Production of sustainable aviation fuels

A techno-economic analysis of power-based concepts

Vom Promotionsausschuss der
Technischen Universität Hamburg
zur Erlangung des akademischen Grades

Doktor-Ingenieur (Dr.-Ing.)

genehmigte Dissertation (kumulativ)

von
Stefan Bube

aus
Stade

2025

1. Gutachter: Prof. Dr.-Ing. Martin Kaltschmitt

2. Gutachter: Prof. Dr.-Ing. Christian Breyer

Vorsitzender des Prüfungsausschusses: Prof. Dr.-Ing. Mirko Skiborowski

Tag der mündlichen Prüfung: 19.11.2025

DOI: https://doi.org/10.15480/882.16258

Handle: https://hdl.handle.net/11420/59267

ORCID: https://orcid.org/0000-0001-7623-3773

Abstract

In the context of ongoing global warming, international aviation faces the challenge of defossilizing its fuel consumption as quickly as possible. Substituting fossil kerosene with kerosene-type sustainable aviation fuels (SAF) is a key instrument in achieving aviation's climate targets. Given the expected increase in SAF demand in the coming years and the limited availability of sustainably sourced biomass, substantial amounts of power-based kerosene will most likely be required. The use of electrical energy can, on the one hand, produce kerosene independently of biomass-derived energy and, on the other hand, when combined with biomass-based SAF production, significantly reduce the specific biomass demand. However, different conversion pathways exist for the synthetic production of power-based SAF, each with distinct techno-economic characteristics. Thus, the overarching research objective is to investigate how kerosene-type SAF can be efficiently produced using electricity from renewable sources of energy as the primary energy input.

The analysis investigates electricity utilization via hybrid production concepts, integrating power-derived hydrogen into biomass-based fuel (methanol) synthesis and via purely power-based production relying on CO_2 and H_2 from water electrolysis. Power-based kerosene production is analyzed by comparing Fischer-Tropsch (FT) synthesis with downstream hydrotreatment (FT pathway) and methanol (MeOH) synthesis with a subsequent methanol-to-kerosene conversion (MeOH pathway). The analyses are conducted at the plant system level using steady-state process simulations. The key figures analyzed include carbon efficiency, energy efficiency, and production costs. Analyzing electrical energy utilization for carbon-efficient fuel production highlights the potential of integrating "green" electricity into biomass-based fuel production. This hybrid production approach enables nearly complete utilization of the carbon contained in the feedstock and thus significantly reduces the specific biomass demand. The analyzed small-scale power-and-biogas-to-methanol concepts reach cost parity with purely biomass-based production due to economies of scale despite the high cost of power-based hydrogen. Purely power-based methanol production achieves almost complete carbon (CO_2) utilization; however, the high hydrogen demand leads to high production costs. The comparative analyses of the power-based kerosene production pathways reveal higher efficiencies for the FT pathway than for the MeOH pathway, referring to the total fuel fraction. However, a higher kerosene selectivity reveals advantages for the MeOH pathway regarding kerosene-related carbon and energy efficiencies. Kerosene production costs range between 3,500 and 5,500 €/t, depending mainly on by-product allocation/revenues and feedstock costs. The FT pathway achieves lower costs when by-products are considered equally valuable to kerosene. However, higher costs result compared to the MeOH pathway when by-product revenues are not considered. Overall, the costs of fuel production utilizing electrical energy depend mainly on feedstock costs (H_2 and CO_2) and utilization efficiency rather than investment costs. Thus, optimizing conversion efficiency and enhancing product selectivity is particularly crucial for power-based production.

Table of contents

List of acronyms

Acronym	Expansion
ASF	Anderson-Schulz-Flory
ASME	American Society of Mechanical Engineers
ASTM	American Society for Testing and Materials
AtJ	Alcohol-to-Jet
BG	Biogas
BGtM	Biogas-to-Methanol
BiRef	Bi-reforming
BP	By-product
BtL	Biomass-to-Liquid
CAPEX	Capital expenditures
CEPCI	Chemical plant cost index
COP	Coefficient of performance
CSDR	Combining steam and dry reforming
DAC	Direct air capture
DME	Dimethyl ether
FRL	Fuel readiness level
FT	Fischer-Tropsch
GHG	Greenhouse gas
GtL	Gas-to-Liquid
HC	Hydrocracking
HEFA	Hydroprocessed esters and fatty acids
HHV	Higher heating value
HT-DAC	High-temperature direct air capture
HTFT	High-temperature Fischer-Tropsch
IATA	International Air Transport Association
ICAO	International Civil Aviation Organization
IGF	Inert gas fraction
K	Kerosene
KPC	Kerosene production costs
LHV	Lower heating value
LT-DAC	Low-temperature direct air capture
LTFT	Low-temperature Fischer-Tropsch
MeOH	Methanol
MOGD	Mobil's Olefins to Gasoline and Distillate

Acronym	Expansion
MPC	Methanol production costs
MtG	Methanol-to-Gasoline
MtJ	Methanol-to-Jet
MtK	Methanol-to-Kerosene
MtO	Methanol-to-Olefins
NRTL	Non-random two-liquid
PBGtM	Power- and Biogas-to-Methanol
PBtL	Power- and Biomass-to-Liquid
PR-BM	Peng-Robinson with Boston-Mathias modification
pri	primary
PtL	Power-to-Liquid
PtM	Power-to-Methanol
PtX	Power-to-X
PV	Parameter variation
RC	Reference case
RK	Redlich-Kwong
RQ	Research question
RWGS	Reverse water-gas shift
SAF	Sustainable aviation fuel
sec	secondary
SG	Syngas
SRK	Soave-Redlich-Kwong
ter	tertiary
TF	Total fuel
TriRef	Tri-reforming
TRL	Technology readiness level
WACC	Weighted average cost of capital
WGS	Water-gas shift

List of symbols

Symbol	Expansion	Unit
α	Chain growth probability	-
A	Size attribute	e.g., m^2,kW,m^3
ACC	Annual capital costs	€/a
$AFLH$	Annual full load hours	h/a
ATC	Annual total cost	€/a
β	Mark-up factors for contingency and fee costs	-
BPR	By-product revenue	€/t
c	Adjustment parameter	-
$\dot{C}$	Carbon flow	mol_C/s
C^0	Bare module cost at standard conditions	€
γ	Mark-up factors for auxiliary costs	-
COR	Carbon oxide ratio	-
FCI	Fixed capital investment	€
F_{BM}	Equipment-specific mark-up factor (under operating conditions)	-
F_{BM}^0	Equipment-specific mark-up factor (under standard conditions)	-
ΔH_{R}	Enthalpy of reaction	kJ/mol
HHV	Higher heating value	MJ/kg
i	Weighted average cost of capital	%
K	Empirical correlation parameter	-
KPC	Kerosene production cost	€/t
LHV	Lower heating value	MJ/kg
m	Mass	t
$\dot{m}$	Mass flow	t/h
MPC	Methanol production cost	€/t
n	Depreciation period	a
η_{C}	Carbon efficiency	%
η_{e}	Energy efficiency	%
O/P	Olefin to paraffin ratio	-
$OPEX_{\mathrm{f}}$	Fixed operational expenditures	€/a
$OPEX_{\mathrm{v}}$	Variable operational expenditures	€/a
$OxyN$	Oxidizing agent ration	-
P_{el}	Electrical power	MW
$\dot{Q}_{\mathrm{th}}$	Thermal power	MW
SN	Stoichiometric number	-

Symbol	Expansion	Unit
ΔT	Temperature difference	K
W_{n}	Weight fraction of chain length n	wt%
ω	Working capital share	%
x	Adjustment parameter	-
$[x]$	Molar fraction of component x	mol%

1 Background

The increase in greenhouse gas (GHG) concentration in the Earth's atmosphere is mainly attributable to human activities, such as the combustion of fossil fuels and the degradation of the biosphere (e.g., deforestation, drainage of wetlands) [1]. The resulting anthropogenic global warming poses an existential threat to existing ecosystems and the essential conditions for life on Earth [1–3]. A necessary measure to limit the increase in GHG concentration and the resulting ongoing warming is the rapid abandonment of fossil carbon-based energy carriers, as the contained carbon is predominantly released into the atmosphere as carbon dioxide (CO_2) either during and/or at the end of their lifecycle. The substitution of these fossil fuel-based carbon-containing energy carriers with alternatives of renewable origin, required for the transition towards climate neutrality, is known as defossilization.

International commercial aviation is currently responsible for ca. 2 to 3 % of global CO_2 emissions, while its actual contribution to the overall GHG effect is even higher [4, 5]. According to current knowledge, CO_2 emissions account for only roughly one-third of aviation's effective radiative forcing, with the remaining two-thirds resulting from so-called "non-CO_2 effects"; under this term, among others, contrails and NO_x emissions are summarized [6, 7]. Nevertheless, commercial aviation continues to rely almost exclusively on kerosene derived from fossil fuel energy (primarily crude oil), which is inherently associated with the release of climate-impacting GHG emissions during combustion and the causation of "non-CO_2 effects" on global climate.

Current projections anticipate a significant growth in commercial aviation over the coming decades, which, without adequate countermeasures, would lead to a strong further increase in aviation-related climate effects [8]. In contrast, the civil aviation industry is increasingly compelled to effectively perform a climate-compatible transformation of the sector in the context of slowing down the ongoing global warming. Consequently, international aviation organizations have published a commitment stating that their members will reduce aviation-related CO_2 emissions to net zero by 2050 [9, 10]. Thus, the global civil aviation industry shows a significant discrepancy between the aimed GHG reduction targets and the projected GHG emissions developments (Figure 1-1).

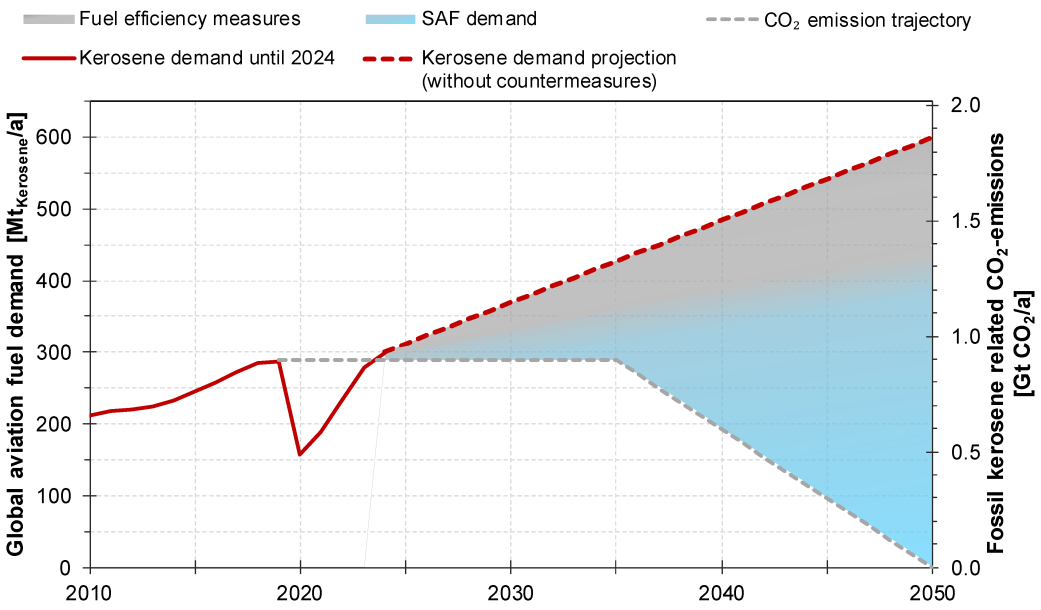

Figure 1-1: Aviation's fuel defossilization requirements until 2050 (only combustion-related CO_2 emissions considered; linear growth between 2024 to 2050 and climate neutral growth until 2035 [11] assumed; data according to [11–15]; SAF: Sustainable aviation fuel).

Increased fuel efficiency due to fleet renewal is characterized by a GHG emission reduction potential of around 20 to 30 % compared to the current civil aircraft fleet [5, 15]. Operational measures, like airline operation optimization and air traffic management improvements, can further reduce GHG emissions – but most likely only to a neglectable amount. All over, the potential of such measures is expected to be clearly below 10 % [15]. As a result, most CO_2 avoidance will depend necessarily on using sustainable aviation fuels[1] (SAF) [16].

The resulting future SAF demand of the global civil aviation industry needed to achieve aviation's net-zero CO_2 emission target will primarily depend on the development of air traffic volume and the extent of technologically achievable and economically feasible fuel efficiency measures. Current analyses predict that the fuel demand of global civil aviation will increase to more than 400 Mt of sustainable kerosene annually by 2050 if the CO_2 reduction goals are to be fulfilled [5, 11, 13].

In the last three years, global SAF production has doubled annually, from 0.3 Mt in 2022 to 0.5 Mt in 2023, and reached ca. 1.0 Mt in 2024. However, with a total kerosene demand of around 300 Mt/a, SAF currently accounts for just 0.3 % of the global kerosene demand [17, 18]. The majority of SAF produced today is derived from hydroprocessed esters and fatty acids (HEFA), sourced, e.g., from biogenic waste products such as used cooking oils (UCO) and animal fats from slaughterhouses [18]. While the majority of SAF production will most likely continue to be provided as HEFA with still increasing volumes in the next few years, the availability of sustainably exploitable unused potentials for the provision

[1] Sustainable aviation fuel (SAF) is defined variably across different contexts. In the context of this thesis, SAF refers specifically to non-fossil aviation fuels produced from renewable sources of energy.

of such a SAF is clearly limited. Thus, to meet the necessarily growing demand for SAF to achieve the CO_2 reduction goals, additional production technologies/options are essential to expand the range of usable resources and ensure long-term scalability.

Against the background described above, the following sections first provide an overview of different SAF types and their respective feedstocks before discussing selected SAF production approaches and technologies in more detail.

1.1 Sustainable aviation fuel options

In principle, a wide range of energy carriers can be considered as adequate substitutes for fossil fuel-based aviation fuels (i.e., kerosene, Jet A1). These options can be categorized based on pre-defined fuel properties or the origin of the energy bound within the SAF during production.

1.1.1 Categorization by properties

To ensure a safe and internationally applicable fuel supply, defined standards exist for conventional aviation fuels, specifying fuel properties that must be met to allow the respective fuel to be used for commercial air flight operations. Due to the near-exclusive reliance on fossil fuel-based kerosene to date, these standards, as well as the associated infrastructure and propulsion technologies, have been specifically tailored to these hydrocarbon-based fuels. SAF can either resemble conventional aviation fuel in terms of molecular composition and properties (kerosene-type SAF) or exhibit entirely different molecular structures and characteristics (non-kerosene-type SAF).

- *Non-kerosene-type SAFs* discussed today are, among others, electricity stored in batteries, hydrogen (H_2), or alcohols. State-of-the-art battery cells currently achieve less than 5 % of the gravimetric and less than 10 % of the volumetric energy density of conventional kerosene [19, 20], making them suitable only for urban and, to a limited extent, regional air traffic [21, 22]. However, most aviation CO_2 emissions are released by medium- and long-haul flights [23]. A similar challenge arises with the substitution of fossil fuel-based kerosene using hydrogen derived from renewable sources of energy. While hydrogen has nearly three times the gravimetric energy density of conventional kerosene, it achieves only about a quarter of the volumetric energy density even after energy-intensive liquefaction and thus a cooling down below −253 °C. Alcohols such as methanol or ethanol also have significantly lower gravimetric and volumetric energy densities compared to conventional kerosene; thus, the use of such fuels would substantially reduce range and/or payload [24]. In addition to the challenge of the energy density, adopting non-kerosene-type energy carriers (especially carbon-free options) would require significant modifications within the overall fuel provision infrastructure, mainly at the airports and in particular within the existing aircraft fleets. For direct-electric and hydrogen-based aviation, entirely new aircraft concepts

must be developed and tested – a process that commonly takes 20 to 30 years from the design phase to serial production [25] – and market penetration follows afterward. Considering the average lifespan of a typical commercial aircraft ranging between 25 and 35 years [25], the market penetration of alternative aircraft technologies most likely extends well beyond 2050. Given the ca. 25 years remaining to achieve the net-zero target defined by the Paris Agreement and the International Air Traffic Organizations, a significant contribution of non-kerosene-type SAF within corresponding aircraft concepts to target fulfillment appears most unlikely from today's perspective [24, 26].

- *Kerosene-type SAF* shares similar physical properties and shows a comparable chemical composition like fossil fuel-based kerosene, primarily consisting of hydrocarbons within a boiling range of 175 to 300 °C. For commercial use, SAF must be certified according to ASTM D7566. This certification process defines the production technology and the necessary fuel properties (e.g., density, distillation residues, viscosity). Currently, eleven conversion processes are approved, allowing the blending of up to 50 % SAF into conventional (fossil fuel-based) jet fuel [27, 28]. However, the origin of the feedstock and energy used is not specified within the basically globally applied ASTM certification, meaning that while alternative aviation fuels must be ASTM-conform for use, these alternative fuels do not need to be necessarily sustainable. The exact composition (type and proportion of hydrocarbons) can vary for both fossil fuel-based kerosene (primarily depending on the crude oil used) and kerosene-type SAF (depending on the production process employed) [29]. The main components typically include n-alkanes, iso-alkanes, cycloalkanes, and aromatic compounds [30]. When sustainably produced from non-fossil feedstocks, a significant advantage of these fuels is their compatibility with the existing fuel provision infrastructure up to the injection into the airplane and the aircraft fleets currently under operation, allowing for immediate reductions in fossil fuel-based CO_2 emissions. In addition, these fuels can also contribute to the reduction of non-CO_2 effects [31].

In contrast to other transportation sectors, such as road transport, where direct electrification through battery-electric vehicles seems to be the most efficient and potentially cost-effective option [32–35], medium- to long-haul commercial aviation relies necessarily on liquid energy carriers characterized by a high gravimetric and volumetric energy density to maintain today's payload capacities [24]. Therefore, and due to the lengthy implementation process of non-kerosene-type SAF in commercial aviation systems, in the coming decades, the necessary defossilization of aviation will primarily depend on "green" liquid hydrocarbon fuels, i.e., kerosene-type SAF. Beyond 2050, however, non-kerosene-type technologies might play increasingly a major role, as they offer potential efficiency advantages and may even contribute to mitigating non-CO_2 effects.

1.1.2 Categorization by energy origin

The production of SAF requires sustainable, non-fossil feedstocks that serve as the material and energy basis for the fuel. Suitable feedstocks contributing to CO_2 mitigation include biomass and electricity from renewable sources of energy, eventually combined with non-energy feedstocks (H_2O and CO_2). According to current regulations [36], the distinction between biomass- and power-based SAF is made solely based on the origin of the energy bound within the fuel.

- *In biomass-based SAF* production, biomass is the main material and energy source. Biomass encompasses a wide range of organic materials (i.e., carbon-, oxygen- and hydrogen-containing chemical compounds) formed through photosynthesis and downstream biochemical reactions within plants. Since this process removes CO_2 from the atmosphere, the CO_2 released during the processing and utilization of such plant material (biomass) can be considered CO_2-neutral, provided that biomass is regenerated/regrown at an equivalent rate (i.e., in a sustainable way). Depending on the type of molecules included within the biomass, processing this material into kerosene, fulfilling the given fuel standards, can be realized via a wide variety of bio- and thermochemical processes, which in turn can be combined within different process pathways. Oil- and fat-containing biomass can be converted relatively easily via hydrotreatment, typically consisting of the three sub-processes: hydrogenation, isomerization, and hydrocracking. Sugar-, starch-, or even lignocellulose-rich biomass is primarily considered for conversion through alcoholic fermentation followed by alcohol-to-jet processing; the latter is realized by the three processes: dehydration, oligomerization, and hydrogenation. Additionally, producing synthesis gas (syngas) via thermochemical gasification or anaerobic digestion, followed by reforming, synthesis, and conversion, represents another viable pathway for kerosene production. Synthesis-based pathways are particularly advantageous for biomass mixtures containing diverse feedstocks that are difficult to separate and cannot be processed individually.
  Besides the molecular basis, biomass is often classified according to its occurrence into cultivated biomass (e.g., maize, rapeseed) as well as the group of residues, by-products, and wastes (e.g., straw, food waste, sewage sludge). Due to the given demand for sustainably provided biomass across various sectors of the overall economy, as well as challenges such as elaborate sourcing, limited infrastructure, and availability, the resource potential for residues, by-products, and waste is necessarily limited. The cultivation of biomass for kerosene production often directly competes with fertile land for food and feed production, as well as areas needed to provide necessary ecosystem services [37]. While estimates for the available biomass potential vary significantly, the abovementioned factors suggest that sustainably provided biomass will not be available in sufficient quantities to meet the forecasted total SAF demand to allow for GHG-neutral commercial aviation in 2050 [11, 38].

- *In power-based SAF* production, energy and material supply are separated, utilizing electricity from renewable sources of energy for energy provision and non-energetic feedstocks, such as H_2O and CO_2, for material provision. As all the energy within the end product originates from electrical energy, the production of power-based SAF requires necessarily significant amounts of electricity. Photovoltaic systems, wind power plants, and hydropower plants are the most widely available options for providing "green" electricity potentially available for such a purpose. Photovoltaic and wind power plants have rapidly gained market importance in recent decades and today are characterized by relatively cost-effective power generation [39]. Given the current state of technology and the globally existing unexploited resource potential, it is expected that in the coming decades, the demand for an increase in the provision of electrical energy will most likely come primarily from photovoltaic systems and wind power plants [40, 41]. Compared to biomass, this energy provision is less land-consuming and also feasible on non-fertile land. While the technical potential fully covers or even exceeds future global primary energy demands [42, 43], the expansion of generation facilities and the corresponding grid and storage infrastructure effectively limits the availability of electricity from renewable sources of energy in the coming decades.

  Electrical energy is converted into chemical energy through electrochemical water splitting into H_2 and O_2 within an electrolyzer. Together with CO_2 from external sources, this H_2 can then be converted into liquid carbon-based synthesis products using chemical synthesis processes. These intermediate synthesis products are then further processed into hydrocarbons, fulfilling the respective fuel specifications for kerosene. Typically, the provision of fresh water for H_2 production is not considered a major techno-economic constraint (even if a water desalination unit is required to allow for the use of seawater), as it contributes only marginally to the overall expenditure of H_2 production [44, 45]. However, the provision of "sustainable" CO_2 is limited to non-fossil CO_2 sources, like biogenic CO_2 point sources or CO_2 separation from the air (direct air capture: DAC), which are either limited in availability or demanding from a techno-economic point of view.

Since current studies indicate that biomass-based SAF shows substantially lower production costs compared to power-based SAF [46–50], the former will most likely dominate the SAF market in the near future (this development is already visible in early/mid-2025 due to the global market expansion in plant oil-based SAF production). Nevertheless, due to the a priori limited availability of sustainably sourced biomass and the transition towards electricity from renewable sources of energy as the primary energy source (and the accompanying cost reductions), power-based kerosene-type SAF will most likely be needed to utilize non-fossil feedstocks and sufficiently fulfill future SAF demands.

1.2 Synthesis-based production

Depending on the feedstock used, the production of kerosene-type SAF can occur via various production pathways utilizing different technologies. However, according to the current state of technology, power-based SAF production relies on synthesis-based production pathways that apply synthesis processes followed by further downstream conversion and treatment steps. Similarly, synthesis-based production pathways can produce biomass-based SAF from a wide range of biogenic residues, by-products, and waste; this is particularly true for non-oil/fat-containing organic materials (i.e., lignocellulosic biomass). Such a biomass-based SAF provision involves other syngas production technologies compared to purely power-based production approaches. Nevertheless, downstream of syngas production, the processing relies largely on the same subsequent synthesis and conversion processes as power-based SAF pathways. Moreover, combinations of power- and biomass-based approaches within so-called hybrid processes are also possible and – based on current knowledge – seem to be quite promising. Figure 1-2 illustrates the general production concepts and the respective technologies for providing kerosene-type SAF, as described in detail below.

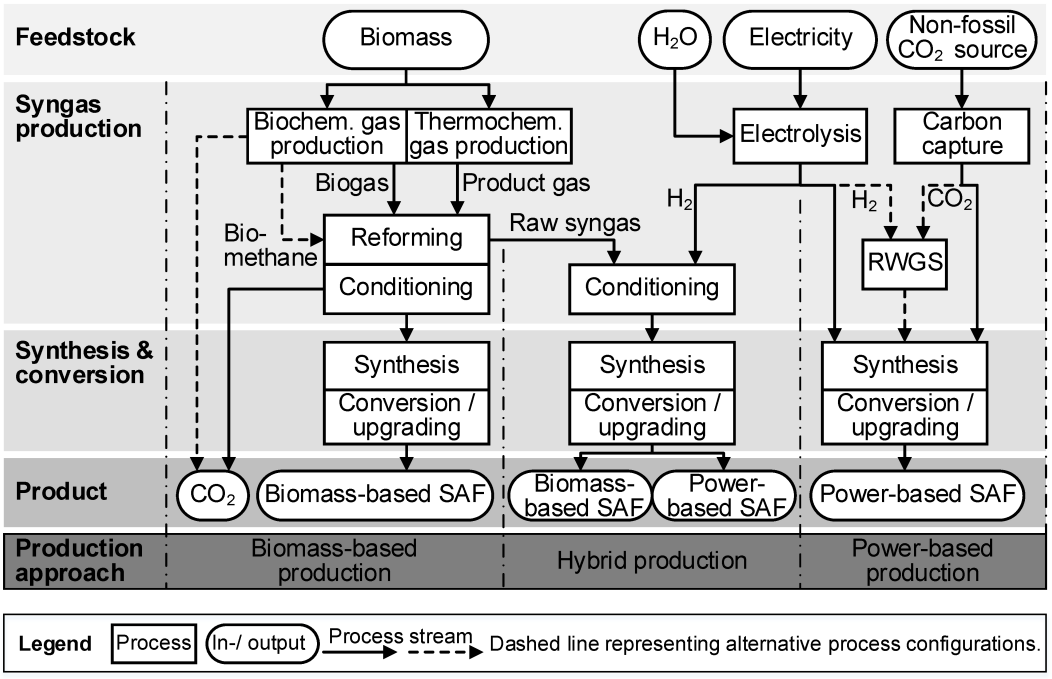

Figure 1-2: Production concepts for biomass, hybrid, and power-based SAF production via synthesis processes (Biochem.: Biochemical, Thermochem.: Thermochemical).

1.2.1 Production approaches

According to current regulations, the distinction between the production approaches described below is based solely on the origin of the energy bound within the fuel. It thus relates to the energy-containing feedstocks utilized (biomass and/or electricity).

- The purely *biomass-based production approach* is shown on the left side of Figure 1-2. The conversion of the biogenic feedstock into SAF is carried out by converting biomass components into a gas mixture, subsequently reformed and conditioned to syngas. This syngas is then converted to kerosene by a respective synthesis step and additional downstream processing of the synthesis products. Most biomasses, except lipids used within the HEFA process, exhibit a significantly lower hydrogen-to-carbon (H:C) ratio compared to the desired hydrocarbon products, such as paraffinic aviation fuels. Therefore, surplus carbon needs to be inevitably removed from the biogenic material during biomass conversion into the desired downstream products, typically in the form of CO_2 to be released into the atmosphere. Additionally, the hydrogen deficit is increased by the oxygen atoms already present in the biomass or added during syngas production (e.g., (thermochemical) gasification, reforming, and conditioning). Since this oxygen must also be removed from the feedstock molecules in the form of water, it acts as a hydrogen sink, increasing the overall hydrogen demand related to the desired hydrocarbon product(s). This hydrogen deficit and the resulting CO_2 separation strongly reduce biomass-based fuel production processes' material efficiency, respectively increase the specific biomass demand.

- The right side of Figure 1-2 shows how hydrogen (H_2) produced from water within an electrolysis process can utilize excess CO_2 from biomass conversion or other non-fossil CO_2 sources within the purely *power-based production approach*. H_2 and CO_2 are supplied separately and mixed in the appropriate ratio. If required, a further conversion into CO-rich syngas might be necessary before the subsequent downstream synthesis. The purely power-based production (utilizing the non-energetic feedstocks H_2O and CO_2) enables SAF production to be fully decoupled spatially and temporally from biomass use, allowing for a diversification of the CO_2 sources.

- The middle of Figure 1-2 depicts the direct integration of power-derived H_2 production into biomass-based production to overcome the hydrogen deficit in the biomass-based raw syngas within a so-called *hybrid production approach*. Here, some energy within the produced SAF originates from biomass, and another part from electrical energy (via H_2). No carbon is released as CO_2 for conditioning within such a concept. Instead, the available CO_2 is theoretically fully converted into syngas and subsequently into synthesis products. Thus, such a hybrid production enables a clearly more efficient utilization of the biogenic carbon. Additionally, as no further oxidation of CO to CO_2 is required for H_2 production, less H_2 from electrolysis is needed compared to a separate biomass-based production with subsequent CO_2 utilization in a standalone power-based process.

As the availability of sustainably provided biomass for SAF production is limited due to the limited availability of fertile land on Earth, utilizing electricity for SAF production – either through purely power-based or hybrid approaches – can significantly increase the utilization of biogenic carbon and thus expand the overall production potential. However,

this increased carbon use efficiency is "purchased" by substantially utilizing electricity for power-based H_2 production.

1.2.2 Syngas production technologies

The syngas production technologies applied depend mainly on the production approach and, thus, on the feedstock utilized.

Biomass-based syngas production. The production of syngas from biomass (e.g., lignocellulosic material, wet organic waste materials like organic urban waste) typically requires multiple conversion steps, primarily involving first gas production and second reforming and/or conditioning. Depending on the feedstock and the technology, syngas composition varies, with H_2, CO, and CO_2 being typically the main components. The conversion of the feedstock (organic material) into such a gas stream is mainly realized via biochemical anaerobic digestion or thermochemical gasification [46].

- *Anaerobic digestion* is a widely established biochemical process. Here, within a watery environment, organic matter is successively degraded under oxygen-free conditions by various groups of microorganisms (i.e., bacteria and archaea). The final product of this biochemical degradation process is primarily biogas, being a mixture of mainly methane (CH_4) (50 to 60 $vol\%_{Dry}$) and CO_2 (40 to 50 $vol\%_{Dry}$) [51]. Anaerobic digestion can be conducted at various temperature levels; however, processes operating in the mesophilic range (ca. 37 °C) dominate the market since they offer a good balance between the gas yield and the required process energy [52]. Since the produced gas mixture (biogas) is typically saturated with moisture and contains impurities that can act as catalyst poisons within subsequent catalytic-controlled synthesis processes – particularly sulfur compounds – biogas must be purified before reforming. The respective purification technologies depend primarily on the type of biomass feedstock (upstream) and the required gas purity (downstream). Anaerobic digestion is commonly applied to organic material streams that have a rather high water content (e.g., sewage sludge, organic urban waste fraction, liquid manure). Due to the nature of the necessary feedstock characteristics, this option is favored for waste valorization and decentralized applications, as the high moisture content of such organic material makes long-distance transportation economically unattractive [51]. Prior to subsequent reforming, some or all of the CO_2 contained within the biogas needs to be separated to achieve the desired syngas composition in the reforming process without additional subsequent conditioning.

- *Thermochemical gasification* is a heat-induced conversion process in which mainly solid biomass (lignocellulosic material) is partially oxidized at a temperature level between 700 and 1,500 °C [53–55] to provide a mixture of CO, H_2, CO_2, and light hydrocarbons, known as product gas. The proportion of these gas components varies greatly

depending on the feedstock composition, the gasification technology, and the oxidization agent employed; for syngas production, typically oxygen or water vapor is applied. Compared to anaerobic digestion, thermochemical gasification offers higher syngas yields but requires relatively dry organic material. Additionally, equipment design and process operation are more demanding. Since the product gas typically includes various impurities (e.g., particles, alkalis, tar, nitrogen, sulfur, halogen compounds), extensive gas cleaning is necessarily required before the subsequent downstream processing can be realized [53].

Reforming processes aim to convert hydrocarbon-containing gases, such as biogas or product gas, into (raw) syngas with a composition close to the specified synthesis requirements. This is achieved through partially oxidizing the hydrocarbons to produce a H_2- and CO-rich gas. Common reforming technologies primarily differ in the oxidizing agent used. Typically, H_2O, O_2, and/or CO_2 (if not already present in sufficient amounts within the feed gas) are added and utilized for the partial oxidation of hydrocarbons at temperatures often well above 700 °C with the help of a catalyst.

- In *steam reforming*, light hydrocarbons react with water steam to produce a CO- and H_2-rich gas mixture. Since both the hydrocarbon and the water act as hydrogen sources, high H:C ratios within the reforming product can be achieved. The strongly endothermic reaction occurs over a nickel-based catalyst (e.g., Ni/Al_2O_3) at temperatures above 800 °C and under elevated pressure conditions [56]. It is evident that steam reforming reactors necessitate substantial quantities of high-temperature heat; consequently, they need to be heated externally [57].

- *Partial oxidation* is a sub-stoichiometric combustion (i.e., oxidation with oxygen) of light hydrocarbons and, thus, an exothermic reaction, eliminating the need for external heating. The reaction requires temperatures above 1,000 °C without a catalyst to proceed efficiently. However, when using a reforming catalyst, the reaction can occur at moderately lower temperatures (< 1,000 °C) while maintaining high conversion efficiencies [56, 57]. Since no additional hydrogen is introduced via the used oxidizing agent, the resulting syngas shows a low H:C ratio, often significantly below the requirements for the subsequent downstream synthesis process [56–58].

- In *dry reforming*, CO_2 is utilized to oxidize light hydrocarbons. This highly endothermic reaction occurs at temperatures above 700 °C and elevated pressures, typically utilizing nickel-based catalysts [59]. Due to the high concentration of carbon-containing compounds within the feed gas, dry reforming is prone to coke formation and metal sintering, posing significant challenges for practical implementation [60]. Compared to steam reforming, the resulting raw syngas typically shows a lower H:C ratio, falling below the requirements for many synthesis processes [61]. Reforming with CO_2 or other oxidizing agents is particularly relevant for feed gases with a naturally high CO_2 content, such as biogas.

The oxidizing agents used in the different reforming technologies can also be combined to adjust the composition of the resulting raw syngas as closely as possible to the required synthesis gas specifications or to influence the reactor's thermal management. For example, combining endothermic steam reforming with exothermic partial oxidation enables autothermal reforming [56]. When CO_2 is used as an oxidizing agent, its combination with steam reforming (known as combined dry and steam reforming or bi-reforming) significantly reduces the risk of coking while achieving higher H:C ratios [62]. By additionally introducing oxygen, this process can also be conducted autothermally, referred to as tri-reforming [63].

The conditioning of raw syngas from the reforming process aims to adjust the syngas composition to meet the specific synthesis requirements, particularly when the desired ratio cannot be achieved directly during the reforming step.

Syngas from partial oxidation, dry reforming, and autothermal reforming often exhibit a significant hydrogen deficit. In purely biomass-based production approaches, additional H_2 is first generated via the water-gas shift reaction. Subsequently, CO_2 is separated to optimize the syngas ratio for CO_2-converting syntheses or to increase reactants' partial pressure and to reduce the volume flows in non-CO_2-converting synthesis processes.

- In the *water-gas shift* (WGS) reaction, carbon monoxide (CO) is further oxidized with water (H_2O), producing carbon dioxide (CO_2) and hydrogen (H_2). This slightly exothermic equilibrium reaction is catalytically driven and takes place at temperatures between 200 and 550 °C and pressures of up to 30 bar. Either a portion of the raw syngas can be fed into a two-stage WGS process, where the CO is almost completely converted, and H_2 is fed back to the main syngas stream. Alternatively, the entire raw syngas stream can undergo a single-stage WGS with only partial CO conversion and a subsequent CO_2 separation.

- *CO_2 separation* from syngas can be achieved by various technologies, including absorption, adsorption, cryogenic separation, or membrane-based processes. Among these, physical absorption has become the most widely established method for syngas conditioning; the Rectisol and Selexol process are commonly used processes within the chemical industry. Both are washing processes in which a liquid solvent absorbs CO_2 within an absorber column and subsequently desorbs CO_2 at elevated temperatures and/or reduced pressure levels within another stripper column. In the Rectisol process, methanol is used as the absorption medium at pressures above 20 bar and temperatures of roughly −40 °C. In contrast, the Selexol process employs a specialized solvent mixture, primarily composed of polyethylene glycol dimethyl ether. While Selexol also operates at high pressures above 20 bar, it allows for higher absorption temperatures compared to Rectisol [64]. Both methods not only facilitate CO_2 removal but also enable the extraction of sulfur contaminants from the syngas [57].

Power-based syngas production. Power-based syngas production fundamentally differs from biomass-based syngas production. Instead of energy-rich molecules, H_2O and CO_2 serve as the primary feedstock, with electricity from renewable sources of energy providing the required energy input. The key processes include water electrolysis for H_2 production and the provision of pure CO_2 through carbon capture from non-fossil sources. Additionally, a CO_2 reduction to CO may be required depending on the synthesis applied downstream, which can be achieved via the reverse water-gas shift (RWGS) reaction.

Electrolysis enables the electrochemical splitting of water into H_2 and O_2, thus converting electrical energy into chemical energy ("green" molecules). This process can be conducted at different temperature levels, utilizing either liquid water (low-temperature electrolysis) or steam (high-temperature electrolysis).

- *Low-temperature electrolysis* operates at temperatures below 100 °C within an exothermic operation, requiring cooling due to ohmic losses within the electrolyzer cell. The most common technologies include proton exchange membrane electrolysis (PEMEL) and alkaline electrolysis (AEL), achieving stack efficiencies of up to 68 % based on the electricity input and the lower heating value (LHV) of the produced H_2. AEL is the most technologically mature option, while PEMEL offers advantages in load flexibility, making it particularly suitable for the integration of electricity from fluctuating renewable sources of energy [65–68].

- *High-temperature electrolysis* operates at temperatures above 700 °C, typically in an endothermic or thermoneutral operation. The integration of (waste) heat enables high efficiencies of potentially up to 100 %; i.e., a part of the energy to split water is provided by electrical energy and another part by thermal energy. This makes this technology particularly beneficial if (cheap) waste heat above 100 °C is available. The electrolyzer is designed as a solid oxide electrolyzer (SOEL). Co-electrolysis of CO_2 and H_2O to directly produce a CO- and H_2-rich syngas is also possible within high-temperature electrolysis. However, due to the relatively low technological maturity, large-scale commercial deployment of high-temperature electrolysis is still associated with significant technical and economic risks [65, 66].

CO_2 capture can be performed from gas streams with elevated CO_2 concentrations (point sources, typically 3 to 100 vol% [69]) or from the atmosphere, where CO_2 is highly diluted (ca. 0.042 vol% in 2023 [70]). Capturing CO_2 from the air via so-called direct air capture (DAC) systems requires significantly more energy and construction effort compared to systems capturing CO_2 from point sources. Examples of non-fossil point sources are biomass-processing facilities, such as anaerobic digestion plants or alcoholic fermentation units.

- For *point source carbon capture*, amine scrubbing is the most widely used technology, achieving capture rates of above 90 % and CO_2 purities above 99 vol% [69, 71]. The desorption process requires significant amounts of thermal energy (at 100 to 140 °C),

making it the most energy-intensive step within the overall CO_2 provision. Physical absorption technologies like Rectisol and Selexol processes require higher pressure levels and are typically used for gas streams with high CO_2 partial pressures. Membrane-based separation and pressure swing adsorption (PSA) are alternative approaches but might yield lower CO_2 purities.

- *Direct air capture* (DAC) technologies are categorized into low-temperature DAC (LT-DAC) and high-temperature DAC (HT-DAC). LT-DAC technologies (using solid sorbents, amine-based) are more technically mature but require higher total energy input compared to HT-DAC (using aqueous solutions, KOH, or NaOH) for the same amount of CO_2 captured. While HT-DAC requires desorption temperatures above 800 °C, LT-DAC adsorption processes are operated on the regeneration side at moderate temperatures of about 100 to 120 °C [72]. The energy needed for DAC operation can be supplied as a combination of heat and electricity or entirely through electrical power. Due to the low atmospheric concentration of CO_2, DAC is technically demanding; therefore, it is most likely that this option remains significantly more expensive than point source carbon capture [69, 73, 74].

If the syngas-utilizing synthesis process does not allow for the direct conversion of CO_2, the reduction of CO_2 to CO must be integrated into the overall syngas provision concept. Using H_2, this can be realized through the reverse water-gas shift (RWGS) reaction. This endothermic equilibrium reaction reduces CO_2 by oxidizing H_2 to H_2O, requiring temperatures above 700 °C to realize a sufficient CO yield under techno-economic constraints. Operating pressures range between 1 and 30 bar; higher pressures typically result in an increased methane formation [75]. The reaction is catalyzed by nickel (Ni) or noble metal-based catalysts in heterogeneous catalysis [76]. The required thermal energy for the high-temperature endothermic reaction can be supplied, e.g., through electrical energy [77].

Hybrid syngas production. The hybrid, power- and biomass-based syngas production combines the process steps of the raw syngas production from biomass and the H_2 production via electrolysis from the power-based production. Conditioning via water-gas shift and CO_2 separation is replaced by adjusting the hydrogen deficit with H_2 from electrolysis. No additional technologies are required for such a hybrid production.

1.2.3 Synthesis and conversion pathways

The two most widely discussed synthesis and conversion pathways for kerosene-type SAF production are the Fischer-Tropsch (FT) and the methanol (MeOH) pathway. Since both pathways differ significantly in terms of the technologies and reactions applied (see below), different efficiencies and production costs are expected for kerosene-type SAF production depending on the applied process pathway.

Fischer-Tropsch (FT) pathway. The FT pathway includes the FT synthesis and further downstream conversion through subsequent hydrotreatment of the synthesized products. The FT synthesis is a well-established technology for producing hydrocarbon fuels from a CO- and H_2-rich syngas, with its first large-scale application dating back to the 1930's. However, the direct conversion of CO_2 into long-chain hydrocarbons remains challenging due to insufficient selectivity of the so far available catalysts and, thus, a too-low conversion efficiency. Consequently, for the time being, a CO- and H_2-rich syngas is required to perform a low-temperature FT synthesis, typically used for long-chain hydrocarbon production. Here, H_2 and CO react with each other to form hydrocarbon chains, yielding synthetic crude oil (syncrude) containing hydrocarbon molecules ranging from light gases (e.g., methane) to long-chain hydrocarbons (i.e., waxes).

Due to the diverse composition of this syncrude, additional downstream hydrotreatment is required to produce aviation fuel that meets the respective specification standards. Therefore, hydrocracking is applied to break down long-chain molecules (waxes) into fuel components accompanied by a parallel occurring isomerization. Hydrogenation to saturate unsaturated bonds is further required to yield a stable, standard-compliant product. A separate/additional hydroisomerization might become necessary when the share of hydrocracked (and therefore iso-paraffinic) fuel components is (too) low within the overall kerosene fraction. The required fuel fractions to meet the given fuel standards are separated from the product spectrum of these treatment steps via conventional distillation/rectification.

Methanol (MeOH) pathway. The MeOH pathway consists of methanol synthesis and the subsequent conversion into a kerosene-rich hydrocarbon fuel mixture through methanol-to-kerosene (MtK) conversion (also known as Methanol-to-Jet: MtJ).

The methanol synthesis allows for the direct conversion of CO_2 and H_2 into methanol and thus eliminates the need for a prior CO_2 reduction step. This synthesis process produces a methanol-water mixture, which needs to be separated via distillation to provide pure methanol.

Similar to other alcohol-based fuel production pathways (Alcohol-to-Jet: AtJ), the MtK conversion route consists of olefins formation through dehydration, oligomerization of short olefins into higher olefins and hydrogenation, converting unsaturated hydrocarbons into alkanes. As within the FT pathway, the hydrocarbon share fulfilling the specification of synthetic kerosene-type SAF is subsequently separated from the hydrocarbon mixture via rectification. The conversion of methanol into hydrocarbons was first developed in the 1970s and later commercialized in the 1980s, primarily for gasoline production [78]. Process concepts for producing heavier hydrocarbons have not yet focused on kerosene production [79, 80].

2 Research gaps, objectives, and outline

The background outlined above underscores the significant disparity between commercial aviation's current CO_2 emission projections and its net-zero target, making the large-scale adoption of kerosene-type sustainable aviation fuels (SAF) essential for the achievement of the agreed CO_2 reduction target and compliance with existing legal requirements. Due to the a priori limited availability of sustainably sourced biomass, SAF production based on "green" electricity from renewable sources of energy is expected to contribute necessarily with a relevant proportion to the overall SAF demanded on a global level, even if the non-fossil carbon utilized within such conversion concepts is also limited or can only be provided at considerable expense. Electricity can be utilized within synthesis-based production pathways, either in purely power-based processes that rely on non-fossil CO_2 sources or in combination with biomass-based production approaches in so-called hybrid processes aiming to maximize biogenic carbon utilization.

Against this background, below the existing research gaps in the field of electricity utilization for carbon-efficient kerosene production are derived. Based on this, the objectives of this thesis and the corresponding research questions are formulated, followed by a description of the thesis outline.

2.1 Research gaps

The conversion of electrical energy for utilization in technical applications that cannot be directly electrified (power-to-x) has gained increasing attention in research and public discourse in recent years. However, there are still open questions to be answered. These knowledge gaps can be categorized into three key research areas outlined below.

Integration of "green" electricity in biomass-based fuel production for carbon-efficient hybrid production systems. While the HEFA process is so far the only commercially utilized SAF production pathway at a large scale in various countries, numerous other biomass-based pathways for the production of kerosene-type SAF or intermediates of synthetic kerosene have been extensively researched and, in some cases, even successfully tested in practical applications [46, 81, 82]. Due to the unfavorable relation between carbon atoms and hydrogen atoms typically occurring in organic matter (biomass) relative to the needed carbon-to-hydrogen ratio within SAF-like hydrocarbons, "classical" biomass-based fuel production processes require the discharging of carbon/carbon compounds, usually as CO_2 released into the atmosphere. However, this CO_2 can also be seen as a loss, especially since providing sustainable CO_2 from ambient air is an energy-inten-

sive and, thus, quite expensive process. Against this background, the efficient use of biogenic carbon gains more and more attention in biomass-based processes for the provision of kerosene-type SAF. Integrating "green" electrical energy within SAF production concepts allows for maximizing carbon utilization and, thus, reducing the specific biomass demands. However, such considerations have not been the main focus of previous investigations. Various technological approaches to realize such a hybrid production – where the product's energy originates both from biomass and "green" electricity (i.e., from renewable sources of energy) – are technically possible. Such innovative hybrid concepts can improve carbon utilization but may significantly change the overall energy efficiency and, thus also, the production costs of such process concepts. So far, only limited insights are available into the technical integration of such processes and the associated techno-economic implications. Consequently, there is a clear research gap regarding the technical requirements and implications of fuel production concepts based on such hybrid process approaches, the efficiency gains that can be achieved, and their economic feasibility compared to pure biomass- or power-based production processes.

Conversion pathways for efficient power-based kerosene production. Power-to-kerosene production pathways, where carbon is utilized in the form of CO_2 and energy is entirely supplied by electricity, have seen increased attention in recent years. Despite this, only a handful of small research and demonstration facilities addressing such concepts have been implemented or are under development [50]. Related to the respective maturity (technology and fuel readiness level), currently, two production pathways are mainly discussed as the primary options for large-scale industrial production: the Fischer-Tropsch (FT) and the methanol (MeOH) pathway.

The FT synthesis followed by downstream hydrotreatment has been studied extensively in recent years [83–87]. Furthermore, fossil fuel-based production via the FT pathway has been commercially used on an industrial scale for various fuel and chemical products for decades [58, 86]. However, kerosene production has not been the primary focus, and syngas provision from CO_2, H_2O, and electrical energy has not been used as a feedstock on a large scale.

Methanol (CH_3OH) is one of the most widely produced primary chemicals, supported by a well-established global infrastructure and a wide range of potential downstream applications within the chemical industry and fuel production facilities. Although methanol is produced almost exclusively from natural gas or coal today, its highly selective synthesis process, technically feasible across a broad range of possible production capacities, makes it particularly well-suited for power-based production. Such methanol production concepts have been extensively studied and implemented in demonstration plants as well as initial commercial facilities [88–93]. Based on this development, methanol-to-kerosene processing has recently gained traction as an alternative to the FT pathway. However, the methanol pathway toward kerosene production is still underexplored relative to the FT pathway. Although several technology providers have recently announced plans for ASTM

certification of methanol-based kerosene, comprehensive, publicly available studies on process concepts remain scarce. This underscores critical research gaps in methanol-based kerosene production. Specifically, there is a lack of techno-economic analyses to contextualize the technology, particularly concerning power-based kerosene production.

Influence of uncertain/unknown technical and economic assumptions. A fundamental challenge in analyzing "new" and/or innovative processes/production pathways is that assumptions of certain technical and numerous economic parameters must be made while being aware that the respective values are subject to uncertainty due to a priori limited knowledge. This fundamental problem, valid for basically all assessments of "new" processes, might result in misleading interpretations of the results of such an analysis. To mitigate the resulting uncertainties, the key parameter in question can be varied within the respective uncertainty range to analyze the impact of the assumption on the overall results and to derive possible outcome ranges. However, such an approach is rarely realized within publicly accessible investigations, e.g., due to the necessary extensive modeling and evaluation efforts. Additionally, such an assessment approach is typically applied mainly to economic parameters and, to a clearly lesser extent, to technical key factors.

Concerning the analysis of the power-based and hybrid fuel production pathways, the lack of valid investigations of the impact of critical and result-determining assumptions can be identified as another research gap. Beyond establishing consistent system boundaries and robust overall process design concepts, it is necessary to consider the uncertainty of the assumed techno-economic key parameters within realistic ranges to improve the overall understanding of the process and strengthen the robustness of the results/conclusions.

2.2 Research objectives

Based on the above-described background, the overarching research objective of this thesis is to explore how kerosene-type SAF can be efficiently produced using electricity from renewable sources of energy. To address the identified research gaps, the thesis aims to analyze the use of "green" electricity in purely power-based and hybrid production concepts, generating techno-economic insights and identifying key differences between these production approaches. Furthermore, the main synthesis and conversion pathways for power-based kerosene production are to be examined in detail related to selected technical and economic parameters. In this context, the impact of uncertain/unknown techno-economic parameters on the overall results shall be assessed and quantified.

The following research questions arise based on the objective outlined above.

1. How, and with what implications, can electrical energy enhance the efficient utilization of non-fossil carbon in "green" fuel production approaches? This research question aims to determine the carbon efficiency of electricity utilizing process concepts and the associated energy efficiencies and production costs.

2. How do the Fischer-Tropsch (FT) and the methanol (MeOH) pathway for power-based kerosene production differ regarding selected technical and economic key parameters? Research question 2 seeks to assess synthesis and conversion pathways for power-based kerosene production in terms of carbon and energy efficiency, as well as kerosene production costs, enabling a fair and sound comparison of the analyzed pathways.

3. Which technical and economic key parameters determine the technical efficiencies and costs of "green" fuel production from electrical energy? This last research question addresses the challenge of incorporating the uncertainty of potentially decisive technical and economic assumptions, generating a deeper understanding of their influence on the overall results.

2.3 Outline

Besides the background chapter and the section discussing the research gaps, the objectives, and the outline, this thesis comprises three scientific publications, a synthesis chapter, and a chapter with overall final considerations. The publications contain detailed analyses of the processes examined and tackle the research questions by providing detailed process-specific results. The synthesis chapter answers the research questions by extracting and synthesizing the findings discussed within the three research papers at a superordinate level. Finally, the elaborated results are summarized, and an outlook regarding further research needs is provided. The chapters address the stated research questions as listed in Table 2-1.

Table 2-1: Addressed research questions within the overall thesis structure (RQ: Research question).

Chapter		**RQ 1**	**RQ 2**	**RQ 3**
3	Power and biogas to methanol – A techno-economic analysis of carbon-maximized green methanol production via two reforming approaches	×		×
4	Kerosene production from power-based syngas – A technical comparison of the Fischer-Tropsch and methanol pathway	×	×	×
5	Cost analysis of kerosene production from power-based syngas via the Fischer-Tropsch and methanol pathway		×	×

As introduced in Section 1.2, the use of "green" electricity from renewable sources of energy for sustainable fuel production can occur in two ways: first, through direct integration into biomass-based production processes (hybrid production), and second, through the exclusive use of electrical energy to convert non-energetic feedstocks such as H_2O and CO_2. Chapter 3 analyzes the direct integration of electrical energy using hybrid production pathways exemplarily for power- and biogas-to-methanol (PBGtM) production. Chapter 4 and 5 provide a detailed examination of purely power-based production. The focus is particularly on the synthesis and conversion processes for power-based kerosene via the Fischer-Tropsch and the methanol pathway. Below, a short outline of the main chapters is given.

Chapter 1: Background

The first chapter introduces the research topic within the broader context of anthropogenic global warming, emphasizing the necessity of SAF. It provides a classification of potential SAF options based on their properties and the origin of the respective fuel energy. Finally, synthesis-based production approaches and the associated technologies are presented, focusing on different concepts for kerosene production utilizing electricity.

Chapter 2: Research gaps, objectives, and outline

This chapter identifies critical gaps within the published research results related to power-based and hybrid fuel production concepts. It defines the overarching research objective and presents the structure of the thesis.

Chapter 3: Power and biogas to methanol – A techno-economic analysis of carbon-maximized green methanol production via two reforming approaches

This chapter examines the integration of power-based H_2 into biomass-based production processes, focusing on maximizing carbon utilization to minimize the overall biomass demand. The conversion of biogas to methanol is chosen as an example because biogas is already produced in more than 8,000 commercially operated biogas plants in Germany. Additionally, biogas can be sourced from a wide range of biogenic feedstock, indicating a considerable biogas production potential. Regarding the integration of "green" electricity, biogas offers a good basis because the use of this gas together with electrical energy is characterized by a substantial potential to increase carbon efficiency since 30 to 50 % of the carbon contained within biogas is available as CO_2, typically remaining unused by releasing this gas component into the atmosphere. Methanol is selected as the target product due to its suitability for small-scale synthesis processes and as an intermediate for synthetic kerosene production. Units for such a small-scale methanol production are commercially available, and methanol's favorable handling properties allow for simple storage and transportation to centralized/large-scale facilities for further processing – such as its conversion into kerosene. This makes methanol a promising candidate for demonstrating hybrid fuel production from electricity and biogas.

The developed hybrid production system incorporates "green" electricity in two distinct configurations: electrically heated bi-reforming and autothermal tri-reforming. These configurations are evaluated to understand how electricity can be integrated into the process from a technical and economic perspective. Based on the gathered results, research questions 1 and 3 are directly addressed.

- Concerning research question 1, the chapter analyzes the extent of carbon utilization and the potential benefits and disadvantages of such hybrid production concepts compared to solely biomass or power-based production approaches.

- Research question 3 is addressed by extensive parameter variation, varying technical parameters, and economic boundary conditions.

Chapter 4: Kerosene production from power-based syngas – A technical comparison of the Fischer-Tropsch and methanol pathway

This chapter presents a technical analysis of power-based kerosene production via the Fischer-Tropsch and the methanol pathway. The analysis is based on detailed process design and stationary process simulations, enabling insights into the process streams and sub-processes interactions within the overall plant concept. Regarding the comparative analysis of kerosene production pathways, the system boundaries are defined around the synthesis and conversion processes, considering H_2 and CO_2 as feedstocks. This focus enables a detailed examination of the differences between the two pathways. The analysis addresses all research questions.

- Research question 1 is examined in the context of purely power-based production, where non-fossil carbon in the form of CO_2 is converted into fuel.

- Research question 2 is addressed regarding technical aspects by analyzing carbon and overall energy efficiency, including various options for CO_2 and H_2 supply.

- Concerning research question 3, a variation of technical higher-level process parameters is conducted to evaluate the respective impact on carbon and energy efficiency, aiming to quantify technical optimization potentials and uncertainties within the analysis.

Chapter 5: Cost analysis of kerosene production from power-based syngas via the Fischer-Tropsch and methanol pathway

The fifth chapter presents the economic analysis of the power-based kerosene production pathways. The technical results detailed in Chapter 4 are used to determine specific process demands and the fixed capital investment requirements of the corresponding production plants that contribute to the respective kerosene production costs. The system boundaries are chosen similarly to Chapter 4, focusing on the synthesis and conversion processes, enabling a more precise assessment of the cost differences between the two pathways and variations in feedstock costs. Thus, this chapter addresses research questions 2 and 3 regarding cost aspects.

- The economic characteristics and differences between the FT and MeOH pathways are derived through production cost analysis, directly addressing research question 2.

- Research question 3 is tackled through variations of the technical and economic parameters to analyze their effects on the overall kerosene production costs. Further-

more, different cost allocation methods and variations in by-product revenues are employed to identify boundary conditions and parameter ranges where each pathway shows economic advantages.

Chapter 6: Synthesis and limitations of results

The sixth chapter provides a synthesis of the results given in detail within Chapters 3 to 5 by compiling the broader findings concerning the formulated research gaps. In addition to answering the research questions, the key findings from the respective chapters are summarized. Additionally, the limitations of the investigation approach and the conducted process analyses are identified and discussed.

Chapter 7: Final considerations

The last chapter summarizes the thesis results and gives an outlook on further research needs.

3 Power and biogas to methanol – A techno-economic analysis of carbon-maximized green methanol production via two reforming approaches

Bube S, Sens L, Drawer C, Kaltschmitt M (2024): Power and biogas to methanol – A techno-economic analysis of carbon-maximized green methanol production via two reforming approaches. In Energy Conversion and Management 304 118220. DOI: 10.1016/j.enconman.2024.118220.

The article can be found online at
https://doi.org/10.1016/j.enconman.2024.118220

Formatting and wording are slightly adjusted to ensure consistency throughout this thesis.

Abstract

The limited potential of sustainably available biomass requires efficient conversion to defossilize future demands of carbon-based chemicals and energy carriers. Therefore, integrating electricity-derived hydrogen into biomass-based production concepts appears promising, maximizing carbon utilization while minimizing biomass requirement. However, specific process concepts and analyses are still lacking to quantify the potential technical and economic benefits of such hybrid production processes. Thus, this research paper investigates this novel approach for decentralized methanol production from biogas within a techno-economic analysis, considering two production configurations. One configuration (BiRef) utilizes electrically heated bi-reforming for syngas generation, while the other configuration (TriRef) uses autothermal tri-reforming. Based on stationary process simulations, in-depth knowledge about process behavior is gained, efficiencies and costs are determined, and influencing factors are assessed. Within the reference case, the BiRef configuration achieves a carbon efficiency of 93 %, while the TriRef configuration reaches 97 % due to its enhanced methane conversion. Energy efficiency is 5 %pt higher within the BiRef configuration (74 %), primarily due to the lower hydrogen demand. Carbon and energy efficiency are crucially affected by reforming temperature and inert gas fraction in the syngas. The economic analysis shows methanol production costs of ca. 1,300 €$_{2022}$/t for both configurations. Variations in economic parameters emphasize advantages for the TriRef configuration when low hydrogen costs (<6 €$_{2022}$/kg) are achievable. The comparison with purely biogas-based methanol production shows that hydrogen addition increases production capacity by up to 67 %. Cost advantages result against purely power-based production, while cost parity is achieved with purely biogas-based production. This paper demonstrates the potential of hybrid methanol production for efficient biogas utilization and highlights decisive parameters influencing technical and economic efficiency.

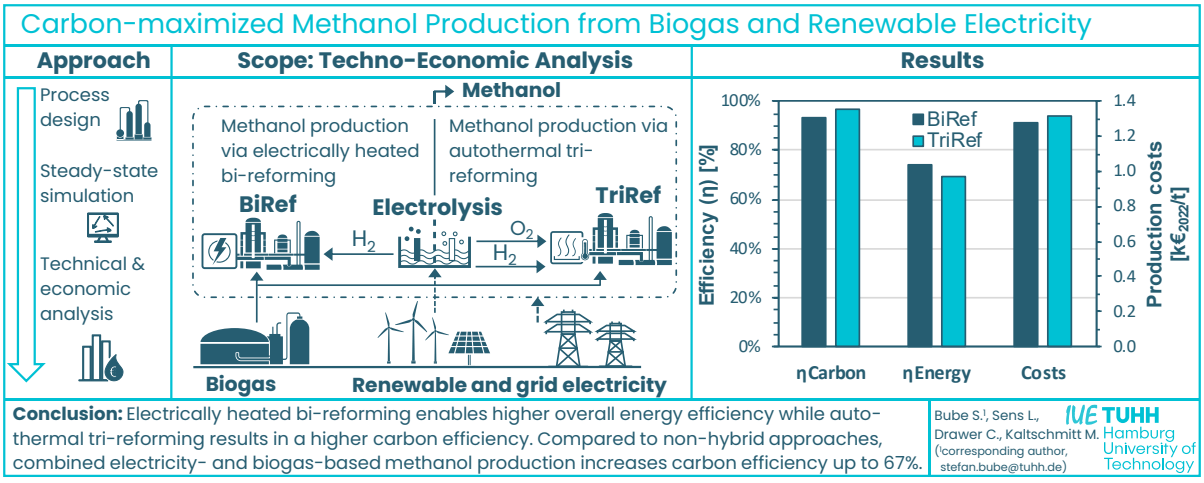

Figure 3-1: Graphical abstract of the publication “Power and biogas to methanol”.

3.1 Introduction

The imperative necessity of defossilizing the highly industrialized economy to mitigate anthropogenic climate change requires a transformation of all sectors toward the utilization of renewable sources of energy and materials. However, from today's perspective, some sectors, such as the chemical industry and most likely also specific segments within the transportation sector (e.g., long-haul air transport), will persist in their reliance on carbon-based molecules over the long term due to the absence of viable decarbonization alternatives. The non-fossil (so-called "green") production of these substances requires significant amounts of energy from renewable sources and sustainable carbon. The latter is either obtained from biomass or extracted as carbon dioxide from the atmosphere. Due to the comparable low atmospheric concentration (approximately 420 ppm [94]), such a direct air capture (DAC) process requires significantly higher energy and engineering efforts compared to carbon supply from biomass processing, making these approaches much more expensive [69, 72]. However, sustainably available biomass is severely limited due to competition in land use and utilization. Hence, maximizing the utilization of the carbon inventory from biomass needs to be prioritized for efficiency reasons, provided a sustainable origin of the utilized biomass can be ensured.

Sustainable biomass, such as manure or straw, is primarily generated within agriculture. So far, these materials are typically, if at all, utilized energetically – i.e., for electricity and heat production – commonly realized through anaerobic biomass fermentation and biogas combustion. Instead of this most widely realized utilization pathway, biogas – which typically consists mainly of methane (CH_4) and carbon dioxide (CO_2) – can also be converted into higher-value substances through reforming and subsequent synthesis processes. Due to its selective and small-scale implementable synthesis technology, methanol (CH_3OH) is particularly suitable as a target product [95, 86]. Methanol is one of the most important organic primary chemicals, with a global (fossil-based) production exceeding 100 Mt/a [91, 96]. Thus, "green" methanol can potentially contribute to defossilization within various sectors of the economy [78, 91].

Biogas-based methanol production (biogas-to-methanol; BGtM) takes place through syngas production and subsequent conversion into methanol. Depending on the biogas composition and the reforming process, the syngas produced has a greater or lesser hydrogen (H_2) deficit compared to the stoichiometric ratio required for methanol synthesis. Conventionally, this deficit can be balanced by CO_2 separation, possibly involving an additional water–gas shift (WGS) reaction. However, this is associated with significant carbon losses and an increased relative biogas demand. A novel approach to compensate for the hydrogen deficit and, thus, to maximize carbon utilization is depicted in Figure 3-2 and involves the addition of "green" H_2 produced from "renewable" electricity.[2] The power-

[2] Refers in this work always to electricity generated from renewable sources of energy.

based H_2 production converts electrical energy into chemical energy via water-electrolysis and is predominantly discussed under the general term “power-to-x” (PtX). The combined overall concept (power- and biogas-to-methanol; PBGtM) enables the complete utilization of the biogas carbon potential, consequently reducing the specific biogas demand for methanol production and potentially realizing higher production capacities based on the available biogas quantity.

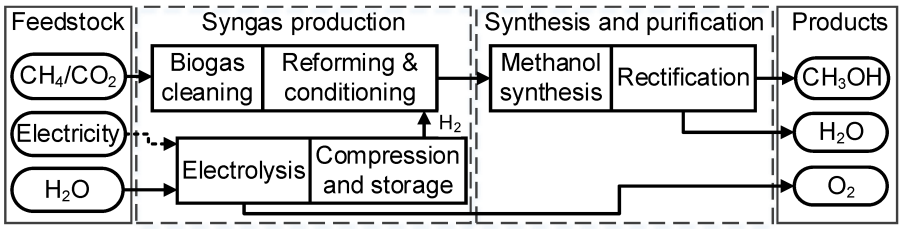

Figure 3-2: Power- and biogas-to-methanol concept.

Concerning the operation of the plant, it has to be taken into account that the availability of renewable electricity used for H_2 generation is often volatile due to the characteristics of renewable energy sources like wind power and solar radiation. In contrast, biogas production is a (more or less) stationary process. Additionally, reforming favors steady-state operation due to high temperatures and heat transfer requirements, even when advanced synthesis concepts allow for dynamic methanol syntheses downstream. Thus, to operate such a PBGtM concept, sufficient storage options are required to smooth volatile electricity and/or H_2 generation and to enable a constant H_2 supply.

In recent years, various studies have been carried out on the synthesis-based conversion of biogas-like gases into higher-value products like methanol. Since dry reforming only allows stoichiometrically complete reforming when the biogas composition is equimolar ($CH_4/CO_2 = 1$) and encounters issues with coke formation, current investigations primarily explore concepts involving additional oxidation agents for reforming (i.e., H_2O for bi-reforming or H_2O and O_2 for tri-reforming). Respective techno-economic analyses for bi-reforming-based methanol production from biogas and similar mixtures are available, focusing mainly on the reforming parameters and achievable syngas compositions (e.g., Entesari and Goeppert [97], Acquarola et al. [98, 99] and Chein et al. [100]). Tri-reforming of biogas for synthesis product generation has been investigated, also focusing mainly on syngas production (e.g., Hernández and Martín [101], Chein and Hsu [102], Farsi and Lari [103], Zhang et al. [104]). Regarding hybrid methanol production, Lim et al. [105] projected methanol production costs from natural gas and CO_2 via tri-reforming in the range of 500 to 850 €/t, considering different electrolysis processes for H_2 production. Techno-economic and environmental assessments have also been carried out for methanol production from landfill gas via dry and bi-reforming (Choe et al. [106]). Additionally, Moioli and Schildhauer [107] compared different methanol production concepts from biogas, showing that the additional utilization of H_2 potentially enables higher carbon utilization and, therefore, higher productivity. However, a detailed comparison of the mainly dis-

cussed reforming technologies within the overall production concept for the carbon-maximized biogas conversion to methanol is missing. Therefore, further investigations are necessary to assess the overall concept of hybrid methanol production from biogas regarding the available reforming technologies and the influence of decisive process and framework parameters.

Against this background, this research paper aims to conduct an in-depth techno-economic assessment of carbon-maximized methanol production from biogas and renewable electricity within a novel decentralized production concept. Two process configurations relying on different reforming technologies are designed and compared to assess the hybrid methanol production concept and evaluate the advantages and disadvantages of the considered reforming technologies within the overall concept. The influence of decisive operating parameters and technical and economic framework conditions are obtained as further novel results. For this purpose, both configurations are modeled using steady-state process simulations. Carbon and energy flow diagrams visualize the simulation results to indicate losses and accumulations. Furthermore, techno-economic key figures are derived and assessed under parameter variation.

Annex A provides technical information on the considered process steps and further detailed information about process modeling data, analysis, and results.

3.2 Methodology

The techno-economic analysis of the previously outlined PBGtM concept is conducted based on process modeling results. Within the scope of the analysis, two process configurations, relying on either bi-reforming or tri-reforming (Section 3.3.1), are compared. Figure 3-3 presents the applied overall assessment approach. The respective tools and methodologies used are described below.

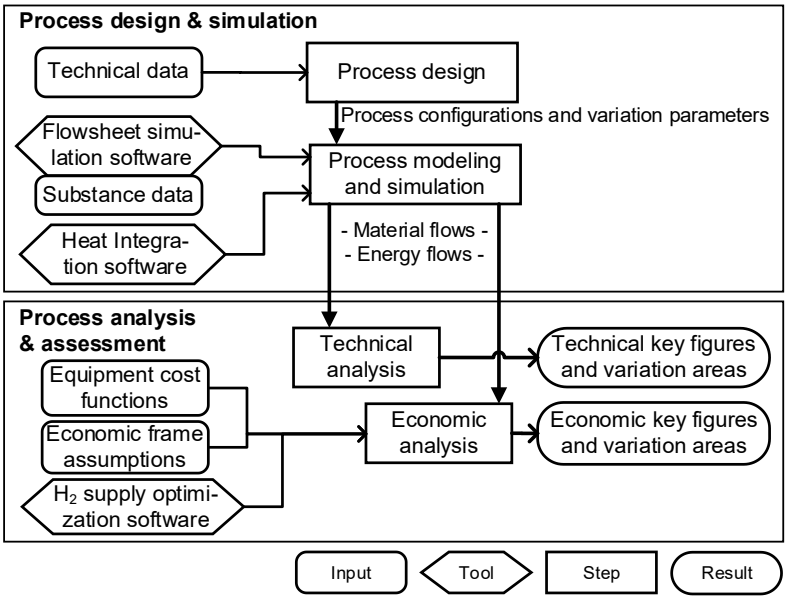

Figure 3-3: Assessment approach of the techno-economic analysis.

3.2.1 Process design and simulation

The design and the simulation of the process configurations form the basis of the analysis and the assessment.

3.2.1.1 Process design

Two process configurations are designed according to the general concept of PBGtM, differing regarding the reforming technologies considered: the bi-reforming (BiRef) and tri-reforming (TriRef) of biogas. Preferably, only technically mature technologies or at least technologies that have been extensively investigated and for which sufficient literature data are available are selected. Parameters for which a significant influence on the overall processes can be expected and/or for which literature shows large value ranges are identified and varied within the simulation (parameter variation). Due to the stationary operating characteristics of biogas plants and the limited dynamics of the biogas reforming step, hydrogen production is designed for a constant supply [108].

3.2.1.2 Process modeling and simulation

A steady-state flowsheet simulation is used to determine the mass and energy flows in the analyzed processes. The commercial simulation software Aspen Plus® is used to determine the occurring material and energy streams. Details about the included methodology, simulation structure, and software databases are provided by [109]. The respective process blocks are interconnected through material, heat, or power streams. Simulation results are used to make iterative adjustments to the process design, optimizing the overall process within the expected technical limitations. No internal integration of heat streams is assumed at this stage. Minimal external heating and cooling requirements are determined via a pinch analysis using the Aspen Energy Analyzer®.

3.2.2 Process analysis and assessment

For both process configurations, a reference case (RC) as well as various technical and economic parameter variations (PV) are analyzed. The ranges of parameter variation are determined based on literature and simulation data to assess the extent of potential deviations from the reference case. The analysis includes the technical and economic key figures described in the following.

3.2.2.1 Technical analysis

The derived mass and energy balances are visualized for the technical analysis regarding carbon and energy flows, enabling a comprehensive understanding of the overall process schemes. The technical key figures carbon and energy efficiency are defined according to Eq. 3-1 and Eq. 3-2.

Carbon efficiency (η_{C}) describes the amount of carbon bound in the target product ($\dot{C}_{\mathrm{Product}}$) compared to the amount of carbon contained within the feedstock ($\dot{C}_{\mathrm{Feed}}$) by considering the respective carbon flows. Since methanol is the only carbon-containing product within the investigated concept, carbon efficiency directly correlates with the methanol production rate.

$$\eta_{\mathrm{C,Product}} = \frac{\dot{C}_{\mathrm{Product}}}{\dot{C}_{\mathrm{Feed}}} \qquad \text{Eq. 3-1}$$

Energy efficiency ($\eta_{\mathrm{e,Product}}$) is used to assess the process configurations regarding their overall energy demands. The chemical energy of the product is related to the energetic effort of production, considering the chemical energy of the feedstock plus the demand for electrical energy (P_{el}) and thermal process energy ($\dot{Q}_{\mathrm{th}}$). Chemical energy is calculated by multiplying the mass flow of the respective product ($\dot{m}_{\mathrm{Product}}$) or feed ($\dot{m}_{\mathrm{Feed}}$) with the respective higher heating value (HHV).

$$\eta_{\mathrm{e,Product}} = \frac{\dot{m}_{\mathrm{Product}}\,\mathrm{HHV}_{\mathrm{Product}}}{\dot{m}_{\mathrm{Feed}}\,\mathrm{HHV}_{\mathrm{Feed}} + P_{\mathrm{el}} + \dot{Q}_{\mathrm{th}}} \qquad \text{Eq. 3-2}$$

3.2.2.2 Economic analysis

The primary objective of the economic analysis is to derive and compare methanol production cost (*MPC*) from the analyzed process configurations under defined economic framework conditions. The *MPC*s represent the minimum required selling prices to achieve economic feasibility in methanol production. The costs are calculated according to Eq. 3-3 for a market-mature process (n$^{\mathrm{th}}$-of-a-kind plant) built on a green field. The *MPCs* consist of the annual capital costs (*ACC*), the fixed operational expenditures ($OPEX_{\mathrm{f}}$) and the variable operational expenditures ($OPEX_{\mathrm{v}}$). The latter represent the feedstock and energy costs, while the fixed operational expenditures are independent of the product amount (e.g., labor, taxes, overheads, maintenance). The overall annual costs are related to the annual production given by the hourly nominal production ($\dot{m}_{\mathrm{Product}}$) and annual full load hours (*AFLH*) of the plant.

$$MPC = \frac{ACC + OPEX_{\mathrm{f}} + OPEX_{\mathrm{v}}}{\dot{m}_{\mathrm{Product}}\,AFLH} \qquad \text{Eq. 3-3}$$

The annuity method (Eq. 3-4) is used to determine the annual capital cost (*ACC*). The capital required for the construction of the plant (fixed capital investment; *FCI*) is depreciated over the depreciation period (n), taking into account the real weighted average cost of capital (*WACC*, i) and the working capital share (ω).

$$ACC = FCI\,\frac{i\,(1+i)^n}{(1+i)^n - 1} + FCI\,\omega\,i \qquad \text{Eq. 3-4}$$

The *FCI* is derived using the module costing technique, which is generally accepted as an approach for preliminary cost estimates [110]. This estimate is based on the major process equipment, which is roughly dimensioned based on the process design and simulation. This cost calculation method can be classified as a study estimate[3] with an expected accuracy range of -30 to +50 % [111]. Detailed calculation principles and assumptions are described in Annex A.

Since constant hydrogen supply from volatile energy sources requires dimensioning based inter alia on representative renewable energy production profiles, hydrogen supply costs are derived using hydrogen supply optimization methodology [108], aiming to minimize the hydrogen supply cost by scaling the individual process steps. Hydrogen costs are considered as $OPEX_{\mathrm{v}}$ and derived for a production in Germany.

3.3 Process configurations

The following describes the designed PBGtM process configurations (BiRef and TriRef) and the assumed data and framework conditions.

3.3.1 Process description

The two considered process configurations are listed in Table 3-1.

- BiRef. Combining steam reforming and dry reforming (CSDR), the bi-reforming process appears to be significantly advantageous over dry reforming, particularly concerning coke formation and product composition [63]. Instead of a fired reactor system, conventionally used for endothermic reforming processes, an electrically heated reformer is considered to avoid carbon losses related to the combustion of biogas[4] and offers the advantage of directly and very efficiently harnessing renewable electricity for chemical processes [112, 113]; such electrical heated reforming reactors have already been successfully demonstrated [114, 115].

- TriRef. The tri-reforming process is a variation of the bi-reforming process, whereby pure O_2 is fed into the reforming reaction chamber to provide the required heat through concurrently occurring exothermic oxidation. This approach eliminates the need for external energy input or removal (autothermal operation). Autothermal reforming is already commercially employed in the production of syngas from methane [57, 116]. Within the TriRef configuration, sufficient O_2 is available from water-electrolysis.

[3] Also known as Major Equipment Estimate; Estimation Class 4 according to AACE Recommended Practice No. 17R-97.

[4] In-house simulations have shown carbon losses of about 25 % when biogas is used for heating.

Table 3-1: Process configurations considered.

Configuration abbreviation	Reforming technology	Heat provision
BiRef	Bi-reforming	Electrical heated
TriRef	Tri-reforming	Autothermal

The process flowsheet depicted in Figure 3-4 applies to both configurations. Biogas is first purified in an adsorber bed filled with doped activated carbon without pressure or temperature adjustments[5]. Then, the cleaned biogas is compressed and mixed with steam (bi-reforming) or steam and oxygen (tri-reforming), depending on the respective process configuration; the reactant composition can be described with the ratio given by Eq. 3-5. Afterward, the gas mixture is pre-heated and fed to the reforming reactor. The reformer product is then cooled down to condense the contained water. The remaining gas mixture (raw syngas) is compressed, mixed with light gases from the purification process (predominantly CO_2), and conditioned with pure hydrogen. The hydrogen can be supplied directly from the electrolyzer or the intermediate hydrogen storage tank. The stoichiometric number (*SN*, Eq. 3-6) and the carbon oxide ratio (*COR*, Eq. 3-7) characterize the syngas composition according to its molar composition.

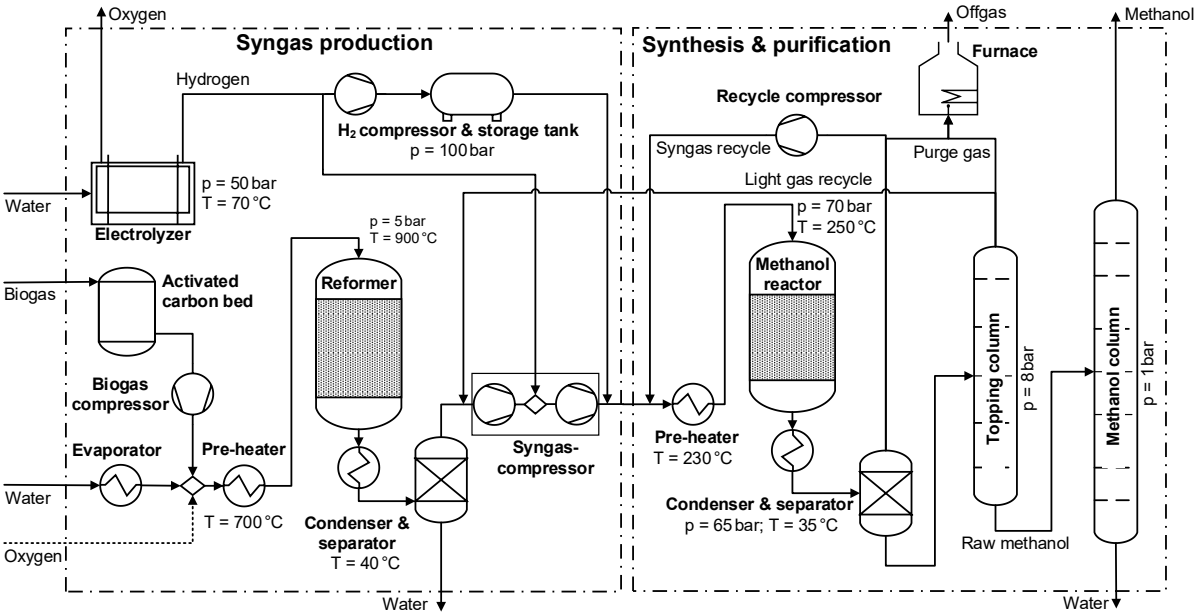

Figure 3-4: PBGtM process flowsheet with main operating conditions (dotted line only in case of tri-reforming).

$$OxyN = \frac{[CO_2] + [H_2O]}{[CH_4]} \qquad \text{Eq. 3-5}$$

$$SN = \frac{[H_2] - [CO_2]}{[CO] + [CO_2]} \qquad \text{Eq. 3-6}$$

[5] Since the activated carbon filter has no relevant influence on the mass and energy flows of the overall process, it is not included in the modeling.

$$COR = \frac{[CO_2]}{[CO] + [CO_2]} \quad \text{Eq. 3-7}$$

[x] Molar fraction of the respective component (x).

The conditioned syngas is pre-heated and fed to the methanol reactor in the synthesis and purification section. The reactor output is cooled down to condensate methanol and water, separated from the remaining gas stream. The remaining gas phase, consisting mainly of unreacted syngas components and inert gases, is recycled to the reactor. A proportion of the recycle gas is purged to avoid an uncontrolled accumulation of inert gases and light by-products. The methanol-water mixture contains small amounts of dissolved gases and heavier by-products and is purified in a two-stage column system. The first column (topping column) mainly separates light components via the column head. Afterward, the second column (methanol column) separates water and heavier components via the column bottom, allowing pure methanol to be recovered as the top product.

3.3.2 Data and assumptions

Below, data and assumptions needed for the modeling and techno-economic assessment are outlined. Annex A provides further data and descriptions.

3.3.2.1 Technical data

The main data used to model the technical processes are listed in Table 3-2. The CH_4/CO_2-ratio, the inert gas fraction (IGF), and the water content define the biogas composition. Since the composition of biogas can vary significantly, the inert gas fraction and the CH_4/CO_2 ratio are considered in the parameter variation. Electrolysis is assumed stoichiometrically, with electrical and thermal flows derived from the assumed electrical efficiency of the electrolyzer. Due to the high operating temperatures of the reforming processes, equilibrium composition is assumed at the reactor outlets. The oxidation number is set to 1.5 (Eq. 3-5) to ensure an excess of oxidants and to prevent coking. The influence of the reforming temperature is analyzed within parameter variation. Syngas conditioning is controlled via design specifications, adjusting the stochiometric number (*SN*, Eq. 3-6) at the reactor entry to 2.05 and the inert gas fraction of the syngas to 20 %. The latter is also considered within parameter variation.

The methanol synthesis is modeled with a temperature approach considering the three main reactions; i.e., the conversion rate depends on the chemical equilibrium, whereby the respective temperature difference gives the offset from the equilibrium. The formation of by-products correlates linearly with the amount of methanol produced. Downstream separation is designed to enable methanol purity according to the quality of methanol grade AA.

Table 3-2: Technical modeling data (LHV: Lower heating value, PV: Parameter variation, RC: Reference case).

Stream/ Process	Parameter		Value	Reference
Biogas	Composition	CH_4/CO_2-ratio	RC: 1.5 | PV:1–3	[117–119]
		N_2 [vol%$_{Dry}$]	RC: 2 | PV 0–5	[117, 118]
		Dew point [°C]	10	[117]
Electrolysis	Conversion	$H_2O \rightarrow H_2 + 0.5\ O_2$	1	[-]
	Energy demand	Electrical efficiency [%$_{LHV, H2}$]	67	[65]
Reforming	Operating conditions	T [°C]	RC: 900 | PV: 800–1,000	[62, 119]
		p [bar]	5	[62]
	Condition	*OxyN* (Eq. 3-5)	1.5	[62]
	Equilibrium conversion	Products considered: CO, CO_2, H_2O, H_2, CH_4, O_2, N_2		[63, 83]
Methanol synthesis	Operating conditions	T [°C]	250	[86, 120, 121]
		p | Δp [bar]	75 | −5	[86, 92]
		Inert gas share	RC: 0.20 | PV: 0.02–0.50	[-]
	Equilibrium conversion with temperature approach [K]	$CO + 2\ H_2 \leftrightharpoons CH_3OH$	15	[120]
		$CO_2 + 3\ H_2 \leftrightharpoons CH_3OH + H_2O$	15	[120]
		$CO + H_2O \leftrightharpoons CO_2 + H_2$	15	[120]
Methanol	Share in final product	CH_3OH [wt%]	99.85	[95]

3.3.2.2 Economic data

In addition to technical parameters directly influencing the relative mass and energy balances, other technical parameters predominantly affect economic figures and do not change technical results. Furthermore, various economic assumptions can significantly impact economic key figures. The respective values and framework assumptions are listed in Table 3-3. The costs are given in euro currency and adjusted according to the chemical plant cost index (CEPCI) for 2022.

Technical parameter. The installed nominal capacity of the PBGtM plant is, from a technical perspective, limited by the availability of biogas at the plant site. The nominal capacity of the production facility typically does not affect the carbon and energy efficiency[6]. Still, it does influence the specific plant costs (economies of scale) and, consequently, the methanol production costs (*MPCs*). In the reference case, the plant size is designed for an available biogas quantity of 670 Nm^3/h, corresponding to a medium- to large-scale biogas plant. The influence of the plant size on the production costs is analyzed as part of economic parameter variation, where the plant size is varied using a scale factor concerning

[6] Assuming the process concept, including process integration, remains unchanged, and the equipment is adapted to the respective performance classes. In very small-scale plants, the influence of heat losses can lead to reduced efficiencies.

the reference case (scale factor 1). The annual plant's full load hours (*AFLH*) determine the annual production quantity at a given plant capacity, thus impacting the production costs. The annual full load hours are dependent not only on market-related factors but also on the technical availability of the biogas plant and the PBGtM plant itself. In the reference case, ca. 7,500 h/a (full load) are assumed (plant utilization of 85 %), constrained by the typical annual full load hours of biogas plants [122].

Economic parameter. The fixed capital investment (*FCI*) depreciation period is assumed to align with the plant's operating life. Uncertainties associated with estimating plant costs are assessed through the variation of annual capital costs (*ACC*) within the expected uncertainty range. The specific costs for biogas are determined based on the literature. Biogas production costs vary significantly depending on the utilized substrate and the plant capacity. The value provided in the reference case is at the lower end of the range, with higher values arising, especially for small-scale plants and potentially more complex substrates (e.g., straw). The biogas costs are currently predominantly assessed based on the energy content [€$_{2022}$/MWh$_{LHV}$], with no value attributed to the contained CO_2. The costs for continuously available electricity are estimated based on the European average price (2008 to 2020) for non-household electricity contracts. This value is in the same cost range as constant electricity supply costs from renewable power in the EU derived by [123]. Hydrogen supply costs are determined using an optimization model [108] by considering the 3rd. Quartile of the German onsite hydrogen supply cost for 2022 (see Annex A, A.4 for extended results).

Table 3-3: Economic data and assumptions (*ACC*: Annual capital cost, *AFLH*: Annual full load hours, PV: Parameter variation, RC: Reference case, *WACC*: Weighted average cost of capital).

Process	Parameter	Unit	Value	Reference
Plant related	Biogas capacity | Scale factor	[Nm^3/h] | [-]	RC: 670 | PV: 0.1–100	[-]
	AFLH	[h/a]	RC: 7,500 | PV: 6,500–8,760	[122]
Capital related	*WACC* (*i*)	[%]	RC: 6 | PV: 0–12	[108]
	Depreciation period (*n*)	[a]	20	[124, 125]
	ACC uncertainty (Factor)	[-]	0.7–1.5	[111]
Costs	Biogas	[€$_{2022}$/MWh$_{LHV}$]	RC: 72 | PV: 45–185	[126, 127]
	Electricity	[€$_{2022}$/MWh]	RC: 130 | PV: 90–230	[123, 128]
	Hydrogen	[€$_{2022}$/kg]	RC: 7.0 | PV: 5.0–9.0	Annex A, A.4

3.4 Technical results

Firstly, the process configurations are analyzed regarding the occurring carbon and energy flows in the reference case. Secondly, the influence of selected parameters on the technical key figures is shown. Lastly, the results are assessed and compared to non-hybrid production concepts regarding carbon utilization.

3.4.1 Process flow analysis

The process simulation results are used to visualize and evaluate the process configurations' relative carbon and energy flows under the reference case assumptions.

3.4.1.1 Carbon flows

The carbon flows are depicted relative to the overall carbon input stream. Stoichiometrically, the carbon input can be bound entirely within the methanol product (carbon efficiency of 100 %) since the formation reactions do not include carbon-containing by-products. However, since conversions and separation processes are usually non-ideal, accumulations and losses occur, which are visualized in the flow diagrams. Hydrogen production is not depicted in the visualization since no carbon is involved.

BiRef. Figure 3-5 shows the carbon flows of the BiRef configuration. Here, biogas is the only carbon-containing input. No relevant carbon losses occur during biogas conversion into syngas within bi-reforming and conditioning. However, as methane is not fully converted in the reforming process, methane is carried into the methanol synthesis as an inert gas in addition to nitrogen. Due to the equilibrium-limited syngas conversion in the methanol synthesis, which requires significant syngas recycling, carbon accumulation occurs within the synthesis loop.

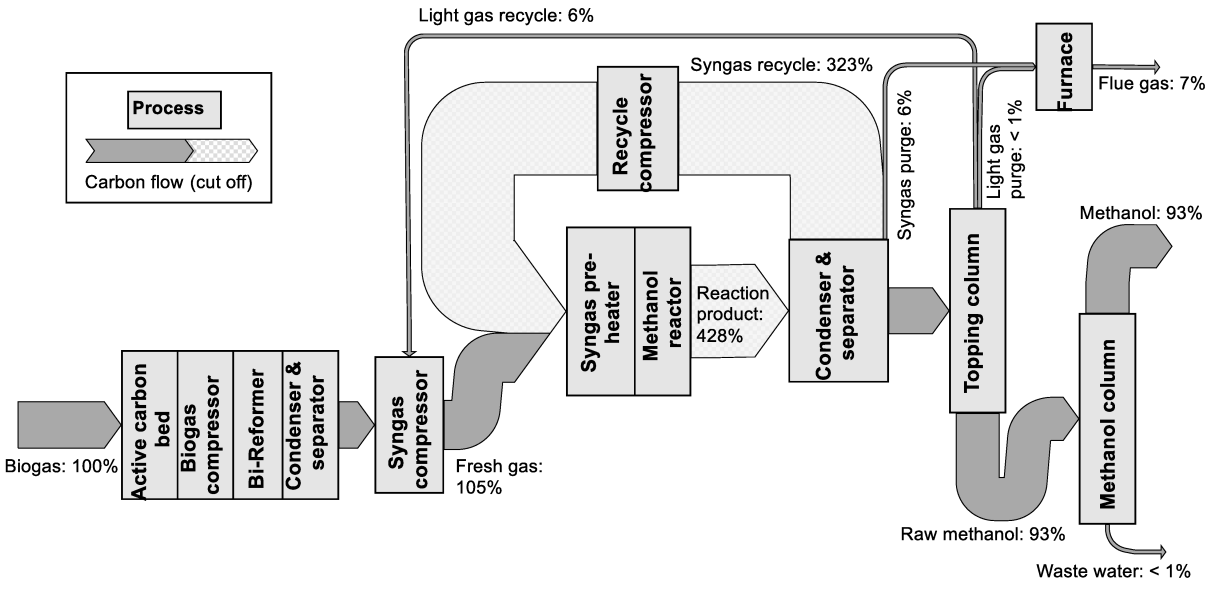

Figure 3-5: Relative carbon flows of the bi-reforming configuration (BiRef).

Here, carbon losses occur through purge gas release, which is required to avoid excessive inert gas accumulation. Methane represents more than 55 % of the inert components within the purge gas, resulting in purge-related carbon losses of 6 %.

The liquid synthesis product still includes 99 % of the utilized carbon when it's fed into the topping column. After separating dissolved gases (mainly CO_2), the raw methanol contains 93 % of the overall carbon input. Within the methanol column, methanol is sharply separated through multistage rectification; no further carbon losses occur at this stage.

The resulting overall carbon efficiency is 93 %, with the remaining carbon (7 %) released as flue gas. The assumed biogas input of 670 Nm^3/h enables a methanol production of 860 kg/h. The specific biogas demand is, therefore, 0.78 Nm^3_{BG}/kg_{MeOH}.

TriRef. Figure 3-6 shows the carbon flows of the TriRef configuration. As in the BiRef configuration, no carbon losses occur during biogas conversion to syngas. However, gas composition at the reformer outlet differs significantly due to the additional oxygen injection into the autothermal reformer (Table 3-4). The higher carbon oxide ratio (Eq. 3-3) results in a lower per-pass conversion within the methanol reactor. Nevertheless, the carbon flow of syngas recycling is only slightly higher as in the BiRef configuration due to the significantly lower methane share of the inert gases (< 15 %). Considering also carbon-free components, the volume flow of syngas in the TriRef configuration is 40 % higher than in the BiRef configuration. Since less inert gas is present in the fresh syngas, the carbon losses related to purge gas only account for 3 % of the utilized carbon, leading to an overall carbon efficiency of 97 % (i.e., 4 %pt more than the BiRef configuration). In the reference case, a 900 kg/h methanol production capacity is reached based on a 670 Nm^3/h biogas feed, corresponding to a specific biogas demand of 0.74 Nm^3_{BG}/kg_{MeOH}.

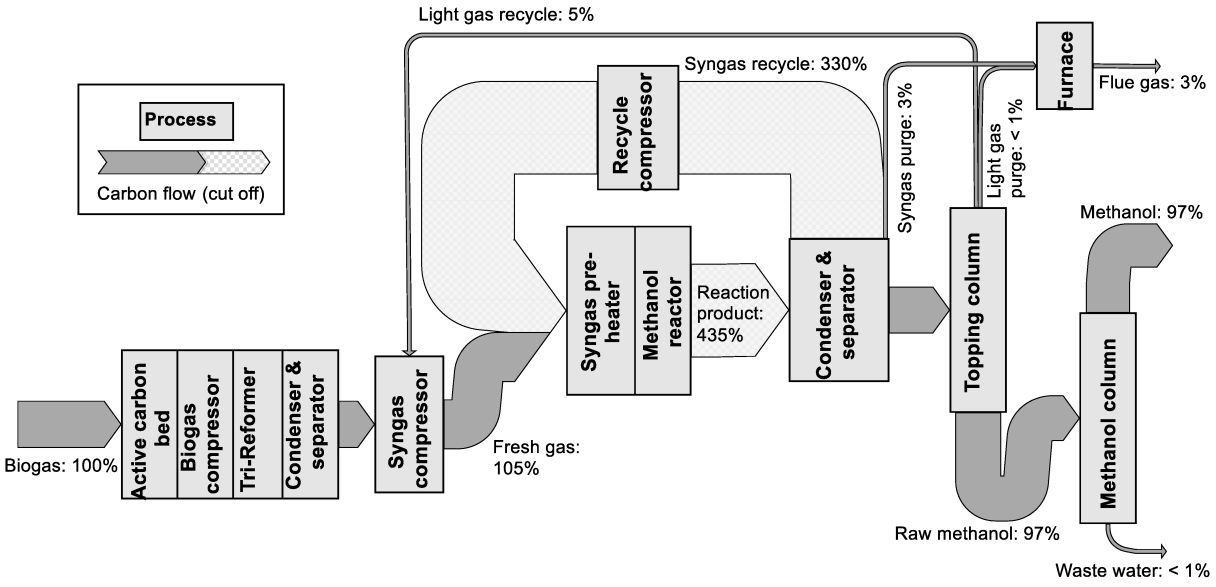

Figure 3-6: Relative carbon flows of the tri-reforming configuration (TriRef).

Table 3-4: Gas properties of both process configurations (*COR*: Carbon oxide ratio, *SN*: Stoichiometric number, IGF: Inert gas fraction).

	BiRef configuration		TriRef configuration	
Parameter	**Reformer product**	**Reactor feed**	**Reformer product**	**Reactor feed**
SN (Eq. 3-2)	1.36	2.05	0.75	2.05
COR (Eq. 3-3)	0.11	0.42	0.32	0.62
IGF [%]	2	20	1	20

3.4.1.2 Energy flows

The process energy flows are normalized to the total energy input of the overall process to analyze and assess the major energy demands and losses of the process configurations. Thereby, chemical energy (related to the higher heating value; HHV), electrical energy, and thermal energy (heating and cooling demands) are considered. Annex A, Section A.3.2 lists further information regarding heat integration.

BiRef. The energy flows of the BiRef configuration are depicted in Figure 3-7, indicating that the main energy input takes place through biogas (59 %). The remaining energy is provided by electricity needed for H_2 production (25 %), heating requirements (12 %), and gas compression (4 %). Heating requirements (in the form of electrical power) are needed within the bi-reforming reactor since only a small part of the required heat can be integrated from internal heat sources (see Annex A.4). Internal heat sources like methanol synthesis can satisfy other internal heat demands.

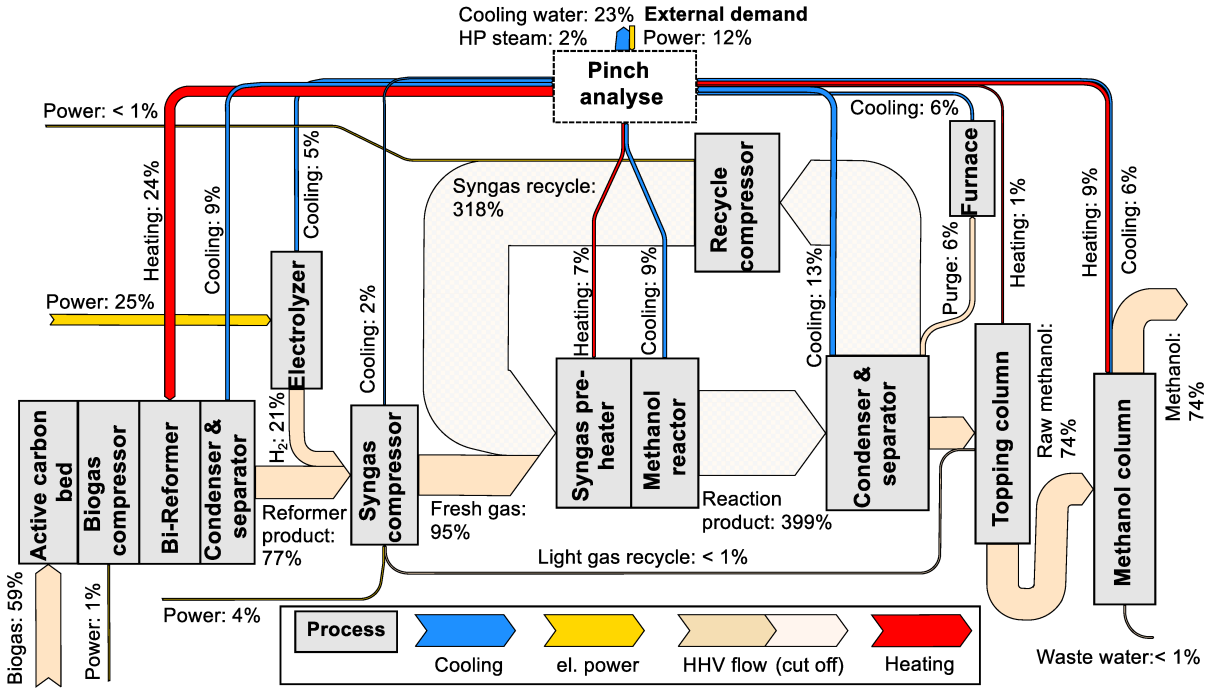

Figure 3-7: Energy flows (rounded) of the biogas bi-reforming (BiRef) configuration (heating and cooling below 1 % not depicted; el.: electrical, HHV: Higher heating value).

The overall energy efficiency is 74 %, while the remaining energy is released as waste heat, i.e., mainly via cooling water. The electricity demand of the electrolyzer under steady-state conditions is 1.8 MW_{el}, enabling a methanol output of 5.5 MW_{HHV}.

TriRef. Figure 3-8 shows the energy flows of the TriRef configuration. Here, biogas represents 52 % of the overall energy input. Like in the BiRef configuration, electrical energy provides the remaining energy. However, in the TriRef configuration, the energy required for H_2 production is almost twice as high (3.6 MW_{el}) as in the BiRef configuration. This increase is due to the lower stoichiometric number of the reforming product (Table 3-4), caused by the additional O_2 input and the associated higher CO_2 and H_2O formation. However, due to the autothermal reforming, no external heating demands exist, which partially compensates for the higher energy requirement of the electrolysis. Despite significantly larger amounts of H_2, the recycling loop's energy stream is lower than the respective stream in the BiRef configuration, as the methane contained in the BiRef configuration overcompensates for this. The overall energy efficiency results in 69 % (compared to 74 % for the BiRef configuration), while the remaining energy is released into the environment as low-temperature waste heat. The methanol production capacity in the reference case is about 5.7 MW_{HHV}.

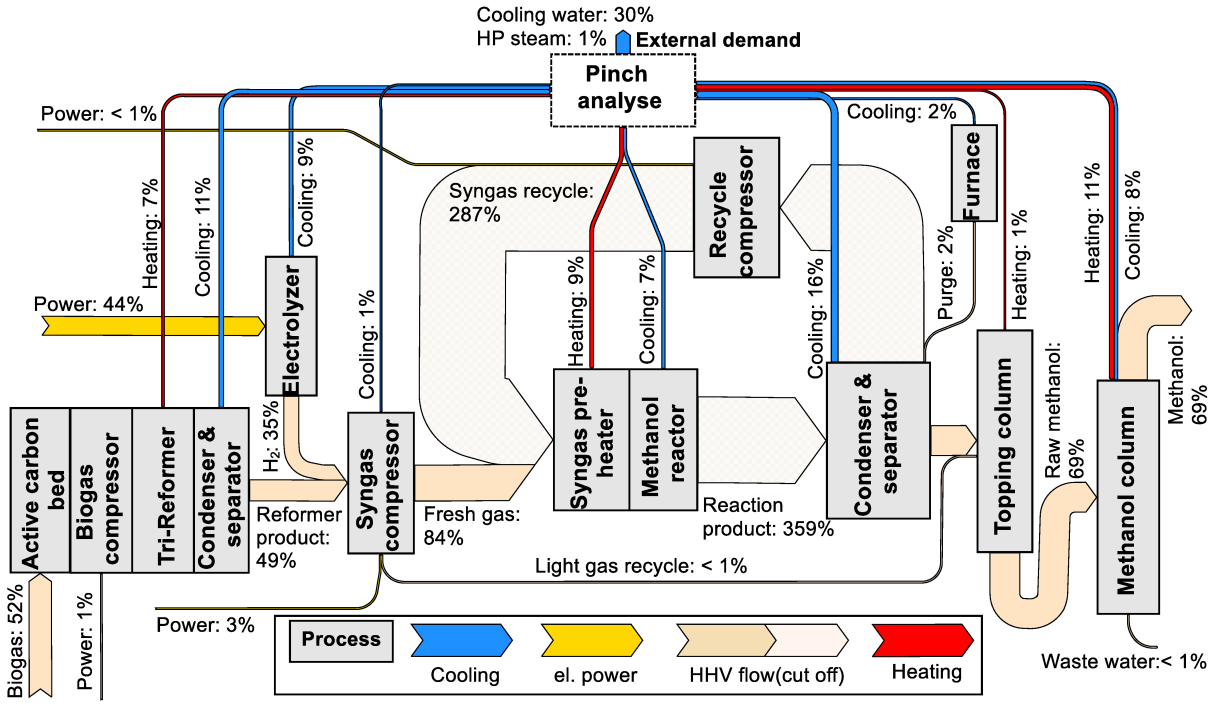

Figure 3-8: Energy flows (rounded) of the biogas tri-reforming (TriRef) configuration (heating and cooling below 1 % not depicted; el.: electrical, HHV: Higher heating value).

3.4.2 Parameter variation

This section analyzes and compares the effects of changing parameters on the technical key figures of the overall process configurations. On the one hand, this results in quantitative findings on the impact of biogas-specific properties. On the other hand, technically advantageous operating ranges and associated optimization potentials can be identified.

The analysis of the reference cases shows that the TriRef configuration has a higher carbon efficiency than the BiRef configuration at the expense of a lower energy efficiency. Therefore, parameter variation is first analyzed in terms of carbon efficiency (Figure 3-9 and Figure 3-10, left), and following regarding energy efficiency (Figure 3-9 and Figure 3-10, right). Lines that do not cover the entire parameter variation range result from physical limitations of the modeled processes, where within the specified parameter ranges, the given design specifications can no longer be met, and therefore, no solutions exist for these parameters.

3.4.2.1 Carbon efficiency

Figure 3-9 (left) shows the impact of different biogas compositions on the carbon efficiencies of the investigated process configurations. In the reference case, the inert gas fraction (IGF) (solid lines) is assumed to be 0.02, and the CH_4/CO_2 ratio (dashed lines) is 1.5.

- **Biogas – Inert gas fraction.** An increasing inert gas fraction of the utilized biogas negatively affects the carbon efficiencies for both process configurations. The BiRef configuration's carbon efficiency decreases almost linearly within the varied area from 94.6 to 90.7 %. The carbon efficiency of the TriRef configuration responds slightly stronger to an increasing inert gas fraction and decreases from 98.8 to 94.5 %.
  In both configurations, the carbon losses are caused by increasing amounts of purge gas, which is only used energetically. The slightly lower sensitivity in the BiRef configuration is due to the anyway higher amount of inert gas present through unreacted methane.

- **Biogas ratio – CH_4/CO_2.** Since a linear variation of the CH_4/CO_2 ratio leads to a non-linear change in the respective CH_4 and CO_2 fraction, these variations also affect the carbon efficiency non-linear. An increasing ratio thereby decreases the carbon efficiency. Concerning the BiRef configuration, carbon efficiency decreases from 94.1 to 91.8 % in the varied area. The TriRef configuration shows almost no response to the parameter variation and decreases only minimally from 97.3 to 96.9 %.
  Since an increasing CH_4/CO_2 ratio implies an increasing CH_4 content, CH_4 conversion becomes more important with an increasing ratio. As the CH_4 content increases, the amount of unconverted methane in the reformer product also increases, which leads to higher purge gas amounts. Since lower conversions are achieved in the BiRef configuration, the effect is stronger than in the TriRef configuration.

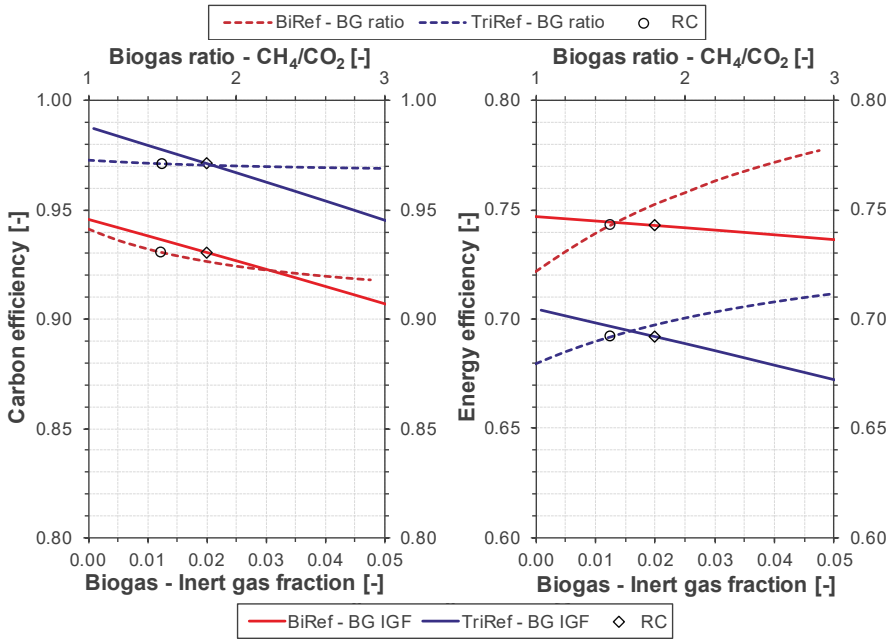

Figure 3-9: Carbon (left) and energy (right) efficiency under variation of biogas inert gas fraction and biogas ratio (BG: Biogas, BiRef: Process configuration with electrically heated bi-reforming, IGF: Inert gas fraction, RC: Reference case, TriRef: Process configuration with autothermal tri-reforming).

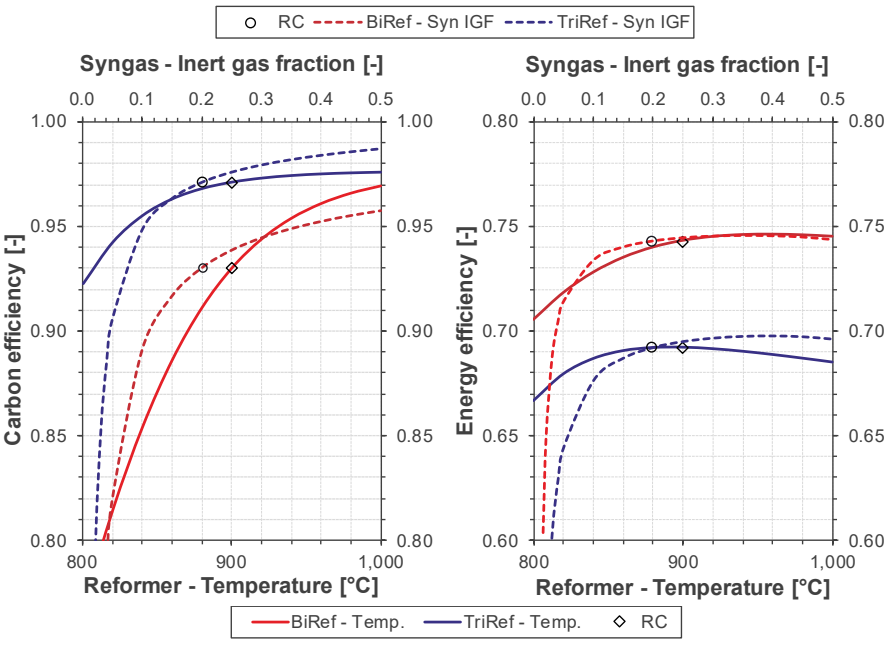

Figure 3-10: Carbon (left) and energy (right) efficiency under variation of reformer temperature and inert gas fraction in syngas (BiRef: Process configuration with electrically heated bi-reforming, RC: Reference case, Temp: Temperature, TriRef: Process configuration with autothermal tri-reforming, Syn: Syngas).

Figure 3-10 (left) shows the impact of changing process parameters on the carbon efficiencies of the investigated process configurations. In the reference case, the reformer temperature is set to 900 °C (solid lines), and the inert gas share in the reactor feed (dashed lines) is adjusted to 0.2.

- **Reformer – Temperature.** An increasing reformer temperature leads to a strongly non-linear increase in carbon efficiency. Especially in the lower temperature region analyzed, a rapid decrease of the key figure occurs. The carbon efficiency of the BiRef concept decreases sharply with reformer temperatures below 900 °C (93.0 to 76.8 %). Above 900 °C, the impact of increasing temperature decreases while carbon efficiency continues to grow (93.0 to 97.0 %). The curve of the TriRef configuration is similar but not quite as steep, and the shallow run-out begins at lower temperatures of about 820 °C. Carbon efficiency increases from 92.2 % to 97.6 % in the varied range.
  The reforming temperature decisively determines the chemical equilibrium of the reforming reactions. Since high temperatures shift the equilibrium towards syngas formation, CH_4 conversion increases with increasing temperature, meaning less CH_4 enters the synthesis loop, and thus, less purge gas has to be purged. The significantly stronger influence on the BiRef configuration results from the lower oxidant amount compared to the TriRef configuration. Here, in addition to water and CO_2, O_2 is present as a very active oxidant, resulting in higher methane conversions even at lower temperatures.

- **Syngas – Inert gas fraction.** The inert gas fraction in the reactor feed results from the inert gas contained in the fresh gas concentrating with increasing recycling of unreacted syngas. The removal of purge gas controls the inert gas fraction (IGF). Thus, the curves resulting from the variation of the permitted inert gas fraction show an increase in carbon efficiency with increasing inert gas fraction. The curves are divided into an almost vertical part (IGF < 0.1) and a more horizontal part (IGF > 0.2). Starting from the reference case fraction (IGF = 0.2), the carbon efficiency drops steeply with decreasing permitted inert gas fraction. In both configurations, the carbon efficiency trends against the per-pass conversion when the inert gas fraction approaches the fresh gas inert gas fraction. In the area right of the reference case value, the carbon efficiency of the BiRef configuration increases up to 95.8 %. In the TriRef configuration, carbon efficiency increases up to 98.7 %.
  In both configurations, the losses once again stem from purge gas. With increasing inert gas fraction in the synthesis loop, more inert components and fewer reactants are purged out within the same amount of purge gas. Again, the higher conversion enabled by tri-reforming shows advantages in the investigated area.

3.4.2.2 Energy efficiency

Biogas properties and process parameters positively affecting carbon efficiency can lead to higher energetic efforts, which can exceed the energy benefit of higher production outputs. Below, the influence of parameter variation on energy efficiency is therefore analyzed in more detail. Figure 3-9 (right) shows the impact of different biogas compositions on energy efficiency.

- **Biogas – Inert gas fraction.** The energy efficiency under variation of the biogas inert gas fraction (solid lines) shows a similar, almost linear trend as the carbon efficiency in the analyzed range. In both configurations, efficiency decreases with an increasing inert gas fraction. However, regarding the BiRef configuration, the slope is clearly lower compared to the carbon efficiency analysis. The energy efficiency decreases only slightly from 74.7 to 73.7 %. The TriRef configurations' energy efficiency responds stronger to an increasing biogas inert gas fraction, similar to the carbon efficiency, decreasing from 70.4 to 67.2 %.
  The changes in energy efficiency result mainly from changes in methanol production (carbon efficiency). However, in the BiRef configuration, the increasing purge gas also increases the high-temperature heat utilized for bi-reforming. This additional heat reduces the electrical power demand and partly counteracts energy losses. Autothermal tri-reforming demands no external heating. Therefore, the heat of purge gas combustion can only be used if external heat sinks are available at the production site, which is not assumed within the analyzed configurations.

- **Biogas ratio – CH_4/CO_2.** The variation of the biogas ratio (dashed lines) shows that high ratios positively affect the energy efficiency of the configurations. Despite decreasing carbon efficiency, energy efficiency significantly increases in both configurations. In the case of the BiRef configuration, the energy efficiency rises from 72.2 to 77.7 %. The increase for the TriRef configuration is slightly lower, increasing from 68.0 to 71.1 %.
  The variations in energy efficiency are primarily driven by the decreasing H_2 demand with increasing CH_4 content in the biogas, reducing the amount of electrical energy for the electrolysis. In comparison to biogas-based H_2 production (via reforming), this process is associated with higher losses. However, the additional O_2 input in tri-reforming requires additional H_2, even at high CH_4/CO_2 ratios. For the BiRef configuration, the external H_2 demand approaches zero for ratios close to three.

The influences of the process parameters reforming temperature (solid lines) and syngas inert gas fraction (dashed lines) on the overall energy efficiencies for both configurations are depicted in Figure 3-10 (right).

- **Reformer – Temperature.** The energy efficiency of both process configurations exhibits an initially increasing trend as the reforming temperature increases, followed by a slight decrease after reaching a maximum. In the case of the BiRef configuration, the maximum is located at 960 °C and reaches 74.6 %. With a further temperature increase to 1,000 °C, the efficiency decreases slightly by 0.1 %. For the TriRef configuration, the maximum is reached at 900 °C with 69.2 %. Subsequently, the efficiency decreases by up to 0.7 % at 1,000 °C. In the range left of the maximum, the efficiencies of the BiRef and TriRef configuration drop to 70.5 and 66.7 %, respectively.
  From a process level perspective, the trend in both curves results from, on the one

hand, the increasing methanol yield (carbon efficiency) with rising reforming temperature and, on the other hand, the counteracting increase in energy demand for reforming. As the positive impact of higher reforming temperatures on the methanol output decreases, particularly in the TriRef configuration, the increasing energy demand predominates, leading to a decrease in energy efficiency beyond the maximum.
In the case of bi-reforming, the additional energy demand is provided through electrical heating with an efficiency of 100 %. In the case of tri-reforming, the increase in temperature is achieved by increasing the oxygen input, which in turn raises the H_2 demand. However, H_2 production involves losses due to the electrolyzer efficiency of approximately 79 %$_{HHV}$.

- **Syngas – Inert gas fraction.** The trend of the energy efficiency curves fundamentally exhibits similarities to those of carbon efficiency. However, the curves attain a maximum within high inert gas fractions before falling slightly again. In the varied area of permitted syngas inert gas fractions, the BiRef configurations' energy efficiency increases from 64.9 % at 2 %$_{IGF}$ to 74.6 % at 35 %$_{IGF}$, which decreases then to 74.4 % at 50 %$_{IGF}$. The TriRef configurations' energy efficiency increases from 55.3 % at 2 %$_{IGF}$ to 69.7 % at 40 %$_{IGF}$. The efficiency then decreases slightly to 69.6 % at 50 %$_{IGF}$.
In both configurations, efficiency gains driven by increasing methanol production predominate up to the maximum. Furthermore, due to the slightly over-stoichiometrically operated syngas, fresh gas H_2 demand and the associated electrolysis power decrease with increasing recirculation. However, beyond the maximum, the exponentially increasing quantity of recycling gas and the consequent electrical energy demand of the recycling compressor outweigh the benefits.

3.4.3 Assessment

The following summarizes and assesses the technical results (Figure 3-11). The reference analysis (red and blue horizontal lines) shows differences in carbon and energy efficiency between the BiRef and the TriRef configuration. The advantage of the TriRef configuration in terms of carbon efficiency and the associated lower biogas demand result from the higher methane conversion in the reforming process caused by the addition of oxygen. However, this is accompanied by an increase in hydrogen demand. Since converting electricity into heat (Bi-Reformer) is more efficient than converting electricity into hydrogen (electrolysis), the BiRef configuration enables a higher energy efficiency despite the lower methanol output.

The composition of the biogas can vary significantly depending on the substrate used and the operating conditions of the biogas plant. The influences on the efficiency of the PBGtM concept determined in the parameter variation are assessed as moderate. A low N_2 content in the biogas is generally favorable and increases carbon and energy efficiency. A high methane content in the biogas reduces the electrolysis demand and thus increases the

overall energy efficiency, while the carbon efficiency is mainly unaffected, especially when using tri-reforming.

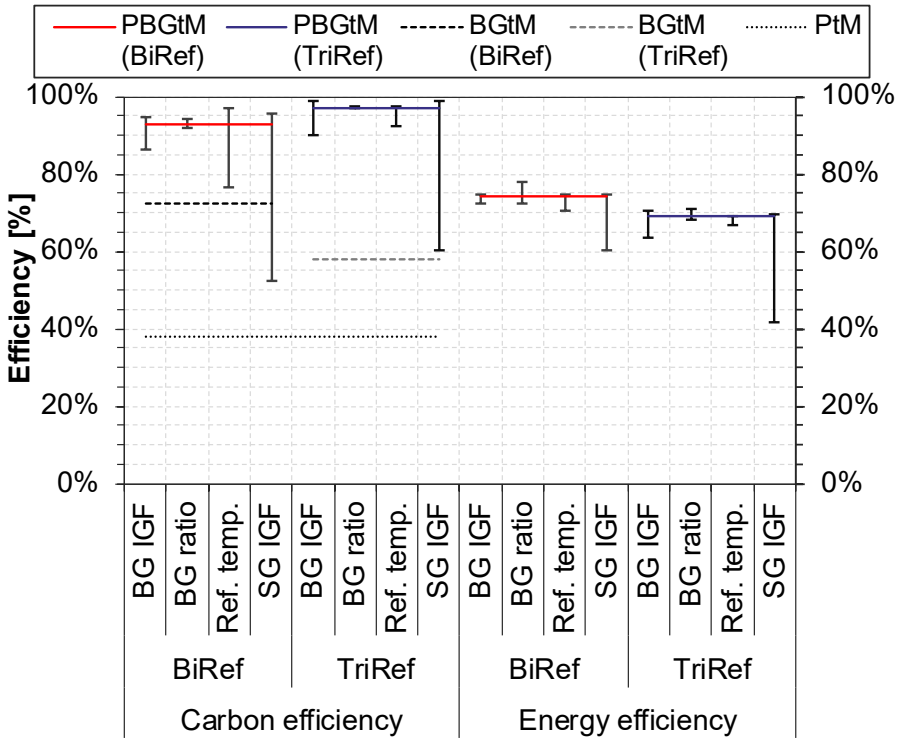

Figure 3-11: Summary comparison of technical reference case and parameter variation results (BG: biogas, BGtM: Biogas-to-Methanol, BiRef: Process configuration with electrically heated bi-reforming, IGF: Inert gas fraction, PtM: Power-to-Methanol, RC: Reference case, Ref. temp.: Reformer temperature, SG: Syngas, TriRef: Process configuration with autothermal tri-reforming).

In contrast to the given properties of biogas, process parameters can be directly influenced by process design and operation. Therefore, parameter variation results represent potential for technical process optimization. The influence of the reformer temperature and the syngas inert gas fraction on the technical key figures is very strong; however, only limited improvements can be achieved compared to the reference case. Significant improvements can only be achieved in the BiRef configuration. Specifically, elevated reformer temperatures enable an increase in carbon efficiency up to the level of the TriRef configuration. An increase in the permissible inert gas fraction also increases carbon efficiency. However, regarding energy efficiency, increasing process-related energy demands prevent enhancements from both process parameters.

Comparison with non-hybrid methanol production from biogas in (Figure 3-11) reveals that integrating power-based hydrogen increases carbon efficiency substantially. For purely power-based production (PtM), utilizing only the CO_2 share of the biogas, carbon efficiency decreases to only 38 %[7]. Purely biogas-based production (BGtM) achieves car-

[7] Carbon capture rate of 95 % assumed.

bon efficiencies of 72.5 % with electrically heated bi-reforming and 58.2 % with tri-reforming. Since carbon efficiency directly correlates with methanol production, non-hybrid concepts produce significantly lower quantities of methanol. For the biogas composition assumed within the reference case, an increase in methanol yield of 28 % (BiRef) and 67 % (TriRef) is achieved compared to the purely biogas-based concepts. The hybrid approach is particularly advantageous when the biogas has a high CO_2 content while the significance of adding power-based hydrogen diminishes as the CH_4 share increases. Considering a biogas ratio (CH_4/CO_2) of three within a bi-reforming-based configuration, carbon efficiency increases by only 2 %pt through additional hydrogen input. However, considering tri-reforming, hydrogen addition still increases carbon efficiency by 24 %pt. In summary, the assessment shows that both PBGtM configurations significantly increase the targeted carbon utilization compared to non-hybrid concepts.

3.5 Economic results

First, the methanol production costs resulting from the reference case are discussed, followed by an analysis of various influencing parameters and the assessment compared to non-hybrid product concepts.

3.5.1 Production costs

Figure 3-12 (left columns) illustrates the methanol production costs resulting from both process configurations in the reference case. The costs are compared with those of non-hybrid concepts (right columns) and fossil fuel-based production in Section 3.5.3.

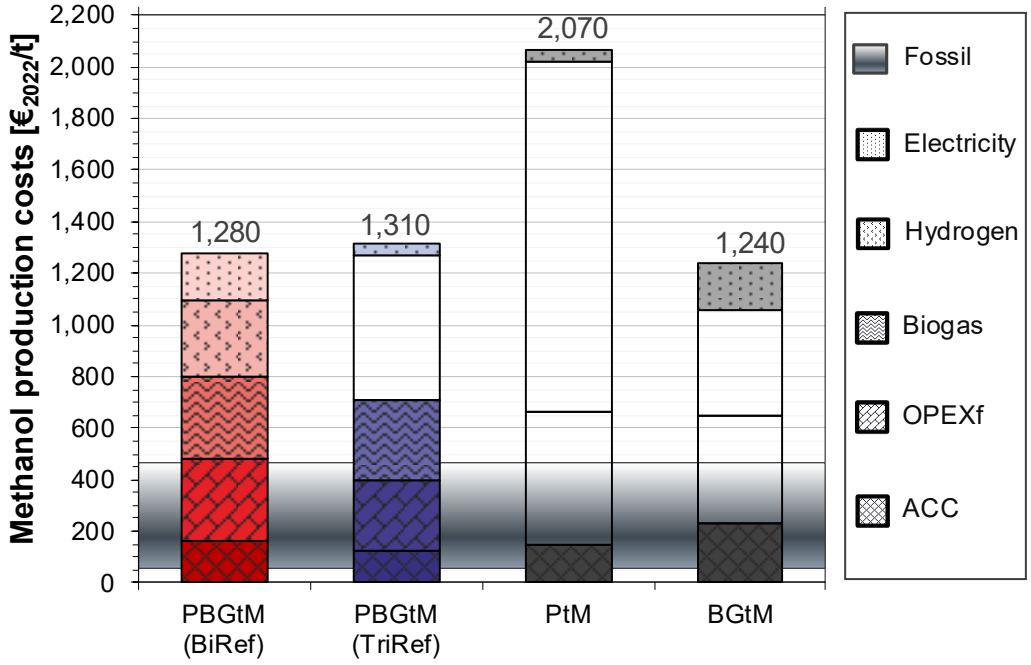

Figure 3-12: Methanol production costs for the reference case (Assumptions for PtM and BGtM see Annex A, fossil cost range according to [91, 129]; *ACC*: Annual capital cost, BGtM: Biogas-to-Methanol, PtM: Power-to-Methanol; *OPEXf*: Fixed operational expenditures).

Estimating production costs for methanol in the BiRef configuration reveals a relatively even distribution of the various cost components. The largest share of costs is attributed to biogas supply. The second largest cost contribution is fixed operational expenditures, predominantly determined by various labor expenses and maintenance. Hydrogen costs are also substantial, while electricity and annual capital costs are slightly lower.

In the TriRef configuration, nearly identical methanol production costs result. Due to the absence of heating in the tri-reforming reactor, the TriRef configuration requires slightly lower fixed capital investments, leading to annual capital costs and parts of the fixed operational expenditures being lower than those in the BiRef configuration. Biogas costs are also slightly lower due to higher carbon efficiency. The largest cost component results from hydrogen supply, accounting for 42 % of the methanol production costs. Electricity costs are relatively low compared to the BiRef configuration due to the lower relative demand.

3.5.2 Parameter variation

The following analyzes the impacts of various technical and economic parameters on methanol production cost (*MPC*) by parameter variation. The investigation areas are defined to follow the technical results from parameter variation and typical market and project-related cost ranges.

3.5.2.1 Technical parameters

In the context of the technical analysis, the parameter variation revealed different carbon and energy efficiencies for the investigated plant configurations. The influences of these efficiencies on the *MPCs* are depicted in Figure 3-13.

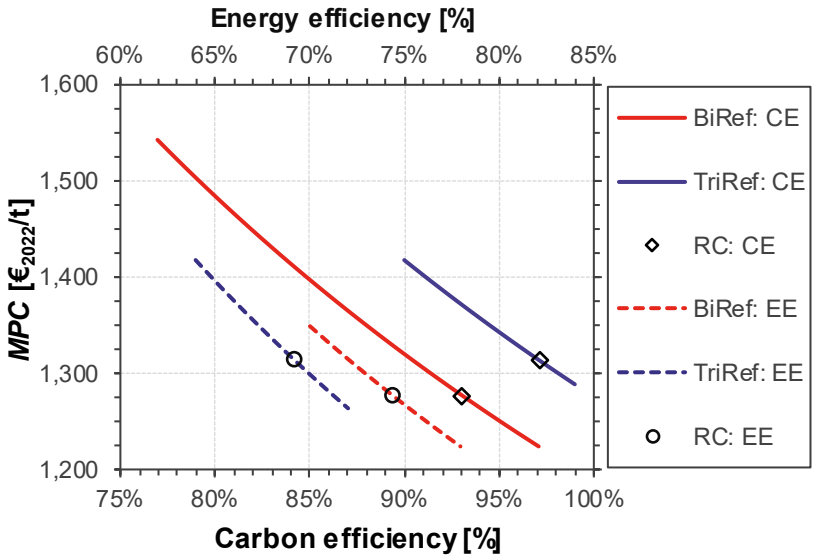

Figure 3-13: Effect of carbon and energy efficiency variation on methanol production cost (CE: Carbon efficiency, EE: Energy efficiency, *MPC*: Methanol production cost, RC: Reference case).

For both configurations, the parameter variation shows only marginal cost reductions with improvements in efficiency compared to the reference case. Across the entire range of technical key figures, the *MPCs* fluctuate by around 150 €$_{2022}$/t. An exception to this is the variation in carbon efficiency in the case of the BiRef configuration. Here, insufficient reforming temperatures or very low permissible inert gas concentrations in the syngas can significantly increase costs due to reduced product formation. However, these losses can be avoided through suitable plant design and operation.

The impacts of annual full load hours (*AFLH*) and plant capacity (scale factor) on *MPCs* are illustrated in Figure 3-14.

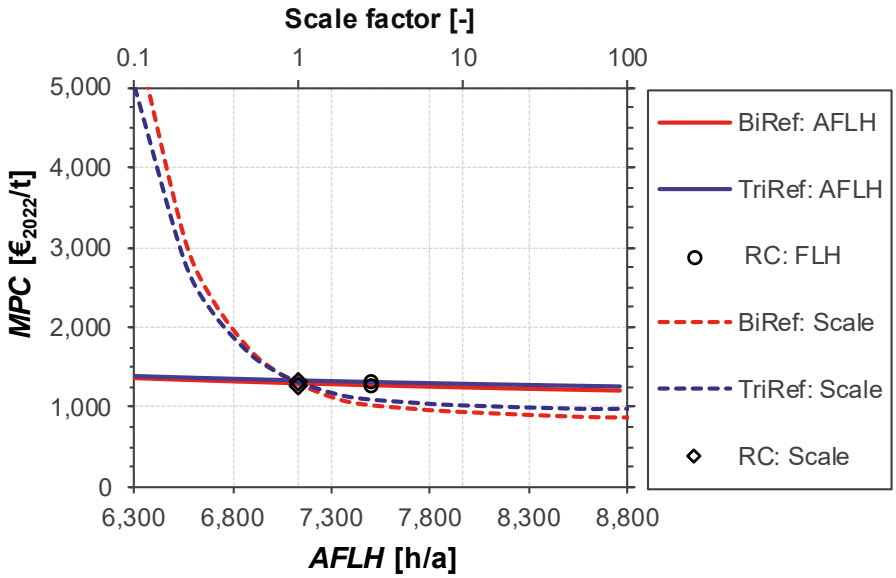

Figure 3-14: Effect of *AFLH* and plant scale on methanol production cost (Scale factor 1 corresponds to the reference case with 670 Nm^{3}BG/h; *AFLH*: Annual full load hours, *MPC*: Methanol production cost, RC: Reference case).

The variation of annual full load hours, which is varied around ± 16 % from the reference case (RC), results in an *MPC* variation of about 160 €$_{2022}$/t and 130 €$_{2022}$/t for the BiRef and TriRef configuration, respectively. Increasing annual full load hours from the reference case to a hypothetical annual full load (8,760 h/a) leads to cost reductions of around 5 % for both configurations.

The variation in plant capacity spans a wide scaling range (factor 1,000). Here, reducing the assumed reference case capacity has a stronger effect than increasing it. Doubling the capacity results in a relative *MPC* reduction of 17 % (BiRef) and 14 % (TriRef), while halving the capacity leads to an *MPC* increase of 34 % (BiRef) and 28 % (TriRef). Sensitivity to changes in plant size is somewhat more pronounced for the BiRef configuration than for the TriRef configuration. Increasing capacity by a factor of 10 reduces *MPC* by approximately 27 % (BiRef) or 22 % (TriRef). However, decreasing capacities affect the *MPC* much more strongly.

3.5.2.2 Economic parameters

Figure 3-15 shows the influence of annual capital cost (*ACC*) and weighted average capital cost (*WACC*) on *MPC*. The annual capital cost variation shows a linear trend with a higher gradient for the BiRef configuration. However, *MPCs* vary less than −50 €$_{2022}$/t and +100 €$_{2022}$/t from the reference case for both configurations. The weighted average capital costs have a non-linear impact on *MPC*. Higher fixed capital investments are more affected by changing weighted average capital costs. Therefore, the costs from the BiRef configuration change slightly more than in the TriRef configuration. However, the influence of the weighted average capital costs for the assumed variation areas is only marginally higher than the variation of the annual capital cost.

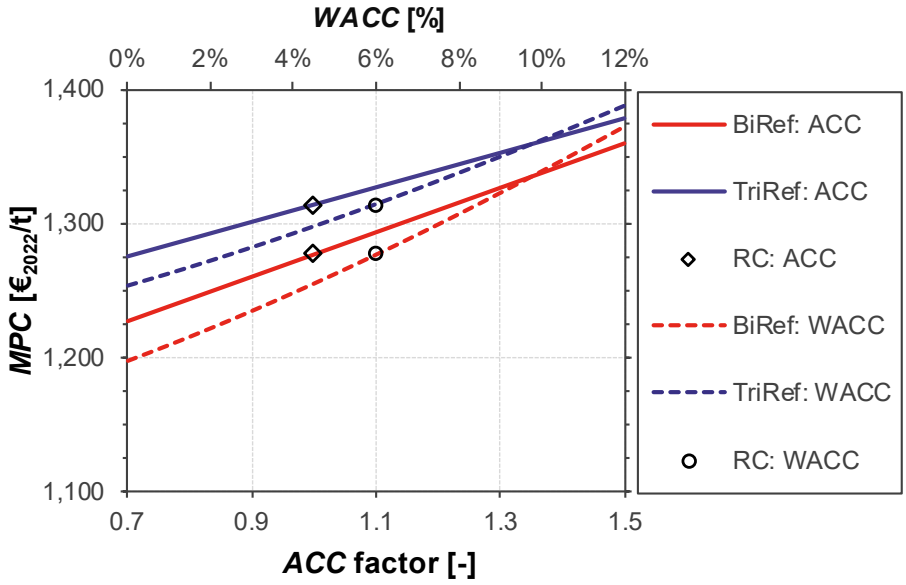

Figure 3-15: Effect of *ACC* and *WACC* on methanol production cost (*ACC*: Annual capital cost, *MPC*: Methanol production cost, RC: Reference case, *WACC*: Weighted average cost of capital).

Figure 3-16 depicts the influences of material and energy feedstock costs on *MPC*. Due to the wide cost range of biogas (variation factor of 4), which can increase significantly from the reference case, especially for small-scale biogas plants and complex substrates, parameter variation can also lead to significant changes in *MPC.* A 50 % increase in the biogas costs results in an *MPC* increase of around 12 % in both configurations compared to the reference case. However, since biogas production costs can also vary to a much greater extent, the change in *MPC* from the reference case can range from −121 €$_{2022}$/t (10 %) to +507 €$_{2022}$/t (40 %) in the case of the BiRef configuration and from −116 €$_{2022}$/t (9 %) to +486 €$_{2022}$/t (37 %) in the case of the TriRef configuration.

The considered electricity costs vary by a factor of 2.6 across the entire range. A 50 % increase in electricity costs results in a 91 €$_{2022}$/t (7 %) cost increase in the BiRef configuration and 24 €$_{2022}$/t (2 %) in the TriRef configuration. Across the entire variation range, there is a cost change relative to the reference case ranging from −56 €$_{2022}$/t (4 %) to +140 €$_{2022}$/t (11 %) in the case of the BiRef configuration and from −15 €$_{2022}$/t (1 %) to

+37 €2022/t (3 %) in the case of the TriRef configuration. The BiRef configuration shows lower *MPC* until electricity costs reach 170 €2022/MWh.

The costs of constant hydrogen supply vary by ca. ±30 % across the optimization scenarios (see Annex A.4). Given the significantly higher hydrogen demand of the TriRef configuration, cost sensitivity is notably higher compared to the BiRef configuration. The fluctuations in the *MPC* amount to ±84 €2022/t (7 %) in the BiRef configuration and ±159 €2022/t (12 %) in the TriRef configuration. Cost advantages for the TriRef configuration are realized when hydrogen costs fall below 6 €2022/kgH2.

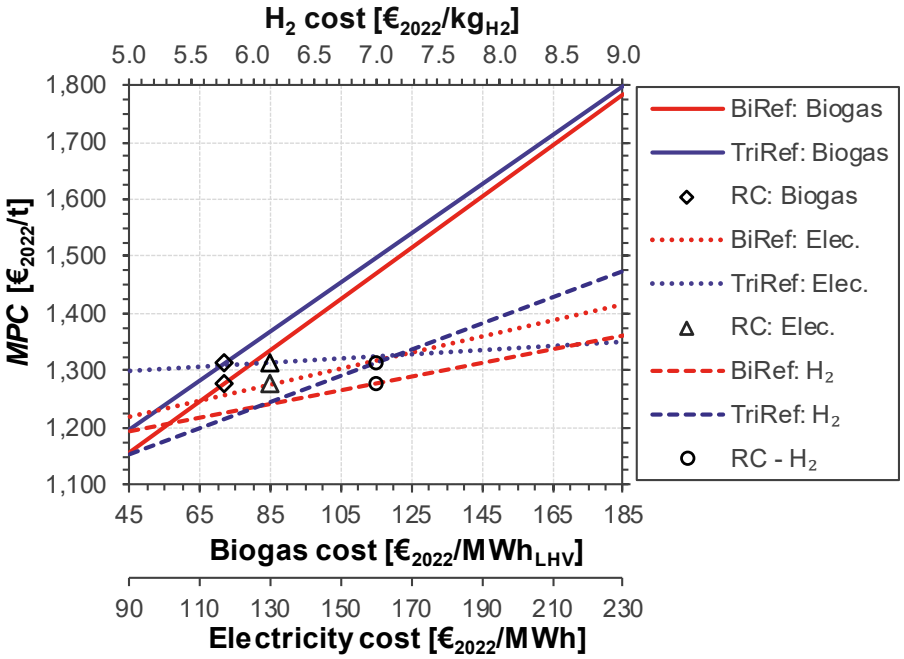

Figure 3-16: Effect of biogas, electricity, and hydrogen cost on methanol production cost (RC: Reference case, Elec: Electricity cost, MPC: Methanol production cost).

3.5.3 Assessment

The following summarizes and assesses the results of the economic analysis. The *MPCs* in the reference case are similar for both configurations, with the BiRef configuration leading to slightly lower costs primarily due to the lower hydrogen demand. Both PBGtM configurations exhibit a relatively even distribution of cost components. The main cost difference between the configurations lies in the proportions of hydrogen and electricity costs. Due to the significantly higher hydrogen demand, the associated costs are notably higher in the TriRef configuration. This cost difference is only partially offset by the higher electricity costs in the BiRef configuration. Besides the uncertainties inherently associated with calculating equipment costs, an increased uncertainty arises for the costs of the electrically heated reformer since the current literature does not provide the respective cost functions. However, considering the relatively low impact of the annual capital costs, significant deviations from the presented findings are not to be expected.

The parameter variation reveals that the ranges for expected efficiencies from the technical analysis have little impact on *MPCs*. The same applies to the impact of annual full load hours within the considered range. The installed plant capacity significantly impacts *MPCs*, particularly due to the broad variation range and strong economies of scale effects. Increasing the plant size leads to significant specific cost reductions compared to the reference case. Conversely, lower plant capacities have an even more pronounced effect; halving the capacity results in an *MPC* increase of around 30 %. Concerning the reference case, *MPC* reduction of over 20 % results for plants with tenfold capacity. However, only a few biogas plants worldwide have the necessary capacity to supply the needed amount of biogas for such a scale. Changes in economic framework assumptions within the varied limits lead to minor *MPC* variations (<±10 % from the reference case). Significant *MPC* changes, on the other hand, can result from cost fluctuations of material and energy feedstocks. In particular, considering biogas production costs from the upper literature range can lead to an increase in the *MPC* of almost 40 %. The impact of hydrogen costs is especially relevant for the TriRef configuration. However, changes in the *MPCs* are below 12 %.

Compared to the literature, the determined costs of approximately 1,300 €$_{2022}$/t are above those reported for biomass-based methanol [91]. Compared to power-based methanol, the costs fall within the lower range of current estimations [91]. However, biogas as well as electricity-derived methanol, exhibit significant cost variations depending on the assumed process concept, feedstock, plant size, and economic parameters. Within the framework conditions applied here, PBGtM shows a clear cost advantage over purely power-based methanol (PtM) (Figure 3-12). This advantage is due to the high costs of hydrogen supply and the significantly lower production capacity (assuming the same biogas potential). Purely biogas-based *MPCs* are in the same cost range as hybrid production. The advantage of BGtM lies in the absence of any additional hydrogen-related costs. However, lower product output disadvantageously offsets this due to higher specific fixed capital investments and fixed operational expenditures.

The *MPCs* of fossil fuel-based methanol from natural gas or coal range from 60 to 470 €$_{2022}$/t (without considering the costs of fossil CO_2 emission) [129], significantly lower than the achievable costs here. These low production costs for fossil-based methanol are achieved in countries with low natural gas or coal costs. The production facilities have capacities of up to 10,000 t/d, resulting in significantly reduced specific labor and maintenance costs compared to the decentralized PBGtM concept. Furthermore, the specific equipment costs are considerably lower due to economies of scale effects. Given the global overcapacity for fossil-based methanol production, market prices are closely aligned with production costs. Assuming costs for CO_2 certificates of 81 €$_{2022}$/t [130] would lead to fossil *MPCs* increase of ca. 40 to 300 €$_{2022}$/t considering only process emissions according to [91, 131, 132]. Compared to conventional large-scale production plants, the PBGtM concept shows high fixed operational expenditures resulting mainly from high specific labor, maintenance, and plant costs.

Without an additional GHG emission-related incentive compared to fossil fuel-based methanol, PBGtM-based methanol is not economically viable. The CO_2 mitigation costs are around 600 €$_{2022}$/t_{CO2} for natural gas-based methanol and 250 €$_{2022}$/t_{CO2} for hard coal-based methanol[8]. Economic advantages of the PBGtM concept over pure biogas- or power-based concepts primarily stem from downstream economies of scale benefits due to the higher utilization of feedstock (high carbon efficiency) and consequently larger methanol production capacities, as well as the cost-free supply of CO_2. Potential cost reduction for the concept lies in the standardized manufacturing of the plant as an end-of-pipe technology and in extensive automation for remote operation, as it is already common in biogas upgrading facilities.

3.6 Conclusion

The overall objective of the paper is to determine the efficiencies and costs of combined electricity- and biogas-based methanol production and to assess the concept compared to non-hybrid production approaches. Two process configurations based on different reforming technologies, i.e., BiRef configuration and TriRef configuration, were simulated and analyzed in a reference case and in a parameter variation. The key technical results can be concluded as follows:

- The BiRef configuration achieves a carbon efficiency of 93 %, while the TriRef configuration reaches 97 % (both for the reference case). Carbon efficiency advantages result from the higher methane conversion of tri-reforming, achieved through the additional use of oxygen as an oxidizing agent, allowing for lower purge gas quantities in the synthesis loop.

- The energy efficiency of the BiRef configuration reaches 74 %, while the TriRef configuration shows a lower efficiency of 69 % (both for the reference case and based on the higher heating value). The higher energy demand of the TriRef configuration primarily results from the higher hydrogen deficit of the reformer product, which must be compensated for by increased electrolysis capacity. In comparison, electrically heated bi-reforming utilizes electrical energy more efficiently.

- Changes in biogas composition only have a moderate effect on the efficiency of the configurations. A lower inert gas content in the biogas is advantageous for achieving higher carbon efficiencies. The demand for electricity-derived hydrogen decreases with an increasing CH_4/CO_2-ratio. The process parameters, reforming temperature, and syngas inert gas fraction significantly influence the investigated key figures. Generally, increasing these process parameters improves the carbon efficiencies of the configurations. However, the maximum energy efficiencies are not at the upper limit

[8] Assuming: GHG-neutral PBGtM production, fossil methanol combustion emissions of 1.375 $t_{CO2}/t_{Methanol}$, process emission of 0.5 $t_{CO2}/t_{Methanol}$ and 3.0 $t_{CO2}/t_{Methanol}$ for natural gas- and coal-based methanol production [91, 131, 132].

of the parameter range, as the increased energy demands surpass the elevated product formation.

- Compared to purely biogas-based methanol production (BGtM), the additional integration of power-based hydrogen can significantly increase carbon efficiency. For the reference case, efficiency enhancements of 21 %pt (BiRef) and 39 %pt (TriRef) are observed. Consequently, methanol yield can be increased by 28 % and 67 %, respectively. The significance of hydrogen addition is particularly important when employing tri-reforming and dealing with low methane content in biogas.

The results of the economic analysis can be concluded as follows:

- Under the assumed conditions applied in the reference case, the methanol production costs for both PBGtM configurations are around 1,300 €$_{2022}$/t, with minor advantages for the BiRef configuration. The hydrogen costs strongly drive the methanol production costs of the TriRef configuration. The cost shares of the BiRef configurations are more balanced, with biogas, hydrogen, and fixed operational expenditures being the main cost components.

- The methanol production costs are only slightly affected within the expected carbon and energy efficiency ranges. In contrast, plant capacity significantly affects production costs, showing cost reductions of over 20 % for plants with methanol production capacities exceeding 9 t/h, compared to 0.9 t/h in the reference case. While economic parameters show only minor effects on the methanol production costs, the availability of inexpensive biogas is essential, as high biogas costs can lead to cost increases of more than 37 %.

- Cost advantages compared to non-hybrid concepts (BGtM and PtM) arise from higher production capacities and the cost-free utilization of CO_2. However, the high costs associated with hydrogen supply result in methanol production costs at a similar level to those of purely biogas-based production. Due to the comparatively small production capacity and the more cost-intensive input materials, the production costs significantly exceed current fossil fuel-based methanol costs, resulting in CO_2 avoidance costs of between 250 €$_{2022}$/t$_{CO2}$ and 600 €$_{2022}$/t$_{CO2}$.

The investigated production concept offers the opportunity to make sustainable biomass resources available for material use and significantly increases carbon efficiency and production capacity compared to purely biogas-based concepts. However, challenges exist in the technical implementation of the complex production process in a decentralized, non-industrial setting and in the economic competitiveness with fossil fuel-based and purely biomass-based production concepts. However, the PBGtM concept can efficiently unlock additional carbon potentials, becoming increasingly important with the growing scarcity of available biomass and GHG-neutral carbon.

4 Kerosene production from power-based syngas – A technical comparison of the Fischer-Tropsch and methanol pathway

Bube S, Bullerdiek N, Voß S, Kaltschmitt M (2024): Kerosene production from power-based syngas – A technical comparison of the Fischer-Tropsch and methanol pathway. In Fuel 366 (2024) 131269. DOI: 10.1016/j.fuel.2024.131269

The article can be found online at
https://doi.org/10.1016/j.fuel.2024.131269

Formatting and wording are slightly adjusted to ensure consistency throughout this thesis.

Abstract

To achieve long-term greenhouse gas (GHG) neutrality within the aviation sector, substituting fossil aviation fuels with sustainable aviation fuels (SAF) derived from renewable energy sources is essential. Among the synthetic SAF options produced through power-to-liquid (PtL) processes, the Fischer-Tropsch (FT) and methanol pathway are of significant interest. However, to assess and compare these pathways, detailed technical process analyses are required to provide a sound basis for economic and environmental assessments. Thus, this research paper investigates and compares both SAF production pathways starting from power-derived syngas within an in-depth technical analysis, providing novel insights into overall process characteristics and efficiencies. Carbon and energy flows are derived from steady-state flowsheet simulations. A variation of technical parameters (FT pathway: FT chain growth probability and hydrocracking behavior, Methanol pathway: Dehydration olefin-selectivity and oligomerization product distribution) is carried out to assess impacts on carbon and energy efficiency, indicating uncertainties and parameter ranges for optimized kerosene production. The results show a very high carbon efficiency of the FT pathway (98 to 99 %) regarding the total fuel products, while the carbon efficiency regarding kerosene lies between 60 and 77 %. For the methanol pathway, a higher kerosene carbon efficiency can be achieved (60 to 90 %); however, the total fuel efficiency (74 to 92 %) is notably lower. The energy efficiencies of both pathways behave similarly to carbon efficiency, with the methanol pathway benefiting from thermodynamic advantages, leading to higher energy efficiency at equal carbon efficiency. Within the FT pathway, kerosene efficiency increases at high chain growth probabilities, while a high olefin-selectivity is crucial for efficient kerosene production within the methanol pathway. The analysis results provide comprehensive insights into the technical behavior of the overall processes which contributes to an improved understanding of the production pathways.

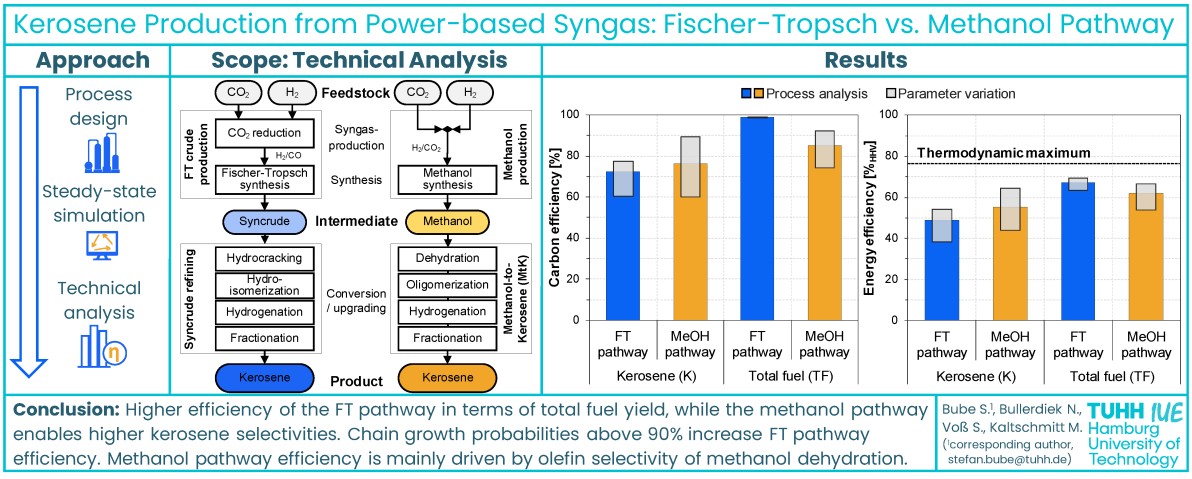

Figure 4-1: Graphical abstract of the publication “Kerosene production from power-based syngas” (FT: Fischer-Tropsch, MeOH: Methanol, K: Kerosene, TF: Total fuel).

4.1 Introduction

The global aviation sector shows a significant disparity between the targeted and projected greenhouse gas (GHG) emissions. On the one hand, both the International Civil Aviation Organization (ICAO) as well as the International Air Transport Association (IATA) have announced the goal of reducing CO_2 emissions to net zero by 2050 [9, 10]. On the other hand, demand for air transportation increases continuously worldwide, resulting in increasing aviation-related CO_2 emissions if no appropriate measures are implemented [8]. To decouple the projected growth in aviation from an increase in GHG emissions and achieve long-term GHG neutrality, fossil fuel-based aviation fuels need to be increasingly replaced by fuel options based on renewable sources of energy. From today's perspective, the use of carbon-free energy carriers used in respective aircraft concepts (e.g., liquid hydrogen or battery-electric aircraft) appears to be rather challenging and, if at all, technologically only feasible in the longer term, as this requires the design of fully new aircraft and a built-up of a proper fuel infrastructure alongside with the existing aviation fuel infrastructure for kerosene-type aviation fuels [24, 26].

Against this background, renewable aviation fuels should not only provide significantly lower GHG emissions but also be technically compatible with existing aircraft fleets and fuel infrastructure used for conventional kerosene so far. Such kerosene-type fuels that can be produced based on renewable energy sources are commonly referred to as sustainable aviation fuels (SAF)[9].

Different process pathways enable the utilization of various energetic (e.g., biomethane, electrical power) and material feedstock options (e.g., carbon dioxide, water) for kerosene-type fuel production. Currently, commercially used SAFs are almost exclusively produced based on vegetable oils and lipid wastes such as hydroprocessed esters and fatty acids (HEFA). In addition, with the start-up of the first production facilities, a ramp-up of conversion processes, mainly for advanced bio-kerosene production, is taking place [134]. However, due to the a priori limited potential of sustainable provided biomass and the much-discussed plate vs. tank issue, a massive expansion of these types of bio-kerosene to cover the existing as well as the emerging demand is doubtful [38]. Alternatively, fuels from renewable electricity and sustainable CO_2 (e-fuels) can be a promising fuel option characterized by a clearly greater production potential. The production of such e-fuels through so-called power-to-liquid (PtL) processes takes place via power-based synthesis gas (syngas) production, a synthesis step, and the subsequent downstream processing; thus, the fuels are also referred to as synthetic fuels. As of today, the main process routes discussed are the Fischer-Tropsch (FT) and the methanol pathway. While SAF from FT processes is already approved according to ASTM D7566 as drop-in aviation fuel, the

[9] Unlike climate-effective CO_2 emissions, aviation-related non-CO_2 effects cannot be fully mitigated by the combustion-based utilization of such fuel [4, 133]. Non-CO_2-effects are effects that are not directly related to the emission of CO_2 but also contribute to global warming. Examples are e.g., contrail formation or NO_x and sulfur emissions.

approval of methanol-based SAF production is currently undergoing the respective approval process (ASTM D4054). Accordingly, there are presently no methanol-to-kerosene production plants in commercial operation. However, methanol-based aviation fuel is a frequently discussed option, offering potential advantages against other production routes [135].

4.1.1 Conversion pathways

Power-based SAF production starts from the feedstocks water (H_2O) and carbon dioxide (CO_2). The energy converted into the chemical energy of the fuel and the energy needed for processing is primarily provided in the form of electricity. Electrochemical water splitting (electrolysis) produces hydrogen (H_2), and CO_2 is provided via capturing processes from respective "sustainable" carbon sources. Starting from these two gases, the FT- and methanol-based conversion pathway differ in the subsequent process chain (Figure 4-2).

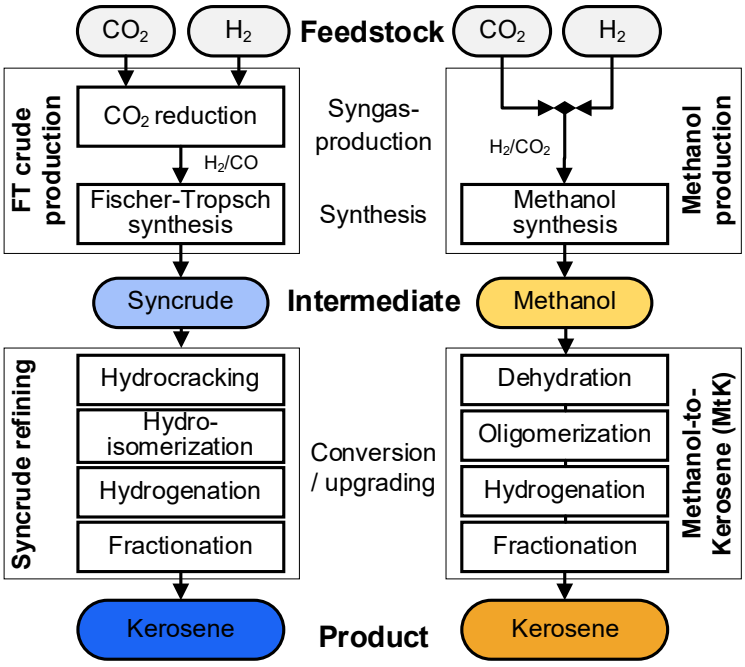

Figure 4-2: Fischer-Tropsch- and methanol-based kerosene production pathways.

4.1.1.1 Fischer-Tropsch pathway

The FT synthesis from carbon monoxide (CO)- and H_2-rich syngas is a state-of-the-art technology with its first commercial implementation in the 1930s [58, 86]. However, the direct conversion of CO_2 into long-chain hydrocarbons is not yet feasible with sufficient selectivity and conversion and requires further research for future applications [86, 136]. Thus, a CO_2 reduction to CO is needed to provide appropriate syngas for the subsequent kerosene production. Converting H_2 and CO into hydrocarbon chains within the FT synthesis yields synthetic crude oil (syncrude), ranging from light gases (e.g., methane) to long-chain hydrocarbons (waxes). Therefore, producing specification-compliant aviation

fuel requires further downstream refining by hydrotreatment and fractionation. Thereby, unsaturated hydrocarbons are saturated (hydrogenation), and waxes can be converted into fuel components by chain breaking (hydrocracking). If the cold flow properties required by the ASTM D7566 specification are not reached, additional hydroisomerization can be applied for branching the linear molecules.

4.1.1.2 Methanol pathway

The methanol pathway can be divided into the actual methanol synthesis, allowing highly selective methanol production, and the subsequent conversion of methanol into a hydrocarbon fuel mixture rich in kerosene components (Methanol-to-Kerosene: MtK, also Methanol-to-Jet: MtJ). Methanol synthesis enables the direct conversion of CO_2 and H_2 into methanol, making a previous CO_2 reduction obsolete. The CO_2-based methanol synthesis yields a mixture of methanol and water subsequently separated through distillation. Processes to convert methanol into hydrocarbons were developed mainly in the 1970s and commercialized in the 1980s [78, 137]. However, the focus was rather on producing products with a shorter carbon chain length, such as gasoline. Thus, no kerosene-specific concepts have been implemented to date. Like all alcohol-based conversion routes (Alcohol-to-Jet: AtJ), the methanol-to-kerosene conversion includes olefin formation within a dehydration process and a subsequent oligomerization into higher olefins. Further downstream hydrogenation converts the unsaturated hydrocarbons to alkanes, which are subsequently fractionated via distillation processes to obtain the desired fuel fractions [81].

4.1.2 Target and scope

The above-presented background highlights the necessity of renewable aviation fuels in air transport and the potential significance of both process pathways for power-based SAF production. However, comprehensive analyses are currently lacking a technical comparison of the FT and methanol pathway, preventing detailed economic and environmental studies. Atsonios et al. recently analyzed different production routes for e-kerosene in terms of carbon utilization and energy efficiency, with the results indicating particular advantages of the FT pathway [138]. However, the comprehensive analysis focuses on comparing several process routes based on fixed process assumptions, whereby no analysis of specific influencing variables was carried out. Further studies are therefore required to identify uncertainties and optimization potentials and to contribute toward enhanced process understanding.

Against this background, this research paper aims to assess and compare the production of synthetic kerosene from power-derived syngas via the Fischer-Tropsch and the methanol pathway within a technical analysis. Novel results arise particularly from the in-depth investigation of the process concepts and assessing critical process parameters regarding their impacts on process efficiencies. Figure 4-3 depicts the considered system boundaries within a generic supply and production chain.

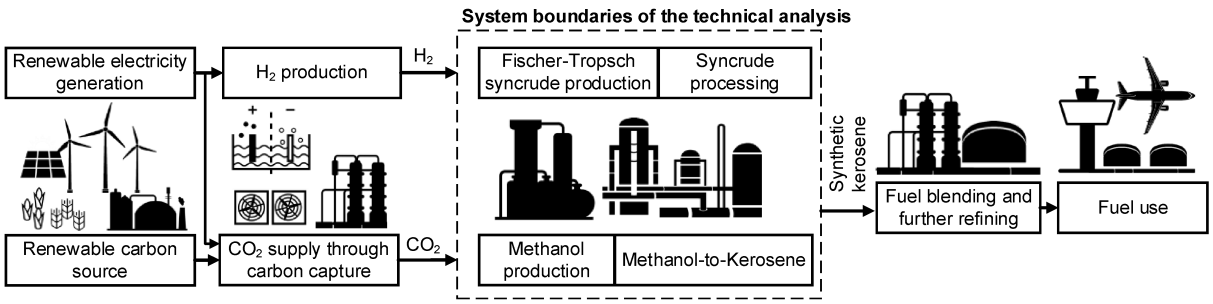

Figure 4-3: System boundaries within a generic supply chain of power-based Fischer-Tropsch- and methanol-based kerosene production.

The analysis focuses on the synthesis and downstream processes, considering H_2 and CO_2 as given feedstocks. A synthetic kerosene fraction represents the target product of both pathways at the end of the system boundaries considered. Thus, subsequent refining, logistics, or blending steps are not relevant for the comparative evaluation of the two production pathways and, therefore, not covered by the system boundaries of this analysis. A steady-state flowsheet simulation of the processes forms the basis of the analysis. The results of the reference cases are presented in carbon and energy flow diagrams. An extensive variation of the most critical parameters is carried out to estimate technical uncertainties and the influences of different process properties regarding carbon and energy efficiency.

4.2 Methodology

The technical analysis and comparison of kerosene production via the Fischer-Tropsch and the methanol pathway is based on an analysis of important technical key figures (here: carbon and energy efficiency) and the respective sensitivities. The overall assessment approach applied is shown in Figure 4-4. Following this, the design and simulation of reference production concepts are used as a basis for the subsequent process analysis and evaluation. The simulation results are utilized for visualizing and evaluating the carbon and energy flows, enabling a comprehensive understanding of the processes. Within the process assessment, the influences of selected technology parameters on the key figures – and thus the resulting uncertainties and optimization possibilities – are evaluated through parameter variations. The applied steps, software tools, and methods are described below.

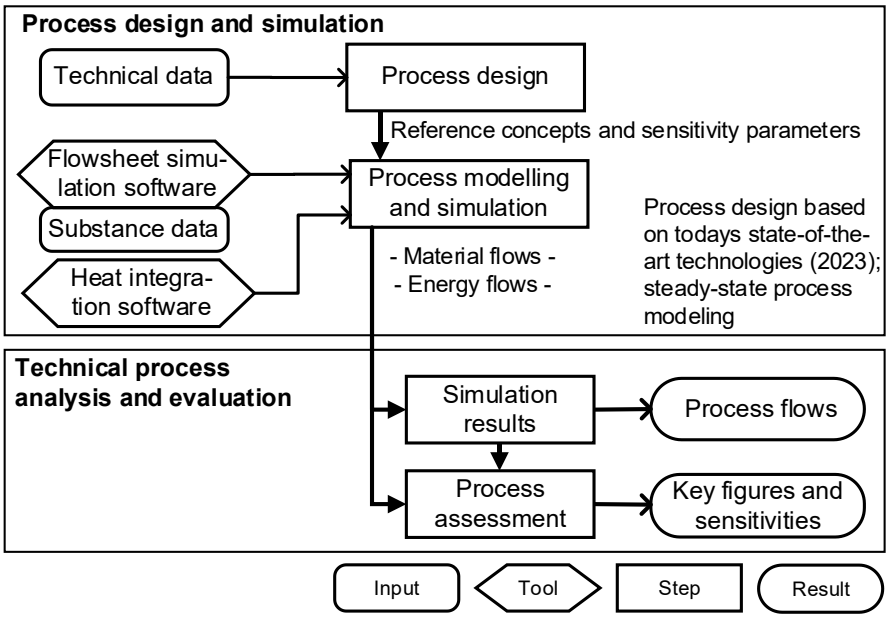

Figure 4-4: Overarching assessment approach.

4.2.1 Process design

Process modeling and simulation are based on the design of representative and fair-comparable processes (reference concepts). The design of such processes depends on the assumed feedstock and the desired target product. Based on these cornerstones, the reference concepts are developed by integrating single reference processes. Only sub-processes with a technology readiness level (TRL) ≥ 6 are considered. This procedure ensures that the reference concepts can be commercially realized in the short-term – at least from a technical perspective. All process data – i.e., conversion rates, selectivities, and operating conditions – are based on literature and adapted to a kerosene-maximized production. By-products in the fuel range of naphtha (gasoline) and diesel are considered valuable outputs; i.e., no "kerosene-only" concepts are considered.

4.2.2 Process modeling and simulation

A steady-state flowsheet simulation determines the mass and energy flows in the analyzed processes. For this purpose, the reference concepts are modeled using the commercial simulation software Aspen Plus®, allowing to determine the occurring material and energy streams based on well-approved thermodynamic calculation methods and material databases. Therefore, the considered components and the applied property methods are specified. The process flowsheet can be modeled using preconfigured or specially constructed unit operations [109]. The respective process blocks are connected with material, heat, or power streams. No internal integration of heat streams is assumed within the simulation model. Further information on the simulation program can be found in the specialist literature [139–141].

A pinch analysis using the Aspen Energy Analyzer® is carried out to address heat integration appropriately, providing information on the minimal external heating and cooling demands. Based on the simulated heat flows, the heat integration is approximated without the specific design of equipment. The minimum temperature differences of the heat transfer and the available "external" utilities are chosen within the model.

4.2.3 Process assessment

For the analysis of the simulation results, the derived mass and energy balances from the process modeling are used to determine technical key figures of the overall process. Therefore, two assessment figures – carbon and energy efficiency – are defined. The sensitivity of these assessment figures is analyzed based on a parameter variation.

Both key figures are related to the production of kerosene (K) as the target product as well as to the total fuel product (TF), including the naphtha (gasoline), kerosene, and diesel fraction.

4.2.3.1 Carbon efficiency

Carbon efficiency is a product-independent comparative figure for material efficiency due to its molar reference. Furthermore, the limited availability of sustainable carbon from biomass underlines the need for efficient carbon use as it directly impacts economic competitiveness. It indicates the selectivity of the process concerning the target product relative to the input material; i.e., this figure describes the amount of carbon bound in the target product compared to the amount of carbon contained in the feedstock (Eq. 4-1). The reference to molar carbon enables a comparison independent of the actual mass of the substance used or the product obtained.

$$\eta_{\mathrm{C,Product}} = \frac{\dot{C}_{\mathrm{Product}}}{\dot{C}_{\mathrm{Feed}}} \qquad \text{Eq. 4-1}$$

η_{C} Carbon efficiency [-]
$\dot{C}$ Carbon flow [$\mathrm{mol_C/s}$]

4.2.3.2 Energy efficiency

Energy efficiency is a commonly used key figure allowing to assess processes regarding their overall energy expenditure. Here, energy efficiency describes the energy content of the product compared to the energetic effort of production (i.e., chemical energy from the feedstock plus additionally needed electrical and thermal process energy) (Eq. 4-2). Here, chemical energy is always related to the energy carrier's higher heating value (HHV), unless otherwise stated.

$$\eta_{\mathrm{e,Product}} = \frac{\dot{m}_{\mathrm{Product}}\,\mathrm{HHV}_{\mathrm{Product}}}{\dot{m}_{\mathrm{Feed}}\,\mathrm{HHV}_{\mathrm{Feed}} + P_{\mathrm{el}} + \dot{Q}_{\mathrm{th}}} \qquad \text{Eq. 4-2}$$

η_{e} Energy efficiency [-]
$\dot{m}$ Mass flow [kg/s]
HHV Higher heating value (HHV) [MJ/kg]
P_{el} External electricity demand [MW]
$\dot{Q}_{\mathrm{th}}$ External heat demand [MW]

4.3 Reference concepts and data

This section describes the defined reference concepts. A detailed description of the technologies considered can be found in Annex B, Section B.1. According to Figure 4-3, both pathways are distinguished into two process sections.

4.3.1 Reference concepts

4.3.1.1 Process inputs and output

The provision of power-based H_2 and sustainable CO_2 falls outside the system boundaries of this analysis. Thus, it is assumed that H_2 at 50 bar (i.e., a pressure level achievable with advanced low-temperature electrolyzers [65, 142]) and CO_2 are available at the plant; the latter is available at atmospheric pressure with a concentration of 99 vol% CO_2 and 1 vol% nitrogen (N_2) [71]. Concerning the carbon chain length, the target product kerosene is defined as the C_8 to C_{16} fraction of the hydrocarbon product mixture [143, 144]. Besides kerosene, a light naphtha fraction (C_5 to C_7) and a heavy diesel fraction (C_{17} to C_{20}) are considered valuable by-products. Further material outputs like fuel gas are considered to be burned for energy recovery within both pathways.

4.3.1.2 Fischer-Tropsch pathway

The Fischer-Tropsch pathway includes the process sections “FT syncrude production” and “Syncrude refining”.

Fischer-Tropsch syncrude production. Figure 4-5 shows the flowsheet of the FT syncrude production section. The process uses a low-temperature Fischer-Tropsch (LTFT) synthesis, enabling the production of a paraffinic syncrude that is well-suited for kerosene production. A CO and H_2-rich syngas is required, as CO_2 behaves inertly under most LTFT catalysts [56, 58, 86]. FT synthesis with direct CO_2 utilization is a promising alternative and the focus of current research. However, thus far, this has only been demonstrated on a small scale and at higher temperatures for producing olefins, aromatics, and short-chain fractions [145–148]. Thus, applying power-based syngas today requires an additional CO_2-reduction step, here considered via a reverse water–gas shift (RWGS) reaction (Eq. 4-3) [86].

$$CO_2 + H_2 \leftrightharpoons CO + H_2O \qquad \Delta H_{R(298\,K)} = 42\,\mathrm{kJ/mol} \qquad \text{Eq. 4-3}$$

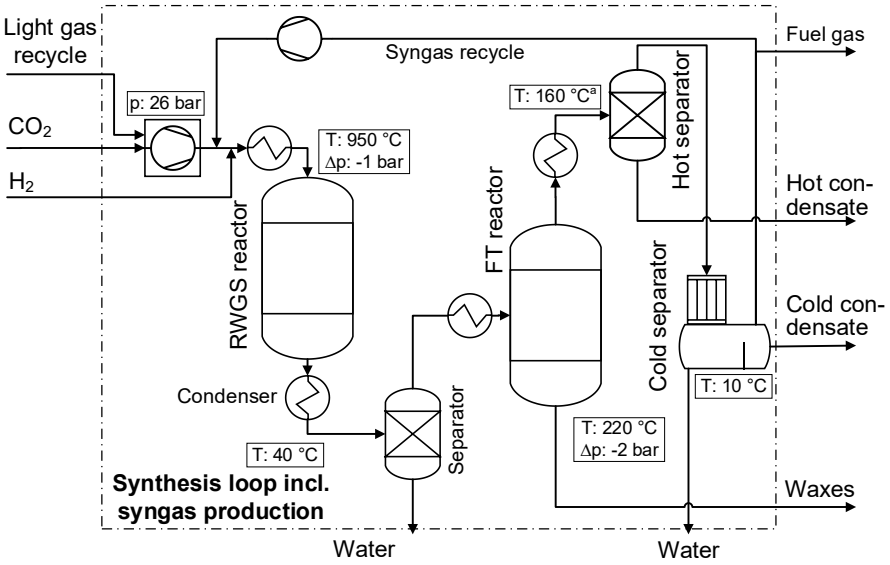

Figure 4-5: Fischer-Tropsch syncrude production flowsheet ([a] temperature control prevents water condensation. Minor equipment and auxiliary currents are neglected; RWGS: Reverse water–gas shift).

First, CO_2 is compressed together with the synthesis loop recycle gas, mixed with H_2, and heated up to 950 °C to enable high conversion rates and to avoid coking at the catalyst. The RWGS reactor is assumed to operate isothermally, providing the required heat via electrical heating. The reaction product is dried by cooling and condensation before it is fed to the FT reactor. Due to the elevated RWGS operation pressure (26 bar), intermediate compression between the reactors is avoided. Eq. 4-4 shows the strongly exothermic FT reaction. The Anderson-Schulz-Flory (ASF) distribution (Eq. 4-5) can describe the chain length distribution of the FT product. The chain length-dependent olefin to paraffin formation can be described with Eq. 4-6 [149].

$$n\mathrm{CO} + (2n+1)\mathrm{H_2} \rightarrow \mathrm{C}_n\mathrm{H}_{2n+2} + n\mathrm{H_2O} \qquad \Delta H_{R(298\,K)} \approx n(-150\,\mathrm{kJ/mol}) \qquad \text{Eq. 4-4}$$

$$W_n = n(1-\alpha)^2\alpha^{n-1} \qquad \text{Eq. 4-5}$$

$$(O/P)_n = \mathrm{e}^{-c\,n} \qquad \text{Eq. 4-6}$$

n Carbon chain length [-]
W_n Weight fraction [-]
α Chain growth probability [-]
O/P Olefin to paraffin ratio [-]
c Adjustment parameter [-]

The FT syncrude is separated into three different liquid streams – a liquid wax fraction, a hot condensate, and a cold condensate. The wax fraction is already liquid under reaction conditions and can be directly separated from the gaseous product stream. Depending on

the reactor design, the liquid wax phase separation can already occur in the reactor or downstream in a conventional gas/liquid separator. The gas phase is cooled to about 160 °C in a first separator, where an additional waxy hot condensate can be separated, but parallel water condensation is avoided. In a cold separator, the remaining gas is further cooled to about 10 °C to condense lighter hydrocarbons and water, which can be decanted as a separate liquid phase. The remaining light gases – consisting mainly of N_2 accumulations, unconverted reactants (H_2, CO), CH_4, and CO_2 – are recycled and partly purged (fuel gas). Since cobalt-catalyzed LTFT only enables the conversion of CO, with CO_2 and hydrocarbons behaving inertly, internal recycling of short-chain products is not considered. However, external recycling – i.e., recycling, which includes equipment outside the FT synthesis loop, is considered with the co-reforming of light C_1 to C_4 hydrocarbons in the RWGS reactor [150].

Syncrude refining. The technologies and the configuration of the FT downstream processing depend mainly on the applied FT synthesis technology and the target products. With a prioritized production of kerosene, extensive hydrotreatment (including hydrogenation, hydrocracking, and/or hydroisomerization (see Annex B, Section B.1), is required. In addition, the thermal separation process of rectification is applied to separate the different fuel fractions (fractionation). The flowsheet of the FT syncrude refining is shown in Figure 4-6.

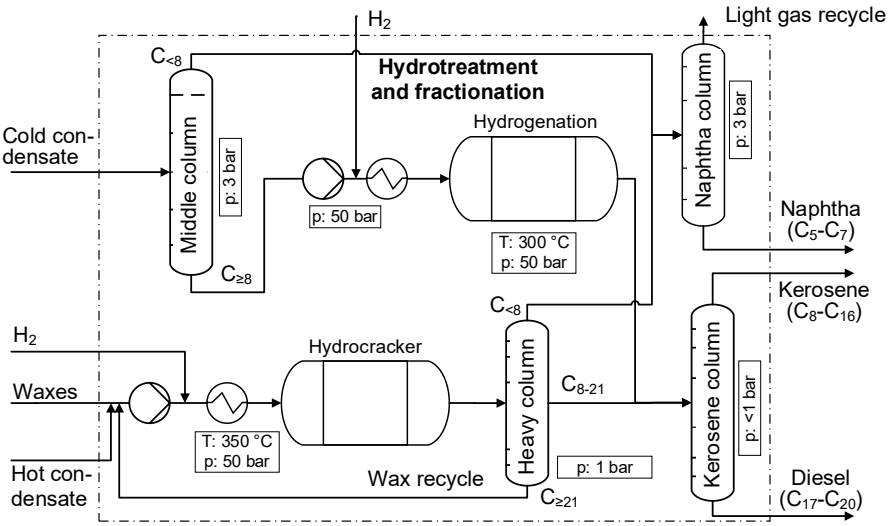

Figure 4-6: FT syncrude refining flowsheet (minor equipment and auxiliary currents neglected).

The wax fraction is mixed with hot condensate and hydrogen before the mixture is heated and fed to the hydrocracking reactor. The product consists of various saturated hydrocarbons fractionated within a downstream-located rectification column. Heavy components ($\geq C_{21}$) are fed back for further cracking, while a lighter kerosene/diesel fraction and a light gas/naphtha fraction are extracted for additional separation. Since the combination of LTFT synthesis and downstream hydrocracking – with parallel isomerization – leads to a product mixture with high proportions of singly branched hydrocarbons, separate hydroisomerization is most likely not necessary [83, 144]. The cold condensate is rectified

to separate light gases and naphtha from the heavier fractions. The light stream is separated in another column into naphtha and light gas, where the latter is recycled back to the synthesis section. The bottom stream from the middle (distillate) column is hydrogenated and fractionated to derive the desired kerosene fraction and diesel as a by-product.

4.3.1.3 Methanol pathway

The methanol pathway is distinguished into the process sections “Methanol production” and the subsequent “Methanol-to-Kerosene”.

Methanol production. The direct synthetic conversion of CO_2 via direct methanol synthesis is already demonstrated and commercially realized on a small scale (TRL 8 to 9) [86, 144]. Thus, starting from pure H_2 and CO_2, syngas is produced by mixing both substances in the required ratio. The stoichiometric number (SN) can quantify the intended ratio on a molar level (Eq. 4-7). Within the methanol synthesis (Eq. 4-8), slightly over-stoichiometric ratios of 2.05 to 2.10 are realized, positively affecting the synthesis [78, 151, 152].

$$SN = \frac{[H_2] - [CO_2]}{[CO] + [CO_2]} \qquad \text{Eq. 4-7}$$

SN Stoichiometric number [-]
$[x]$ Molar fraction of component x [-]

$$CO_2 + 3\,H_2 \rightleftharpoons CH_3OH + H_2O \qquad \Delta H_{R(298\,K)} = -49.2\ \text{kJ/mol} \qquad \text{Eq. 4-8}$$

Figure 4-7 shows the flowsheet for a direct CO_2-converting methanol synthesis. As shown, CO_2 and H_2 are fed into a multi-stage syngas compressor and mixed with light gases from the first purification column, which mainly consist of CO_2. The compressed gas stream is then mixed with recycled syngas and preheated before it is fed into the methanol reactor. The reaction product is cooled and partially condensed. Part of the unconverted syngas is purged out of the process to avoid an accumulation of inert gases or light synthesis by-products. The remaining part of the gas phase is compressed again to overcome the pressure drop of the synthesis reactor. The liquid raw methanol, a mixture of mainly methanol, water, and solved gases, is fed to the so-called topping column, where the solved gases and light by-products are separated from the mixture. The methanol–water mixture builds the bottom product and is fed to the methanol column to provide pure methanol as the main product.

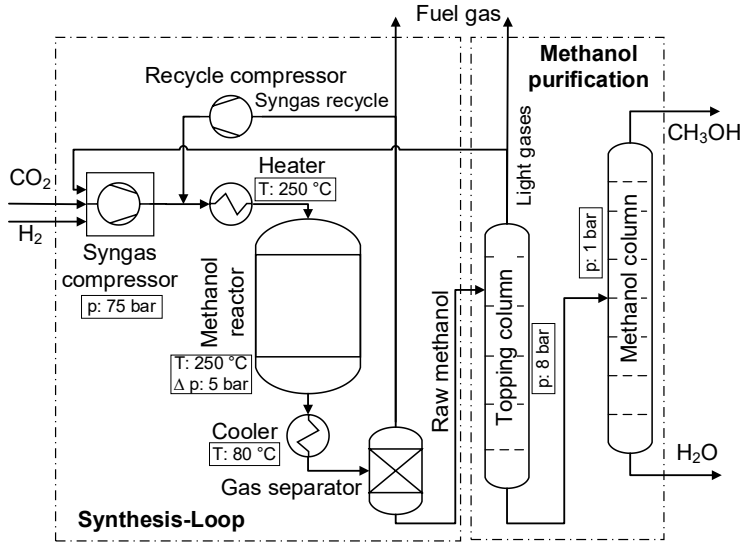

Figure 4-7: Methanol production flowsheet (minor equipment and auxiliary currents neglected).

Methanol-to-Kerosene process. The Methanol-to-Kerosene (MtK) process, analogous to common alcohol-to-hydrocarbon processes, consists of dehydration, oligomerization, and hydrogenation (Annex B, Section B.1). The decisive factor for the product formed is the combination of dehydration and oligomerization**.** Figure 4-8 shows the process flowsheet of the MtK process derived.

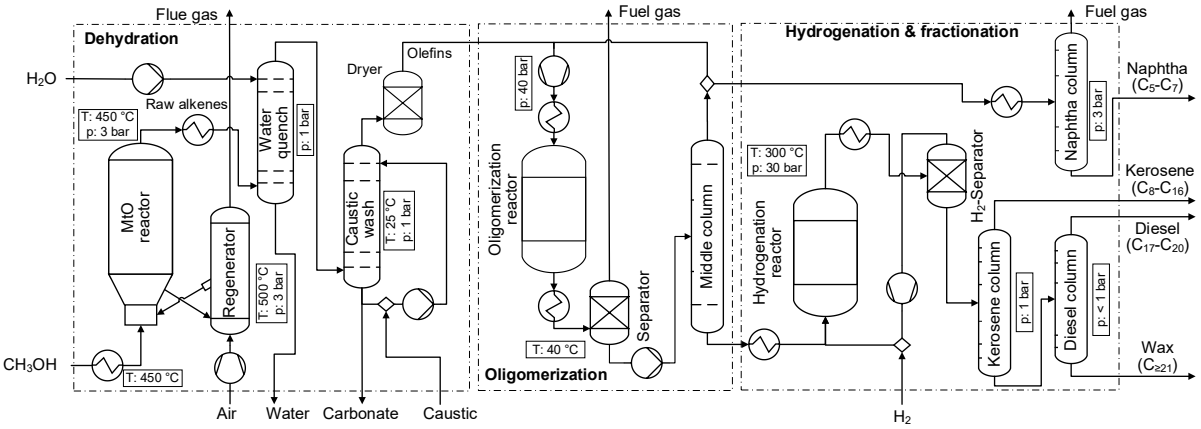

Figure 4-8: Methanol-to-Kerosene flowsheet with main components (minor equipment and auxiliary currents neglected).

The methanol is compressed and enters the Methanol-to-Olefins (MtO) reactor to generate light olefins. The MtO section is designed based on the UOP/Norsk Hydro MtO process without further olefin separation [81]. The raw olefin stream is then fed in a water separation column and subsequently washed with caustic soda for CO_2 separation. After the olefin stream is further dried through a molecular sieve, it enters the oligomerization unit. The product distribution of most oligomerization processes can be approximated with a generic ASF distribution [153–155]. Considering that the starting point of the distribution – i.e., regarding the product with the shortest carbon chain length – is affected by the carbon chain length of the olefin feedstock, the adjusted ASF distribution can be described by Eq. 4-9.

$$W_n = (n - x - 1)(1 - \alpha)^2 \alpha^{n-x-2} \qquad \text{for } n \geq x \qquad \text{Eq. 4-9}$$

n Carbon chain length [-]
W_n Weight fraction [-]
α Chain growth probability [-]
x Adjustment parameter [-]

The weight fraction (W_n) of the product with the chain length (n) depends on the chain growth probability (α) and the starting point adjustment variable (x). Assuming a complete per-pass conversion, x = 2 represents an ethene-ethene, x = 3 an ethene-propene, and x = 4 a propene-propene dimer as the lightest component. For the formation of hydrocarbons in the kerosene range, operating conditions from 150 to 300 °C and 40 to 100 bar seem practical [78, 137]. The oligomerization reactor product is cooled to 40 °C to separate light MtO by-products, predominantly light alkanes. To achieve a maximized kerosene output, the liquid stream is fed into a distillation column, which further separates light gases and naphtha from the higher olefins. The light fraction is mainly recycled to the oligomerization reactor, while a purge stream is extracted to avoid an accumulation of higher alkanes. Multi-stage oligomerization is also conceivable, but due to the generic modeling approach, it is not considered here. The bottom stream of the column is then hydrogenated and fractionated.

4.3.2 Data and assumptions

The following section outlines the most important data and assumptions of process modeling. For additional modeling data, refer to Annex B, Section B.2.

4.3.2.1 Fischer-Tropsch pathway

Fischer-Tropsch syncrude production. Table 4-1 presents the most important parameters and assumptions for modeling the FT syncrude production. The RWGS product mixture is assumed to be in a chemical equilibrium at the applied operating conditions (i.e., fast kinetics at these temperatures) [156]. The operating pressure of the FT reactor and the pressure drop of the RWGS reactor determine the outlet pressure of the syngas compression, avoiding intermediate compression. The H_2:CO ratio in the FT feed is set to 2.05. The total share of reactants (CO and H_2) is set to 70 %, with the rest resulting from accumulated inert components and unconverted RWGS products (CH_4 and CO_2). The chain growth probability (Eq. 4-5) differs depending on the process technology, which is varied to evaluate the influence on the overall process. Within the reference case, chain growth probability is set to yield a maximum straight-run kerosene fraction. Some of the considered ASF distributions are exemplarily shown in Figure 4-9 (left). However, the selectivities for C_1 and C_2 products deviating from the actual ASF are adjusted in the model accord-

ing to [58]. High-temperature (HT) condensate is separated under the restriction that water condensation is avoided (temperature control). Cold condensate is separated at 10 °C to avoid recycling of higher alkanes to the RWGS reactor.

Table 4-1: Key modeling parameter of the FT syncrude production (RC: Reference case, *T*: temperature, *p*: pressure, PV: Parameter variation).

Process	Parameter		Value	Reference
RWGS reactor	Operating conditions	T [°C]	950	[83, 144, 150]
		p_{in} | Δp [bar]	26 | −1	[144] | [150]
	Equilibrium conversion	Products considered: CO, CO_2, H_2O, H_2, CH_4		[75, 76]
FT reactor	Operating conditions	T [°C]	220	[58, 86]
		p_{in} | Δp [bar]	25 | −2	[83, 86]|[157]
	Reaction parameter	Chain growth probability (Eq. 4-5)[a]	RC: 0.85 PV: 0.75–0.95[b]	[58]
		Per-pass conversion [%]	65	[86]
	By-product formation	c in olefin share, Eq. 4-6	0.3	[149]

[a] C_1 to C_2 selectivity adjusted according to [58], [b] see Annex B, Section B.2

Syncrude refining. Table 4-2 shows data and assumptions for the syncrude refining concept. Ideal hydrocracking is assumed [158]. The selectivities to all C_4 to C_{n-4} products derived from a C_n reactant are equal, while the selectivities to C_3 and C_{n-3} products are assumed to be only half as high. Products with a carbon chain length of < C_2 products are not formed. Since the cracking activity of hydrocarbons increases exponentially with increasing carbon chain length, the conversion is determined component-specifically between C_8 and C_{17} using an exponential function. No reaction is assumed for hydrocarbon chains smaller than C_8, while components larger than C_{17} are completely converted. In the reference case, each cracked component can undergo secondary cracking with a probability dependent on its new chain length.

Table 4-2: Key modeling parameter of the syncrude refining (RC: Reference case, *T*: temperature, *p*: pressure, PV: Parameter variation).

Process	Parameter		Value	Reference
Hydrocracker	Operating conditions	T [°C] | p [bar]	350 | 50	[83, 158, 159]
	Reaction parameter	Ideal cracking with chain length depending conversion; RC: Secondary cracking; PV: Primary to tertiary cracking		Based a.o. on [144, 158]
Hydrogenation	Operating conditions	T [°C] | p [bar]	300 | 40	[159, 160]
	Reaction parameter	Conversion [%]	100	[159, 160]

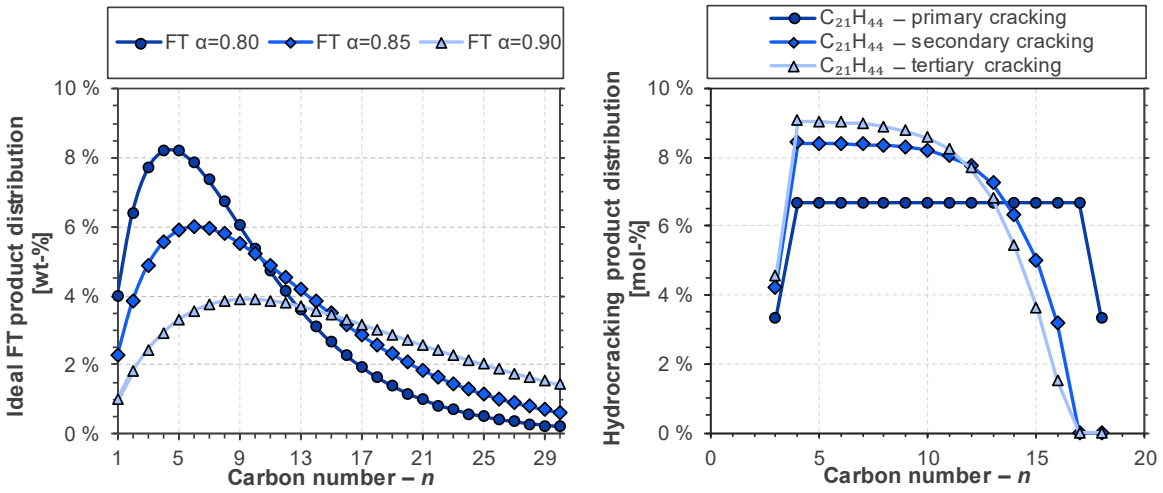

Figure 4-9: Exemplary FT and hydrocracker product distributions according to model assumptions (α: chain growth probability; FT: Fischer-Tropsch).

To evaluate the influence of different hydrocracking behaviors, the process assessment also takes into account single cracking (primary) and triple cracking (tertiary). The resulting product distributions using the example of a single component are shown in Figure 4-9 (right).

4.3.2.2 Methanol pathway

Methanol production. Essential assumptions and data used for modeling the methanol production section are presented in Table 4-3. The syngas conversion is assumed to be close to equilibrium using a temperature approach [78, 120]. The formation of by-products is considered proportional to the methanol formation and calculated from selectivity data according to [86]. To account for occurring syngas losses due to purge gas, the purge gas volume is adjusted to achieve a common recycle ratio of 4.5 [86, 161]. The rectification columns are designed so that the effluent meets the purity requirements of internationally traded methanol. Since no significant uncertainties regarding the modeling of the methanol synthesis are evaluated, no sensitivity parameters are considered.

Table 4-3: Key modeling data of the methanol production (DME: Dimethyl ether, *T*: temperature, *p*: pressure).

Process	Parameter		Value	Reference
Methanol reactor	Operating conditions	T [°C]	250	[86, 95]
		p_{in} | Δp [bar]	75 | −5	[86]|[92]
	Equilibrium conversion with temperature approach	$CO + 2\ H_2 \leftrightharpoons CH_3OH$	15 K	[120]
		$CO_2 + 3\ H_2 \leftrightharpoons CH_3OH + H_2O$	15 K	[120]
		$CO_2 + H_2 \leftrightharpoons CO + H_2O$	15 K	[120]
	By-product formation	Ethanol | DME | methyl formate [w ppm]	89 | 145 |14	[86]
Syngas purge	Recycle gas ratio [a] [mol%], controlled by syngas purge		450	[86, 161]

[a] Ratio = Recycle (mol/s)/fresh gas (mol/s)

Methanol-to-Kerosene process. Table 4-4 shows the key modeling data of the Methanol-to-Kerosene process section. Since the olefin-selectivity of the MtO reaction is decisive for the assumed oligomerization and literature values differ, its influence is investigated through parameter variation. Therefore, the respective MtO reactions are adjusted by an olefin-selectivity factor (S_0). Oligomerization is modeled generically according to Eq. 4-9. Since MtO can yield olefins in the range of mainly C_2 to C_4, besides the chain growth probability (α), starting point variation of ASF distribution is also considered through a parameter variation (Section 4.4.2). This is conducted via an additional parameter referred to as x in this analysis (Eq. 4-9). Some of the adjusted ASF distributions are exemplarily shown in Figure 4-10. Hydrogenation is modeled analogously to FT syncrude upgrading.

Table 4-4: Key modeling data of the Methanol-to-Kerosene process (RC: Reference case, MtO: Methanol-to-Olefins, p: pressure, PV: Parameter variation, S_0: Olefin-Selectivity, T: Temperature).

Process	Parameter		Value	Reference
MtO reactor	Operating conditions	T [°C] | p [bar]	450 | 3	[162, 163]
	Reaction parameter	Olefin-selectivity (S_0) [$\%_C$][a]	RC: 90; PV: 85–95	[164–168]
		Conversion [%]	100	[162, 163, 168]
	Reaction conversion [%]	2 CH_3OH → C_2H_4 + 2 H_2O	46.00 · S_0	according to [79, 164, 165, 169, 170]
		3 CH_3OH → C_3H_6 + 3 H_2O	42.89 · S_0	
		4 CH_3OH → C_4H_8 + 4 H_2O	11.11 · S_0	
		13 CH_3OH → 2 CO_2 + 9 H_2O + 2 CH_4+ C_2H_6 + C_3H_8 + C_4H_{10} + H_2	100 − S_0 − 3.81	
		14 CH_3OH → Coke + 14 H_2O + 3 CH_4	3.81	
Regeneration reactor	Operating conditions	T [°C] | p [bar]	500 | 3	[80, 164]
	Reaction parameter	Coke combustion [%]	100	[80, 164]
Oligomerization	Operating conditions	T [°C] | p [bar]	250 | 50	[78, 137, 171]
	Reaction parameter	x (Eq. 4-9)	RC: 3; PV: 2–4	-
		α (Eq. 4-9)	RC: 0.69; PV: 0.60–078[b]	-
	Inert gas fraction, controlled by recycle purge		30	-
Hydrogenation	Operating conditions	T [°C] | p [bar]	300 | 50	[159, 160, 171]
	Reaction parameter	Conversion [%]	100	[159, 172]

[a] $\%_C$: percentage of carbon input, [b] see Annex B, Section B.2

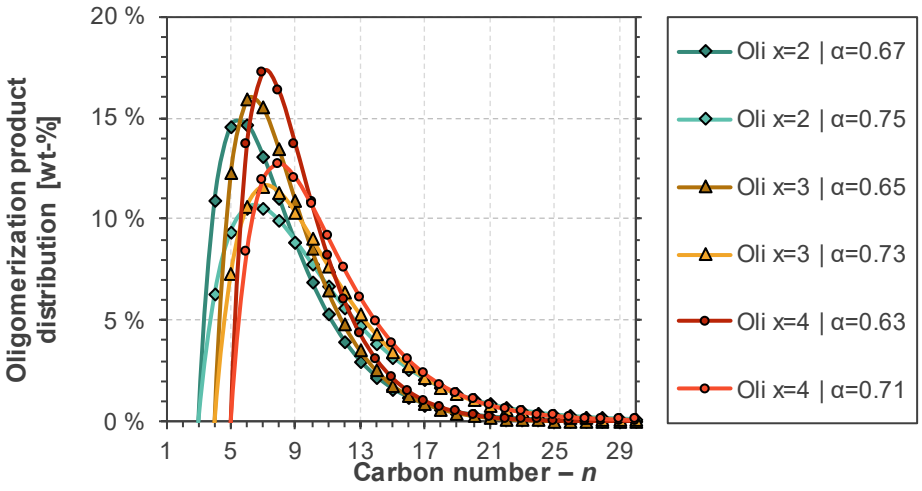

Figure 4-10: Exemplary oligomerization product distributions according to model assumptions (α: chain growth probability; Oli: oligomerization; *x*: parameter of Eq. 4-9).

Here, an ASF distribution starting at butene (x = 2) could be representative of an ethene-based oligomerization with complete conversion. An x-value of 3 leads to a starting point at pentene, which can correspond to an ethene-propene dimer. A completely propene-based oligomerization could lead to a starting point at hexene – assuming complete conversion. Nevertheless, since oligomerization from an olefin mixture is generally assumed, both even and odd carbon chains are present in the product.

4.4 Results and discussion

In this section, the results of the flowsheet simulation are presented and assessed. First, the simulation results are shown in terms of carbon and energy flows. Additionally, the hydrogen flows are depicted in Annex B, Section B.3. The influences of the varied technical parameters on carbon and energy efficiency are presented in the process assessment. Subsequently, the process-specific results of the FT and methanol pathways are comparatively discussed and shown as PtL efficiency (incl. H_2 and CO_2 supply).

4.4.1 Process simulation

The process simulation results are used to visualize and evaluate the relative carbon and energy flows of the reference case processes.

4.4.1.1 Carbon flows

Below, the carbon flows are expressed in relation to the overall carbon input stream for both processes. Theoretically, the carbon can be entirely bound in the kerosene since no carbon-containing by-products occur within the main building reactions. However, due to impurities, side reactions, and only limited controllable chain length distributions, by-products, and carbon losses occur, which are visualized in the flow diagrams (Figure 4-11 and Figure 4-12).

Fischer-Tropsch pathway. Figure 4-11 shows the relative carbon flows of the analyzed FT plant concept. The only carbon input into the process is the CO_2 input steam. This CO_2 is supplied to the RWGS reactor along with the synthesis gas recycle (in terms of carbon, primarily CO, CO_2, and CH_4). Despite the high operation pressure, the high temperature suppresses methane formation within the RWGS reactor. As the methane formed in the FT reactor is largely recycled, RWGS methane reforming outweighs methane formation (RWGS feed: 5.1 mol%$_{CH4}$, RWGS product: 4.4 mol%$_{CH4}$). To prevent the accumulation of inert components, a purge gas stream is diverted from the recycle stream (cold separator) and exits the process after combustion in the form of CO_2 in the flue gas; this results in carbon losses of less than 1 %. Other carbon losses, such as dissolved components in wastewater, are below 0.1 % (and thus not shown in Figure 4-11).

Downstream, approximately 30 % of the FT product consists of heavy components (wax and hot condensate) directed to the hydrocracking unit. Around 7 % of the hydrocracking products are light components (C_{7-}), while about 25 % are within the kerosene and diesel fraction (C_{8+}). The cold condensate divides into about 18 % naphtha and lighter components (C_{7-}) and approx. 54 % kerosene and heavier components (C_{8+}). The light and heavy fractions are fed to a naphtha column and a kerosene column, respectively, to obtain the individual target product fractions. Here, 73 % of the produced liquid products account for the target product kerosene, 21 % for naphtha, and only 6 % for diesel.

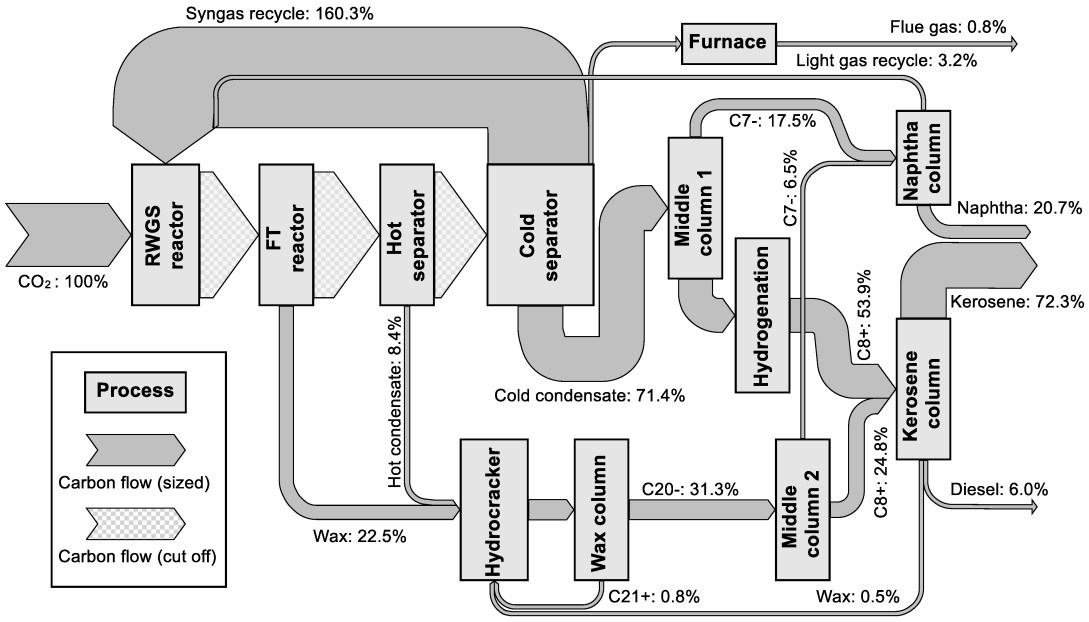

Figure 4-11: Relative carbon flows of the FT pathway (only carbon flow affecting process blocks are shown; RWGS: reverse water-gas shift).

Methanol pathway. The relative carbon flows of the methanol pathway are shown in Figure 4-12. Again, the CO_2 stream serves as the only carbon input. Upstream, methanol production yields a carbon efficiency of almost 98 %, with purge gases being the only significant losses. The major carbon losses occur downstream (i.e., in the MtK process section). During methanol dehydration, approximately 3 % of the carbon is discharged from the

process as coke, which is released as CO_2 in the subsequent catalyst regeneration. In the oligomerization process, carbon losses occur due to removing light alkanes (purge from separator) and regulating inert components (middle column purge), amounting to about 3 and 7 %. The latter can be added to the naphtha fraction in certain proportions. Additionally, carbon losses occur due to heavy components (wax) utilized as an energy carrier within the furnace.

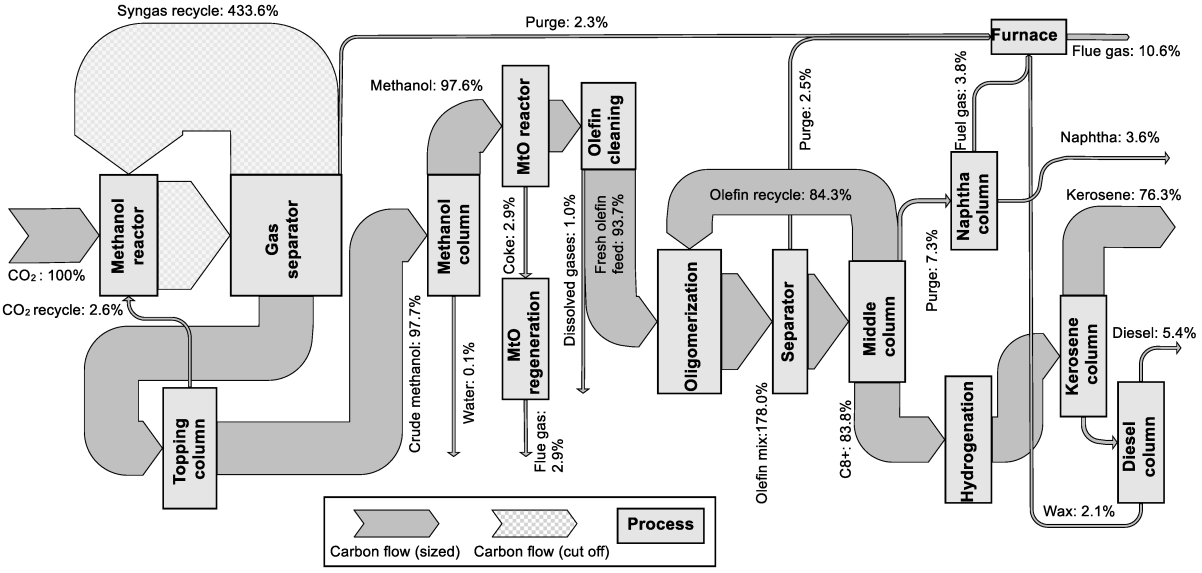

Figure 4-12: Relative carbon flows of the methanol pathway (only carbon flow affecting process blocks are shown; MtO: Methanol-to-Olefins).

With regard to the carbon flows, the kerosene fraction accounts for almost 90 % of the liquid products, while naphtha and diesel represent only 4 and 6 %, respectively.

4.4.1.2 Energetic flows

The specific energy flows are normalized to the total energy input of each pathway to analyze and assess the major energy demands and losses of the process concepts. Thereby, chemical energy (related to the higher heating value), electrical power, as well as heating and cooling demands (thermal energy) are distinguished as energy streams.

Fischer-Tropsch pathway. In the FT pathway (Figure 4-13), hydrogen input accounts for 89 % of the total energy input. The FT synthesis operates at a relatively low pressure level (25 bar) (i.e., no further hydrogen compression is needed). Additionally, the comparatively high syngas conversion of 65 % leads to a rather low recycling ratio. This results in an electricity demand for compression below 2 % of the total energetic input. However, there is a high energy demand for the RWGS process, which cannot be fully supplied through heat integration alone and requires significant additional thermal energy provided by electricity (electrical heating). Due to the efficient recycling steps upstream and further downstream processing of by-products, only a small amount of heat is generated from combusting waste streams in the furnace. A significant cooling demand arises

from the FT synthesis and the product condensation. After heat integration, the overall cooling demand via cooling water is estimated at 9 %, while a further 24 % of the energy can be used for external steam supply; i.e., about 33 % of the energy used in the process is dissipated in the form of heat. Around 10 % of the overall energy is required for heating demands and is provided by electricity. At the end of the overall process, 67 % of the input energy exits in the form of liquid products. Of this, 73 % can be allocated to the kerosene fraction, resulting in a kerosene energetic efficiency of 49 %.

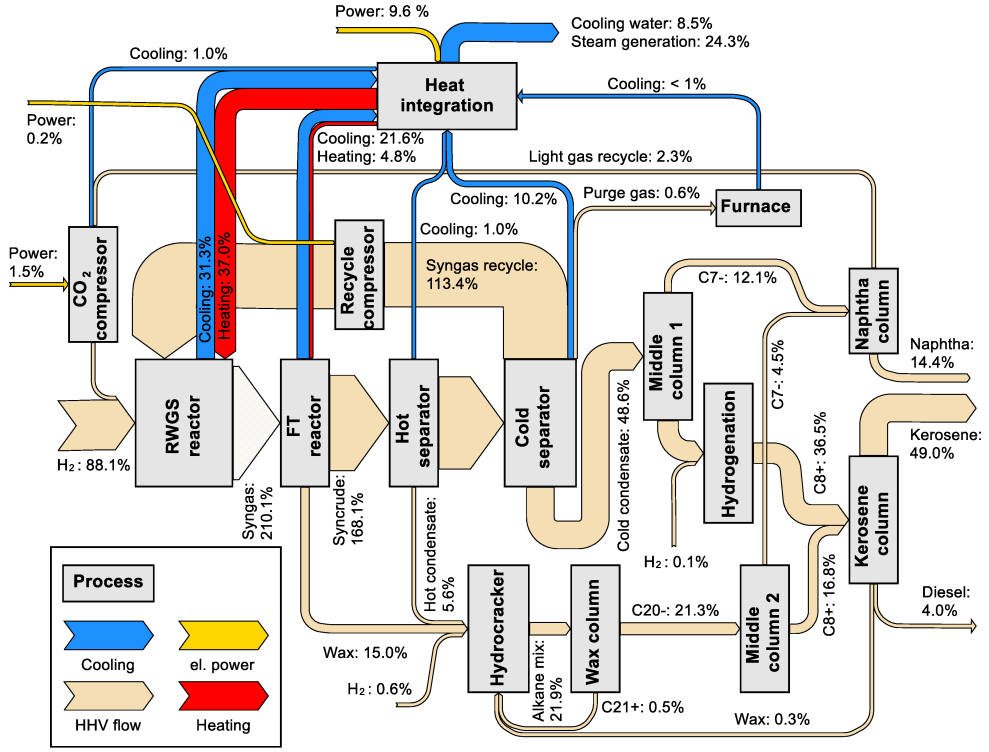

Figure 4-13: Relative energy flows of the FT pathway (heating and cooling below 1 % not depicted; HHV higher heating value; RWGS: reverse water-gas shift).

Methanol pathway. In the methanol pathway (Figure 4-14), the hydrogen input accounts for 94 % of the total energy input. Around 6 % of the total energy input (electrical power) is consumed for gas compression, particularly for the high pressures required for methanol synthesis. As all conversion processes are exothermic, no externally provided heat is required. There are losses associated with the exothermic methanol synthesis reaction. However, significant amounts of heat are needed for methanol purification. The combustion of waste streams generates heat at higher temperature levels (> 900 °C) but leads to lower energy efficiency for the production of liquid fuel products at the same time. After heat integration, the overall cooling demand is estimated to be 38 % (i.e., 62 % cooling water and 38 % steam generation). The liquid product of the process accounts for 62 % of the total energy input; the kerosene fraction amounts to 90 % of these.

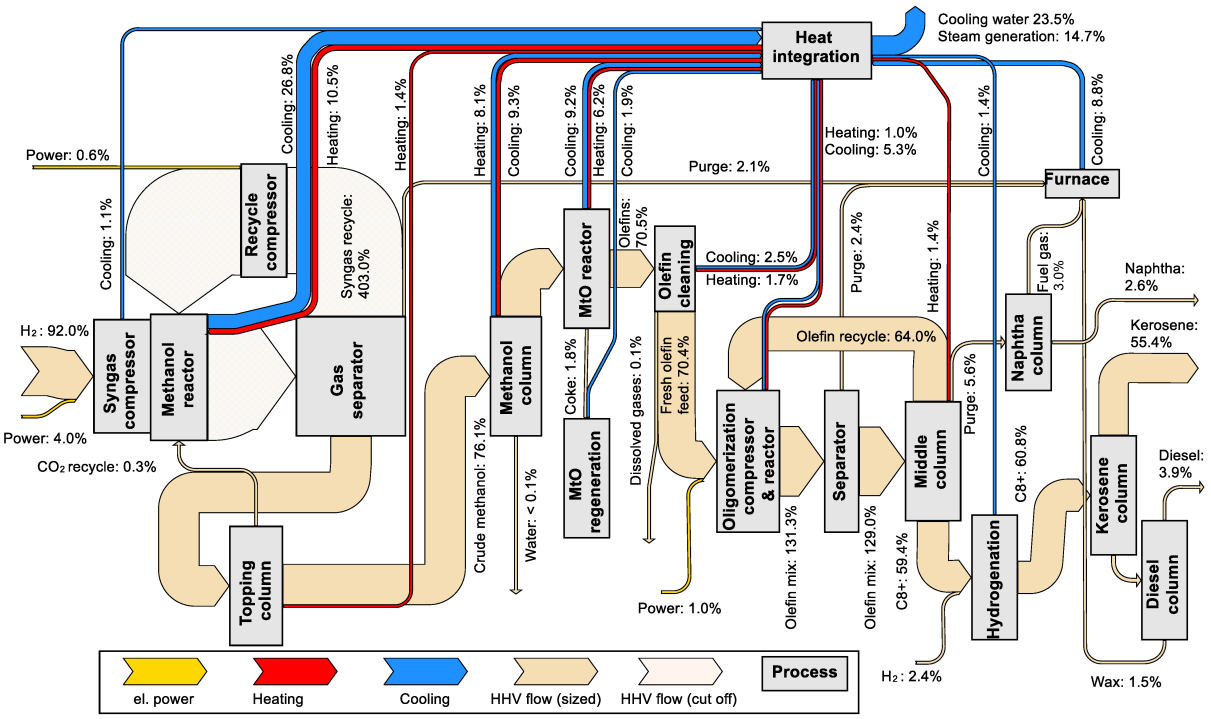

Figure 4-14: Relative energy flows of the methanol pathway (heating and cooling below 1 % not depicted; MtO: Methanol-to-Olefins).

4.4.2 Process assessment

Based on the simulation results described above, the process assessment is carried out. The carbon efficiencies (Section 4.4.2.1) and energy efficiencies (Section 4.4.2.2) of the overall pathways are derived for the reference cases, while the influences of the underlying technology parameter assumptions are assessed through parameter variation. The sensitivity of the key figures regarding the varied parameters also indicates uncertainties and potentially desirable parameter ranges for optimized production.

4.4.2.1 Carbon efficiency

The relative carbon flows shown in Section 4.4.1 represent the carbon efficiencies of the individual product fraction. Figure 4-15 presents the carbon efficiencies applied over the chain growth probability resulting from the simulation of the overall plant. Minor changes compared to the reference case (< 1 %) result from simplified rectification models in parameter variation simulation (Annex B, Section B.2). Below, the results of the FT and the methanol pathway are described.

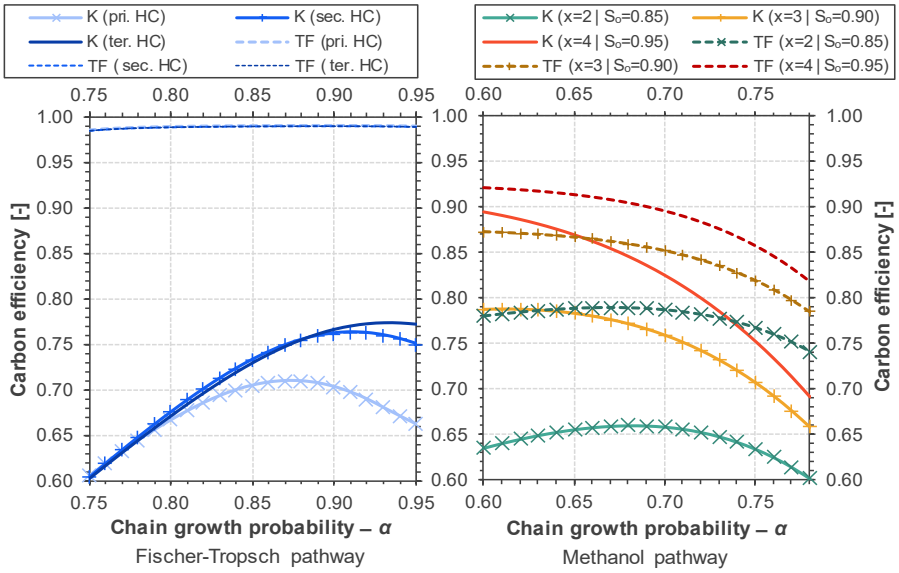

Figure 4-15: Carbon efficiencies of overall Fischer-Tropsch and methanol pathway under parameter variation (HC: Hydrocracking, K: Kerosene, pri.: primary, sec.: secondary, S_0: Olefin-selectivity, ter.: tertiary, TF: Total fuel, x: parameter of Eq. 4-9).

Fischer-Tropsch pathway. In the reference case (secondary hydrocracking, α = 0.85), the kerosene (K) carbon efficiency, which refers to the kerosene fraction, is around 72 %. Together with the naphtha and diesel fractions, this results in an almost ideal total fuel (TF) carbon efficiency of 99 %. In Figure 4-15, left, the influences of the assumed chain growth probability and the considered hydrocracking behaviors on the carbon efficiency are depicted.

- Influence of chain growth probability (α). The chain growth probability is uniformly varied around the reference case (α = 0.85), representing the maximum for straight-run kerosene. The TF carbon efficiency shows minimal changes over the variation range (98 to 99 %). The trend gradually increases, reaching a maximum of 99 % at α-values of 0.90. Shifting left from the maximum, lighter components in the syncrude increase, requiring reforming through the RWGS process and recycling into the synthesis loop. As recycling increases, losses through purge gases increase, leading to decreased TF efficiency. Higher α-values also increase the wax content that subsequently undergoes hydrocracking. The resulting light by-products are also fed back into the RWGS and subsequently into the synthesis loop. As cracking intensifies, the quantity of lighter components formed in the hydrocracker outweighs those formed in the synthesis, leading to a decline in TF efficiency to the right of the maximum with further increasing chain growth probabilities. Regarding the carbon efficiency of K, the maximum shifts towards higher α-values. This is because the decrease in straight-run kerosene is less significant up to a certain point compared to the increase in kerosene formed through hydrocracking. After this chain growth probability is reached, the K carbon efficiency decreases as the diesel fraction within the cracking products increases. This decrease is particularly evident in the case of primary and secondary

cracking, as significantly more C_{17}-C_{20} molecules are formed here, which are subsequently not recycled in the wax column but are removed as diesel in the kerosene column. Therefore, the location of the maximum kerosene efficiency depends on the hydrocracking behavior considered.

- Influence of hydrocracking behavior. The variation of the hydrocracking behavior comprises three cases in which the number of cracking events per-pass is varied (Section 4.3.2). Across all three cracking cases, the K carbon efficiency values range from 60 to 77 %, depending on the α-value. In the case of primary cracking, for chain growth probabilities higher than 0.80, the K carbon efficiency is clearly lower than in the other hydrocracking cases, and thus also the maximum K carbon efficiency (71 % at α = 0.87). However, this maximum shifts towards α-values above 0.90 for secondary and tertiary hydrocracking, with over 76 % (α = 0.91, secondary cracking) and 77 % (α = 0.94, tertiary cracking) of the carbon input bound in kerosene. The differences in K carbon efficiencies concerning the considered cracking scenarios primarily arise from the differential cracking of the diesel fraction (C_{17} to C_{20}). While, in the case of primary cracking, the diesel fraction is separated from the product mixture after hydrocracking, substantial portions of the fraction undergo further cracking in secondary and tertiary processes, diverting them to the naphtha and kerosene fractions instead of ending up in the diesel fraction. Even if the number of cracking operations cannot be controlled to the same extent as in the analysis, the same effect can be achieved in actual plant operation by selectively feeding diesel components back into the hydrocracker, which also allows higher kerosene efficiencies.

Methanol pathway. In the reference case of the methanol pathway (S_0 = 90 %, x = 3, α = 0.69), a TF carbon efficiency of about 85 % is obtained, while the K carbon efficiency reaches 76 %. Figure 4-15, right, illustrates the influences of the ASF starting point (parameter x of Eq. 4-9) and the considered olefin-selectivity over the chain growth probability (α). To independently assess the individual impacts of the varied parameters, the carbon efficiency profiles for the assumed olefin-selectivities are presented separately in Figure 4-16. Subsequently, the influences of the varied parameters are explained separately. However, the influences of the varied parameters are partially interdependent. As a result, the effects cannot be discussed completely separately from each other.

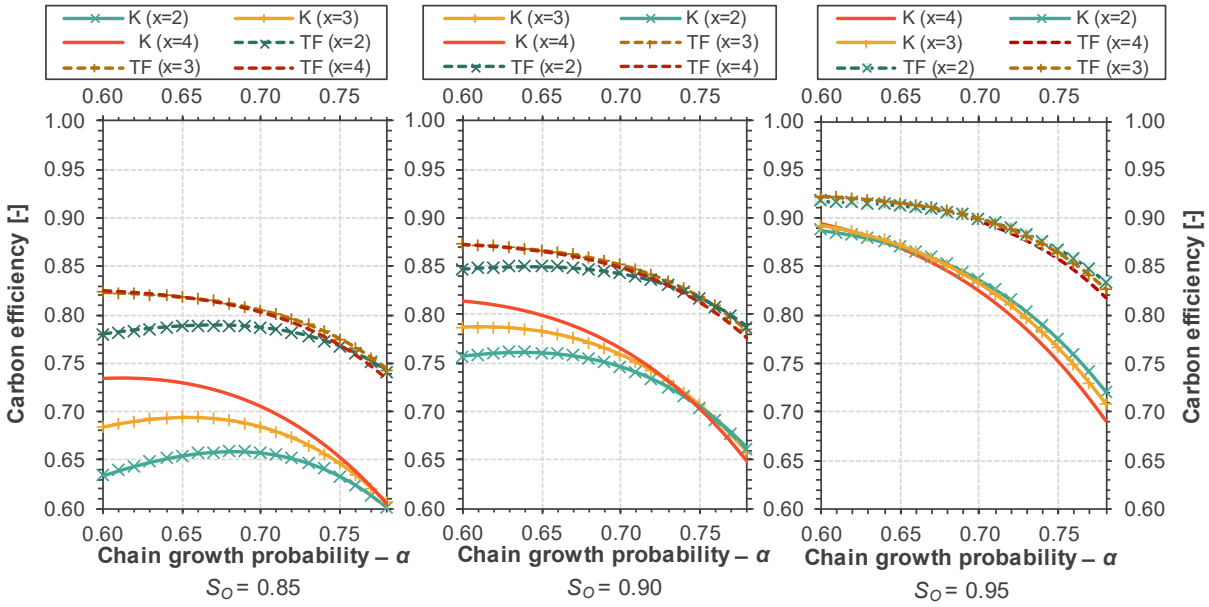

Figure 4-16: Carbon efficiencies of overall methanol pathway under separate S_0 and x-variation (K: Kerosene, S_0: Olefin-selectivity, TF: Total fuel, x: parameter of Eq. 4-9).

- Influence of chain growth probability (α). The chain growth probability is varied below the α-value of maximum straight-run kerosene output (Annex B, Section B.2). This is done because, in the overall process, the lighter naphtha fraction is fed back into the oligomerization, potentially increasing the overall kerosene fraction. The results of the parameter variation confirm this effect since a lower α-value generally leads to a higher K carbon efficiency. Furthermore, the TF efficiency is also positively influenced in most cases by a lower α-value, as the wax fraction, that is used only energetically, decreases.

- Influence of olefin-selectivity (S_0). The results of the parameter variation show that the olefin-selectivity is a decisive parameter that strongly affects the achievable carbon efficiencies. At an olefin-selectivity of 85 % the K carbon efficiency and the TF carbon efficiency are limited to 60 to 73 % and 74 to 82 %, respectively. Raising the olefin-selectivity to 95 %, K carbon efficiency and the TF carbon efficiency are increased to 69 to 90 % and 82 to 92 %, respectively. Direct losses caused by non-ideal olefin-selectivity occur as by-products (alkanes) do not oligomerize and are therefore not further processed into any of the desired product fractions. Indirect losses additionally arise due to the increasing purge requirements with rising amounts of inert alkanes, as this also results in the removal of more valuable olefins – i.e., olefins that could be further processed into the desired product fractions.

- Influence of ASF starting point. The impact of the ASF starting point – which approximates the influence of the olefin-feedstock (monomer) size – on the overall process is also dependent on S_0, which is evidently illustrated by different diagrams. At rather low olefin-selectivities (S_0 = 0.85), a positive influence of larger monomers as oligomerization feed (higher x-values) can be observed. However, this influence of the monomer size on both the K and the TF carbon efficiency decreases significantly with

increasing olefin-selectivities. At higher S_O-values, the carbon efficiencies achieved become increasingly less dependent on the monomer size. Additionally, with higher chain growth probabilities and particularly at increasing S_O-values, the influence of the monomer size even reverses; i.e., the achievable carbon efficiencies decrease as the monomer size increases. This inverse effect is observed for olefin-selectivities of S_O = 0.95 when the chain growth probabilities exceed approximately 0.65 for K carbon efficiency and 0.68 for TF carbon efficiency. The decreasing impact of ASF starting point with increasing S_O primarily results from a lower purge requirement, allowing for more efficient recycling of lighter naphtha. The transition from a positive to a negative effect of larger monomer sizes with increasing chain growth probabilities regarding the K carbon efficiency is primarily due to the shift of the straight-run kerosene fraction towards diesel. Regarding the TF carbon efficiency, this effect is primarily attributed to increased wax formation with higher chain growth probabilities.

Across all variations, the methanol pathway shows high kerosene yields, especially for chain growth probabilities well below the straight-run optimum. This is primarily a result of the direct recycling of the light naphtha fraction. The olefin-selectivity (S_O) of the MtO process is identified as a crucial process parameter, as it strongly influences both kerosene yield and overall yield under the assumptions made. The results suggest that a high olefin-selectivity is more important for the efficiencies of the process than a high straight-run kerosene fraction. Furthermore, the results obtained by the underlying assumptions suggest that low chain growth probabilities starting from higher olefins (x = 4) achieve higher kerosene yields than starting from very light olefins (x = 2) with higher chain growth probabilities. Starting from higher olefins might also influence the smoothness of the product distribution, which is not analyzed here.

4.4.2.2 Energy efficiency

Figure 4-17 shows the energy efficiencies applied over the chain growth probability (α) resulting from the simulation of the overall plant. Minor changes compared to the base case analysis (< 1 %) result from simplified fractionation models in parameter variation (see Annex B, Section B.2). Based on the higher heating values (HHV), a theoretical maximum energy efficiency of 77 % can be cited. The theoretical efficiency is calculated by dividing the energy of the products (assumed here to be $C_{10}H_{22}$ and H_2O) by that of the reactants (H_2 and CO_2), and thus takes into account the losses of the reaction enthalpy of the overall reaction. Since the energy streams of the product fractions are proportional to the respective carbon flows, carbon efficiency directly affects energy efficiency. Furthermore, the main energy input of both pathways results from hydrogen, which also supports a correlation of energy with carbon efficiency as a parameter of material utilization. In tendency, the effects are, therefore, similar to the results shown in Figure 4-15. However, the

variation of technical parameters influences internal process flows and energy requirements, eventually affecting energy efficiency. The resulting deviations from the carbon efficiency and the key figure areas are explained below.

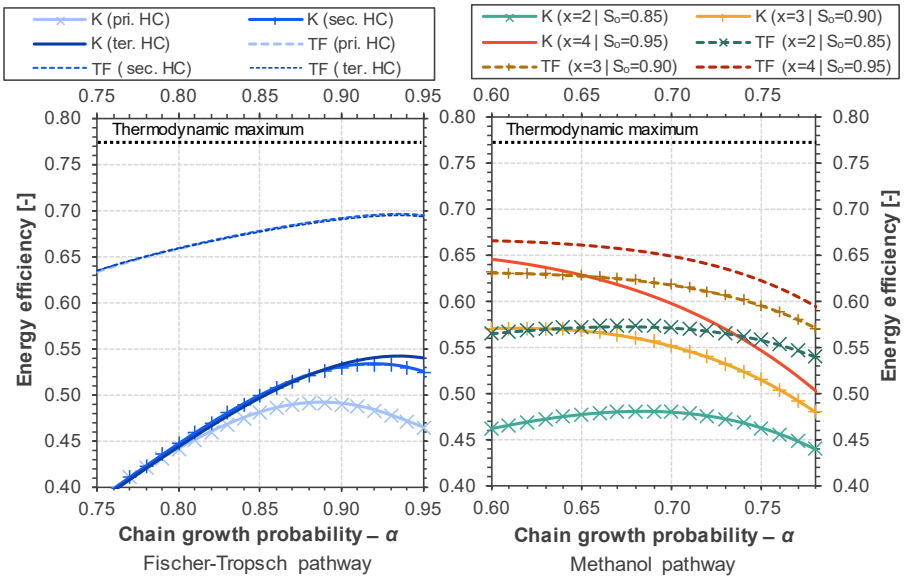

Figure 4-17: Energy efficiencies of overall Fischer-Tropsch and methanol pathway under parameter variation (HC: Hydrocracking, K: Kerosene, pri.: primary, sec.: secondary, S_O: Olefin-selectivity, ter.: tertiary, TF: Total fuel, x: parameter of Eq. 4-9).

Fischer-Tropsch pathway. The energy efficiency in the reference case shown in Section 4.4.1.2 is determined to be 49 % with regard to the energy content of the produced kerosene. The TF energy efficiency, considering the naphtha, kerosene, and diesel fraction, reaches 67 %. Figure 4-17 left, shows the influence of the assumed chain growth probability and the considered hydrocracking behavior on the energy efficiency.

- Influence of chain growth probability (α). The TF energy efficiency shows a stronger sensitivity regarding the chain length probability compared to the carbon efficiency, ranging from 63 to 70 %. This is because at low α-values, the amount of light components reformed in the RWGS (reverse water-gas shift) process significantly increases. The additional energy required for this needs to be covered by external energy (electrical power), resulting in an overall increase in energy demand while the fuel product quantity remains nearly constant. Regarding kerosene, both the amount of produced kerosene (carbon efficiency) and the required energy quantity in the RWGS process decrease with increasing α-values. Therefore, the K energy efficiency still varies in a larger range from 39 to 54 %. The changes in compressor power due to varying process streams are negligible with respect to the overall energy demand.

- Influence of hydrocracking behavior. Between the hydrocracking cases, energy efficiencies behave almost identically to the carbon efficiencies. This is because the different hydrocracking cases have no significant impact on the energy requirements of the overall process, which means that energy efficiency correlates directly with the product quantity.

Methanol pathway. The K energy efficiency of the methanol pathways reference case is determined to be 55 %, while the TF energy efficiency amounts to about 62 %. Figure 4-17 right, shows the influence of the considered ASF starting points and olefin-selectivity over the chain growth probability on the energy efficiency. The results of the parameter variation show a wide range of K energy efficiency (44 to 65 %) and the TF energy efficiency (54 to 67 %).

Since the energy efficiency in the methanol pathway is almost exclusively influenced by the material efficiency, the resulting curves from parameter variation behave similarly to those of the carbon efficiency. More precisely, this is because the varied parameters have no influence on the methanol production efficiency, and changes in the oligomerization recycle with regard to the compressor power are below 0.5 %. For the discussion of the individual influences of the varied parameters, reference is made to the above-described section on carbon efficiency.

4.4.3 Overall comparison

The key figures of both pathways are compared in Figure 4-18. In the following, these are discussed for the carbon efficiency and the energy efficiency. To enable an assessment of the pathways in relation to the entire PtL process chain, the provision of the feedstocks H_2 and CO_2 is additionally included in the energy efficiency at the end of this section.

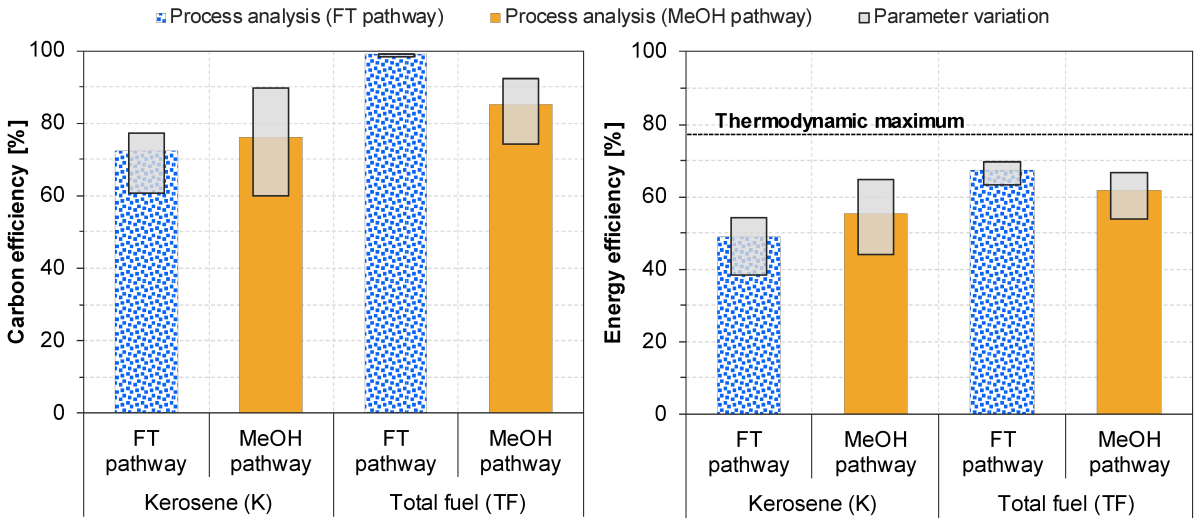

Figure 4-18: Key overall figures of the FT and methanol pathway (FT: Fischer-Tropsch, MeOH: Methanol).

4.4.3.1 Carbon efficiency

Total fuel carbon efficiency. Compared to the methanol pathway, the FT pathway enables a higher TF carbon efficiency through upstream reforming of lighter components and downstream hydrocracking of heavier components, with only minor losses occurring in the synthesis loop. The carbon efficiency sums up to approximately 99 %, varying only

within a relatively small range within the parameter variation. While the methanol synthesis itself is highly selective, the lower per-pass conversion results in purge losses exceeding those of the FT synthesis. However, the major carbon losses in the methanol pathway occur in the MtK process due to a limited selectivity in dehydration, which also determines carbon losses in oligomerization. Overall, this leads to a lower TF carbon efficiency of about 85 %. The value shows a higher variation from 74 to 92 % in the parameter variation compared to almost constant TF carbon efficiency in the FT pathway.

Kerosene carbon efficiency. Despite the overall carbon losses in the reference case, the methanol pathway has a higher K carbon efficiency (76 %) compared to the FT pathway (72 %). This is due to the narrower product distribution and the recycling of the light naphtha product fraction. Nevertheless, depending on the parameters considered, the parameter variation shows a wide range from 60 to 90 %, whereby the influence on the technical parameters and, thus, the achievable efficiencies currently appear to be limited. The range in the FT pathway is also comparably wide, reaching from 61 to 77 %. However, since the chain growth probability in the FT synthesis can be well adjusted through catalysts and process conditions, optimizing the overall process towards the upper values of kerosene efficiency is realistic.

In addition to the kerosene yield, the composition of the fraction also differs (Annex B, Section B.3). The methanol pathway analyzed here yields a kerosene fraction with a high proportion of light components. In contrast, the kerosene fraction formed in the FT pathway is more uniform and potentially easier to process into ASTM-compliant fuel.

4.4.3.2 Energy efficiency

The comparison of the FT against the methanol pathway depicted in Figure 4-18, shows that, compared to the carbon efficiency (left), the methanol pathway has shifted upwards in terms of the energy efficiency (right). This can be explained due to the thermodynamic advantage of the methanol pathway, where only exothermic processes occur, and no additional energy is required for CO_2 reduction or recycle gas reforming.

Total fuel energy efficiency. Concerning energy efficiency, hydrogen is the largest energy input for both pathways. The FT pathway also requires a significant additional heating demand, mainly caused by the RWGS. In the methanol pathway, all reaction steps are exothermic, allowing to cover all heating demands through heat integration. However, higher electrical energy requirements for compression are needed compared to the FT pathway. Due to the low material losses, manifesting as energy losses due to combustion in the furnace, the FT pathway achieves higher total fuel (TF) energy efficiencies (67 %) than the methanol pathway (62 %) in the reference case. The parameter variation of the FT pathway shows a wider range of TF energy efficiency (63 to 70 %) compared to the TF carbon efficiency. This is due to an increasing energy demand of the RWGS at lower chain

growth probabilities, which leads to a higher reforming effort. In contrast, almost no energetic influences besides the material efficiency occur in the methanol pathway; i.e., the energy efficiency behaves similarly to its carbon efficiency ranging from 54 to 67 %.

Kerosene energy efficiency. In terms of K energy efficiency, both pathways show a similar behavior as with regard to carbon efficiency. However, the methanol pathway is more clearly above the FT pathway in terms of energy than is the case for carbon. The reference case results are 55 % and 49 %, respectively. The methanol pathway ranges from 44 to 65 %, while the FT pathway reaches 38 to 54 %. Comparing the lower end of the K efficiencies demonstrates the thermodynamic advantage of the methanol pathway. While both pathways are almost equal in terms of carbon, the methanol pathway exceeds the FT pathway in terms of energy by more than 5 %.

Power-to-liquid efficiency. The previously discussed efficiencies pertain to the system boundaries chosen within the analysis, i.e., H_2 and CO_2 are available as pure components. To make statements about the efficiencies of the entire production chain of power-based kerosene, the efforts or losses in feedstock supply must be considered. The energy efficiency starting from electrical power, including H_2 provision and CO_2 capture, is depicted in Figure 4-19. The energy requirements of electrolysis depend on the chosen technology and vary within the efficiency range for low-temperature electrolyzers. The energy expenditure for CO_2 capture is highly contingent on the CO_2 source and the availability of heat ($T > 100$ °C). The illustration distinguishes three cases. In one case, pure CO_2 ("pure"), e.g., from ethanol fermentation, is considered, eliminating the need for further efforts. Case two ("point") represents capture via amine scrubbing from point sources (10 to 40 vol% CO_2). Additionally, capture through a direct air capture facility ("DAC") is considered. In both capture cases, no heat integration is assumed.

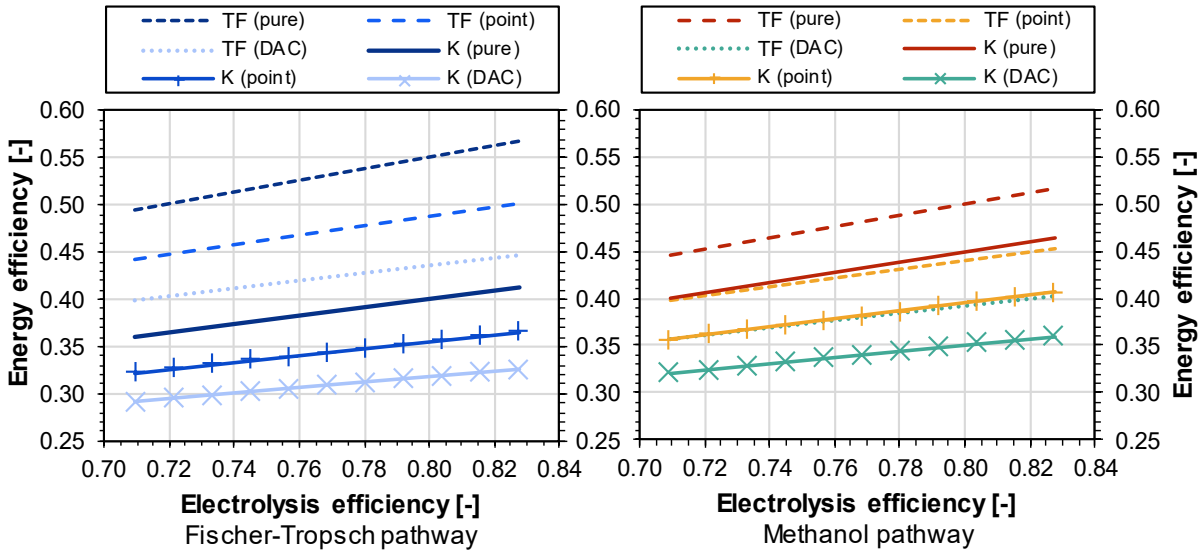

Figure 4-19: Energy efficiency considering H_2 production and CO_2 supply (all efficiencies based on HHV; DAC: Direct air capture, K: Kerosene, point: CO_2 point source, pure: pure CO_2, TF: Total fuel).

Depending on the electrolyzer efficiency, the total fuel (TF) efficiency in both pathways decreases by 10 to 18 %pt. The overall efficiency is thus 49 to 57 % (46 to 53 %$_{LHV}$) for the FT pathway and 45 to 52 % (41 to 48 %$_{LHV}$) for the methanol pathway. If CO_2 needs to be additionally captured from a point source with no heat integration possible, the efficiency further decreases by approximately 6 %pt to 44 to 50 % (41 to 47 %$_{LHV}$) for the FT pathway and 40 to 45 % (37 to 42 %$_{LHV}$) for the methanol pathway. In the absence of a point source, requiring CO_2 to be captured from the air, the efficiencies further decline to 40 to 45 % (37 to 42 %$_{LHV}$) for the FT pathway and 36 to 40 % (33 to 37 %$_{LHV}$) for the methanol pathway. The provision of feedstocks H_2 and CO_2 plays a significant role in overall efficiency. Since the efficiency of synthesis and downstream processes directly determines the demand for feedstock, any conversion losses occurring here directly increase the losses in feedstock provision.

4.5 Conclusion

This research paper investigates and compares the FT and methanol pathway from power-derived syngas within an in-depth technical analysis. The main findings can be summarized as follows.

- Concerning carbon efficiency, the FT pathway enables very high efficiencies regarding to the total fuel (TF) yield (approx. 98 to 99 %). However, due to FT synthesis's relatively broad product distribution, the specific kerosene selectivity and, thus, the kerosene (K) carbon efficiency are clearly lower (approx. 60 to 79 %). The concept of the methanol pathway exhibits a higher K efficiency (approx. 60 to 90 %) but a significantly lower TF efficiency (approx. 74 to 92 %). This is due to, on the one hand, the high proportion of straight-run kerosene and the recycling of light olefins (naphtha fraction), but, on the other hand, losses through limited olefin-selectivities and the inability to further process heavy components.

- Concerning energy efficiency, hydrogen feed accounts for the highest energy input in both pathways, constituting more than 89 %. Therefore, energy efficiency is closely linked to material efficiency, meaning that higher material or hydrogen losses within the overall process result in a lower energy efficiency. Consequently, due to minor material losses, the FT pathway shows a higher TF energy efficiency of 67 % (72 %$_{LHV}$) compared to the methanol pathway with 62 % (67 %$_{LHV}$). However, the latter still shows a higher kerosene energy efficiency of 55 % (60 %$_{LHV}$) against 49 % (53 %$_{LHV}$) within the FT pathway. Also, the methanol pathway offers advantages since no high-temperature heat is required. In the FT pathway, the RWGS reaction necessitates significant energy input, which is subsequently released at a lower energy level in the FT synthesis. A CO_2-based methanol synthesis ensures that the entire methanol pathway consists of exothermic processes and minimizes losses from a thermodynamic perspective. To determine the overall PtL efficiency, the H_2 and CO_2 supply must also be

taken into account, which significantly reduces the energy efficiencies of the overall production.

- Based on the parameter variation, significantly higher uncertainties arise with regard to the evaluation of the methanol pathway. This is indicated by the strong sensitivity in K and TF efficiency, especially concerning the olefin-selectivity and the chain growth probability. In contrast, the FT pathway's assumptions, parameters, and results suggest lower uncertainties since more data are available in the literature, and the overall process shows lower sensitivities regarding the varied parameters.

Building upon this technical analysis, further theoretical considerations can be pursued to enable a more comprehensive evaluation of the two pathways. This includes additional technical analysis considering different plant concepts (e.g., 100 % kerosene plants or combined technology approaches) and economic and environmental analysis. Furthermore, theoretical and practical product quality investigations are necessary to optimize both pathways in terms of yield and fuel quality.

5 Cost analysis of kerosene production from power-based syngas via the Fischer-Tropsch and methanol pathway

Bube S, Voß S, Quante, G, Kaltschmitt M (2024): Cost analysis of kerosene production from power-based syngas via the Fischer-Tropsch and methanol pathway. In Fuel 384 133901. DOI: 10.1016/j.fuel.2024.133901

The article can be found online at
https://doi.org/10.1016/j.fuel.2024.133901

Formatting and wording are slightly adjusted to ensure consistency throughout this thesis.

Abstract

Current estimates for power-based kerosene production costs are up to ten times higher than conventional, fossil fuel-based kerosene prices. Therefore, successful market integration necessitates a thorough understanding of the cost structure and the key factors influencing kerosene production costs. This paper provides an extensive cost analysis of power-based kerosene production comparing two different plant concepts, one using the Fischer-Tropsch synthesis and hydrotreatment (FT pathway), the other applying direct methanol synthesis with downstream dehydration and oligomerization (MeOH pathway). Two cost allocation methods are applied to address uncertainties associated with unpredictable by-product revenues: allocating costs solely to the kerosene fraction, without considering by-product revenues, establishes the upper cost limit, while allocating costs at the total fuel fraction, defines the lower cost boundary. For these two cases, possible cost ranges are evaluated by varying technical and economic frame conditions. For the "total fuel allocation", the FT pathway yields lower kerosene production cost than the methanol pathway (FT: 3,630 €/t, MeOH: 4,240 €/t). But contrarily for the "kerosene allocation", the MeOH pathway shows lower cost (FT: 5,070 €/t, MeOH: 4,660 €/t). By-product revenue variation indicates benefits for the FT pathway if naphtha prices above 30 % of the kerosene production cost can be achieved. In all cases, costs are mainly affected by the supply of H_2 and CO_2; thus, feedstock conversion efficiency is the most important factor determining the production costs besides feedstock prices. While variations in the H_2 price (3 to 7 €/kg) significantly influence kerosene production costs for both pathways (ca. ±25 %), CO_2 prices at the level of CO_2 supply costs from DAC (1,000 €/t) can lead to even higher cost increases of up to 75 % compared to CO_2 prices related to carbon capture costs from point sources (150 €/t). Thus, this analysis provides novel insights into the cost composition and the most important influencing parameters for the two most widely discussed production pathways for power-based kerosene production and enables comparison and assessment of production costs under different framework conditions.

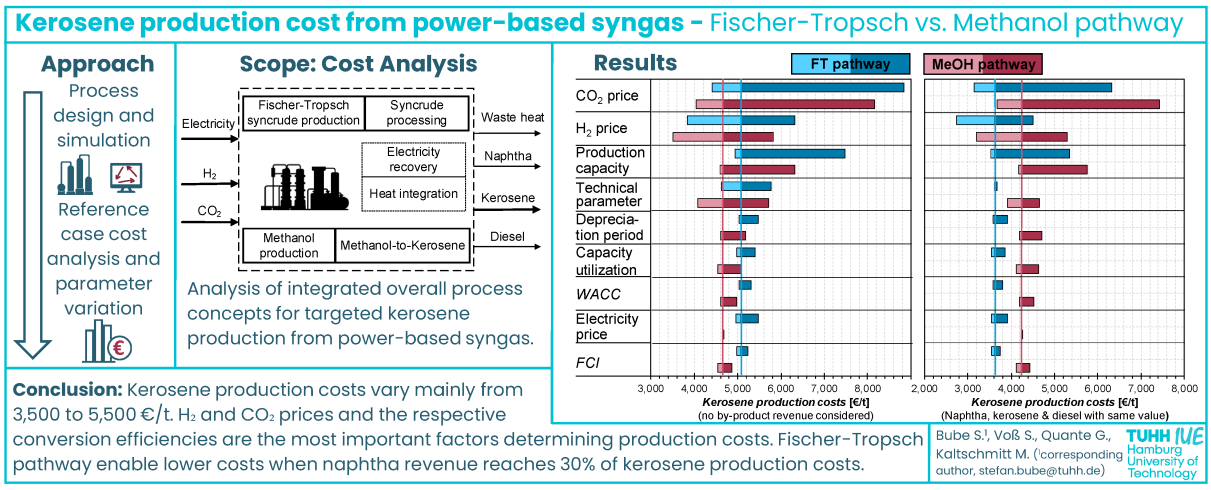

Figure 5-1: Graphical abstract of the publication "Cost analysis of kerosene production from power-based syngas" (*WACC*: Weighted average cost of capital, *FCI*: Fixed capital investment).

5.1 Introduction

The global aviation sector strives to achieve net carbon dioxide neutrality by 2050 [9, 10]. However, extensive decarbonization through direct electrification or using hydrogen (H_2), the most widely discussed options for land transport, seems technically and systemically unfeasible on a large scale for air transportation in the coming decades [38, 173, 174]. Furthermore, the globally available potential of biomass-based kerosene is limited due to the a priori restricted availability of sustainable biomass, enforced by significant competition from other sectors [11]. Consequently, fuels produced from renewable electricity and non-energetic feedstock (H_2O and CO_2), so-called power-based[10] or e-kerosene, are expected to play an essential role in reducing aviation's carbon dioxide emissions. The most common and widely developed pathways for producing power-based kerosene are the Fischer-Tropsch (FT) and the methanol (MeOH) pathway.

Technically, the production of power-based kerosene is feasible, though it has not yet been commercially implemented [50, 175]. The primary reason for the lack of commercially operated, large-scale production plants is economic uncertainty despite manageable technical risks. There is currently no established market for power-based kerosene, making long-term revenue projections difficult. Furthermore, studies indicate up to ten times higher production costs than fossil fuel-based kerosene and two- to threefold higher costs than biomass-based kerosene [46–49, 83, 176, 177]. In a comprehensive analysis, Seymour et al. [178] analyzed the influence of geographical location on the production costs of power-to-liquid fuels and showed that in the medium term, even in very promising locations, the production costs are still significantly higher compared to conventional kerosene prices. Colelli et al. [179] analyzed a. o. production costs for power-based kerosene from FT synthesis, assessing indirect FT synthesis (incl. reverse water-gas shift reaction (RWGS) for CO_2 reduction) as technically and economically more beneficial compared to a direct CO_2-converting FT synthesis. The analysis from Raab and Dietrich [180] also takes supply chain aspects into account and finds that these only make a small contribution to the overall power-based kerosene costs. In a recently published detailed analysis of decentralized Fischer-Tropsch concepts, Meurer et al. [181] demonstrate that the advantages of decentralized production primarily stem from the reduction of indirect plant costs for modular units, although there are also disadvantages due to efficiency losses. Peacock et al. [182] investigated large-scale SAF production using FT synthesis, emphasizing the importance of a constant energy supply to achieve lower fuel production costs. While many available analyses provide a sound basis for general cost estimates of power-based fuel, differences within possible production pathways and influences of by-product revenues (and the respective cost allocations) are rarely considered. Moreover, most studies assume fixed technical and economic parameters, sometimes greatly influencing the cost outcomes and thus limiting the usability of the results. However, detailed

[10] In this paper, power is used as a substitute for electricity, as the production technology is a power-to-x process, whereby power is used as an accepted term for electricity.

consideration of process requirements and frame conditions is essential to compare different process pathways and identify the respective advantages and disadvantages. Recent technical analyses that compare process pathways at a high level of detail provide a suitable basis for economic considerations [138, 175, 183].

Against this background, this paper addresses these research gaps by providing a comprehensive cost analysis of kerosene production from power-based syngas, comparing two different plant concepts, one using the Fischer-Tropsch synthesis and hydrotreatment, the other applying direct methanol synthesis with downstream dehydration and oligomerization. This study provides valuable insights into both pathways' economic differences and advantages by evaluating the individual kerosene production cost based on identical system boundaries and framework conditions. Different cost allocations are applied to address uncertainties associated with unpredictable by-product revenues. An extensive variation of technical and economic parameters is carried out to derive sound cost ranges and to identify advantageous conditions for the respective process pathways.

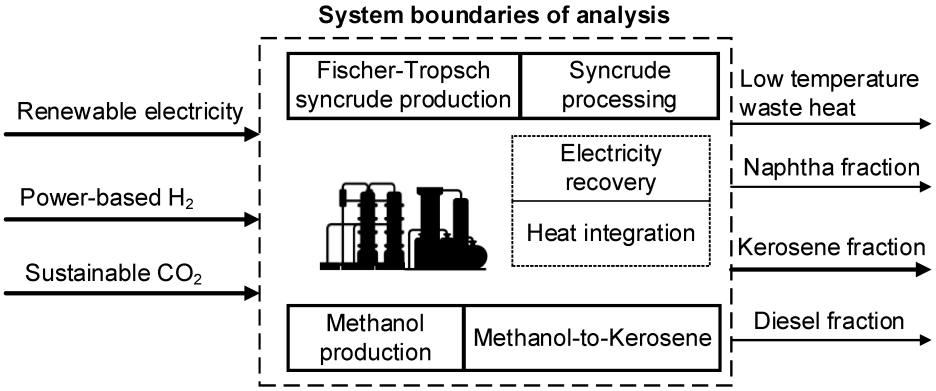

Figure 5-2: System boundaries of considered power-based kerosene production pathways.

The considered system boundaries with the primary process in- and outputs are depicted in Figure 5-2. The analysis focuses on the synthesis and downstream processing, considering H_2 and CO_2 as feedstock. Kerosene is the targeted product, while naphtha and diesel are considered as by-products. The fuel fractions are categorized based on the chain length of the molecules. According to the system boundaries and in line with the general power-to-liquid (PtL) concept, electricity is considered as the primary energy source and, therefore, also for heat provision. Internally produced heat that exceeds the integrable quantity is considered for re-electrification via steam turbines so that only low-temperature heat (removed via cooling water) is produced in addition to the fuel products. The underlying concepts for the respective technical processes and simulation approaches are based on an in-depth technical analysis conducted by Bube et al. [175] (Chapter 4). Therefore, only the main technical results are outlined in this study.

This paper is structured as follows. The methodology section details the production cost calculation methodology and the considered cost allocations. The subsequent section pre-

sents the main technical and economic assumptions, including the technical process concepts, feedstock prices, capital and operating expenditures, and variation parameters. The results of the analysis are then presented, including the process simulation results, detailed cost breakdowns, and parameter variation analysis. Finally, the results are summarized and discussed, and conclusions are derived.

5.2 Cost analysis methodology

Figure 5-3 sketches the methodology used for the cost analysis based on prior process design and simulation. Cost calculation requires technical process data like operating conditions as well as mass and energy flows. The respective data is derived using steady-state flowsheet simulation, whereby the process design and simulation are mainly based on Bube et al. [175]. Modifications to the process concepts and modeling are defined in Section 5.3.1 and Annex C. The cost analysis of the investigated process pathways is conducted for the presented process configurations and based on the described modeling approaches. Thus, the results are directly related to the specific process design, while alternative process concepts may lead to different results.

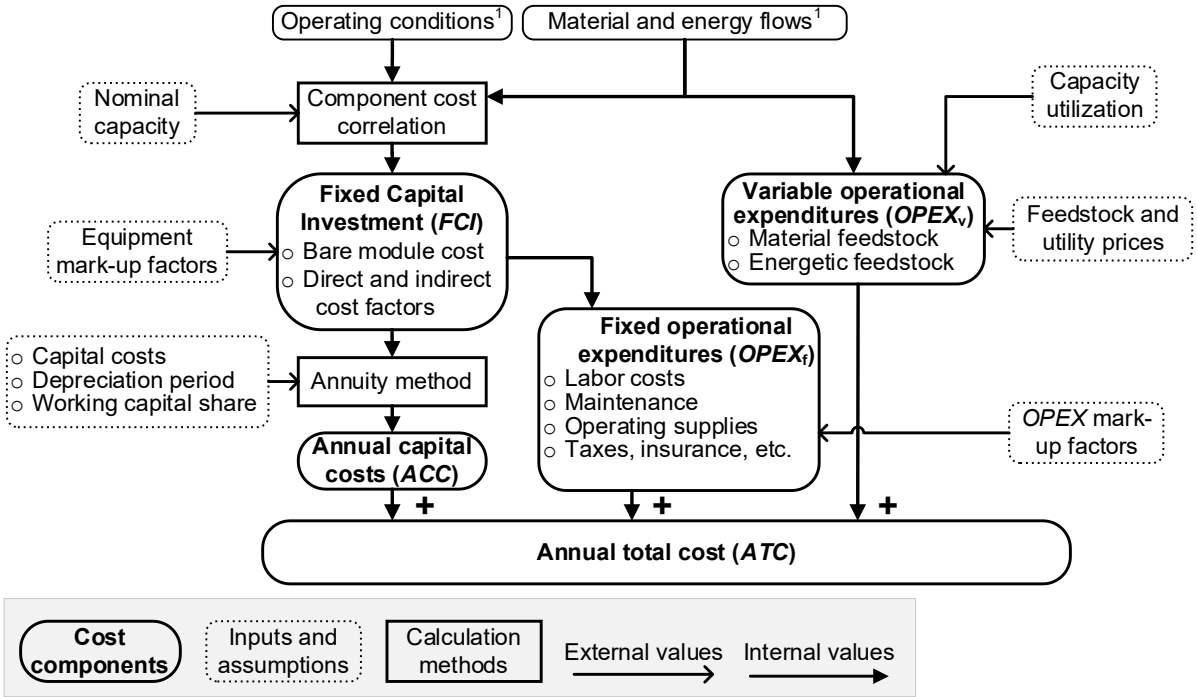

Figure 5-3: Overall production cost calculation methodology ([1] based on process design and simulation in accordance with [175]).

The cost analysis aims to derive and compare kerosene production costs from the analyzed process concepts under defined framework conditions. The individual cost components are analyzed at fixed technical and economic parameters (reference case, RC) (Section 5.4.2). The influence of selected parameters on total costs is examined within a parameter variation (PV) (Section 5.4.3).

The kerosene production cost represents the minimum required selling price to achieve economic feasibility in power-based fuel production (i.e., to cover all costs without assuming profit). According to Eq. 5-1, the annual total cost (ATC) consists of the annual capital costs (ACC), the fixed operational expenditures ($OPEX_{\mathrm{f}}$) and the variable operational expenditures ($OPEX_{\mathrm{v}}$). The latter represent the material and energy feedstock, while the fixed operational expenditures are costs considered to be independent of the product amount (e.g., labor, taxes, overheads, maintenance). The annual total cost can be transformed into kerosene production costs (KPC) according to Eq. 5-2, using different allocations with or without considering by-product revenues. Within multi-product generation plants, achievable prices for the by-products (here, power-based naphtha and diesel) can significantly impact the production cost of the targeted product (here, kerosene). Given the absence of established markets for power-based fuels and the reliance of their future value on the evolving regulatory framework, it is currently difficult to make reliable price assumptions. This analysis employs two different cost allocation approaches to address this challenge, providing an upper and lower bound for kerosene production costs and defining an expected cost range. The cost allocations impacting Eq. 5-2 are presented in Table 5-1.

- Within the kerosene allocation (KPC_{K}), only the kerosene fraction is considered a valuable product, with no by-product revenues accounted for, establishing the upper cost boundary.
- Conversely, the total fuel allocation (KPC_{TF}) assumes all fuel fractions (naphtha, kerosene, diesel) as valuable products, resulting in equal production costs for all fractions and defining the lower cost boundary.
- A variation of by-product revenues (BPR) is used to analyze trends in kerosene production costs (KPC) across both pathways and identify favorable BPR ranges for each pathway.

$$ATC = ACC + OPEX_{\mathrm{f}} + OPEX_{\mathrm{v}} \qquad \text{Eq. 5-1}$$

$$KPC = \frac{ATC - m_{\mathrm{BP}}\, BPR}{m_{\mathrm{P}}} \qquad \text{Eq. 5-2}$$

Table 5-1: Allocation cases according to Eq. 5-2 (BPR: By-product revenue).

Key figure	Abbreviation	Product ($_{\mathrm{P}}$) | By-product ($_{\mathrm{BP}}$) [t]	BPR [€/t_{BP}]
Kerosene allocation	KPC_{K}	Kerosene | none	0
Total fuel allocation	KPC_{TF}	Naphtha, kerosene, diesel | none	0
Kerosene production cost	KPC	Kerosene | naphtha, diesel	varied

The annual production (m) is given by the nominal hourly output ($\dot{m}$) multiplied by the average capacity utilization (u) and the hours of one year (Eq. 5-3).

$$m = \dot{m}\ u\ \ 8{,}760\,\mathrm{h/a} \qquad \text{Eq. 5-3}$$

Annual capital cost. The annuity method (Eq. 5-4) determines the annual capital cost. The capital required for the construction of the plant (fixed capital investment; *FCI*) is depreciated over the depreciation period (n [a]), taking into account the real weighted average cost of capital (*WACC*, i) and the working capital share (ω) [144].

$$ACC = FCI\ \frac{i\ (1+i)^n}{(1+i)^n - 1} + FCI\ \omega\ i \qquad \text{Eq. 5-4}$$

The fixed capital investment is derived using the module costing technique, a method for providing preliminary investment estimates for a.o. chemical plants [144]. This estimate is based on the major process equipment (k), which is roughly dimensioned using process design and simulation data. The size attribute A (e.g., area, volume, power, etc.) is used to calculate bare module costs (C_{P}^{0}) via equipment-specific component cost correlations (Eq. 5-5) with empirical correlation parameters (K_{x}) given by Turton et al. [110]. The bare module costs are multiplied by equipment-specific mark-up factors, which depend on ($F_{\mathrm{BM},l}$) or are independent of ($F_{\mathrm{BM},l}^{0}$) operating conditions and construction material. The sum of all equipment costs multiplied by further mark-up factors for contingency and fee costs (γ) and auxiliary costs (β) results the fixed capital investment. This cost calculation method can be classified as a study estimate with an expected accuracy range of −30 to +50 % [111].

$$\log_{10}(C_{\mathrm{P}}^{0}) = K_1 + K_2 \log_{10}(A) + K_3 [\log_{10}(A)]^2 \qquad \text{Eq. 5-5}$$

$$FCI = (1+\gamma) \sum_{l=1}^{k} C_{\mathrm{P},l}^{0}\, F_{\mathrm{BM},l} + \beta \sum_{l=1}^{k} C_{\mathrm{P},l}^{0}\, F_{\mathrm{BM},l}^{0} \qquad \text{Eq. 5-6}$$

Fixed operational expenditures include labor costs, costs for maintenance, operating supplies, and other charges for royalties, distribution and selling, research and development, and so on. These costs are largely independent of production volumes. Empirical factors are used to estimate the individual cost items based on the fixed capital investment. Labor costs calculation is, among others, based on an estimate of the operating employee to allow for an uninterrupted operation throughout a calendar year.

Variable operational expenditures include costs for material and energetic inputs, i.e., H_2, CO_2, and electricity. The respective requirements are based on the process simulation and the technical evaluation of the plant concept specified in Section 5.3. The specific prices to be applied are determined in accordance with the literature and vary within foreseeable ranges in the parameter variation. For feedstock for which there is currently no established market, the prices are defined based on the expected production costs.

Parameter variation. The variation of technical and economic parameters derives potential cost ranges and uncertainties resulting from different framework assumptions. For the variation of technical parameters, higher-level process parameters (e.g., conversion rates, selectivity) were chosen in line with the applied process modeling and, if applicable, defined in accordance with the state-of-the-art. The process concepts are simulated and analyzed for each varied parameter, whereby the same process conditions (e.g., inert gas concentrations, synthesis gas compositions, etc.) are ensured by defined design specifications. Since the varied higher-level process parameters can be achieved through multiple combinations of underlying operating conditions and design aspects (e.g., temperature, pressure, space velocity), which may interact in complex ways, such underlying parameters are considered constant during the parameter variation. This approach enables a more general evaluation at the system level with a manageable number of variables to be adjusted. The economic parameter variation is carried out for the technical reference case.

Further information on kerosene production cost calculation can be found in Annex C.

5.3 Data and assumptions

5.3.1 Technical concept assumptions

The following briefly describes the technical process concepts, the main assumptions, and the decisive technical parameters. Detailed information about the considered technologies, the respective modeling approaches, and the technical process analysis are available in [175], respectively Chapter 4). Below, in particular, the differences made to [175] are highlighted.

The feedstocks H_2 (100 vol%$_{H2}$, 50 bar, 35 °C [65, 142]) and CO_2 (99.5 vol%$_{CO2}$, 0.5 vol%$_{N2}$, 1 bar, 35 °C [184]) are assumed to be available at the plant site. Process energy is constantly available grid electricity, covering the given electricity and heat demands. The fuel fractions naphtha (C_5 to C_8), kerosene (C_9 to C_{17}) [83, 185], and diesel (C_{18} to C_{20}) can occur as material process outputs. The chain lengths included in the kerosene fraction are selected to ensure that ASTM conformity would be expected in real production processes. However, due to the lower component diversity in the simulation (no iso-alkanes, no cyclic components) compared to real products, ASTM conformity cannot be verified within the scope of the study. The properties of the kerosene fractions from the simulation, as well as the ASTM requirements, are presented and discussed in Annex C, Section C.4.

Three utility systems are considered in addition to the main processes. Vacuum generators are considered according to [186] (0.05 bar$_a$), enabling the rectification of heavy hydrocarbons at lower temperatures. Steam turbines serve to recover excess process heat as electricity, while furnaces are employed to generate high-temperature heat from light fuel gases. Heat integration (pinch analysis) is used to reduce external energy demands.

Since excess heat is utilized in the steam turbines, only low-temperature waste heat (cooling water at 25 °C) leaves the system boundaries. A detailed description of the energy integration approach and the considered utilities is provided in Annex C, Section C.1.

5.3.1.1 Fischer-Tropsch pathway

Figure 5-4 shows a block flow diagram of the FT pathway. The synthesis gas (syngas) production is carried out via a high-temperature (950 °C) reverse water-gas shift (RWGS) reaction, enabling parallel reforming of light hydrocarbons. The H_2:CO ratio in the produced syngas is set to 2.05 by adjusting the H_2 feed into the RWGS reactor. As the heat integration of the RWGS has a major influence on the overall efficiency of the process [187], feed gas preheating with the product gas is assumed. However, to counteract coking and metal dusting, the steam-to-carbon ratio in the reactor feed is set to 0.5[11]. Furthermore, preheating with product gas is limited to 200 K below the reactor temperature to enable rapid product gas cooling[12]. High-alloy nickel clad is chosen as a constructional countermeasure for the affected RWGS equipment [189]. The syngas is converted into synthetic crude oil (syncrude) using a low-temperature FT synthesis (LTFT) to produce a product mixture rich in long-chain hydrocarbons that is favorable in terms of overall process efficiency [175]. Heavy hydrocarbons (C_{18+}) are cracked via hydrocracking. Deviating to [175], hydrocracking is also applied to the diesel fraction. Thus, only naphtha and kerosene are produced.

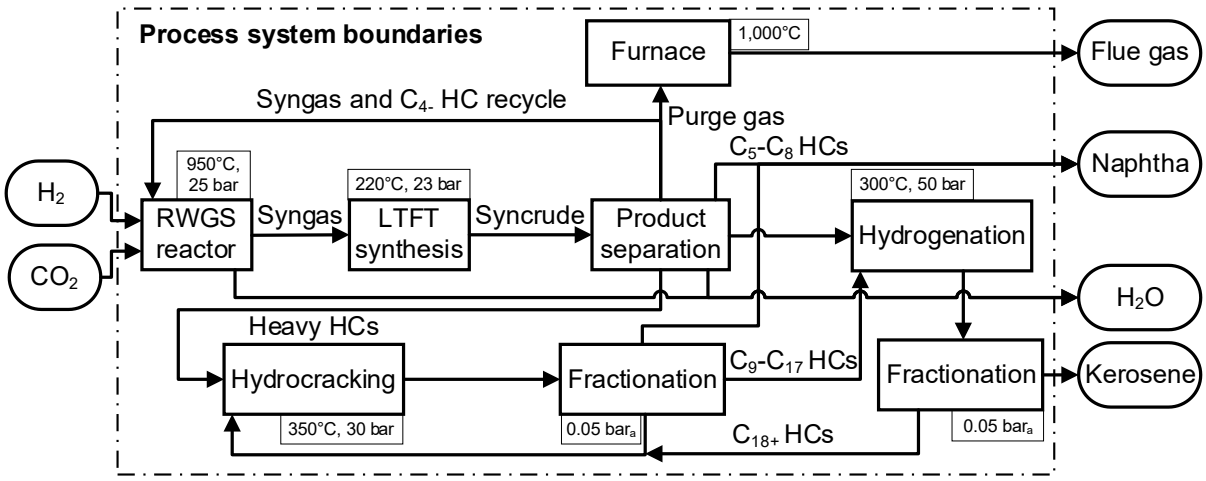

Figure 5-4: Fischer-Tropsch pathway block flow diagram (only main processes shown; LTFT: Low-temperature Fischer-Tropsch, HC: Hydrocarbon, RWGS: Reverse water-gas shift).

[11] In steam methane reforming the steam-to-carbon ratio is usually around 1.5, but water is consumed during the reaction in a similar proportion as CO is formed [188]. Since the RWGS reaction is a steam generating reaction, the ratio in the RWGS was adjusted accordingly to 0.5.

[12] Metal dusting occurs with CO rich gases mainly between 400 and 800 °C [188, 189]. The risk of metal dusting can be reduced via fast cooling (commonly performed in a high pressure steam quench [57]) to restrict carbon formation kinetically.

Some technical parameters have a major influence on technical and, therefore, potentially also economic key figures. As described in the methodology, higher-level parameters are varied which can be influenced by different operating conditions and design aspects. In FT synthesis, a key parameter is the chain growth probability (α). It is the determining factor for the chain length distribution, i.e., mass fractions (W_n) of a component with the chain length n, in the FT product (Eq. 5-7). This value typically ranges between 0.8 and 0.95 in the LTFT process and can be affected by factors such as temperature, syngas composition, pressure, residence time, and the catalyst used [56, 58, 86, 190]. High chain growth probabilities can be achieved with cobalt catalysts under low temperatures (180 to 240 °C), elevated pressures, and sufficient residence time.

$$W_n = n(1-\alpha)^2\alpha^{n-1} \qquad \text{Eq. 5-7}$$

Another critical parameter in the FT pathway is the intensity of hydrocracking. In real processes, the intensity of hydrocracking is primarily adjusted by the reaction temperature and the catalyst used. Higher temperatures and more active catalysts increase the probability of cracking reactions. In the idealized cracking model used here, as described in [158, 175], the intensity is approximated by the number of possible cracking reactions per molecule per reactor pass. Mild cracking is modeled assuming only one chain break (primary cracking), while severe cracking enables up to three cracking reactions per-pass (tertiary cracking). The technical parameters assumed within the reference case and the parameter variation of the FT pathway are listed in Table 5-2.

Table 5-2: Technical parameters for the reference case and parameter variation of the Fischer-Tropsch pathway (RC: Reference case, PV: Parameter variation).

Process	Parameter	Value
FT synthesis	Chain growth probability (α_{FT})	RC: 0.89 PV: 0.84–0.94
Hydrocracking	Ideal cracking; chain length depending conversion	RC: Secondary cracking PV: Primary to tertiary cracking

5.3.1.2 Methanol pathway

No design changes are made in the methanol pathway compared to [175]. Figure 5-5 shows the simplified block flow diagram of the respective process concept. The methanol produced in the direct (CO_2-converting) methanol synthesis is converted via dehydration (methanol-to-olefin, MtO) into light olefins (mainly ethene and propene). The product mixture is cleaned (water and caustic wash, drying via molecular sieves) and fed into the oligomerization. Different catalysts in multi-stage or multi-bed reactors are used to ensure high conversions of all olefins. Nickel-based catalysts allow for nearly complete conversion of ethene [191]. Subsequent oligomerization using acid catalysts (e.g., in mesoporous and microporous materials, zeolites, or resins) enables the production of a high pro-

portion of highly branched C_{10+} olefins [191, 192]. The oligomerization product is fractionated into lighter hydrocarbons (C_{8-}), mainly recycled to increase the overall kerosene fraction, and a heavier hydrocarbon fraction (C_{9+}), which is hydrogenated and further fractionated. Since no waxes are formed in this process, no hydrocracker is considered. Therefore, diesel is also produced in addition to kerosene and naphtha.

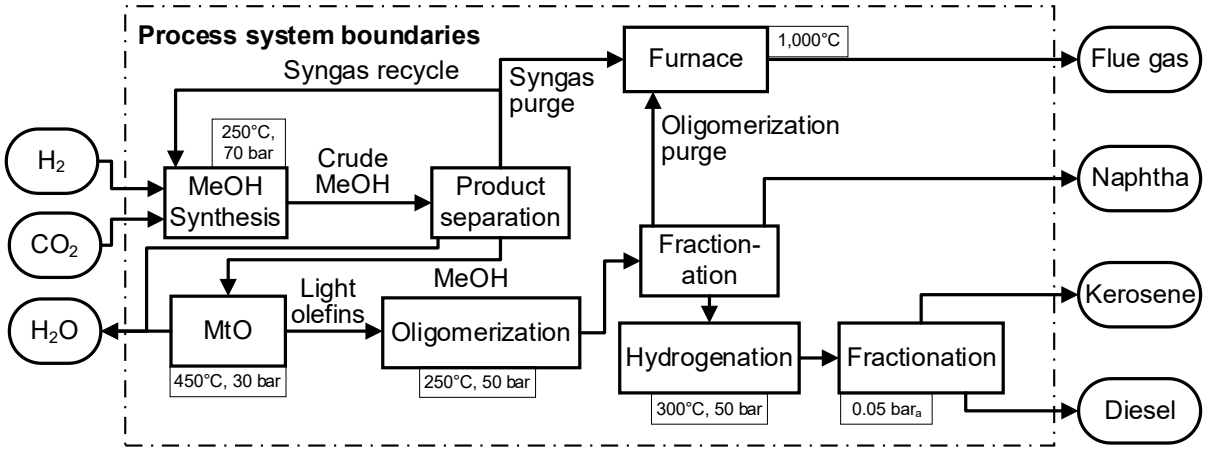

Figure 5-5: Methanol pathway block flow diagram (only main processes shown; MeOH: Methanol, MtO: Methanol-to-Olefins).

Within the MeOH pathway, the technical analysis (see [175]) indicates the strong influence of MtO olefin selectivity (S_O) and oligomerization chain growth probability. The achievable olefin selectivity, defined as the proportion of carbon in methanol that is converted into olefins, is approximately 80 to 90 % in industrial processes [162, 193]. Ongoing research, particularly in catalyst development, is focused on achieving even higher selectivities. As in FT synthesis, oligomerization can also be characterized by chain growth probability. However, the monomers can consist of various olefins from the MtO reactor or the oligomerization recycle stream. Depending on the reactant composition and the target product (i.e., chain length and component type), oligomerization can occur via various technologies, primarily distinguished by the catalysts used. The chain length distribution can be influenced by the catalyst and factors such as reactor temperature, pressure, residence time, and feed composition [191, 192]. High temperatures and short residence times tend to reduce the chain growth probability. The generic model used here for oligomerization is described in detail in Annex C, Section C.1. Due to the variety of oligomerization processes and the large number of influencing parameters, significant differences in product distributions can potentially occur in real oligomerization processes. Therefore, the chain growth probability in this study varies across a wide range within the parameter variation. Table 5-3 lists the parameters considered within the reference case and the parameter variation.

Table 5-3: Technical parameters for the reference case and parameter variation of the methanol pathway (RC: Reference case, PV: Parameter variation).

Process	Parameter	Value
Dehydration (MtO)	Olefin-Selectivity (S_O)	RC: 0.90 PV: 0.85–0.95
Oligomerization	Chain growth probability (α_{Oli})[a]	RC: 0.3 PV: 0.2–0.4

[a] Advanced oligomerization modeling compared to [175] (see Annex C, Section C.1).

5.3.2 Economic data and assumptions

Besides the technical data and assumptions primarily used for process modeling and simulation, further parameters predominantly affect economic figures and do not change technical results. The main economic parameters here are described and listed below (Table 5-4).

The plant investments are calculated for a market-mature process (n^{th}-of-a-kind plant) built on a green field. The installed production capacity for both pathways at 8,760 h/a at nominal load is around 100 kt_{TF}/a, corresponding to the largest PtL projects currently targeted [50]. However, as most of the currently planned projects have significantly lower capacities, while conventional fuel productions (e.g., via gas-to-liquid (GtL)) have significantly higher installed capacities, the production capacity is varied within the parameter variation. The cost functions and factors used to calculate the costs for the construction and commissioning of the plant (fixed capital investment) are listed in detail in Annex C, Section C.3.

The capacity utilization determines the annual production quantity at a given plant capacity, thus impacting the production costs. It depends on the customers' demand, the feedstock availability, and the plant reliability. The cost of feedstock availability, especially for H_2 from renewable energy and CO_2 of sustainable (non-fossil) origin, depends strongly on the plant location (availability and timing of renewable energy) and the infrastructure (existing H_2 and CO_2 grid). Since the constant supply of H_2 requires large, sometimes seasonal, storage facilities and overcapacities of the corresponding production facilities, which increases the cost of H_2 [108], it is assumed that capacity utilization of the conversion plants will be lower than for conventional plants which operate at an average of 75 to 85 % [124]. However, since this can vary greatly depending on the locally given frame conditions, the parameter variation also considers capacity utilization.

The fixed capital investment (*FCI*) depreciation period is assumed to be 15 years. Considering the weighted average cost of capital (*WACC*) of 6 % for production in highly industrialized countries [50], resulting in an annual depreciation of around 11 $\%_{FCI,}$ being in line with the literature [110, 124, 125]. Uncertainties associated with estimating plant costs are assessed through the variation of annual capital costs within the expected uncertainty range (−30/+50 %) [111].

The prices for continuously available electricity are estimated based on the European average price (2008 - 2020) for non-household electricity contracts. This value is in the same range as the constant electricity supply from renewable power in the EU derived by [123]. As there are currently no established markets for non-fossil H_2 and CO_2, the prices are estimated based on current analyses of supply costs. Thus, H_2 and CO_2 prices are varied over a wide range assigned to supply costs from different provisioning cases. The expected H_2 supply cost depends primarily on the production location and the transportation distance; variations by a factor of more than two can result. For the reference case, H_2 prices are set according to European average supply costs for power-based H_2. The expected cost range for CO_2 is even greater. While CO_2 can be provided without additional effort at advantageous point sources [69], capture costs of more than 1,000 €/t_{CO2} are currently realistic for direct air capture (DAC) [73, 74]. CO_2 prices corresponding to capture costs from a point source are assumed for the reference case. However, it should be noted that the market will determine pricing more in the future and that the supply costs represent a lower price limit here.

Table 5-4: Economic data and assumptions (*ACC*: Annual capital cost, PV: Parameter variation, RC: Reference case, *WACC*: Weighted average cost of capital).

Parameter		Unit	Value	Reference
Plant related	Production capacity (total fuel product)	[kt/a]	RC: 100 | PV:10–200	[-]
	Capacity utilization [a]	[%]	RC: 70 | PV: 35–100	[-]
Capital related	*WACC* (*i*)	[%]	RC: 6 | PV: 4–15	[50, 108]
	Depreciation period (*n*)	[a]	15 | 5–20	[124, 125, 194]
	ACC uncertainty (Factor)	[-]	0.7–1.5	[111]
Costs	H_2	[€$_{2023}$/kg]	RC: 5.0 | PV: 3.0–7.0	[108, 195]
	CO_2	[€$_{2023}$/t]	RC: 150 | PV: 0–1,000	[69, 73, 74, 196]
	Electricity	[€$_{2023}$/MWh]	RC: 72 | PV: 40–190	[123, 128]

[a] Capacity utilization of 70 % equals 6,132 annual full load hours.

All costs are given in euro currency and adjusted according to the chemical plant cost index (CEPCI) for 2023. The exchange rate is 1.19 US$/€ and is based on the average for the years 1999 to 2022 [197]. Additional data are provided in Annex C, Section C.3.

5.4 Results and discussion

In this section, the process simulation results are presented first (Section 5.4.1), serving as the basis for subsequent cost analysis. The costs for the reference cases are analyzed in section 5.4.2. Subsequently, the impact of the technical and economic parameter variation on kerosene production cost (*KPC*) is depicted and discussed in section 5.4.3.

5.4.1 Process simulation results

The results of the process simulations, which form the basis for calculating the variable operational expenditures and fixed capital investments, are presented as mass and electricity flows in Figure 5-6 and Figure 5-7. Carbon and energy flow diagrams (incl. heat streams) as well as system efficiencies under technical parameter variation, are described in Annex C, Section C.4.

5.4.1.1 Fischer-Tropsch pathway

For the FT pathway, a specific hydrogen demand of 0.62 t/t_K and 0.44 t/t_{TF} is observed. The CO_2 demand is 4.43 t/t_K and 3.16 t/t_{TF}. Considering heat integration and internal power generation, the external electricity demand (including heating requirements) amounts to 3.38 MWh/t_K and 2.41 MWh/t_{TF}, respectively. Notably, the high power demand of the electrically heated RWGS reactor is evident, which arises from both the endothermic RWGS reaction itself and the endothermic reforming of light components (primarily CH_4) from the syngas recycle and the naphtha column headstream. The water produced during the synthesis reaction is separated by condensation after the RWGS reactor and decantation from the light condensate in the cold separator after the FT synthesis.

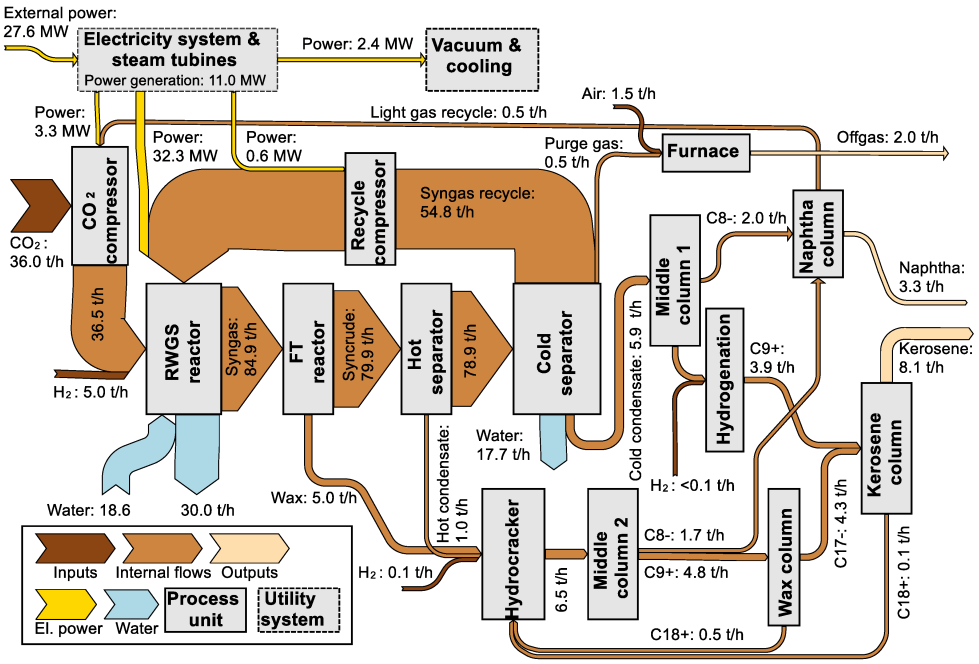

Figure 5-6: Mass and electricity flows of the Fischer-Tropsch pathway (diagram represents the reference case; heat flows are not shown for reasons of visual clarity. Power flows below 0.1 MW not shown; FT: Fischer-Tropsch, RWGS: Reverse water-gas shift).

5.4.1.2 Methanol pathway

The simulation of the methanol pathway shows specific hydrogen demands of 0.58 t/t_K and 0.52 t/t_{TF}. The CO_2 demand is 4.12 t/t_K and 3.74 t/t_{TF}. Steam turbines can almost sup-

ply the entire electricity required for the process by utilizing excess heat, as all main reactions in the process are exothermic. The external electricity demand is 0.06 MWh/t_K and 0.05 MWh/t_{TF}, respectively. Oligomerization allows for the direct recycling of unreacted olefins without the need for reforming. However, material losses occur due to the absence of RWGS (or further reforming options), as the resulting purge gas streams can only be used for energy recovery. The direct CO_2 conversion in methanol synthesis leads to low conversion rates, resulting in large mass flows and corresponding sizing requirements in the synthesis loop.

The higher kerosene selectivity of the MeOH pathway compared to the FT pathway results primarily from the larger monomer building blocks (ethene, propene), which can form hydrocarbons in the kerosene fraction with fewer chain growth reactions (lower chain growth probability). This is further supported by light fractions recycled directly without breaking the already-formed chains (Annex C, Section C.4).

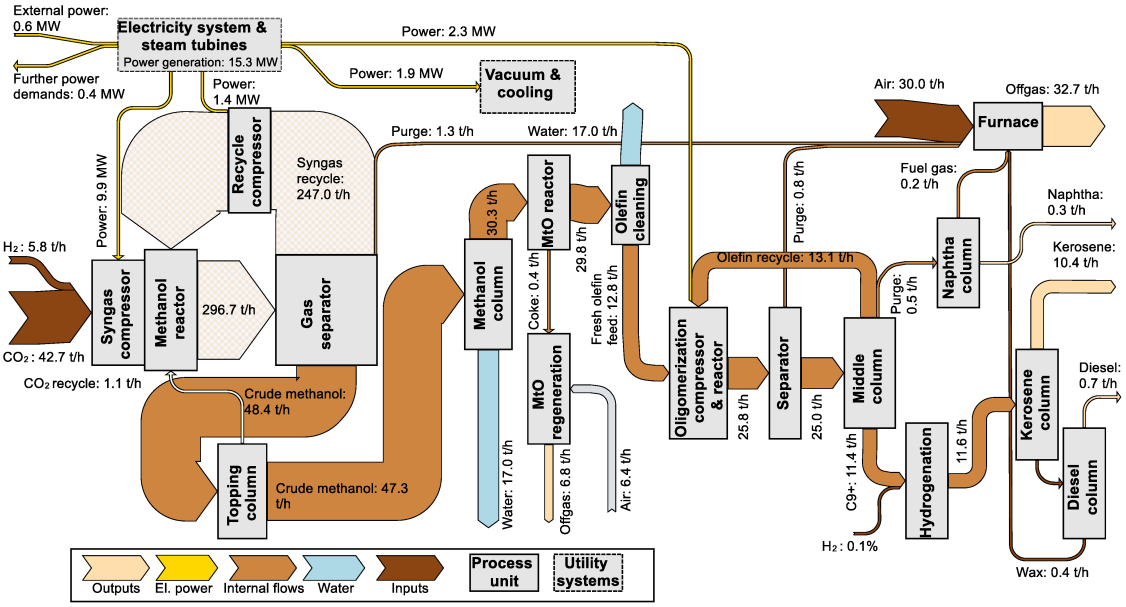

Figure 5-7: Mass and electricity flows of the methanol pathway (diagram represents the reference case; heat flows are not shown for reasons of visual clarity. Power flows below 0.1 MW not shown; MtO: Methanol-to-olefins).

5.4.2 Production costs

Figure 5-8 depicts the kerosene production costs of both pathways (reference case) for both cost allocation methods. The left side of the figure (KPC_K) represents the allocation of costs solely to the kerosene fraction without accounting for by-product revenues, therefore indicating an upper cost limit. The right side represents the equal allocation of costs across all fuel products (naphtha, kerosene, diesel fraction), indicating a lower cost limit (KPC_{TF}). The proportions of the individual cost components shown are equal within both allocations. Electricity production from internal heat conversion is offset against the external electricity supply.

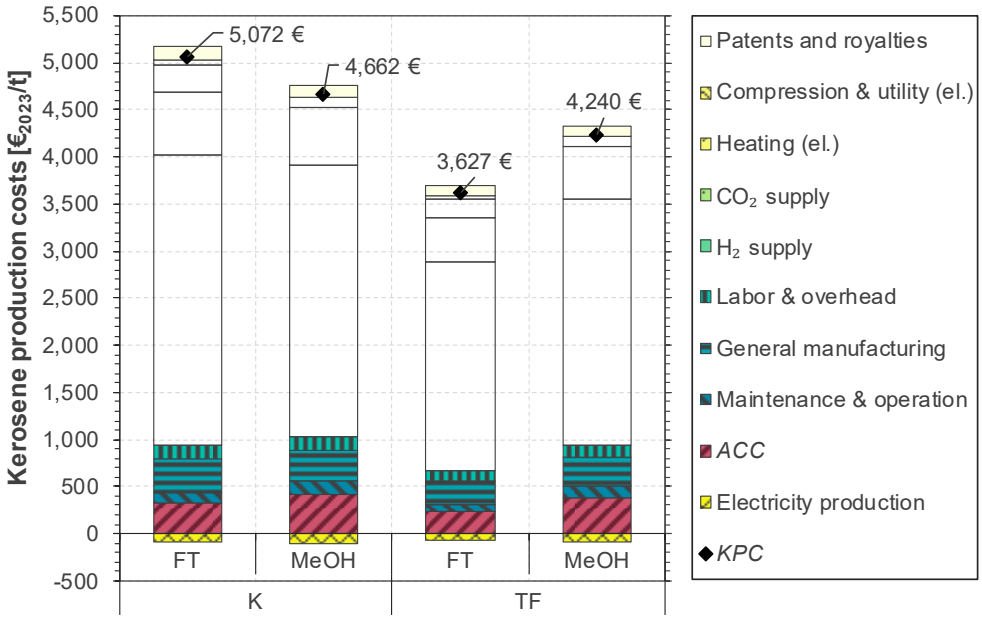

Figure 5-8: Kerosene production costs of the Fischer-Tropsch and methanol pathway in the reference case (K: Kerosene allocation, TF: Total fuel allocation, FT: Fischer-Tropsch, MeOH: Methanol, *ACC*: Annual capital cost, *KPC*: Kerosene production cost).

In the reference case, the FT pathway yields kerosene production costs between 3,630 and 5,070 €/t, depending on the allocation method/the by-product revenues, respectively. For the MeOH pathway, costs are within a smaller range of 4,240 to 4,660 €/t. The costs of both pathways are dominated by the costs of H_2 (FT: 61 %, MeOH 62 %) and CO_2 supply (both 13 %). The shares of the remaining cost components are distributed relatively evenly across the kerosene production costs. The major difference between the cost distribution of the FT and MeOH pathway lies in the electricity cost. The FT pathway requires significantly more electricity (mainly for RWGS heating) than is supplied by internal heat conversion. In contrast, the electricity demand and generation are almost equal within the MeOH pathway. The fixed capital investments, resulting from the major equipment estimate used, are 150 M€ for the FT pathway and 240 M€ for the MeOH pathway (see Annex C, SectionC.5). The higher fixed capital investments required for the MeOH pathway result mainly from the larger synthesis loop and the higher pressure level of the methanol synthesis. Therefore, the resulting share of annual capital cost is also slightly higher for the MeOH pathway (9 %) than for the FT pathway (7 %).

Comparing both pathways' kerosene production costs, the kerosene production via the MeOH pathway results in lower costs when no revenues from naphtha or diesel are considered (KPC_K). However, considering all fuel fractions as (equally) valuable products, the FT pathway enables significantly lower production costs (KPC_{TF}). The first result is caused by the high kerosene selectivity of the olefin oligomerization (MeOH pathway). In contrast, the advantage of the FT pathway regarding KPC_{TF} is due to the low material losses and, thus, the higher total fuel production.

Figure 5-9 depicts the kerosene production cost over varying by-product revenues (*BPR*). Both of the above-described allocations can be found in the figure.

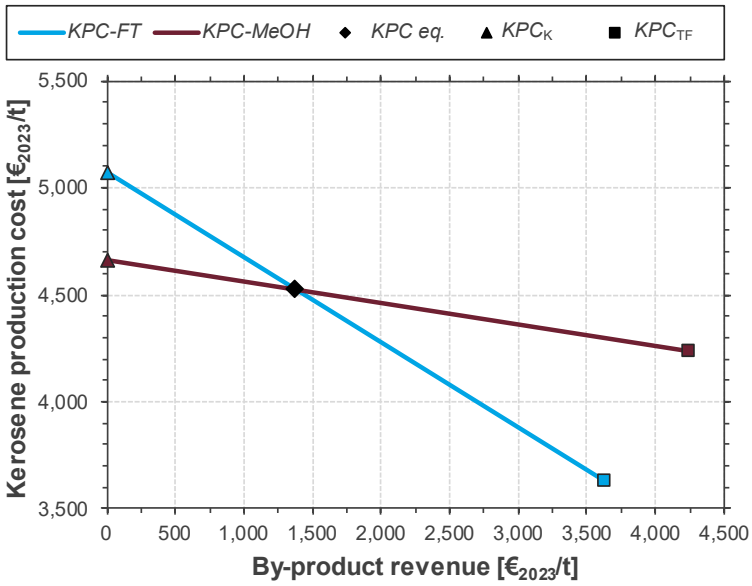

Figure 5-9: Kerosene production cost of the Fischer-Tropsch and methanol pathway under varying by-product revenues (FT: Fischer-Tropsch pathway, MeOH: Methanol pathway, eq.: equal, *KPC*: Kerosene production cost, KPC_K: Kerosene production cost from kerosene allocation, KPC_{TF}: Kerosene production cost from total fuel allocation).

KPC_K occur at a by-product revenue of 0 €/t_{BP}. KPC_{TF} are located where the kerosene production costs are equal to the by-product revenues. Due to the larger by-product quantity, the kerosene production costs of the FT pathway in the analyzed plant concepts are significantly more dependent on the by-product revenues. Equal kerosene production costs for both pathways (*KPC eq.*) occur at a by-product revenue of around 1,370 €/t_{BP}. The respective kerosene production costs are 4,530 €/t. Below this value, the MeOH pathway enables lower kerosene production costs; at higher by-product revenues, the FT pathway enables cheaper kerosene production. In other words, the MeOH pathway would be economically beneficial only for kerosene market prices, which are 3.3 times higher than naphtha or diesel prices. Optimizing the process concepts toward maximized naphtha or diesel production would be economically beneficial if higher revenues are achieved for the by-products than for kerosene.

5.4.3 Parameter variation

In simulation-based techno-economic analyses, the cost calculation results strongly depend on the underlying technical and economic concepts and assumptions. The variation of key parameters is analyzed below to show the respective impacts on kerosene production costs and to determine realistic cost ranges for power-based fuel production.

5.4.3.1 Technical parameters

The results of the technical parameter variation are shown in Figure 5-10. The solid lines represent the kerosene allocation (KPC_K), i.e., excluding by-product revenues, and the dashed lines show the cost allocation to the total fuel fraction (KPC_{TF}). In the FT pathway,

the chain growth probability within the FT reactor and the degree of hydrocracking, i.e., single (pri.), double (sec.), and triple (ter.) cracking possibility per reactor pass, are varied as higher-level process parameters (see Section 5.3.1). The diagram indicates that both parameters have almost no impact in the varied range when costs are allocated to the total fuel product – meaning KPC_{TF} stay nearly constant. This is due to the fact that while the relative proportions of the fuel fractions shift, the overall quantity of fuel produced remains nearly constant. However, energy demand and wax distillation costs increase slightly with increasing chain growth probability, while the energy demand of the RWGS reactor increases with decreasing chain growth probability (increasing recycling of light gases). This leads to minimal KPC_{TF} at chain growth probabilities around 0.9. Mild hydrocracking (pri. HC) and high chain growth probabilities increase the kerosene fraction, reducing kerosene production costs within kerosene allocation (KPC_K).

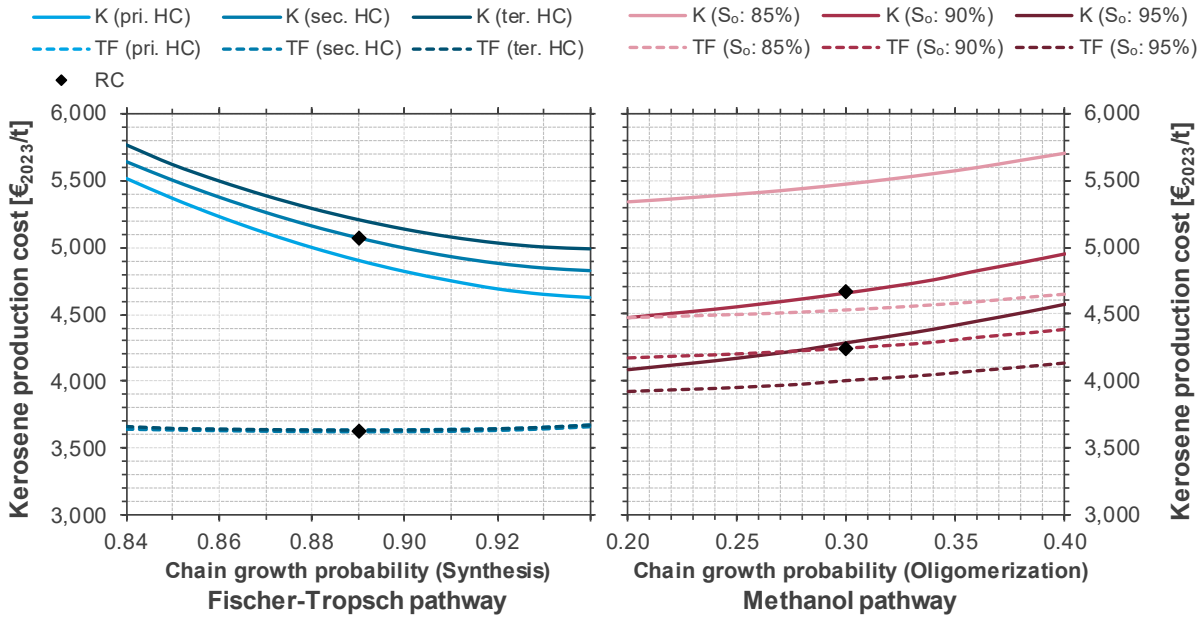

Figure 5-10: Kerosene production cost under technical parameter variation (K: Kerosene allocation, TF: Total fuel allocation, S_O: Olefin selectivity pri.: primary, sec.: secondary, ter.: tertiary, HC: Hydrocracking, RC: Reference case).

Within the MeOH pathway, KPC_K and KPC_{TF} are strongly affected by the varied parameters of olefin selectivity (S_O) and oligomerization chain growth probability since total fuel and kerosene yield change significantly. Generally, low chain growth probabilities and high olefin selectivities positively affect technical efficiencies and kerosene production costs. A comparison of the economic results with the technical results (Annex C, Section C.4) reveals a strong correlation between the production costs and the process efficiencies. As in the FT pathway, the KPC_{TF} are less affected by the chain growth probability as this parameter mainly changes the proportions of fuel fractions. However, with high probabilities of chain growth, an increasing wax fraction occurs, reducing the overall amount of fuel produced. Low chain growth probabilities increase the kerosene selectivity of the overall process as less diesel and waxes are produced. The increasing naphtha fraction is recycled, thus increasing the energy input and dimensioning of the oligomerization loop.

However, this is more than compensated for by the higher efficiency of the process in terms of kerosene production. A higher olefin selectivity directly reduces the amount of purge gas and increases the overall process efficiency.

The methanol pathway shows lower kerosene production costs over a wide range of parameter variations when no revenues for naphtha or diesel are considered (KPC_K). This is due to the higher kerosene selectivity compared to the FT pathway, making by-product revenue less critical. However, cost allocation to all fuel products (KPC_{TF}) shows lower production costs within the FT pathway that cannot be reached by the methanol pathway, even under the most favorable assumptions. Within the FT pathway, the KPC_K varies from 4,630 to 5,770 €/t (RC: 5,070 €/t; −9 %, +14 %). KPC_{TF} change is minimal from 3,630 to 3,670 €/t (RC: 3,630 €/t; −0 %, +1 %). The variation is much stronger in the MeOH pathway, where KPC_K varies from 4,080 to 5,710 €/t (RC: 4,660 €/t; −12 %, +22 %) and KPC_{TF} changes from 3,920 to 4,640 €/t (RC: 4,240 €/t; −8 % +10 %).

5.4.3.2 Economic parameters

Figure 5-11 shows the kerosene production cost under the variation of four economic parameters. The solid lines represent the kerosene allocation (KPC_K), and the dashed lines show the total fuel allocation (KPC_{TF}). The influence of the economic parameters analyzed here on the MeOH pathway is slightly more significant, as the fixed capital investments are higher. However, within the expected parameter ranges, the MeOH pathway always enables lower kerosene production costs when no by-product revenues are assumed (KPC_K), while the FT pathway allows for lower kerosene production costs when all fuel fractions are assumed to have the same value (KPC_{TF}).

Weighted average cost of capital. Within the FT pathway, the KPC_K varies from 5,020 to 5,320 €/t (RC: 5,070 €/t; −1 %, +5 %). The KPC_{TF} varies between 3,590 and 3,800 €/t (RC: 3,630 €/t; −1 %, +5 %). KPC_K in the MeOH pathway varies from 4,600 to 4,970 €/t (RC: 4,660 €/t; −1 %, +7 %), and KPC_{TF} changes between 4,190 and 4,520 €/t (RC: 4,240 €/t; −1 % +7 %). The weighted average cost of capital depends on plant location and numerous further factors. However, the *WACC* has a minor impact on kerosene production costs since annual capital costs only contribute a small fraction of overall costs. This parameter is typically much more important for very capital-intensive production processes (e.g., electricity generation, water-electrolyzer).

Depreciation period. Within the FT pathway, the KPC_K varies from 5,030 to 5,470 €/t (RC: 5,070 €/t; −1 %, +8 %), and the KPC_{TF} ranges from 3,590 to 3,910 €/t (RC: 3,630 €/t; −1 %, +8 %). Again, the MeOH pathway is slightly more affected, with KPC_K between 4,600 and 5,170 €/t (RC: 4,660 €/t; −1 %, +11 %) and KPC_{TF} varying from 4,190 to 4,700 €/t (RC: 4,240 €/t; −1 %, +11 %). The length of the period assumed for investment depreciation has a non-linear influence on the kerosene production costs. Considerable cost in-

creases particularly occur for amortization periods of less than ten years. For amortization periods longer than ten years, the effect is limited due to the relatively small share of annual capital cost within the kerosene production cost.

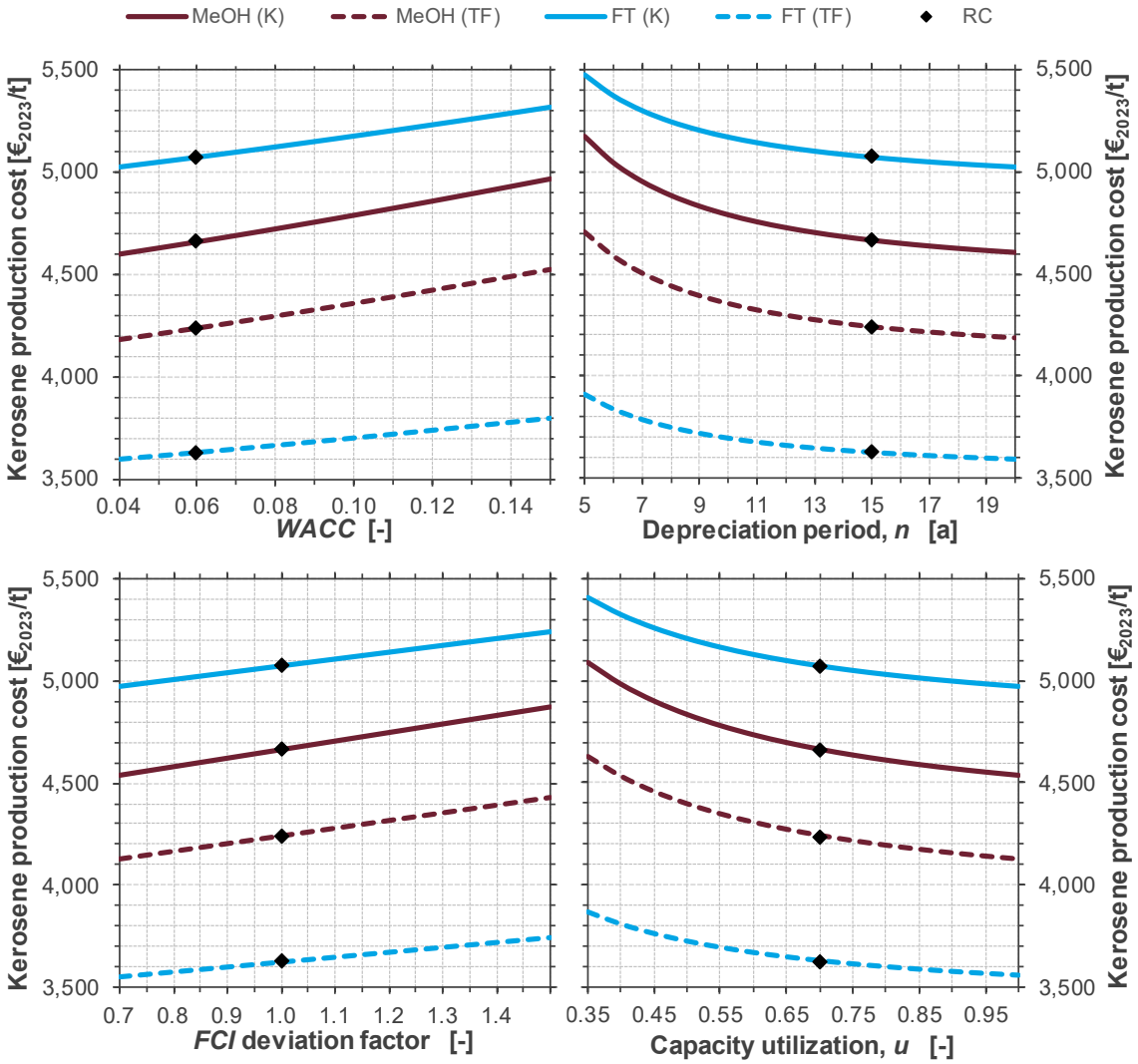

Figure 5-11: Kerosene production costs under economic parameter variation (FT: Fischer-Tropsch pathway, MeOH: Methanol pathway, K: Kerosene allocation, TF: Total fuel allocation, RC: Reference case, *WACC*: Weighted average cost of capital, *FCI*: Fixed capital investment).

Annual capital cost. The major equipment estimate method used for fixed capital investment calculation, by definition, has an accuracy of −30/+50 %, which is reflected here using the fixed capital investment (*FCI*) deviation factor. The kerosene production costs change linearly and relatively flat. Within the FT pathway, KPC_{K} increase from 4,970 to 5,240 €/t (RC: 5,070 €/t; −2 %, +3 %), and the KPC_{TF} increase from 3,560 to 3,750 €/t (RC: 3,630 €/t; −2 %, +3 %). Due to the higher fixed capital investment required for the MeOH pathway, KPC_{K} and KPC_{TF} change slightly stronger from 4,540 to 4,870 €/t (RC: 4,660 €/t; −3 %, +5 %) and 4,120 to 4,430 €/t (RC: 4,240 €/t; −3 %, +5 %) respectively.

Capacity utilization. Capacity utilization is decisive for the amount of product produced to which all fixed costs are related. Accordingly, the impact on kerosene production cost is non-linear and increases in particular at low utilizations. Within the FT pathway, KPC_{K}

and KPC_{TF} can be decreased to 4,970 and 3,560 €/t (−2 % of RC) when nominal load production can be achieved over the entire year. However, the H_2 supply from fluctuating power-based electrolysis might only be made available constantly at much higher prices, making lower capacity utilization economically favorable at certain times. A lower utilization at constant feedstock prices can increase the KPC_K and KPC_{TF} up to 5,410 €/t and 3,870 €/t (+7 %). The same applies to the MeOH pathway, where KPC_K varies from 4,540 to 5,090 €/t (RC: 4,660 €/t; −3 %, +9 %), and KPC_{TF} varies from 4,120 to 4,630 €/t (RC: 4,240 €/t; −3 % +9 %).

The influences of feedstock prices are depicted in Figure 5-12.

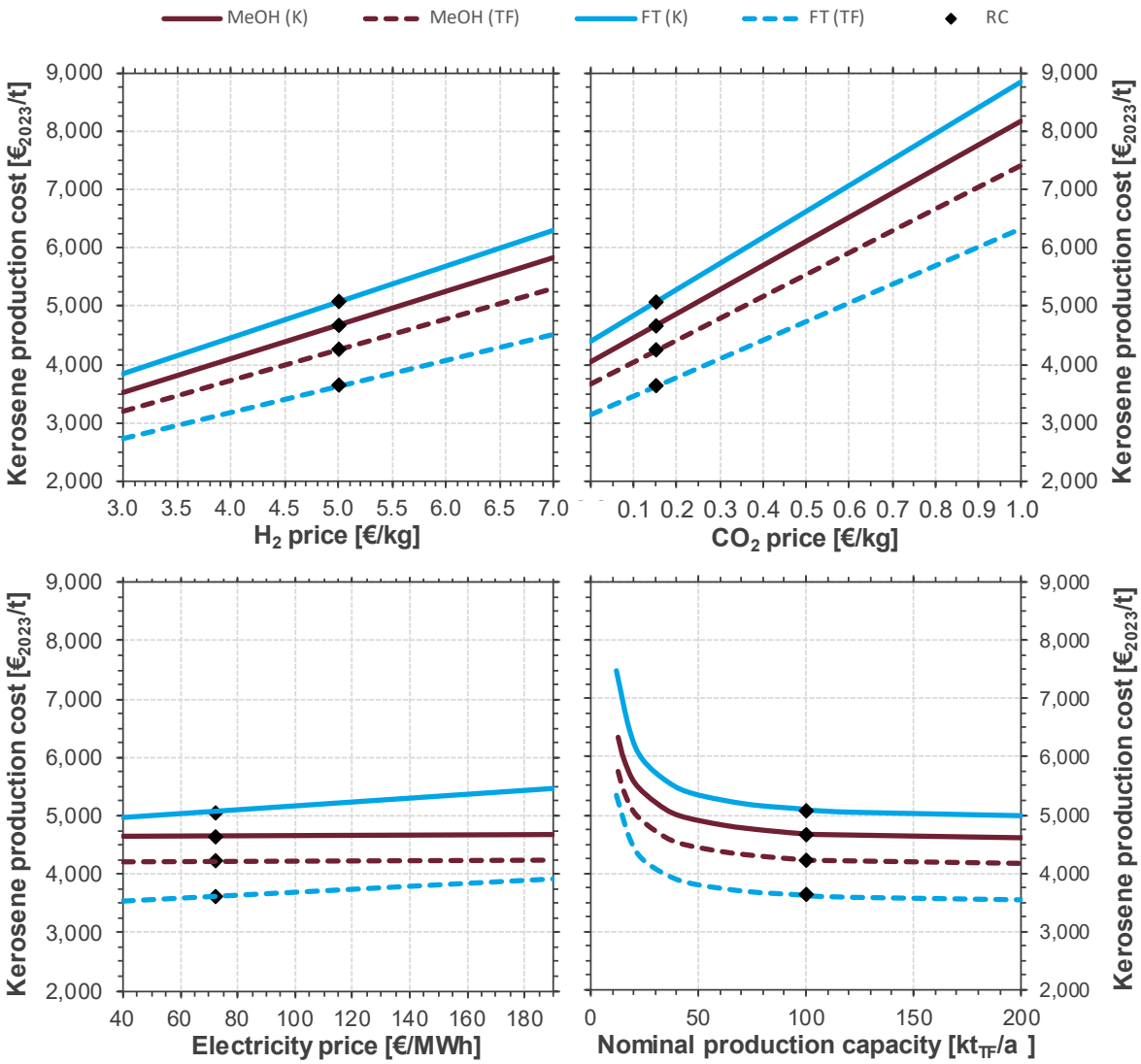

Figure 5-12: Kerosene production cost under feedstock price and nominal production capacity variation (FT: Fischer-Tropsch pathway, MeOH: Methanol pathway, K: Kerosene allocation, TF: Total fuel allocation, RC: Reference case).

H_2 price. Within the assumed H_2 price range, KPC_K and KPC_{TF} vary between ± 24 % (FT) and ± 25 % (MeOH) of the reference case cost. For the FT pathway, the KPC_K ranges from 3,830 to 6,310 €/t and the KPC_{TF} from 2,740 to 4,510 €/t. Within the MeOH pathway, the cost ranges from 3,510 to 5,810 €/t and 3,190 to 5,290 €/t, respectively. Power-based H_2

production is expensive due to the high electricity demand and the high capital investments for the electrolyzer. Furthermore, a significant amount of H_2 is required since it is the main energetic input within the analyzed process pathways. Accordingly, the H_2 price has a high impact on the *KPC*.

CO_2 price. Even if the specific prices of H_2 are significantly higher than those of CO_2, the CO_2 price equally influences the kerosene production costs. This is due, on the one hand, to the (mass-related) higher demand for CO_2 and, on the other hand, to the potentially vast price range depending on the supply option and the market development. Possible cost reductions, for example, if pure CO_2 is produced as a waste product without alternative use (0 €/t_{CO2}), can lead to reduced costs of 13 % compared to the reference cases. In contrast, CO_2 prices that refer to the provision costs via DAC, currently lying around 1,000 €/t_{CO2}, increase the kerosene production cost by 74 % (FT) and 75 % (MeOH) compared to the reference case. The KPC_K in the FT pathway ranges from 4,410 to 8,830 €/t. The KPC_{TF} increases from 3,150 to 6,320 €/t. Within the MeOH pathway, KPC_K and KPC_{TF} vary from 4,040 to 8,160 €/t and 3,680 to 7,420 €/t, respectively.

Electricity price. The influence of electricity prices affects both pathways in very different ways. While MeOH-based production requires almost no external electricity and is therefore widely independent from the electricity price, the variation carried out here results in changes between −2 and +8 % (KPC_K 4,960 to 5,470 €/t; KPC_{TF} 3,550 to 3,910 €/t) in the FT pathway. At an electricity price of around 330 €/MWh and higher, the MeOH pathway would be cheaper even if the costs are allocated to total fuel product (KPC_{TF}). However, such high electricity prices seem unlikely for industrial customers.

Nominal plant capacity. The nominal plant capacity variation depicts the effects of scale on the kerosene production cost. A strong effect of the realized plant sizes can be seen between 10 and 50 kt_{TF}/a. Decreasing equipment size and thus increasing specific equipment costs lead to a significant rise in the share of annual capital costs, particularly for plant capacities below 30 kt_{TF}/a. In contrast, between 100 and 200 kt_{TF}/a, further cost reductions are minimal, among others, as some components reach standard industrial equipment's capacity limits. While in both production cases, only minor cost reductions can be expected through further upscaling (based on the cost method used here, 3 % (FT) to 2 % (MeOH)), the costs for very small-scale systems can lead to production cost increases clearly above 30 % compared to the reference case.

5.4.4 Summary and discussion

The different influences from parameter variation on the kerosene production costs are depicted in Figure 5-13. The left diagram depicts the kerosene production costs excluding

by-product revenues (KPC_K), while the right diagram presents the costs derived by total fuel allocation (KPC_{TF}). Depending on the allocation method/by-product value and the assumed parameters, the kerosene production costs are predominantly between 3,500 and 5,500 €/t. The figure shows that H_2 and CO_2 prices determine kerosene production costs significantly within both pathways; thus, price changes lead to high cost variations. In particular, CO_2 prices equivalent to the current supply costs via direct air capture can nearly double kerosene production costs compared to applying CO_2 supply cost from point sources. The plant's production capacity also significantly affects kerosene production costs within 10 to 50 kt_{TF}/a range. Here, economies of scale effects result in a significant cost increase for small-scale production facilities.

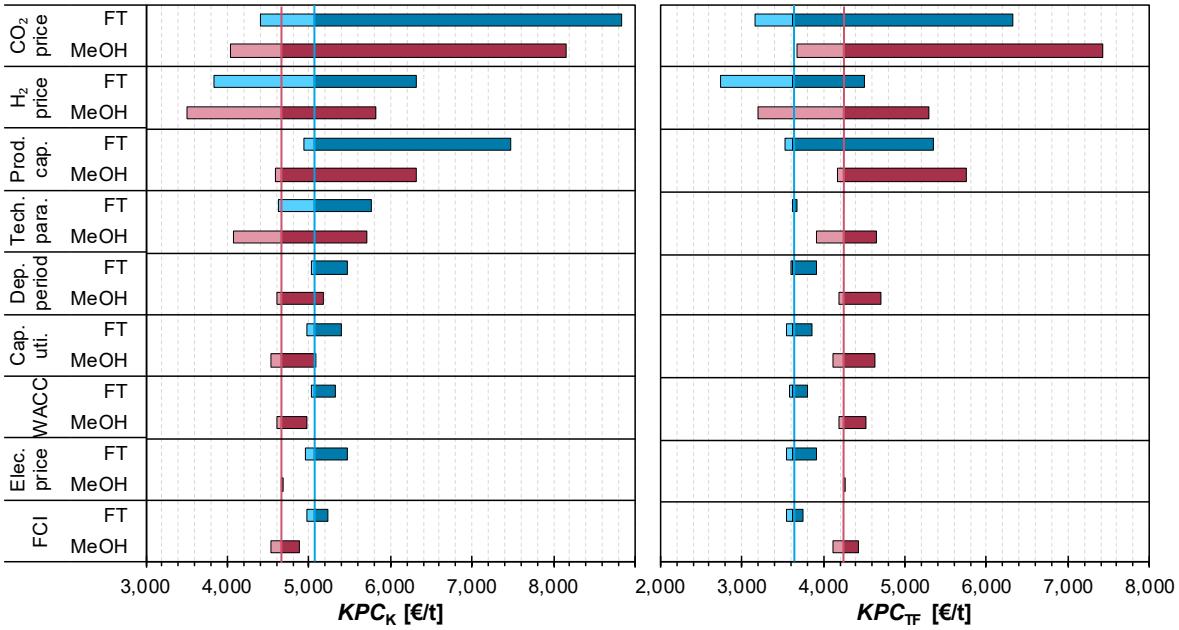

Figure 5-13: Comparison of parameter variation impacts on kerosene production cost (FT: Fischer-Tropsch pathway; MeOH: Methanol pathway; KPC_K: Kerosene production cost based on kerosene allocation; KPC_{TF}: Kerosene production cost based on total fuel allocation; Tech. para.: Technical parameter; *WACC*: Weighted average cost of capital; Dep.: Depreciation; *FCI*: Fixed capital investment, Cap. uti.: Capacity utilization; Elec.: Electricity; Prod. cap.: Production capacity).

Technical parameter variations considerably influence the kerosene production cost of both pathways when no by-product revenue is considered (KPC_K). However, when naphtha, kerosene, and diesel are of equal value (total fuel cost allocation, KPC_{TF}), only the MeOH pathway is affected by technical parameter variation. The economic parameters varied (depreciation period, weighted average cost of capital, fixed capital investment, capacity utilization) show a lower effect on kerosene production cost, with the MeOH pathway being slightly more sensitive due to its higher plant costs. The electricity price only affects the FT pathway since the MeOH pathway has hardly any external electricity demand. However, lower KPC_{TF} only result for the MeOH pathway when applying very high electricity prices of 330 €/MWh and more.

Concerning the technical parameters, the MeOH pathway shows more significant uncertainties than the FT pathway. Based on the utilization of fossil syngas, the FT pathway is commercially used for the synthetic production of various fuels and has been extensively studied and described in the literature [58, 86, 87, 136, 150, 157]. The chain growth probability and hydrocracking intensity can be adjusted through appropriate catalysts and process conditions, making a further maximization of the kerosene fraction (as shown in the parameter variation) feasible. In contrast, there is significantly less data available in the literature for methanol-based kerosene production, while various process concepts are proposed, particularly regarding the combination of dehydration and oligomerization [138, 183, 198]. As a result, the modeling is based on a much smaller data set compared to the FT pathway, leading to greater uncertainties. Therefore, the results from the parameter variation rather represent an uncertainty range surrounding the reference case.

Further uncertainties exist about calculating plant costs (fixed capital investment) using the module costing technique. Although this method has relatively high accuracy (−30/+50 %), corresponding functions are not available in the literature for all types of equipment and process conditions, which can result in larger deviations. The limited validity range of the functions severely restricts a statement beyond the varied size range. Even if the cost reduction slowly flattens out between capacities of 100 and 200 kt_{TF}/a, further cost reductions can potentially occur in larger-scale projects, even if this cannot be evaluated with the cost functions used here [86]. Since many of the fixed operational expenditures are calculated on the basis of fixed capital investments, such uncertainties also apply to parts of these costs.

5.5 Conclusion

The successful market integration of power-based aviation fuels necessitates a thorough understanding of the cost structure and the key factors influencing kerosene production costs. This study presents a comprehensive cost analysis of kerosene production from power-based syngas, comparing two different plant concepts, one using the Fischer-Tropsch synthesis and hydrotreatment, the other applying direct methanol synthesis with downstream dehydration and oligomerization. Two cost allocation methods are applied to address uncertainties associated with unpredictable by-product revenues. Allocating costs solely to the kerosene fraction, without considering by-product revenues, establishes the upper cost limit (KPC_K), while allocating costs across the total fuel fraction, resulting in equal production costs for all fuel products, defines the lower cost boundary (KPC_{TF}). Novel findings result from the detailed comparison of the process pathways based on the same framework conditions and extensive parameter variation.

The main conclusions that can be drawn with regard to the analyzed process concepts in the reference case can be summarized as follows:

- Applying the above-mentioned cost allocations reveals a significantly lower impact of achievable naphtha and diesel revenues on the kerosene production cost in the MeOH pathway due to its high kerosene selectivity. In contrast, kerosene production costs in the FT pathway are more sensitive to variations in by-product revenues, ranging from 3,630 to 5,070 €/t, while in the MeOH pathway, by-product price-related cost changes range from 4,240 to 4,660 €/t.

- Due to its high material efficiency, the FT pathway becomes advantageous compared to the MeOH pathway already at by-product revenues equivalent to 30 % (1,370 €/t) of the associated kerosene production costs (4,530 €/t); i.e., kerosene must be 3.3 times more valuable than naphtha and diesel to result in lower kerosene production costs for the MeOH pathway.

Analyzing the parameter variations yields the following results for the plant concepts investigated here:

- Variations in technical parameters have a more significant impact on the MeOH pathway than on the FT pathway. Both, a more limited availability of process modeling data and a greater sensitivity to the varied parameters cause a higher uncertainty for the MeOH pathway; the KPC_{K} range from −12 to +22 %, and the KPC_{TF} from −8 to +10 %. Within the FT pathway, KPC_{K} and KPC_{TF} vary only by −8 to +13 % and 0 to +1 %, respectively.

- In general, *KPCs* strongly correlate with technical efficiencies, with changes in plant investment (e.g., due to larger equipment dimensions) having only a minor effect on overall costs.

- The H_2 and CO_2 prices have the most significant influence on kerosene production costs. Lowering the costs of H_2 production can reduce kerosene production costs by up to 25 % (within the expected H_2 price range). CO_2 price, especially in the range of current DAC costs, can increase kerosene production costs by up to 75 % compared to price levels referring to point source carbon capture costs.

Since a broad data basis is already available for modeling the industrially established FT pathway and the higher-level process parameters (chain growth probability, hydrocracking intensity) are largely adjustable, the parameter variation results can be considered as a feasible optimization range. The MeOH pathway has significantly greater uncertainties due to the lack of industrial validation and the smaller data basis. Therefore, the results from the parameter variation primarily represent the uncertainties rather than the practically achievable optimization range.

In conclusion, based on the analyzed kerosene production costs, which primarily range between 3,500 and 5,500 €/t, power-based aviation fuels are expected to be significantly more expensive than most biomass-based kerosene alternatives. The primary cost drivers

are found upstream of the synthesis process, i.e., H_2 production and potentially CO_2 supply. Thus, the efficiency of feedstock utilization becomes even more important. This suggests that extensive measures to enhance feedstock conversion efficiency could be economically viable despite increasing plant complexity. Therefore, further studies are needed to develop and optimize concepts with maximized feedstock utilization and kerosene yield.

6 Synthesis and limitations of results

Based on the previously presented results, the objective of this chapter is to compile and discuss the broader findings from the detailed results shown in Chapters 3, 4, and 5 to address and answer the research questions outlined in Chapter 2.

Section 6.1 addresses research question 1, exploring how electrical energy can be utilized to efficiently use non-fossil carbon in "green" fuel production. Section 6.2 focuses on research question 2, highlighting the key differences between the Fischer-Tropsch (FT) and methanol (MeOH) pathways for power-based kerosene production. Research question 3 is covered in Section 6.3, emphasizing the techno-economic parameters that determine the efficiency and costs of producing kerosene or methanol as a potential intermediate product in kerosene production from electrical energy. Finally, Section 6.4 tackles the limitations in the accuracy and applicability of the analysis findings.

6.1 Electricity utilization for carbon-efficient fuel production

This section addresses the question of how, and with what implications, electrical energy can enhance the efficient utilization of non-fossil carbon within "green" fuel production approaches. To this end, hybrid and purely power-based production approaches are qualitatively compared with purely biomass-based production in terms of carbon efficiency, electricity demand, and production costs (Figure 6-1). Key insights are synthesized from Chapters 3 and 4.

The production approaches compared in Figure 6-1 are classified as introduced in Section 1.2. If the energy contained in the final product – specifically kerosene or methanol in the context of this thesis – is derived entirely from "green" electricity provided by renewable, non-biogenic sources of energy, and only non-energetic material feedstocks (H_2O and CO_2) are utilized, the process is classified as a purely power-based production approach (power-to-liquid; PtL). If the fuel product is derived from biogenic energy and electricity is used solely to run the process (e.g., compression, pumping) without being incorporated into the chemical energy of the fuel product, the process is referred to as biomass-to-liquid (BtL). A combination of both approaches, where one part of the energy contained in the product originates from organic matter and the other from "green" electrical energy, is referred to as hybrid production (power- and biomass-to-liquid; PBtL). The results visualized in Figure 6-1 are discussed in the following sections.

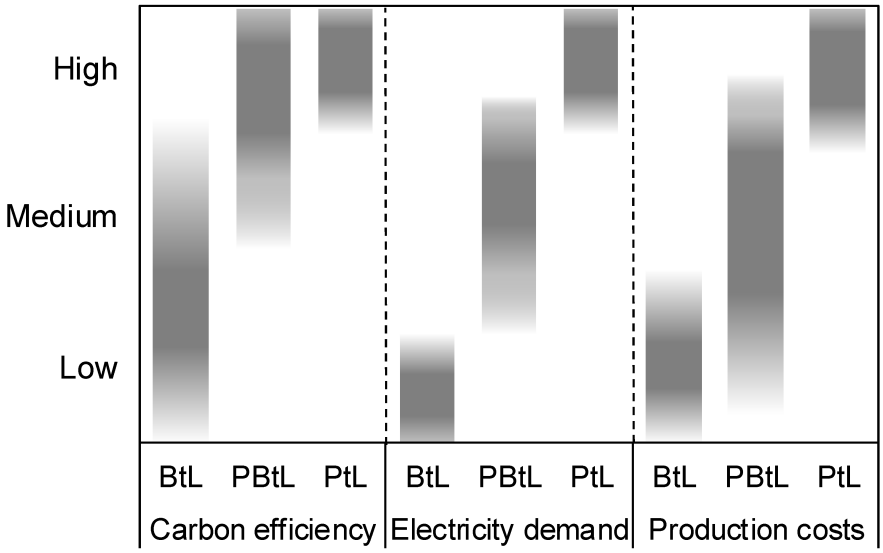

Figure 6-1: Qualitative assessment of biomass-based, hybrid, and power-based fuel production (BtL: Biomass-to-liquid, PBtL: Power- and biomass-to-liquid, PtL: Power-to-liquid).

6.1.1 Carbon efficiency

The carbon efficiency describes the proportion of carbon contained within the feedstock (e.g., in the form of CO_2, within the organic matter) that is chemically bound within the final fuel product. In purely biomass-based fuel production concepts, a portion of the carbon must be discharged from the overall process because the carbon-to-hydrogen ratio in biomass is lower compared to the final fuel product. This excess carbon is typically discharged in the form of CO_2 and released into the atmosphere, which is the final sink. In biomass utilizing synthesis-based production pathways, the necessary addition of oxidizing agents (typically O_2, H_2O, or CO_2) for thermochemical gasification or reforming results in an increased H_2 demand, which has to be compensated within the syngas conditioning step (water-gas shift and CO_2 separation) resulting in additional carbon losses in the form of CO_2. Thus, purely biomass-based fuel production is strongly limited regarding the achievable carbon efficiency. Through carbon-free H_2 production, as enabled by water-electrolysis using electrical energy, the H_2 deficit within the syngas can be balanced, avoiding carbon losses during syngas production and conditioning. Doing so, either separated surplus (and otherwise unused) CO_2 can be utilized in power-based fuel production (PtL), or unconditioned syngas (CO and H_2) can be conditioned by H_2 addition (PBtL) and further processed within the same downstream synthesis process. Therefore, by adding electrical energy in the form of H_2 to such conversion pathways, a complete carbon utilization (carbon efficiency of 100 %) can be achieved in theory within the PBtL and PtL approach. However, the increase in carbon efficiency is directly linked to the amount of H_2 added to such a PBtL process, allowing for a largely arbitrary adjustment of the carbon efficiency between that of BtL processes and theoretical full carbon utilization.

The results of the in-depth analysis described in Chapter 3 show that for the case of converting biogas to methanol (a fuel and a potential intermediate for kerosene production),

the addition of power-based H_2 increases the carbon efficiency of purely biogas-based production, ranging from ca. 58 to 73 %, to over 93 %. Depending on the reforming technology employed, the carbon utilization could be increased by 28 % (bi-reforming configuration: BiRef) or by 67 % (tri-reforming configuration: TriRef). The higher the carbon-to-hydrogen ratio within the feedstock (i.e., the lower the CH_4 to CO_2 ratio in the biogas), the greater the potential of the hybrid production approach to increase the carbon efficiency compared to purely biogas-based production. Within the analyzed hybrid production concepts designed to maximize the carbon use efficiency, carbon losses occur almost exclusively through the removal of purge gases (i.e., a certain share of the gas needs to be removed from the process to prevent an accumulation of inert gases). These losses depend, among other things, on the maximum permitted inert gas concentration within the synthesis loop, the biogas composition, and the per-pass conversion of the reforming technology used.

The purely power-based production of methanol (Chapter 4) achieves a carbon efficiency of over 97 %, excluding potential carbon capture losses (typical carbon capture rates exceed 90 %). Comparable to the hybrid production approach, carbon losses within the power-based production process primarily result from removing purge gases. The required amount of gas to be removed from the overall process is mainly determined by the purity of the feedstock (here: CO_2 and H_2) and the acceptable/allowed concentrations of inert gases within the synthesis loop. While the direct synthesis from CO_2 achieves a lower per-pass conversion rate than the conventional CO-based synthesis used within the hybrid production approach, this may lead to increased syngas losses via purge gas removal. However, since less inert gases can generally be expected in the power-based syngas compared to syngas derived by biogas reforming (N_2 and unconverted CH_4), the overall purge gas demand in power-based production is typically lower, offsetting the syngas losses caused by the lower per-pass conversion.

Summarizing the results of the carbon efficiency investigation, the simulation-based analyses of the hybrid and purely power-based production approaches confirm the great potential of using electrical energy to maximize the utilization of non-fossil carbon. The carbon bound within the feedstock can almost completely be transferred into the desired fuel product. The achievable increase in carbon utilization compared to purely biomass-based fuel production depends mainly on the biogenic feedstock used as well as the syngas production technology utilized.

The carbon efficiency of any subsequent processing into kerosene depends on the selectivity of the following conversion steps (Section 6.2) and does not differ whether the methanol stream originates from biomass, power, or fossil resources.

6.1.2 Electricity demand

In hybrid and purely power-based production approaches, electrical energy is primarily integrated into the targeted product by adding H_2 produced via electrolysis of water. This H_2 is needed to achieve the required syngas ratio (stoichiometric number, Eq. 3-6). The total carbon and part of the required H_2 within the hybrid production approach originate, in this case, from the employed biomass. The carbon contained within the organic matter is typically not fully oxidized during syngas production; instead, for efficiency reasons, it is intended that the carbon remains predominantly in a reduced and not in a fully oxidized form (i.e., the form of CO instead of CO_2). Thus, compared to purely power-based production, where exclusively CO_2 is utilized, and the entire H_2 originates from electrolysis (water splitting), the additional H_2 demand – and so the electricity demand – for hybrid production is significantly lower.

In contrast, the purely power-based production approach requires the entire energy content of the product, along with the occurring conversion losses, to be provided in the form of electrical energy. For exclusively biomass-based production, electricity demand is primarily limited to the provision of energy to operate the respective process components (i.e., compressors, pumps), accounting for a comparatively small portion of the total energy requirements.

The analysis of a hybrid production using biogas and electrical energy to produce methanol (Chapter 3) shows that the electricity demand of such a concept is influenced not only by the hydrogen deficit of the biogas (CH_4 to CO_2 ratio) but also significantly by the chosen process configuration. In addition to supplying power-based H_2, electrical energy can also be converted into chemical energy by providing heat for endothermic reactions. In the process configuration using electrically heated bi-reforming (BiRef), roughly as much energy is required for biogas reforming as for H_2 production via electrolysis. Even with 50 % of this energy supplied through internal heat integration, around 12 % of the input energy is used for heating the respective reforming process. Conversely, in the process configuration with autothermal tri-reforming (TriRef), there is no external energy demand for heating. However, ca. 44 % of the total input energy is needed for H_2 production (compared to only 25 % in the BiRef configuration).

Regarding electricity demand and overall energy efficiency, the analysis reveals that highly efficient electrical heating is energetically advantageous compared to using additional exothermic oxidation reactions for heat generation. The latter approach increases the H_2 deficit, necessitating more H_2 from the energy-intensive electrolysis process. Nevertheless, adding an oxidizing agent (O_2) in the tri-reforming improves methane conversion and reduces downstream purge gas requirements. This slightly increases the carbon efficiency of the TriRef configuration compared to the BiRef configuration. However, this advantage does not fully offset the energy benefits of electrical heating. Thus, with an energy efficiency of 74 $\%_{HHV}$, the BiRef configuration is more energy efficient than the TriRef configuration (69 $\%_{HHV}$).

The purely power-based production approach analyzed in Chapter 4 shows an energetic efficiency of 63 %$_{HHV}$[13]. If CO_2 provision is excluded, more than 92 % of the input energy occurs as H_2, corresponding to an electricity input for electrolysis of 96 %. Additional electricity demands arise for syngas compression and, depending on the heat integration concept, for heating the methanol-water separation. Compared to the CO-based synthesis used in the hybrid process, the CO_2-converting methanol synthesis is less exothermic and produces more water, increasing the separation effort.

To summarize, the electricity demand in hybrid process concepts can vary significantly depending on the feedstock and the technologies used. Within the analyzed concepts, the electricity demands range from 0.55 kWh$_{el}$/kWh$_{HHV}$ (BiRef configuration) to 0.70 kWh$_{el}$/kWh$_{HHV}$ (TriRef configuration). Purely power-based production is associated with the highest electricity demand, being almost entirely utilized for H_2 production from water. Within the analyzed PtM concept, an electricity demand of 1.58 kWh$_{el}$/kWh$_{HHV}$ was determined. The electricity required in purely biomass-based production is usually significantly lower than in PtM and PBtM processes. Since additional electricity is required for H_2 production in PBtM concepts, the electricity demand is necessarily higher than that of the corresponding BtM concept. However, it will most likely remain lower compared to PtM concepts due to the lower H_2 demand for syngas conditioning.

6.1.3 Production costs

Available studies indicate that power-based fuel production is more expensive than biomass-based fuel production [46–49, 83, 176, 177]. This fact is primarily because biomass or biomass-based conversion products (e.g., biogas, ethanol, product gas from gasification) are typically a clearly cheaper feedstock compared to H_2 from water-electrolysis based on “green” electricity. Accordingly, the production costs of hybrid production approaches are expected to fall between those of purely biomass-based and purely power-based production.

However, the cost analysis results (Chapter 3) reveal that in decentralized, small-scale production concepts, where the producible fuel quantity (and thus the designed nominal plant capacity) is limited by the locally available (biogenic) feedstock, methanol production costs from hybrid processes might match those of purely biomass-based production. Here, the cost-intensive production of H_2 – while significantly reducing specific biogas costs – increases the overall feedstock cost share of the total production costs. Nevertheless, within such small-scale production concepts, limited by the locally available amount of biogenic feedstock, the significant increase in production capacity by adding “green” electricity-based H_2 may enable lower specific plant costs due to economies of scale, re-

[13] Assuming electrolysis efficiency of 67 %$_{LHV}$ like in hybrid production (Chapter 3); carbon capture not included.

sulting in reduced annual capital costs. Additional cost reductions are achieved as maintenance and labor expenses are distributed across a larger production volume, leading to a significant decline in these costs compared to purely biogas-based production. Thus, within the analyzed small-scale process concept (Chapter 3), methanol production costs from purely biogas-based and hybrid production are both around 1,300 €$_{2022}$/t.

Nevertheless, the capacity-related advantages of this small-scale application can only be transferred to larger production concepts to a limited extent and only if the availability of biogenic feedstock constitutes the primary limiting design factor. As production capacity increases, the impact of economies of scale, as well as the relative share of maintenance and labor costs decrease. Consequently, higher production costs for hybrid production concepts compared to purely biomass-based approaches are to be expected at larger scales.

The hybrid process configurations analyzed in Chapter 3 utilize continuously available grid power for process energy (including heating) and volatile electricity from photovoltaic systems and wind turbines for H_2 production. Here, a comparison of the two assessed configurations in terms of methanol production costs shows that the BiRef concept (reforming via electrically heated bi-reforming) is advantageous when grid power prices are relatively low, and H_2 production based on photovoltaic and wind power is relatively costly. In contrast, the TriRef configuration (autothermal reforming through O_2 addition) remains largely unaffected by grid power prices but benefits from low H_2 production costs.

Purely power-based production is characterized by the highest production costs of the considered production approaches (i.e., BtL, PBtL, and PtL). This is primarily due to the higher H_2 demand of PtL and the associated high production costs of "green" electricity-based H_2. Additionally, within the biogas-limited small-scale concept analyzed in Chapter 3, the production costs of PtL are further increased by the lower production capacity, exclusively utilizing surplus CO_2 from the local biomethane plant as carbon input. Here, methanol production costs of around 2,100 €$_{2022}$/t – i.e., ca. 60 % higher than those of the other production approaches – result from purely power-based production. Again, the lower production capacity increases the specific investment (economies of scale) and operating costs. Even though these capacity-related effects no longer apply in large-scale PtL production concepts, the costs of purely electricity-based methanol production remain high due to the significant demand for H_2 produced through energy- and capital-intensive water electrolysis.

In accordance with existing literature, the analyses conducted here show higher costs of power-based fuel production compared to biomass-based production. In general, it is expected that the costs of hybrid fuel production will fall between BtL and PtL costs. However, where the feasible production capacity is limited by the locally available amount of biogenic feedstock, hybrid production enables larger production capacities due to the higher utilization of the overall available biogenic carbon (here: CH_4 and CO_2 contained

within the biogas). In such cases, hybrid production enables capacity-related cost savings, potentially offsetting the additional H_2 production costs within selected system configurations.

6.2 Comparison of the Fischer-Tropsch and methanol pathway

This section addresses research question 2 by highlighting the main differences between the FT and MeOH pathway for power-based kerosene production concerning technical, systemic, and economic aspects. These aspects are qualitatively compared in Table 6-1. The results described below are based on the extensive technical analysis (Chapter 4) and the detailed cost analysis (Chapter 5), focusing on carbon efficiency, energy efficiency, and kerosene production cost. The systemic aspects can be derived from the designed process pathways and discussed qualitatively based on the previously presented results.

Table 6-1: Qualitative comparison of the Fischer-Tropsch and methanol pathway (FT: Fischer-Tropsch, MeOH: Methanol).

			FT	**MeOH**
Technical aspects	Carbon efficiency	Total fuel	++	+
		Kerosene	o	+
	Energy efficiency	Total fuel	+	o
		Kerosene	o	++
Systemic aspects	Maturity	Process	+	+
		Fuel	+	o
	Flexibility	Feedstock	++	++
		Products	+	++
		Logistics	o	++
Economic aspects	Production costs	Total fuel	–	––
		Kerosene	––	–

Negative		Neutral		Positive
––	–	o	+	++

6.2.1 Technical aspects

The FT and the MeOH pathway are compared in terms of technical aspects in the following section.

Carbon efficiency. In the power-based kerosene production pathways, CO_2 serves as the sole carbon input/source. Within the process concepts analyzed in Chapters 4 and 5[14], the following efficiencies are derived.

- *Total fuel-related efficiency.* Within the FT pathway, CO_2 can be nearly entirely converted into fuel components, achieving a carbon efficiency of 98 to 99 % related to the total fuel production (i.e., naphtha, kerosene, and diesel) in the reference case and under the variation of technical parameters. Losses occur exclusively through purge gas venting within the synthesis loop. The MeOH pathway achieves a total fuel carbon efficiency of 83 to 85 % in the reference case, with values ranging from 74 to 92 % under technical parameter variations. Losses primarily arise from purge gas in the oligomerization loop, mainly caused by the accumulation of light alkanes that cannot be recycled due to the lack of a reforming option. Additionally, small amounts of wax components are generated, which cannot be utilized due to the absence of a hydrocracker in the defined process concept. These material streams are burned with purge gases from the methanol synthesis for heat generation, which represents a carbon loss due to the assumed release of flue gas into the atmosphere.

- *Kerosene-related efficiency.* The carbon efficiency considering only the kerosene fraction is 70 to 72 % within the FT pathway's reference case, varying between 61 and 78 % under parameter variations. The main by-product is naphtha, which is produced as a straight-run product from the synthesis and during the subsequent hydrocracking step. Within the MeOH pathway, a kerosene carbon efficiency of 76 % can be achieved in the reference case, with values varying between 60 and 90 % under parameter variations.

The FT pathway achieves an almost complete carbon utilization based on the process configurations analyzed here. This is enabled by the subprocesses hydrocracking and reverse water-gas shift (RWGS) converting product fractions outside the fuel range either directly into suitable fuel components or reform them into syngas easily to be recycled. Such technologies are not available within the analyzed MeOH pathway, requiring some intermediate and by-products to be removed from the overall process, resulting in carbon and hydrogen losses. In terms of pure kerosene production, the MeOH pathway enables a more selective production of kerosene due to the longer monomers and the ability to directly

[14] The carbon efficiencies between the analyses carried out in Chapter 4 and 5 slightly differ, as the process concepts and some modeling approaches differ slightly. The value ranges given represent the total range from both analyses.

recycle shorter olefins during oligomerization. In contrast, the FT synthesis allows the recycling of light fuel fractions only after prior reforming. Consequently, the synthesized chains must be fully cracked before chain growth can restart.

Energy efficiency. Since the H_2 feed within both pathways analyzed in Chapters 4 and 5[15] accounts for the highest energy input (> 87 %), energy efficiency is closely linked to material (carbon and hydrogen) efficiency rather than process energy demands. Consequently, due to minor losses of carbon and hydrogen, the FT pathway shows a higher total fuel energy efficiency of 67 %$_{HHV}$ within the reference case and 63 to 70 %$_{HHV}$ under parameter variation. Within the analyzed MeOH pathway, total fuel energy efficiency ranges from 62 to 64 %$_{HHV}$ in the reference case and 54 to 68 %$_{HHV}$ under parameter variation. However, the MeOH pathway shows a higher kerosene energy efficiency of 55 to 58 %$_{HHV}$ (44 to 66 %$_{HHV}$ under parameter variation) against 48 to 49 %$_{HHV}$ within the FT pathway (38 to 54 %$_{HHV}$ under parameter variation). Additionally, the MeOH pathway offers thermodynamic advantages since no high-temperature heat is required. In the FT pathway, the RWGS reaction necessitates significant energy input being subsequently released at a lower temperature level within the FT synthesis. The energy requirements of the RWGS are also increased by the reforming of recycled gases and measures to avoid metal dusting (i.e., the addition of steam and limited heat integration). A CO_2-based methanol synthesis ensures that the entire methanol pathway consists of exothermic processes and minimizes losses from a chemical reaction perspective.

Both process pathways can be considered relatively efficient when compared to the thermodynamic maximum. However, significant losses occur when considering the necessary upstream efforts for water electrolysis and CO_2 capture, which can reduce efficiency by up to 25 %pt (Section 4.2.3.2).

6.2.2 Systemic aspects

Process and fuel maturity. Figure 6-2 illustrates the maturity of Fischer-Tropsch- and methanol-based kerosene production regarding process and fuel readiness. The pathways differ significantly in their conversion reactions and, thus, in the utilized process technologies. Both pathways mainly rely on well-established, commercially used processes/process steps. However, an exception is the process step of the reverse water-gas shift (RWGS) reaction needed within the FT pathway. This process step reduces CO_2 to CO and is not required in fossil and biomass fuel-based syngas production, where CO-rich syngas results from partial oxidation of the hydrocarbons used as feedstock. Therefore, there is not yet a known commercial application of this technology. During recent years, initial pilot-scale implementations of this technology have been developed within the context of power-to-x (PtX) projects, resulting in an increase of the technology readiness

[15] The energy efficiencies between the analyses carried out in Chapter 4 and 5 slightly differ, as the process concepts, some modeling approaches and the energy integration concepts are slightly different. The value ranges given represent the total range from both analyses.

level[16] (TRL) to be now between 5 and 7; i.e., this technology is not yet fully market mature. In contrast, the FT synthesis and the subsequent downstream hydrotreatment steps are fully technologically mature, with a TRL of up to 11. As such, the overall TRL of the FT pathway is currently rated mainly between 6 and 7, determined by the RWGS reaction step and, thus, the lack of a commercial demonstration of the overall process chain.

The direct CO_2-converting methanol synthesis used in the MeOH pathway has been demonstrated multiple times on an industrial-relevant scale and has even seen limited commercial application (TRL 8 to 9). The necessary downstream conversion processes, including dehydration, oligomerization, and hydrogenation, are fully mature for specific applications (up to TRL 11). However, dehydration and oligomerization have not yet been optimized and integrated for fuel products fulfilling the kerosene specification based on the currently valid standards. So far, the dehydration process is predominantly used to produce short-chain olefins such as ethene and propene. However, it can also target C_4 to C_6 olefins. Common oligomerization technologies are mainly used to link pure olefin monomers to gasoline components or specific chemical compounds (e.g., fine chemicals) used within the chemical industry (i.e., as a raw material). Thus, the oligomerization of olefin mixtures for kerosene production lacks commercial demonstration. Due to the pending demonstration of overall concepts enabling standard-conform kerosene production by combining these individually mature process steps, the overall TRL of the MeOH pathway is currently rated between 5 and 7.

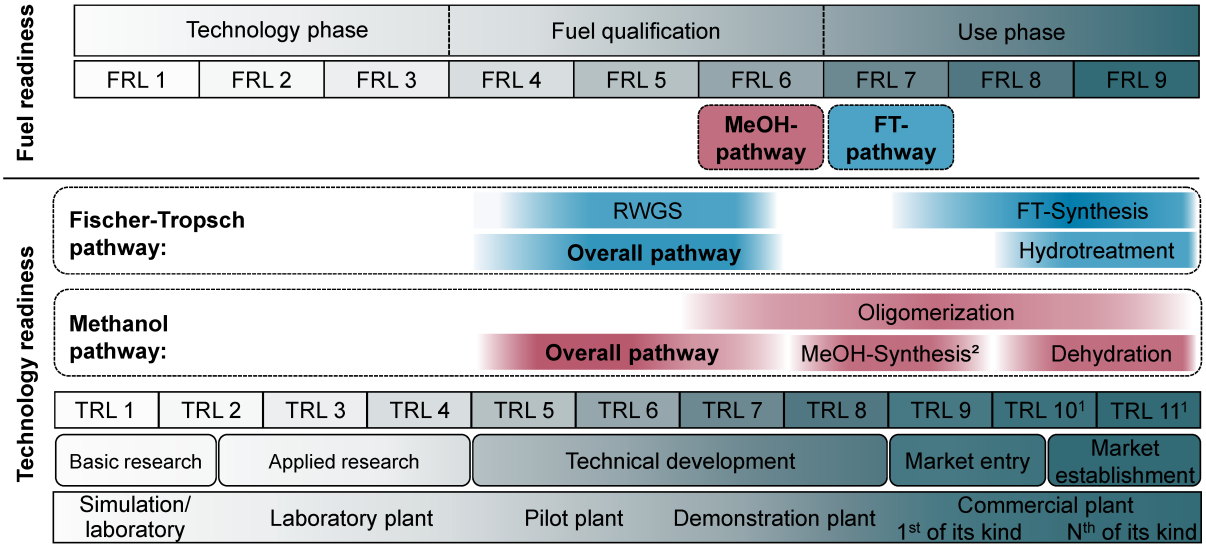

Figure 6-2: Technology (TRL) and fuel readiness level (FRL) of the Fischer-Tropsch (FT) and methanol (MeOH) pathway (color gradient indicates degree of maturity; [1]TRL scale according to IEA ETP Clean Energy Technology Guide [201], [2] direct, CO_2-converting methanol synthesis).

[16] The technology readiness level is a scale from 1 to 9 (expanded to 11 by the IEA) used to classify the development stage of processes and technologies (also see [199–201]).

From a Fuel Readiness Level[17] (FRL) perspective, the FT pathway currently has an advantage, as ASTM certification has already been achieved (FRL 7 to 8). For the MeOH pathway, ASTM approval (FRL 6) is still pending. However, several technology providers are currently undergoing the necessary certification process under ASTM D4054, and approval is expected within the next few years [203].

Feedstock flexibility refers to the range of energy and material feedstocks that can be utilized. The power-based production of kerosene-type SAF relies on electricity as the primary energy feedstock, while H_2O and CO_2 serve as non-energy material feedstocks. Through electrolysis, H_2 is produced from water and combined with CO_2 to produce power-based syngas. This syngas mixture acts as the feedstock for subsequent synthesis and conversion processes, ultimately yielding synthetic kerosene via either the FT pathway or the MeOH pathway. Since both pathways utilize syngas as the basic material, they can, in principle, also be adapted for biomass-based or hybrid production processes. Therefore, concerning technically feasible feedstocks, both conversion pathways are characterized by a high flexibility.

Product flexibility refers to the capability to adjust production in response to market changes. During times of high sustainable aviation fuel (SAF) demands, selectivity for kerosene as the target product is crucial. However, in times of lower SAF demand (e.g., during a pandemic) and thus lower market revenues, the flexibility to produce alternative end products within the kerosene production plant can offer significant advantages.

Kerosene-optimized production concepts based on the FT pathway primarily allow adjustments in the share of fuel fractions produced and the production of additional by-products, such as waxes (e.g., for lubricant manufacturing). These adjustments can be achieved by modifying the operating conditions of the FT synthesis (e.g., temperature, pressure, residence time) within the allowable operating window and/or by redistributing downstream material streams (e.g., directing more or fewer components to hydrocracking).

In the MeOH pathway, methanol synthesis occurs as the first step, yielding pure methanol as an intermediate. With a current global demand of over 100 Mt/a, methanol is one of the most widely produced primary or base chemicals. Furthermore, “green” methanol is expected to be increasingly used within the maritime sector as an alternative fuel. The subsequent conversion to olefins, the first step in the methanol-to-kerosene process chain, is already well-established, with more than 30 Mt/a used for ethene and propene production. Thus, if the demand for kerosene decreases, the MeOH pathway can switch to marketing the intermediate products methanol and olefins, which are already traded in large quantities worldwide. Additionally, during the oligomerization step, some flexibility in the product spectrum is expected through adjusted operation conditions and recycles.

[17] The fuel readiness level is a scale from 1 to 9 used to classify the development stage of a fuel, specifically used within aviation fuel development (see [199, 200, 202]).

However, current applications suggest a shift toward shorter-chain fractions rather than diesel or waxes.

Regarding the flexibility to transition away from kerosene production to other value-added products, if economically required, the MeOH pathway shows an advantage due to the intermediate products generated within the process chain, which can be supplied to established markets as basic or high-value chemicals (also in need of defossilization).

Logistical flexibility refers to the ability to produce and transport products and intermediates with geographical flexibility. In this context, the MeOH pathway offers two significant advantages over the FT pathway. While the latter pathway produces syncrude as an intermediate, which is a diverse mixture with variable composition requiring considerable logistical effort for transportation without additional processing, methanol is a pure substance that can be easily handled based on available and proven technical rules using existing infrastructure. This advantage opens the window for the MeOH pathway to separate the methanol production section and the conversion section geographically (e.g., methanol production in countries with a high potential for renewable energy; methanol conversion within the kerosene-utilizing country) and facilitates a division of production responsibilities between methanol producers and kerosene producers.

Additionally, methanol production is more straightforward to implement in small-scale setups than the FT pathway. This may enable the utilization of smaller quantities of locally available and potentially more affordable feedstocks. The subsequent conversion of methanol to kerosene, requiring significantly less energy compared to methanol production, can then be performed on a large scale, benefiting from economies of scale. In contrast, although innovative reactor designs for small-scale FT synthesis exist, separating FT synthesis from downstream processing is challenging due to the logistical constraints associated with the long-distance transportation of syncrude. In this regard, the MeOH pathway shows clear advantages.

6.2.3 Cost aspects

Chapter 5 provides an extensive cost analysis of power-based kerosene production, comparing the FT and MeOH pathways. Since significant amounts of by-products (such as naphtha and diesel) occur during kerosene production in both pathways, the kerosene production costs also depend heavily on the revenues from naphtha and diesel sales. Thus, two cost allocation methods are applied to address uncertainties associated with unpredictable by-product revenues: (i) allocating costs solely to the kerosene fraction without considering by-product revenues establishes the upper-cost limit, while (ii) allocating costs across the total fuel fraction defines the lower cost boundary. The latter assumes that none of the produced by-products has a higher value than kerosene, as maximizing the more valuable by-product would then be economically more viable than the kerosene maximization examined here.

The total fuel production costs in the FT pathway are lower than in the MeOH pathway (FT: 3,630 €$_{2023}$/t, MeOH: 4,240 €$_{2023}$/t). However, when considering exclusively the kerosene production costs (excluding by-product revenues), the MeOH pathway shows lower costs (FT: 5,070 €$_{2023}$/t, MeOH: 4,660 €$_{2023}$/t). Variations in by-product revenues reveal an advantage for the FT pathway if by-product revenues exceed 30 % of the kerosene production cost.

In both pathways, the costs are predominantly influenced by the supply of H_2 and CO_2. Consequently, feedstock conversion efficiency is one of the most critical factors, alongside feedstock prices, in determining production costs. H_2 price variations (between 3 and 7 €$_{2023}$/kg) result in cost variations of ca. ±25 % for both pathways. CO_2 prices corresponding to supply costs from direct air capture (1,000 €$_{2023}$/t) can lead to cost increases of up to 75 % compared to CO_2 prices associated with point source carbon capture (150 €$_{2023}$/t).

In conclusion, based on the analyzed kerosene production costs, ranging mainly between 3,500 and 5,500 €$_{2023}$/t, power-based aviation fuels are expected to be significantly more expensive than most biomass-based kerosene alternatives [11, 46, 48, 50]. The primary cost drivers are upstream of the synthesis process, particularly H_2 production and CO_2 supply. Due to its lower H_2 and CO_2 demand relative to total fuel production, the FT pathway shows lower production costs if the achievable relative revenue of the different fuel fractions (kerosene, naphtha, diesel) are comparable. However, if the achievable relative revenue of kerosene is significantly higher than that of naphtha or diesel, the MeOH pathway may be economically advantageous due to its higher kerosene selectivity.

6.3 Techno-economic key parameters

In this section, the third research question is addressed by building upon the findings from Chapters 3 to 5. The key parameters determining the efficiencies and costs of fuel, especially kerosene production from electrical energy, are discussed in terms of technical efficiencies and, subsequently, costs.

6.3.1 Efficiency affecting parameters

To analyze the influence of technical parameters on carbon and energy efficiencies, specific operating parameters (e.g., temperature, feedstock composition) and selected process parameters (e.g., conversion rates, selectivities) were identified during process analyses and varied within their expected ranges. Such a procedure allows for identifying potential optimization areas for the overall process concepts while also visualizing uncertainties resulting from assumed parameter values whose actual achievable ranges are not precisely estimable for the time being.

Hybrid methanol production. In the examined power-and-biogas-to-methanol concept, the composition of the biogas stream entering the conversion process (inert gas (N_2) fraction of 0 to 5 vol%; CH_4 to CO_2 ratio of 1 to 3) is identified as a highly variable input factor. Variations can occur in particular due to the substrate used, the fermentation technology, and possible biogas pre-treatments (e.g., biogenic desulfurization). Parameter variation results show that high N_2 concentrations within the biogas have a larger impact on carbon efficiency compared to the CH_4 to CO_2 ratio, leading to carbon losses of up to 5 %pt compared to biogas free of N_2. Energy efficiency is more affected by the CH_4 to CO_2 ratio, especially in the process configuration with electrically heated bi-reforming (BiRef), varying by up to 6 %pt in the analyzed parameter range.

Variations of operating parameters such as reforming temperature (800 to 1,000 °C) and allowable inert gas content during synthesis (0 to 50 vol%) are analyzed. Both parameters show a significantly higher influence on carbon and energy efficiency than biogas composition (in some cases, there is a variation of more than 20 %pt). However, the parameters are manageable through adjustments within the respective reactor design, making them controllable optimization parameters. The results show that the reference cases assumed here are already close to the maximum achievable efficiencies. Therefore, the parameters do not give rise to significant uncertainties, and the optimization potential is relatively low.

Power-based kerosene production. Concerning methanol synthesis based on power-based syngas, no technical parameters are identified that are associated with major uncertainties or cannot be technically controlled. In the comparative analysis of kerosene production from power-based syngas via the FT and MeOH pathways, two process parameters are varied for each pathway. In the FT pathway, the well-controllable chain-growth probability within the FT synthesis and the number of cracking reactions ("activity") within the hydrocracker are varied; the hydrocracking activity can also be influenced by reactor design and operating conditions. In the MeOH pathway, the focus is on the olefin selectivity, which is currently technically limited, and the chain-growth probability during oligomerization. While the chain-growth probability can be influenced by design and operational adjustments, the achievable ranges and product distributions – especially when accounting for recycle streams – remain largely uncertain.

- For the FT pathway, the varied parameters cause minimal changes in total fuel efficiencies, with the energy efficiency (7 %pt) being more affected than the carbon efficiency (1 %pt). However, higher chain-growth probabilities and mild cracking conditions led to improvements in kerosene selectivity. The kerosene-related carbon and energy efficiency vary by about 16 %pt within the technical parameter variation range. Due to the controllability of the chain-growth probability and the hydrocracking intensity, the achievable improvements compared to the reference case are considered to be realistic optimization opportunities rather than uncertainties.

- In the MeOH pathway, a wide variation in total fuel efficiency and kerosene selectivity is observed. The total fuel efficiency varies by around 18 %pt regarding carbon efficiency and about 13 %pt regarding energy efficiency. The kerosene-related carbon and energy efficiency vary even more by about 30 %pt and 21 %pt, respectively. Achieving a high olefin selectivity during dehydration is critical for reaching high carbon and energy efficiencies. Additionally, low chain-growth probabilities, combined with high naphtha recycling rates, enhance kerosene selectivity while reducing the formation of heavier components. However, the extent to which further improvements in olefin selectivity beyond the assumed reference value are possible and the degree to which the product composition of oligomerization can be technically influenced remain uncertain. Therefore, the broad range of results is better interpreted as reflecting uncertainties.

Considering the entire PtL production chain, including the energy-intensive water-electrolysis and the potentially elaborate CO_2 capture, it becomes evident that the main energy demands are upstream of the syngas conversion. Thus, the achievable electrolysis efficiency and the available carbon capture source significantly influence the overall energy efficiency of such a PtL concept. Varying the energy efficiency of the electrolysis step results in variations of the overall energy efficiency of up to about 18 %pt, while the type of available carbon source (i.e., the concentration of CO_2 within the available gas mixture) leads to overall energy efficiency variations of up to ca. 14 %pt. However, this also underlines the importance of an efficient downstream conversion of the elaborately produced power-based syngas.

Comparison. The carbon and energy efficiency of kerosene and kerosene intermediate production utilizing electrical energy is influenced by a broad range of pathway-dependent process parameters. Syngas production in hybrid concepts is strongly affected by the reforming of hydrocarbons and the feedstock composition, which directly further affects the methanol synthesis, especially regarding purge gas amounts. In contrast, purely power-based production mainly depends on the efficient supply of H_2 (electrolysis efficiency) and CO_2 (point source or DAC), with no further effects on methanol synthesis as long as common gas purities are achieved.

Downstream of the synthesis process, no major differences between biomass-, hybrid, or power-based production occur. Regarding the conversion to kerosene, a distinction can be made between total fuel-related efficiency and kerosene-related efficiency. For total fuel efficiency, inert by-products formed within the process chain are particularly relevant, as they lead to increasing amounts of purge gas within the subsequent conversion steps. For kerosene efficiencies, the selectivity of the conversion process and the ability to utilize by-products through recycling play a key role. High recycle streams increasing the energy demand of production are outweighed by the gains achieved through higher product yields.

6.3.2 Cost affecting parameters

Besides efficiency affecting parameters that directly influence production costs, economic parameters were varied. These parameters primarily encompass feedstock costs, production capacities and utilization, as well as capital-related costs. These factors can impact production costs significantly but do not affect technical efficiencies.

Hybrid methanol production. The cost analysis of decentralized, small-scale hybrid production (power- and biogas-to-methanol, Chapter 3) shows that the variations in carbon and energy efficiencies from technical parameter variation result only in minor cost changes (< 10 % from the reference case) within the expected parameter ranges. In contrast, within the assumed small-scale production concept limited by the available amount of biogenic feedstock, the installed methanol production capacity significantly influences the production costs. The considered biogas availability ranges from ca. 70 to 70,000 Nm^3/h, representing relatively small agricultural sites up to the largest industrial-scale facilities currently in operation. Halving the production capacity of the reference case (670 Nm^3/h) leads to an increase of 34 % (BiRef) and 28 % (TriRef), while doubling the capacity shows a production cost reduction of 17 % (BiRef) and 14 % (TriRef). This underscores the positive effect of increasing production capacity via the hybrid production approach within small-scale production concepts, where the availability of biogenic feedstock limits the maximum production capacity. Particularly for production capacities smaller than in the reference case (8,000 t_{MeOH}/a), a strongly nonlinear cost increase is observed, indicating that small-scale production concepts require a minimum capacity to bring costs down to allow for a potentially economically feasible production. For larger production capacities, further cost reductions can be achieved with increasing scale, albeit to a lesser extent. At the same time, the previously described capacity-related advantages of hybrid production diminish as production capacity increases.

Biogas and H_2 prices are particularly important in terms of feedstock costs. Since biogas represents the largest material and energy input, and prices can vary in a wide range, it strongly determines methanol production costs (variations around −10 to +40 % from the reference case). The H_2 price also has a significant influence. However, its impact on the methanol production costs depends strongly on the respective H_2 demand (i.e., the process configuration and the biogas composition (CH_4 to CO_2 ratio)). Other factors, such as the weighted average cost of capital (*WACC*) or annual full-load hours, play only a minor role within the considered ranges (< 10 % from the reference case).

Power-based kerosene production. In power-based production, H_2 and CO_2 costs have the most significant influence on production costs. Reducing H_2 prices from 5 €/kg (reference case) to 3 €/kg can lower kerosene production costs by up to 25 %. Conversely, CO_2 prices – particularly in the range of current direct air capture costs (up to 1 €/kg) – can increase kerosene production costs by up to 75 % compared to levels associated with point source carbon capture costs.

The influence of varying technical parameters differs depending on whether the costs are allocated to all fuel products (total fuel (TF) allocation, representing the assumed lower cost boundary) or whether no revenues from naphtha or diesel are assumed (kerosene (K) allocation, representing the assumed upper cost boundary). Regarding the total fuel allocation, the changes lie between 0 % and +1 % within the FT pathway since the total fuel output stays almost constant. Within the MeOH pathway, the costs vary between −8 % and +10 %, which directly correlate with the total fuel output. Technical parameter variation considering kerosene allocation yields variations of −9 to +14 % within the FT pathway and −12 to +22 % within the MeOH pathway.

Plant production capacity also plays a crucial role in determining the overall costs. Since the reference case capacity (100,000 t_{TF}/a) is already relatively high, further cost reductions from upscaling are expected to be relatively low. However, significant reductions in plant capacity (< 25,000 t_{TF}/a) can increase kerosene production costs by more than 30 %. Other economic parameters show a minor influence on the fuel production costs (< 10 % from the reference case) as long as the production capacity is in the range of the reference case and capital-intensive H_2 production (electrolysis) is outside the respective system boundaries.

Comparison. In hybrid and purely power-based fuel production, production costs are primarily determined by feedstock costs (i.e., H_2 and CO_2 costs) as well as the costs of biogenic feedstocks in hybrid production. Since feedstock costs constitute the largest share of the overall production costs, efficient (technical) conversion to the target product is of great importance. For small-scale concepts, it is evident that economies of scale can cause high specific capital expenditures (fixed capital investments) and operational expenditures. This also amplifies the impact of economic parameters such as *WACC* and depreciation period. The main influences on production costs in hybrid and purely power-based process approaches are, therefore, fundamentally similar, although the importance of H_2 supply plays an even greater role in power-based production, and CO_2 supply is not relevant in hybrid production.

6.4 Limitations of analyses

The detailed techno-economic results described in chapters 3 to 5, as well as the broader findings presented above, are based on the design, modeling, and simulation of process concepts and their technical and economic analysis. In general, the process analyses conducted within the scope of this thesis follow a uniform approach. The resulting limitations regarding the accuracy and applicability of the findings are outlined below.

- *Process design.* The process design aims to develop representative and widely comparable overall processes (reference concepts). To achieve this, sub-technologies for the necessary process steps are selected and integrated into an overarching process flow

diagram. The selection of these subprocesses and their integration can result in various overall concepts characterized by significantly different techno-economic properties. Also, to derive representative and interpretable results, the production approaches are designed as generically as possible, and decisive process parameters are varied. However, the detailed results are directly tied to the analyzed process concepts and can thus only be transferred to other process concepts to a limited extent.

- *Process modeling and simulation*. To calculate the mass and energy flows occurring within the respective process concepts, the overall processes are modeled and simulated under steady-state conditions using appropriate software (Aspen Plus [109]). In line with the conducted analysis, the modeling is performed at the plant system level. The focus of process modeling is less on the detailed representation and analysis of specific chemical reactions (e.g., through kinetic models) and more on translating process characteristics (e.g., product distributions, selectivities, conversion rates) into corresponding reaction units. The approaches implemented in the modeling process significantly influence the techno-economic results, just as the process flow design does. Thus, a generic representation and an additional analysis through parameter variation are essential for the validity of the analysis results. The results are directly related to the assumptions made during modeling and can only be properly interpreted, keeping the respective modeling approaches in mind. The approaches used in modeling the investigated process concepts are largely based on previously published and validated models or process data. However, due to the lack of real-world data, a generic approach had to be developed to represent the product distribution in the oligomerization step of the methanol pathway (see Chapter 4, Annex B, and the enhanced model in Annex C). To reflect the resulting uncertainties, an extensive variation of modeling parameters is conducted. The resulting uncertainties regarding the methanol pathway's results are identified and quantified and must be considered when interpreting the results.

- *Technical analysis.* The process analysis translates the simulation results into relative process flow diagrams (e.g., Sankey diagrams) and assesses them based on carbon and energy efficiency. Estimating the heat integration potential and the resulting external energy requirements is also necessary for energy-related considerations. The applied pinch analysis determines the maximum integration potential under the assumption of a minimal temperature difference. Depending on the defined overall concept and the chosen energy integration approach, different overall energy efficiencies might result. Therefore, the respective energy integration approach is also relevant for interpreting and comparing the results. While there are differences between individual analyses, they remain consistent within each analysis, ensuring comparability within the investigation.

- *Economic analysis.* The simulation results serve as the basis of production cost analysis. The production costs represent the minimum selling price required to ensure the

economic viability of the respective production process. These results are based on the outcomes of the technical analysis and are thus closely linked to the investigated process concepts and modeling approaches (see above). For the calculation of fixed capital investments, the module costing technique [110], a method for providing preliminary investment estimates (e.g., for chemical plants), is applied. This method is characterized by a calculation accuracy of +50 % / −30 %. However, since not all apparatuses used can be exactly represented using the available cost equations, higher cost deviations may occur. Furthermore, such cost calculations are always subject to significant uncertainties because numerous assumptions must be made, relying on, for example, geographic, economic, or political conditions that can vary considerably and are not fully predictable. Consequently, the results of the economic analysis are associated with relatively great uncertainties.
Nevertheless, the calculation of production costs across the different analyses is based on the same methodology. Thus, full comparability is ensured within each publication/chapter. However, for comparisons between publications/chapters, the respective technical and economic framework conditions must be considered.

- *Data availability.* The process design, modeling, and framework assumptions of the economic analyses are based on data available from public sources at the time of the analysis. For the technical assessment, mainly peer-reviewed publications and free accessible real-plant data from existing facilities are used. However, the quality and availability of the data might vary significantly between different process technologies. In particular, when comparing the power-based kerosene production pathways, a broad data foundation is available for modeling the already industrially established FT pathway, whereas the modeling of the less-explored MeOH pathway relies on a more limited dataset, resulting in greater uncertainties. These uncertainties were explicitly addressed during the analyses to prevent any misinterpretation of the results.

The relative results and the general correlations across analyses are largely comparable due to the consistent methodological approach and the similar system boundaries. However, the absolute results are valid only for the underlying process concepts and the assumptions made regarding modeling and analysis. To ensure the interpretability of the results, all process details have been thoroughly described and justified in the publications/chapters and the supplementary information (Annex A to Annex C). To mitigate the effects of case-specific conditions and the uncertainties arising from limited data availability, key technical and economic parameters were varied across broad ranges. Consequently, the results are valid for achieving the defined research objectives and answering the research questions. Nevertheless, the transferability of detailed results to process concepts not examined within the scope of this thesis is limited.

7 Final considerations

In light of the accelerating global warming, the aviation sector faces the urgent challenge of rapidly reducing its reliance on fossil fuels. Replacing conventional kerosene with sustainable aviation fuels (SAF) is crucial for achieving aviation's climate goals. However, given the growing demand for SAF and the a priori limited availability of sustainably sourced biomass, power-based kerosene is expected to play a significant role in meeting future needs – if the GHG reduction targets are taken seriously. Utilizing electrical energy enables kerosene production independent from biomass-derived energy or combined power- and biomass-based SAF production, reducing the specific biomass demands. Additionally, various synthesis pathways exist for power-based SAF production, each with distinct technological and economic implications. Against this background, the overarching research objective of this thesis is to investigate how kerosene-type SAF can be efficiently produced using electricity from renewable sources of energy as the primary energy source. The results quantify the techno-economic characteristics of different production approaches and the most widely discussed synthesis pathways for producing power-based kerosene or kerosene intermediates. The identified research gaps in this context are addressed through three overarching research questions, focusing on (i) the implications of electrical energy utilization for carbon-efficient fuel production, (ii) common production pathways for power-based kerosene production, and (iii) the respective determining technical and economic parameters. The analysis comprises three scientific publications (Chapters 3 to 5). Chapter 3 investigates the hybrid – i.e., power- and biogas-based – production of methanol (a potential intermediate within synthetic kerosene production) via two process configurations, comparing them with purely biogas- and purely power-based production approaches. Chapters 4 and 5 investigate the power-based production of kerosene via the Fischer-Tropsch (FT) and methanol (MeOH) pathway. The broader findings derived from these detailed analyses are synthesized and discussed in Chapter 6.

7.1 Summary

The methodological framework for analyzing the different production approaches and concepts combines process conceptualization and design, modeling, steady-state process simulation, and techno-economic assessment on a plant system level. The key figures assessed within the investigations are carbon efficiency, energy efficiency, and production costs. Process modeling and simulation are based on the design of representative and fair-comparable process concepts derived by integrating the respective individual sub-pro-

cesses into an overall process flowsheet. Process simulation derives mass and energy balances, allowing for a detailed assessment of material (especially carbon and hydrogen) flows and energy demands. Technical key figures are determined from the simulation results, further considering energy integration (e.g., pinch analysis). The variation of operating and process parameters explores impacts on the overall process efficiencies and the associated uncertainties and/or optimization potentials. The economic assessment analyses production cost, also applying technical and economic parameter variations. Building on the described approach, the research questions are answered to achieve the overall research objective.

The following key findings regarding the implications of electrical energy utilization for carbon-efficient fuel production can be summarized.

- Integrating electricity from renewable sources of energy into biomass-based fuel production by adding H_2 from water-electrolysis (hybrid fuel production) enables nearly complete carbon utilization, significantly reducing the specific biomass demand. In the analyzed decentralized power-and-biogas-to-methanol approach, hybrid production leads to carbon efficiencies above 93 %, a clear increase in carbon utilization compared to purely biogas-based production (58 to 73 %). Within this small-scale concept, where the availability of biogenic feedstock is assumed to be the limiting factor for the realizable production capacity, methanol production costs around 1,300 €$_{2022}$/t (similar to those in the purely biogas-based approach) can be achieved, benefitting from economies of scale despite the high cost of power-based H_2 production.

- The comparison of two possible process configurations – one using electrically-heated bi-reforming (BiRef configuration) and the other employing autothermal tri-reforming (TriRef configuration) of biogas – reveals significant differences regarding the integration of electrical energy and its implications on techno-economic key figures. While electrical heating of the endothermic reforming process efficiently converts electrical energy into chemical energy, autothermal reforming requires higher H_2 addition from electrolysis, resulting in higher energy losses. However, the addition of O_2 as an oxidizing agent in tri-reforming enhances conversion efficiency, thus reducing carbon and hydrogen losses and increasing carbon efficiency. The carbon and energy efficiency derived are 93 % and 74 %$_{HHV}$ for the BiRef configuration and 97 % and 69 %$_{HHV}$ in the TriRef configuration. Economically, both process concepts lead to similar fuel production costs (BiRef: 1,280 €$_{2022}$/t, TriRef: 1,310 €$_{2022}$/t), with H_2 costs being the determining factor in selecting the more cost-effective concept.

- Purely power-based methanol production involves converting electrical energy into chemical energy solely through H_2 production via electrolysis. The downstream synthesis enables direct CO_2 conversion into methanol with a very high carbon efficiency (> 97 %). Compared to hybrid production, significantly more H_2 must be produced, as half of the oxygen contained within the CO_2 needs to be removed as water during the

subsequent chemical reactions. In the analyzed small-scale, purely power-based methanol production, production costs amount to ca. 2,100 €/t. The significant cost increase compared to the biogas-based and hybrid approach results from the higher H_2 demand as well as from the lower production capacity, which is restricted in the analyzed concept by the availability of CO_2 from the assumed biogas production facility.

The analysis of kerosene production from power-based syngas, comparing the FT and MeOH pathway, results in the following key insights.

- The FT pathway is characterized by a high total fuel (TF) carbon efficiency of 99 % (including kerosene, naphtha, and potentially diesel). The syncrude produced through the relatively unselective FT synthesis can be upgraded selectively, with light by-products being recycled and reformed into syngas within the reverse water-gas shift (RWGS) reactor. Selective hydrocracking enables the conversion of long-chain waxes into kerosene and naphtha fractions, increasing the kerosene (K) carbon efficiency from around 70 % in the reference case to around 78 % when high chain growth probabilities in the FT synthesis are combined with mild hydrocracking. Due to the high carbon and hydrogen efficiency, energy efficiencies of around 49 %$_{HHV}$ regarding the kerosene yield and around 67 %$_{HHV}$ regarding the total fuel yield can be achieved.

- In the MeOH pathway, hydrocarbon production occurs through methanol synthesis, followed by extensive downstream processing. Methanol is synthesized very selectively but requires a subsequent (downstream) conversion into hydrocarbon chains based on dehydration and oligomerization processes. Due to the larger monomers (C_2 to C_4), compared to the FT reaction (CO monomers), fewer chain-growth reactions are required within the oligomerization to achieve the same product chain length, enabling a more selective production. This is further enhanced by recycling light fuel fractions, such as naphtha, directly back to the oligomerization reactor, clearly reducing the by-product formation. As a result, the MeOH pathway is more kerosene selective (ca. 76 %) than the FT pathway. However, it incurs higher carbon losses due to purge gas venting, primarily from alkane formation during dehydration, resulting in a total fuel carbon efficiency of around 84 %. The efficiency of the pathway is thus primarily determined by olefin selectivity in dehydration. In terms of energy efficiency, the MeOH pathway benefits from a thermodynamic advantage, as it involves only exothermic reactions (kerosene and total fuel energy efficiency of 56 and 63 %$_{HHV}$). In contrast, the FT pathway requires additional energy input for the RWGS reaction, with the energy then released during the FT synthesis at a lower temperature level. However, regarding the total fuel fraction, this reaction-related advantage of the MeOH pathway is more than offset by higher carbon and hydrogen losses.

- The kerosene production costs (*KPC*), depending on the allocation method/by-product value and the assumed parameters, are predominantly between 3,500 and

5,500 €$_{2023}$/t. The FT pathway achieves comparatively lower *KPC* of 3,630 €$_{2023}$/t when costs are allocated to all fuel fractions. However, if no significant revenues can be generated from the by-products, *KPC* increase significantly to about 5,070 €$_{2023}$/t. Production costs for the MeOH pathway are less dependent on by-product revenues due to its higher kerosene selectivity (4,240 to 4,660 €$_{2023}$/t). However, they exceed those of the FT pathway if the achievable by-product prices are higher than 30 % of kerosene production costs.

The results of the analyses are substantially influenced by the respective technical and economic assumptions. To identify optimization potentials, assess uncertainties, and quantify the effects of varying influencing factors, comprehensive parameter variations were conducted. The key findings (quantified in the individual chapters) can be summarized as follows.

- The carbon and energy efficiency of power-based kerosene and its intermediates depend on a wide range of pathway-specific process factors. Upstream of the synthesis, the purity of syngas is critical, being influenced by the purity of the feedstock and, in the case of hybrid production, by the reforming efficiency. As H_2 demand increases, the efficiency of electrolysis becomes increasingly decisive for the energy efficiency of syngas production. Downstream of the synthesis, the efficiency of kerosene production can be divided into total fuel efficiency and kerosene-specific efficiency. For total fuel efficiency, the formation of inert by-products within the process chain is critical, as they contribute to higher purge gas losses within the subsequent conversion steps; this is especially true for the MeOH pathway. For kerosene-specific efficiency, conversion selectivity is paramount. While high recycle streams may increase the energy demand of production, these are likely offset by the higher yields achieved through increased product selectivity.

- The production costs of power-based kerosene from “green” electricity are predominantly driven by feedstock costs (H_2 and CO_2) rather than capital costs of the conversion plant. Since feedstock costs account for the largest share of production costs, achieving high conversion efficiencies and selectivities to the target product is vital for reaching relatively low kerosene production costs. For small-scale production concepts, economies of scale can significantly increase plant costs/fixed capital investments, thereby increasing overall production costs. Further, increasing fixed capital investments magnify the influence of economic parameters, such as the weighted average cost of capital (*WACC*) and the depreciation period.

7.2 Outlook

The analysis, along with the resulting conclusions, also indicate the remaining research gaps and areas requiring further analysis. These are outlined in detail below.

- *Investigations of hybrid production systems.* The analysis of power- and biogas-to-methanol concepts (Chapter 3) demonstrates the carbon utilization potential and its implications using the example of biogas. However, hybrid processes can be based on a variety of biomass or biogenic intermediates, leading to differences in process designs and achievable techno-economic outcomes. While generalized insights into hybrid production are provided here, a comparative analysis of diverse hybrid production concepts could validate these findings, expand knowledge on other application areas, and facilitate cross-concept comparisons.
  Due to the small-scale nature of hybrid production analyzed here, an evaluation of the full kerosene production chain has not been carried out since such an approach at this scale seems not economically feasible. However, given the distinct syngas composition in hybrid production being closer to conventional fossil fuel-based syngas, the reverse water-gas shift reactor required in purely power-based approaches may no longer be necessary for the FT pathway. This could eliminate a significant disadvantage of the FT pathway compared to the MeOH pathway. Thus, a comparative analysis of kerosene production in a large-scale hybrid setup could yield different results than those presented here.

- *Investigation of extended power-to-kerosene conversion concepts.* The results of power-based kerosene production indicate that conversion efficiency is particularly critical due to the limited availability or cost-intensive provision of CO_2 and H_2. Conversely, the capital costs of conversion processes represent a relatively small share of total production costs, especially for large-scale production. This underscores the economic viability of extensive measures to enhance feedstock conversion efficiency, even if they increase plant complexity and, thus, also overall costs. A key area for improvement lies in the recovery and recycling of currently unused purge gas streams, which could be processed using advanced separation technologies such as membrane or adsorption systems.
  In the context of power-based kerosene production, product selectivity might become a more important aspect compared to fossil fuel-based refining. This may result from the fact that the demand for product fractions, such as gasoline or diesel for road transport, may decrease through, e.g., direct electrification or changes in mobility infrastructure. Additionally, given the higher production costs of power-based fuels compared to biomass-based fuels, economic competitiveness relies on higher revenues from the market or targeted subsidies for power-based products. Since such incentives are often limited to specific applications, economic advantages may arise from a more selective production of the target product. For instance, current European regulation [36, 204] incentivizes the use of power-based kerosene (PtL quotas). If such

incentives are not extended to by-products like naphtha and diesel, production pathways with high selectivities for kerosene could prove to be more economically viable, even at the expense of lower total fuel efficiency.
Production concepts can vary significantly depending on boundary conditions, potentially including combinations of pathways and/or extensions of the technologies analyzed here. Therefore, further process analyses are needed to develop and optimize concepts with maximized feedstock utilization and kerosene selectivity. For example, the pathways could be expanded with additional reforming stages (e.g., for naphtha components in the FT pathway or light fuel gases in the MeOH pathway) to increase kerosene yields and minimize by-products or flue gases. Such concepts, designed for 100 % kerosene selectivity and full carbon utilization, could be economically advantageous despite the significant increase in process complexity.

- *Validation through technical concept demonstration.* The concepts analyzed here were designed and simulated based on publicly available data. Validation of these theoretical, simulation-based analyses in real-world, implemented technical concepts at a representative scale remains pending. However, validating the results is challenging due to the high costs of implementation and the limited data accessibility from plant operators and technology providers. However, such validations are crucial for further developing process concepts, accounting for real-world limitations, and increasing the technological maturity of the investigated pathways.

Beyond the production approaches and process configurations examined here, further additional options for power-based kerosene production exist. Future research should focus on optimizing process concepts to enhance both efficiency and selectivity in kerosene production. The findings emphasize that the efficient utilization of non-fossil carbon will be crucial to meet future aviation fuel demands while minimizing environmental and economic impacts.

Annex A – Power and biogas to methanol

This section contains the supplementary information published with the manuscript "Power and biogas to methanol – A techno-economic analysis of carbon-maximized green methanol production via two reforming approaches" (Chapter 3). Formatting and wording are slightly adjusted to ensure consistency throughout this thesis.

A.1 Technology description

A.1.1 Process inputs

The main inputs are briefly described below:

Biogas. Biogas is an energy-rich gas mixture, primarily composed of methane (CH_4) and carbon dioxide (CO_2), derived through anaerobic digestion of biomass [117, 205]. Various organic materials such as starch, proteins, lipids, chitin, or lignocellulose can serve as feedstock (substrates); however, biogas yield and production effort can vary [117]. Additional pre-treatment (mechanical, thermal, or chemical) is required, particularly for biogas production from lignocellulosic biomass [206]. Biogas composition depends on multiple factors, including the substrate, retention time, and the type of fermentation process. Typically, 50 to 75 vol% CH_4, 25 to 45 vol% CO_2, and 2 to 7 vol% H_2O can be expected as main components. Additionally, nitrogen (N_2), oxygen (O_2), ammonia (NH_3), and hydrogen (H_2) impurities occur in the lower single-digit percentage range [118]. Furthermore, sulfur compounds (mainly hydrogen sulfide (H_2S)) and other trace gases may be present in the ppm range. The raw biogas production costs range from 0.04 to 0.19 €/kWh_{LHV}, which strongly depends on the substrate and the plant size [126, 127].

Electricity from renewable sources of energy. According to European legislation, renewable electricity is derived from renewable non-fossil sources, such as solar radiation, wind speed, or hydropower [207]. Photovoltaics and wind turbines exhibit the largest and most cost-effective potential for exploiting these renewable energy sources [208]. The potential and temporal occurrence of these energy sources are highly site-dependent and non-controllable. In favorable locations, electricity from solar radiation and wind power can be generated at costs below 40 €/MWh_{el} (solar) and 60 €/MWh_{el} (wind) [209]. However, the pronounced volatility must be considered. The combination of wind and solar radiation utilization can positively influence the temporal constancy of the supply.

A.1.2 Syngas production

Syngas, a mixture of hydrogen, carbon monoxide (CO), and carbon dioxide, builds the input of the methanol synthesis and must exhibit specific characteristics to enable a selective and efficient synthesis. The stoichiometric number (*SN*; Eq. A-1) and the carbon oxide ratio (*COR*; Eq. A-2) are commonly used to describe the syngas composition. The *SN* is adjusted between 2.05 and 2.15 [78, 95, 151]. Since the water produced during the conversion of CO_2 to methanol has a deactivating effect on many methanol catalysts, the *COR* is kept as low as possible in conventional applications. A *COR* between 0.02 and 0.05 is the optimum ratio for methanol formation since a complete absence of CO_2 hinders conversion [151].

$$SN = \frac{[H_2] - [CO_2]}{[CO] + [CO_2]} \qquad \text{Eq. A-1}$$

$$COR = \frac{[CO_2]}{[CO] + [CO_2]} \qquad \text{Eq. A-2}$$

[x] Molar fraction of the respective component (x).

In addition to the reactants, inert gases and catalyst poisons may also be present in the syngas. The inert gas proportion in the fresh gas[18] should be kept as low as possible to avoid reactive component dilution [151]. However, depending on the feedstock used and the syngas production process, up to 20 vol% is contained in conventional processes today [151, 210]. The requirements regarding catalyst poisons are significantly higher and must be considered for synthesis and reforming catalysts. Considering commonly used Ni- and Cu-catalysts, attention has to be paid to sulfur (< 0.1 ppm) and chlorine (< 1 ppb) compounds, tar (< 1 mg/m^3_N), alkalis (< 0.25 mg/m^3_N) and ammonia (< 1 ppm) [78, 86, 117]. Since electrolysis-based H_2 is usually very pure and not contaminated with poisons, additional cleaning can be reduced to biogas treatment [86, 142, 211].

Biogas cleaning. Due to the relatively high H_2S content in biogas, which can lead to elevated emission levels and corrosion damage to compressors and engines, simple purification processes – biological, chemical, or adsorptive – are commonly employed. Reducing H_2S to below 50 ppm is economically feasible in this context, even for energetic biogas utilization [117]. However, biogas use in catalytic processes requires a significantly lower concentration of sulfur components and other potential catalyst poisons. The necessary fine purification can be achieved using various technologies already employed in natural gas purification. Among others, adsorption on zinc oxide (ZnO) and cryogenic processes are applicable for fine desulfurization to achieve concentrations below 0.2 ppm [212, 213]. However, both approaches are constructively and energetically demanding since they require additional equipment and utilities, making small-scale implementation less

[18] Fresh gas is the gas supplied to the synthesis loop that has not yet been mixed with recycled gases. It is also referred to as make-up gas (MUG).

advantageous. Desulfurization through adsorption using activated carbon is applied today in many biogas plants and can be operated at ambient temperature [212]. Using impregnated activated carbon – i.e., coated with active components (such as potassium compounds) – can enhance adsorption for fine desulfurization and bind other poisoning components, such as halogens. Regeneration of the activated carbon is not possible; however, the adsorption intervals can be extended through intensive pre-cleaning.

Biogas reforming. In contrast to methane reforming, which has been used on a large scale for syngas production for decades, the reforming of CH_4/CO_2 mixtures, as found in biogas, is relatively uncommon. Since both molecules are very stable, high temperatures of 700 to 1,000 °C are applied to achieve high conversion rates [63, 214–216]. Furthermore, reforming increases molar quantity, favoring lower operating pressures [62, 217]. Discussed reforming methods include allothermal dry reforming, bi-reforming, and autothermal tri-reforming. All technologies are heterogeneously catalyzed, mainly on nickel or novel metal catalysts [216].

In dry reforming, the CO_2 contained in the mixture serves as the only oxidizing agent. According to Eq. A-3, complete CH_4 conversion requires at least an equimolar ratio of reactants, leading to an *SN* of 1 and a *COR* of 0.

$$CH_4 + CO_2 \rightleftharpoons 2\,CO + 2\,H_2 \qquad \Delta H_{R\,(298\,K)} = 247\,\text{kJ/mol} \qquad \text{Eq. A-3}$$

However, due to coke formation and metal sintering, long-term operation with high catalyst activity is currently not feasible [60, 216]. The combination of dry reforming with steam reforming (CSDR) is called bi-reforming [62, 218]. In this process, the likewise strongly endothermic reaction Eq. A-4 takes place parallel to Eq. A-3. The resulting *SN* is higher than in dry reforming since steam reforming generates additional H_2 from water. The water-gas shift (WGS) reaction (Eq. A-5) does not influence the *SN* (provided oxygen is available in surplus) but increases *COR*.

$$CH_4 + H_2O \rightleftharpoons CO + 3\,H_2 \qquad \Delta H_{R\,(298\,K)} = 206\,\text{kJ/mol} \qquad \text{Eq. A-4}$$

$$CO + H_2O \rightleftharpoons CO_2 + H_2 \qquad \Delta H_{R\,(298\,K)} = -40.9\,\text{kJ/mol} \qquad \text{Eq. A-5}$$

$$OxyN = \frac{[CO_2] + [H_2O]}{[CH_4]} \qquad \text{Eq. A-6}$$

[x] Molar fraction of the respective component (x).

Even though steam utilization counteracts potential coking, the challenges of this process lie in ensuring long-term catalyst stability and optimizing CH_4 conversion [62, 63]. The ratio of oxidant to methane can be quantified using Eq. A-6. At values above 1.5, coke formation can be sufficiently suppressed. Bi-reforming is not yet commercially established [62]. Pure O_2 can be added to steam to reduce the high thermal energy requirements; this process is called tri-reforming. The exothermic partial oxidation (Eq. A-7) or complete oxidation (Eq. A-8) releases heat, which reduces the required heat demand in the reactor

[219]. Compared to bi-reforming, the *SN* reduces due to the increasing CO_2 content while the *COR* increases. Tri-reforming is also not yet commercially established.

$$CH_4 + 0.5\,O_2 \rightleftharpoons CO + 2\,H_2 \qquad \Delta H_{R\,(298\,K)} = -36\,\text{kJ/mol} \qquad \text{Eq. A-7}$$

$$CO + 0.5\,O_2 \rightleftharpoons CO_2 \qquad \Delta H_{R\,(298\,K)} = -283\,\text{kJ/mol} \qquad \text{Eq. A-8}$$

Hydrogen supply. Power-based state-of-the-art H_2 production can be realized via water-electrolysis (Eq. A-9). The theoretical minimum energy required for electrochemical water-splitting under standard formation conditions corresponds to the enthalpy difference of the reaction.

$$H_2O \rightarrow H_2 + 0.5\,O_2 \qquad \Delta H_{R\,(298\,K)} = 286\ \text{kJ/mol} \qquad \text{Eq. A-9}$$

Alkaline electrolysis (AEL), polymer electrolyte membrane electrolysis (PEMEL), anion exchange membrane electrolysis (AEMEL), and high-temperature electrolysis (HTEL, also performed as HT co-electrolysis) are currently the most widely discussed electrolysis technologies [65–68]. Due to the lack of technological maturity, a commercial implementation of AEMEL and HTEL on a large scale is currently only possible at high technical and economic risks [65, 66]. The AEL and the PEMEL, on the other hand, have been tested on a commercial, small to large scale and are both state-of-the-art. Both technologies are operated below 100 °C and reach system efficiencies of up to 68 %. Due to the high load flexibility (power range and temporal load behavior) and the higher outlet pressures, the PEMEL offers advantages over the AEL for operation with volatile electricity [65, 66].

In addition to hydrogen production, constant hydrogen supply from volatile power supply requires hydrogen storage. This is usually realized for medium capacities through gas storage at pressures up to 700 bar. However, the choice of the optimum storage pressure involves, in each specific case, a trade-off between space requirements, capital expenditure, and energy demand, which is why significantly lower pressures are also common for immobile storage [108, 220].

A.1.3 Synthesis and purification

Methanol synthesis converts the syngas into the target product. The resulting product mixture must be purified downstream according to the required product quality. The globally accepted specification for methanol used in the chemical industry aligns with the Grade AA standards defined by the American Society for Testing and Materials (ASTM). The acceptable concentration level here is 99.85 wt% [95].

Methanol synthesis. Methanol is produced worldwide exclusively by state-of-the-art methanol synthesis (TRL 9, TRL 8–9 for CO_2-based syngas) [86, 95, 144]. Today, the low-

pressure technology is used exclusively for the heterogeneously catalyzed conversion operated at 200 to 300 °C and 40 to 100 bar [86, 95]. The formation of methanol can be described by the reactions shown in Eq. A-10 and Eq. A-11. The water-gas shift (WGS) reaction (Eq. A-5) couples both reactions.

$$CO + 2\,H_2 \rightleftharpoons CH_3OH \qquad \Delta H_{R\,(298\,K)} = -90.8\,\mathrm{kJ/mol} \qquad \text{Eq. A-10}$$

$$CO_2 + 3\,H_2 \rightleftharpoons CH_3OH + H_2O \qquad \Delta H_{R\,(298\,K)} = -49.2\,\mathrm{kJ/mol} \qquad \text{Eq. A-11}$$

Today's commercial catalysts are based on copper oxide (CuO) and zinc oxide (ZnO) stabilized with Al_2O_3 or Cr_2O_3 and spiked with small amounts of promoters [95]. The synthesis enables selectivities above 99.9 %C, slightly increasing with a higher *COR*. However, an increasing *COR* also increases water formation and decreases per-pass conversion [86]. By-products, such as predominantly ethanol, dimethyl ether, and methyl formate, are only formed in very small amounts [86].

Methanol purification. The synthesis output contains the main reaction products (methanol and water) but also additional components (e.g., unreacted synthesis gas and by-products). Methanol and water are separated from unconverted syngas through rapid cooling and condensation, often applied by mixing with already condensed product (quenching). Subsequently, methanol is separated from the condensed mixture using the thermal separation process rectification. Depending on the synthesis selectivity and desired product purity, one- to three-stage column configurations can be implemented for methanol purification.

A.2 Economic calculations

Fixed capital investment (FCI) calculation. The *FCI,* representing the capital required for the plant's construction, is calculated according to Eq. A-12. The applied module costing technique relates all costs to the purchased costs of equipment (purchased costs for base conditions: C_P^0). Contingency and fees (γ) and costs for land, buildings, and auxiliary facilities (auxiliary costs: β) are considered via markup factors. The raw component costs are adjusted with specific cost factors (F_{BM}), taking into account additional design adjustments for pressure and material requirements.

The base equipment is calculated for the major process equipment and can be derived from equipment-specific cost correlations available in the literature (Eq. A-13) [110]. For this purpose, the individual apparatuses are each dimensioned with respect to the equipment-dependent size parameter (A, e.g., volume, area, power) based on the simulation results and further technical specifications (e.g., gas hourly space velocity, bulk density).

$$FCI = (1 + \gamma) \sum_{l=1}^{k} C_{\mathrm{P},l}^{0} F_{\mathrm{BM},l} + \beta \sum_{l=1}^{k} C_{\mathrm{P},l}^{0} F_{\mathrm{BM},l}^{0} \quad \text{Eq. A-12}$$

FCI	Fixed capital investments [€$_{2022}$]
$C_{\mathrm{P},l}^{0}$	Purchased cost for base conditions [€$_{2022}$]
F_{BM}	Component-specific cost factor [-]
$F_{\mathrm{BM}}{}^{0}$	Component-specific cost factor for base conditions [-]
γ	Share of contingency and fee costs [%]
β	Share of auxiliary costs [%]
l	Number of the equipment [-]
k	Total number of equipment [-]

$$\log_{10} C_{\mathrm{P}}^{0} = K_1 + K_2 \log_{10}(A) + K_3 [\log_{10}(A)]^2 \quad \text{Eq. A-13}$$

C_{P}^{0}	Purchased cost for base conditions [€$_{2022}$]
K_{x}	Correlation parameter [-]
A	Capacity or size parameter [m^2, m, kW, etc.]

To adjust the purchased cost for base conditions to non-base-case conditions and to take into account the direct and indirect costs of installation, C_{P}^{0} is multiplied by the bare module factor (F_{BM}) (Eq. A-14). The specific elements of the formula depend on the type of equipment and can be found in the respective literature [110].

$$F_{\mathrm{BM}} = B_1 + B_2 F_P F_M \quad \text{Eq. A-14}$$

F_{BM}	Bare module factor [-]
B_1 & B_2	Installation cost factors [-]
F_P	Pressure factor
F_M	Material factor

A.3 Modeling data

Additional information on the comprehensibility of the simulations and analyses performed is provided below.

A.3.1 Process configuration model data

Thermodynamic models. Different thermodynamic models (equation of state or activity coefficient models) are chosen to calculate the occurring mixture states, mass, and energy flows depending on the interacting components and the process conditions. The syngas production is predominantly modeled using the “Soave-Redlich-Kwong” (SRK) equation-of-state for analyzing hydrocarbon systems [221, 222]. In the methanol synthesis and purification section, streams with considerable proportions of polar components, such as

predominantly water and alcohols, occur. Thus, an equation-of-state model by Schwarzentruber and Renon (SR-Polar) is used [120, 221].

Components. Table A-1 lists the modeled components considered in the process simulation.

Table A-1: List of modeled components.

Component	CAS number
Nitrogen (N_2)	7727-37-9
Oxygen (O_2)	7782-44-7
Hydrogen (H_2)	1333-74-0
Carbon monoxide (CO)	630-08-0
Carbon dioxide (CO_2)	124-38-9
Water (H_2O)	7732-18-5
Methane (CH_4)	74-82-8
Methanol (CH_3OH)	67-56-1
Ethanol (C_2H_5OH)	64-17-5
Dimethyl ether (C_2H_6O)	115-10-6
Methyl formate ($C_2H_4O_2$)	107-31-3
Acetone (C_3H_6O)	67-64-1

Inputs and Outputs. Biogas, water, and oxygen are the material inputs of the process. The considered states of the components are listed in Table A-2. The assumed composition of biogas is defined by the CH_4/CO_2-ratio, the inert gas fraction (IGF), and the water content. For the latter, it is assumed that biogas, as conventionally practiced, is cooled down to 10 °C during pre-purification for drying purposes (outside system boundaries). Oxygen is a by-product of water-electrolysis and is available as a pure substance at elevated pressure. Water is considered available at the plant side as a pure substance. Input and Output streams are set to 35 °C to close the overall energy balance and to avoid impractical cooling demands from pinch analysis.

Table A-2: Definition of process inputs and outputs (PV: Parameter variation, RC: Reference case, *x*: Molar fraction).

Stream	Parameter		Value	Reference
Biogas	Composition	CH_4/CO_2-ratio	RC: 1.5, PV:1–3	[117–119]
		N_2 [$\%_{Dry}$]	RC: 2, PV: 0–5	[117, 118]
		Dew point [°C]	10	[117]
	Conditions	p [bar] | T [°C]	1.045 | 10	[117]
Water	Composition	x_{H2O} [%]	100	[-]
	Conditions	p [bar]; T [°C]	1 | 35	[-]
Oxygen[a]	Composition	x_{O2} [%]	100	[86, 108]
	Conditions	p [bar]; T [°C]	50 | 70	[86, 108]
Methanol	Composition	x_{CH3OH} [%]	99.85	[95]
	Conditions	p [bar]; T [°C]	1 | 35	[-]

[a] from water-electrolysis

Technical. Table A-3 lists extended information on the Aspen plus® process models.

Table A-3: Extended list of technical modeling data and simulation approaches (DS: Design specification, HHV: Higher heating value, LHV: Lower heating value, PV: Parameter variation, RC: Reference case, *SN*: Stoichiometric number, $\dot{Q}$: Thermal energy stream, $\eta_{el.}$: Electrical efficiency).

Process	Model	Parameter	Value	Value	Reference
Electrolysis	Calculator	Electricity demand	Electrical efficiency ($\eta_{el.}$) [$\%_{LHV}$]	67	[86]
		Heating/ cooling	Based on energy balance: $\dot{Q} = \dot{m}_{H2}\left(\mathrm{LHV}\ \eta_{el.}{}^{-1} - \mathrm{HHV}\right)$		[-]
Reforming	RGibbs	Operating conditions	T [°C]	RC: 900 PV: 800–1,000	[62, 119]
			p [bar]	5	[62]
		Equilibrium conversion	Products considered: CO, CO_2, H_2O, H_2, CH_4, O_2, N_2		[83]
	Calculator	Condition	*OxyN*	1.5	[62]
Methanol synthesis	Design spec	Syngas composition	*SN*	2.05	[95, 151]
	REquil	Operating conditions	T [°C]	250	[86, 92]
			$p \mid \Delta p$ [bar]	75 | −5	
		Equilibrium conversion with temperature approach	$CO + 2H_2 \leftrightharpoons CH_3OH$	15 K	[120]
			$CO_2 + 3H_2 \leftrightharpoons CH_3OH + H_2O$	15 K	[120]
			$CO_2 + H_2 \leftrightharpoons CO + H_2O$	15 K	[120]
	Design spec	Amount of purge gas	Inert gas share	RC: 0.2 PV: 0.02–0.50	[-]
	RStoic + Calculator	By-product formation [mol/t_{CH3OH}]	$2CO + 4H_2 \rightarrow C_2H_5OH + H_2O$	16.1	[86]
			$2CO + 2H_2 \rightarrow C_2H_4O_2$	11.5	[86]
			$2CO + 4H_2 \rightarrow C_2H_6O + H_2O$	1.6	[86]
			$3CO + 5H_2 \rightarrow C_3H_6O + 2H_2O$	0.5	[86]
			$CO + 3H_2 \rightarrow CH_4 + H_2O$	5.8	[86]
Topping column	Radfrac	Internal DS	CO_2 purity bottom [wt%]	0.001	[-]
			Top temperature [°C]	30	[-]
Methanol column	Internal DS	Internal DS	CH_3OH purity top [wt%]	99.85	[95]
			CH_3OH recovery top [%]	99.9	[-]

General assumptions for compression modeling. The selected compressor models are designed according to several criteria. Generally, a maximum compression ratio of 3 is permitted [223, 224]. If higher pressure ratios are required for compression, multistage compressors are selected. For the multistage compressor, the same pressure ratios are assumed for all stages since the total work requirement is lowest here [223]. Intermediate cooling is assumed down to 75 °C (air cooler [25 $°C_{Air}$] with minimal temperature difference gas to gas 50 K). The maximum compression temperature is considered to be below

250 °C [224]. All compressions are calculated polytropic using the ASME method (see Aspen Help for further descriptions [109]). Aspen Plus® default compression efficiency (72 %) is used.

General assumptions for purge gas combustion modeling. Fuel gas combustion is modeled using stoichiometric reactor models generating combustion reactions. Oxygen is provided by air (21 vol%$_{O2}$/ 79 vol%$_{N2}$). The combustion ratio is assumed with air in surplus (λ = 1.2) and a combustion temperature of 1,000 °C. The feed gas is pre-heated to 700 °C to consider heat integration potential. SRK equation-of-state is used for calculating thermodynamic properties.

A.3.2 Heat integration

The heat integration carried out by pinch analysis considers a general minimum temperature difference (ΔT) of 20 K. Apart from this, a ΔT of 10 K is assumed for evaporation and condensation processes [225]. In order to approximate an ideal heat integration, heating/cooling and aggregate state changes of pure substances are simulated in separate steps. Table A-4 lists the considered utility streams used in the pinch analysis.

Table A-4: Utility streams considered in heat integration (T: Temperature).

Task	Utility stream	Inlet T [°C]	Outlet T [°C]
Cooling	Water	15	25
	Low-pressure steam generation	124	125
	Medium-pressure steam generation	174	175
	High-pressure steam generation	249	250
Heating	Electrical power	1,001	1,000

A.3.3 Economic analysis

Economic analysis data. Table A-5 and Table A-6 list the assumed values for the general cost calculation. For the operating labor costs (C_{OL}), six operators with a gross of 4,910 €$_{2022}$/month and 13 salaries/a are considered. In addition, non-wage labor costs of 28 % are considered. In the parameter variation of the plant size, the number of necessary operators was increased with increasing plant size (Scale factor/Operator: 5/12, 10/18, 50/24, 100/30).

Table A-5: Assumptions for annual capital cost calculation (Parameters according to A.2 and 3.2).

Parameter	Value	Reference
Share of contingency and fee costs (γ) [-]	0.18	[110]
Share of auxiliary costs (β) [-]	0.5	[110]
Working capital share (ω) [-]	0.15	[110]
Weighted average cost of capital ($WACC$, i) [-]	0.06	[108]
Depreciation period (n) [a]	20	[125]

Table A-6: $OPEX_f$ markup factors according to Turton et al. [110] (C_{OL}: Operating labor costs, *FCI*: Fixed capital investments).

Parameter	Calculation
Direct supervisory and clerical labor (C_{DS})	$0.18C_{OL}$
Maintenance and repairs (C_{MR})	$0.03FCI$
Operating supplies	$0.009FCI$
Laboratory charges	$0.15C_{OL}$
Local taxes and insurance	$0.032FCI$
Plant overhead costs	$0.5(C_{OL} + C_{MR}+C_{DS})$
Administrative costs	$0.15(C_{OL} + C_{MR} + C_{DS})$

Hydrogen supply cost database. The input parameters for the determination of the on-site hydrogen supply cost are listed in Table A-7.

Assumptions for the calculation of the comparative cases PtM and BGtM. Simplified assumptions are made for calculating the methanol production cost (*MPC*) of the non-hybrid concepts PtM and BGtM. For PtM, all apparatus for biogas reforming are excluded from the fixed capital investments (*FCI*). In addition, an amine wash process is included to separate CO_2 from the biogas. The specific costs for the available biogas quantity are assumed to be 1,500 €$_{2022}$/Nm$^3_{BG}$/h [226]. Since, in the reference case, only 40 % of the carbon in the biogas is CO_2, the plant's production capacity is scaled by a factor of 0.4. Given that very low inert gas contents in the feedstock and minimal purge gas losses are expected when using CO_2 and H_2, the carbon efficiency is assumed to be the same as in the TriRef configuration (97 %). The specific electricity requirements for gas compression are assumed to be identical to the TriRef configuration.

The *MPC* of the BGtM concept is based on the apparatus costs of the BiRef configuration since additional O_2 input would significantly lower the production capacity (without additional H_2 generation). Like in the PtM concept, an amine wash process is included to separate the required CO_2 amount from the biogas. The maximum production quantity is determined based on Eq. A-15, resulting in an 80 % capacity compared to the reference case (scale factor 0.8). The specific power requirement is equated to the BiRef configuration due to the electrically heated reforming.

$$3CH_4 + CO_2 + 2\,H_2O \rightarrow 4CO + 8H_2 \rightarrow 4CH_3OH \qquad \text{Eq. A-15}$$

Table A-7 lists the data considered in the optimization model used for hydrogen supply cost calculation.

Table A-7: Input parameters (year 2022) for the onsite hydrogen supply cost determination (Base: baseline scenario, derived from the data median; CAPEX: capital expenditure; Cons: conservative scenario, derived from the worst 25 % percentile of the data; OPEX: operational expenditure; PEMEL: proton exchange membrane electrolyzer; Prog: progressive scenario, derived from the best 25 % percentile of the data).

Component	Parameter	Unit	Base	Prog	Cons	Reference
Compressor (250 bar_{out})	CAPEX	$€_{2022}/(kg_{H2}/h)$	1,980	1,312	4,104	[220, 227, 228]
	Depreciation	a	20	20	20	own assumption
	Efficiency	-	0.79	0.85	0.68	[227, 229, 230]
	OPEX	$\%_{of\ CAPEX}/a$	5	5	5	[220, 228]
Li-Ion-battery	CAPEX	$€_{2022}/kWh_{el}$	326	250	364	[231–234]
	Depreciation	a	20	20	20	own assumption
	Efficiency	-	0.87	0.90	0.85	[231, 232, 234]
	OPEX	$\%_{of\ CAPEX}/a$	3	3	3	[232–234]
PEMEL (50 bar_{out})	CAPEX	$€_{2022}/kW_{el}$	1,386	1,045	1,757	[231, 235–242]
	Depreciation	a	20	20	20	own assumption
	Efficiency (LHV)	-	0.67	0.69	0.63	own assumption
	OPEX	$\%_{of\ CAPEX}/a$	3.5	3.5	3.5	[235, 236, 238–242]
	Water demand	kg_{H2O}/kg_{H2}	10	10	10	[243]
	Water cost	$€_{2022}/m^3_{H2O}$	2.6	2.6	2.6	[244]
Photovoltaic	CAPEX	$€_{2022}/kW_{el}$	625	541	728	[208, 232, 233, 245–249]
	Depreciation	a	20	20	20	own assumption
	OPEX	$\%_{of\ CAPEX}/a$	2.4	2.4	2.4	[232, 233, 245, 246, 248, 249]
Wind turbine (onshore)	CAPEX	$€_{2022}/kW_{el}$	1,402	1,290	1,545	[208, 235, 245, 248–252]
	Depreciation	a	20	20	20	own assumption
	OPEX	$\%_{of\ CAPEX}/a$	2.4	2.4	2.4	[232, 245, 248, 249, 252]
H_2-Tank (200 bar_{max})	CAPEX	$€_{2022}/kg_{H2}$	514	240	665	[220, 228, 253–255]
	Depreciation	a	20	20	20	own assumption
	OPEX	$\%_{of\ CAPEX}/a$	2	2	2	[229]
	Storage pressure	bar	100	100	100	own assumption

A.4 Extended results

A.4.1 Pinch analysis results

Figure A-1 illustrates the composition curves depicting the outcomes of heat integration for an assumed minimum temperature difference of 20 K. In the case of the BiRef configuration, an external heat demand of approximately 0.9 MW arises, which is exclusively required for reforming and provided via electricity. The external cooling demand of

1.9 MW is covered by more than 90 % via cooling water and can only be minimally utilized for steam generation. Up to 2.3 MW can be internally transferred.

In the TriRef configuration, an external cooling demand of 2.5 MW results, which is nearly entirely met by cooling water (98 %). Internal heat recovery can utilize up to 2.3 MW. No external heat is required due to autothermal reforming.

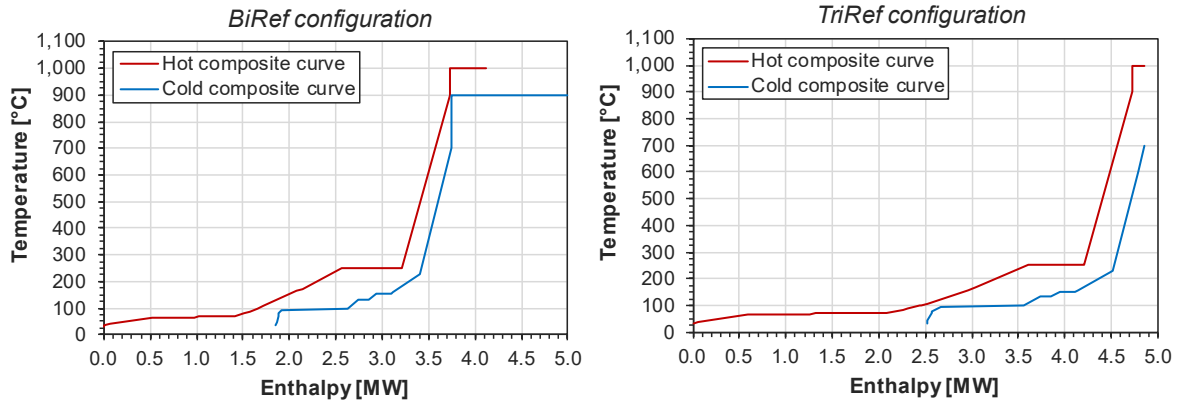

Figure A-1: Compositive curves from heat integration.

A.4.2 Bare module costs

The results of pure component cost calculation for the respective process units are depicted in Figure A-2. The heat integration costs encompass all heat exchangers required for the previously illustrated heat integration. This includes, among others, preheaters, condensers, or boilers, which are accordingly not included in the costs of the listed units. The synthesis unit encompasses the costs of the syngas compression and the methanol reactor. The reformer unit comprises the vessels of the activated carbon filters and the purge gas combustion in addition to the reactors. Since cost functions for electrically heated reforming reactors are so far not available in the literature, the reformer was assumed to be a fired reactor (i.e., including a reactor furnace).

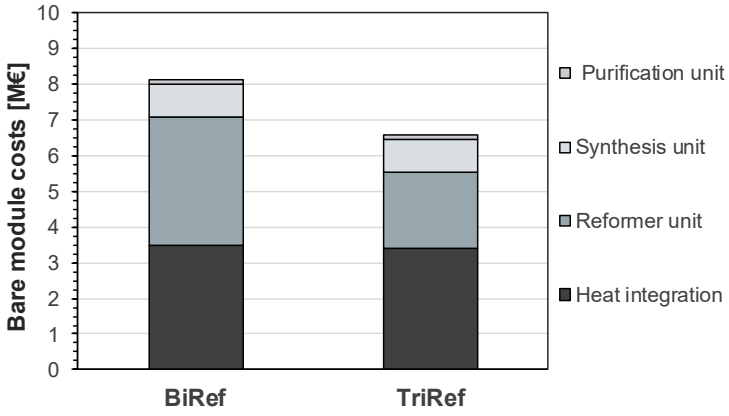

Figure A-2: Bare module costs for BiRef and TriRef configuration.

A.4.3 Hydrogen supply costs

The results of the hydrogen onsite supply costs (year 2022) by applying the optimization model from Sens et al. 2022 [108] are shown in Figure A-3. Based on this, the hydrogen costs are set to 7 €$_{2022}$/kg in the reference case. According to average cost regions in the progressive and conservative scenario, the parameter varies from 5 to 9 €$_{2022}$/kg.

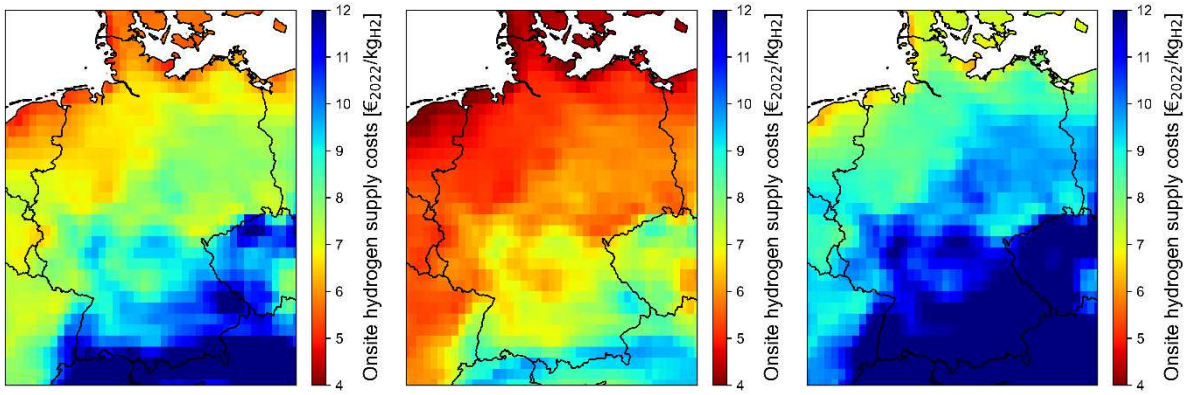

Figure A-3: Costs for a constant onsite green hydrogen supply for the baseline (left), progressive (middle), and conservative (right) scenario in 2022 (determined by applying the optimization model from Sens et al. 2022 [108]).

Annex B – Kerosene production from power-based syngas

This section contains the supplementary information published with the manuscript "Kerosene production from power-based syngas – A technical comparison of the Fischer-Tropsch and methanol pathway" (Chapter 4). Formatting and wording are slightly adjusted to ensure consistency throughout this thesis.

B.1 Technology description

In addition to the flowsheets described in Chapter 4, detailed information on the technologies used are presented in the following, serving as the basis for the design of the reference concepts.

B.1.1 Fischer-Tropsch pathway

The following describes the technologies considered within the Fischer-Tropsch pathway.

Fischer-Tropsch syncrude production

Reverse water-gas shift. The reduction of CO_2 to CO and syngas conditioning is considered via a reverse water-gas shift (RWGS) reaction, using H_2 as a reductant. The respective endothermic equilibrium reaction is shown in Eq. B-1.

$$CO_2 + H_2 \leftrightharpoons CO + H_2O \qquad \Delta H_{R\,(298\,K)} = 42\ \mathrm{kJ/mol} \qquad \text{Eq. B-1}$$

The RWGS reactor operates between 700 and 1,000 °C to enable sufficient CO formation [83]. Operating pressures between 1 and 30 bar are mainly investigated in practical applications, with a rising formation of methane at increased pressure [75, 83]. The required heat for the endothermic reaction at high-temperature levels can be provided by electrical energy or combustion. Nickel (Ni) or noble metal-based catalysts are mainly used to promote the reaction [75]. Since only some research and demonstration RWGS plants exist but no RWGS reactors are commercially used yet, the TRL is estimated to be at about 6 [135, 256].

Low-temperature Fischer-Tropsch synthesis. The low-temperature Fischer-Tropsch (LTFT) synthesis is a heterogeneously catalyzed conversion, mainly producing long-chain n-alkanes in the kerosene, diesel, and wax range. Eq. B-2 shows the strongly exothermic reaction where n represents the carbon chain length of the molecules produced. The chain length distribution can be described by the Anderson-Schulz-Flory (ASF) distribution shown in Eq. B-3, with W_n giving the chain length(n)-related weight fraction according to

the chain growth probability (α). However, considerable deviations occur in particular due to a much higher C_1 and a much lower C_2 production [58].

$$n\mathrm{CO} + (2n+1)\mathrm{H_2} \rightarrow \mathrm{C}_n\mathrm{H}_{2n+2} + n\mathrm{H_2O} \qquad \Delta H_{\mathrm{R\,(298\,K)}} \approx n(-150\,\mathrm{kJ/mol}) \qquad \text{Eq. B-2}$$

$$W_n = n(1-\alpha)^2\alpha^{n-1} \qquad \text{Eq. B-3}$$

The chain growth probability mainly depends on the catalyst used, the composition of the respective syngas, and the operating temperature and pressure within the reactor [190]. Iron (Fe) or cobalt (Co) can be used as an active catalyst component. The higher activity of cobalt leads to improved conversions and is therefore preferred, especially for long-chain hydrocarbon generation [87, 135]. At operating conditions from 180 to 250 °C and 20 to 60 bar, per-pass conversions from 60 to 85 % and chain growth probabilities between 0.80 and 0.95 can be reached [58, 86, 87, 144]. Besides n-alkanes, LTFT produces olefins – whose proportion decreases with increasing chain length – and minor amounts of oxygenates (mainly alcohols) [58, 190, 257]. The chain length (n) dependent olefin (O) to alkane (paraffin; P) formation can be described by Eq. B-4 [149]. The adjustment parameter c lies between 0.19 and 0.49 [258].

$$(O/P)_n = \mathrm{e}^{-c\,n} \qquad \text{Eq. B-4}$$

Syncrude refining

Hydrocracking. Hydrocracking is the catalytic conversion of long-chain hydrocarbons into lighter ones within an H_2-rich environment. Thus, heavy syncrude fractions, especially waxes, can be converted into common fuel fractions. The splitting of carbon double bonds (C-C bonds) is enabled via bi-functional catalysts under elevated pressures and temperatures (35 to 70 bar and 325 to 375 °C [144, 159]). Hydroisomerization reactions always accompany cracking reactions, leading to a product with a higher degree of branching and, therefore, better cold flow properties. The used catalysts have two active centers: an acidic center that causes isomerization and chain breaking and a metallic center with a hydrogenation-dehydrogenation effect [259]. The probability of chain breaking increases with the increasing carbon chain length of the molecules. Ideal cracking is characterized by equal cracking probability along the carbon chain and direct desorption of the cracked molecule from the catalyst. This results in a single cracking event predominantly achieved at mild process conditions [144]. However, secondary and tertiary cracking can also occur, shifting the product distribution to shorter hydrocarbons. Using shape-selective zeolites as catalysts can additionally improve the hydrocracking selectivity. The hydrocracking of FT wax can reach per-pass conversions of 20 to 100 %.

Hydrogenation and fractionation. Hydrogenation of FT-derived kerosene is required to ensure the long-term stability of the molecules, i.e., to avoid undesired reactions of unsaturated hydro-carbons during kerosene storage. Saturating olefins is slightly exothermic and decreases molar quantities, according to Eq. B-5. Complete hydrogenation is achieved under a high hydrogen surplus and elevated pressures (5 to 60 bar [160, 171]) catalyzed by nickel (Ni), platinum (Pt), or palladium (Pd) on alumina (Al_2O_3) [159]. The temperature lies between 50 and 350 °C, depending on the degree of branching and the catalyst used [159, 160]. The amount of hydrogen required corresponds to the amount of olefins in the feedstock, which is relatively low for LTFT products. However, excess hydrogen within the reactor is necessary to achieve complete saturation.

$$C_nH_{2n} + H_2 \rightarrow C_nH_{2n+2} \qquad \text{Eq. B-5}$$

To separate the different fuel fractions, fractionation of the hydrocarbon mixture is performed via rectification. Depending on the mixture, separating into different product fractions can be carried out in one or more interconnected rectification columns. Distillation of high-boiling components might be operated under a vacuum to avoid thermal cracking.

B.1.2 Methanol pathway

The methanol pathway is distinguished into the process sections “Methanol production” and the subsequent “Methanol-to-Kerosene” process.

Methanol production

The methanol synthesis is a heterogeneously catalyzed conversion usually operated in a temperature and pressure range of 200 to 300 °C and 40 to 100 bar [86, 95]. The formation of methanol can be described by the reactions in Eq. B-6 and Eq. B-7. Both reactions are coupled via the water-gas shift (WGS) reaction occurring in parallel (Eq. B-8).

$$CO + 2\,H_2 \rightleftharpoons CH_3OH \qquad \Delta H_{R\,(298\,K)} = -90.8\ \text{kJ/mol} \qquad \text{Eq. B-6}$$

$$CO_2 + 3\,H_2 \rightleftharpoons CH_3OH + H_2O \qquad \Delta H_{R\,(298\,K)} = -49.2\ \text{kJ/mol} \qquad \text{Eq. B-7}$$

$$CO + H_2O \rightleftharpoons CO_2 + H_2 \qquad \Delta H_{R\,(298\,K)} = -40.9\ \text{kJ/mol} \qquad \text{Eq. B-8}$$

Due to the exothermic and volume-decreasing nature of the equilibrium-limited methanol formation reaction, product generation is favored by low temperatures and high pressures [217]. Compared to the conventional CO-converting synthesis, the per-pass conversion for direct CO_2 conversion is significantly lower (< 45 %). However, the selectivity is slightly higher (99.90 to 99.96 %) [86]. Today’s commercial catalysts are based on copper oxide (CuO) and zinc oxide (ZnO) stabilized with Al_2O_3 or chrome oxide (Cr_2O_3) and

spiked with small amounts of promoters [95]. The predominant by-products are ethanol, dimethyl ether, and methyl formate, which are formed only in very small amounts [86].

Methanol-to-Kerosene process

Figure B-1 shows the processes steps of the Methanol-to-Kerosene (MtK) process. Commercially available processes are the Mobil olefins to gasoline and distillate (MOGD) and the MtSynfuel process from Lurgi (today AirLiquide). However, none of these processes is currently optimized for kerosene production.

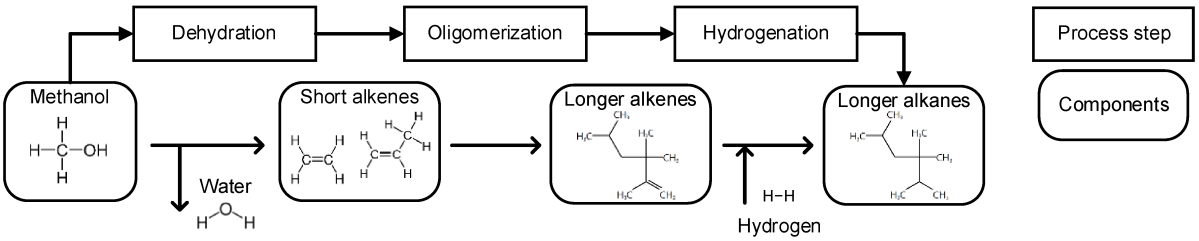

Figure B-1: Basic conversion steps for Methanol-to-Kerosene (MtK) processes.

Dehydration. Methanol dehydration to light olefins is also known as the Methanol-to-Olefins (MtO) process. Around 30 Mt/a of methanol are converted worldwide via MtO, making the process a state-of-the-art technology (TRL 9) [91]. According to Eq. B-9, the separation of the hydroxyl group, takes place by the formation of water and a carbon-to-carbon double bond.

$$n\mathrm{CH_3OH} \rightarrow \mathrm{C}_n\mathrm{H}_{2n} + n\mathrm{H_2O} \qquad \text{with } 2 \leq n \leq 6 \qquad \text{Eq. B-9}$$

Depending on the selected catalyst and the applied operating conditions – i.e., pressure, temperature, and space velocity – predominantly short-chain olefins are formed. Low temperatures and pressures favor the exothermic conversion. However, methanol dehydration needs considerable activation energy, requiring temperatures above 350 °C and catalysts to achieve a complete methanol conversion [81, 168, 260]. Protonated ZSM-5 and SAPO-34 zeolites are common catalysts used. The olefin-selectivity lies between 80 to 90 % related to the carbon input [162, 193]. By-products are mainly coke depositing on the catalyst, short-chain alkanes, and CO_2, which may be separated before the olefins are further processed [79, 169, 170]. Most commercial processes are operated at around 400 °C and pressure levels below 5 bar [78, 162].

Today, MtO is primarily applied to generate ethene and propene as an alternative route to naphtha cracking from crude oil. However, for the downstream oligomerization, olefins with higher carbon chain lengths, like butene or propene, can be a more beneficial starting material for producing higher hydrocarbon fuels [155, 261]. Olefins with a shorter carbon chain length may lead to a more homogenous product distribution, with a smoother distillation curve being more comparable with conventional (crude oil-based) kerosene [262].

Oligomerization. By oligomerization, the carbon double bonds (C=C bonds) of the olefins (monomers) are broken and linked with other olefin molecules by the formation of C-C bonds (Figure B-1). Monounsaturated hydrocarbons (oligomers) are mainly formed. Eq. B-10 shows the exothermic and volume-decreasing reaction with the number of monomers (m) and their carbon number (n).

$$m\mathrm{C}_n\mathrm{H}_{2n} \rightarrow \mathrm{C}_{mn}\mathrm{H}_{2mn} \qquad \text{with } 2 \leq n \leq 4 \qquad \text{Eq. B-10}$$

Depending on the reactant composition and the target product (i.e., chain length and component type), oligomerization can occur via various technologies, primarily distinguished by the catalysts used. For kerosene production, acidic catalysts play a major role, further enabling aromatics production [263]. Homogenous transition-metal catalysis can also produce olefins in the kerosene range [264]. Depending on the MtO product, different single- or multi-stage processes are conceivable. Today, commercial oligomerization applications focus on producing gasoline from C_2 to C_4 olefins.

Pure iso-butene can be used for primary oligomerization on a polymeric acid resin catalyst at temperatures below 100 °C, targeting products in the kerosene range. However, more stable olefins like ethene or propene are not converted to a sufficient amount in such an oligomerization concept. Solid phosphoric acid (SPA) catalysts can also be used at higher temperatures to produce a more diverse and branched product since concomitant oligomerization, cracking, and isomerization occur [155]. Some extensively studied oligomerization catalysts for fuel production are shape-selective, acidic zeolites. Depending on the operating conditions and the pore size, different olefin mixtures can be converted into more or less branched kerosene and diesel fractions. Light olefins in the gasoline range can be recycled to oligomerization, increasing the overall kerosene fraction [79, 155]. In addition to individual oligomerization technologies, combining consecutive oligomerization processes can also enhance the kerosene fraction, particularly when dealing with olefin mixtures [155].

According to a more generic approach, the oligomerization product is described using the adjusted ASF distribution according to Eq. B-11.

$$W_n = (n - x - 1)(1 - \alpha)^2 \alpha^{n-x-2} \qquad \text{for } n \geq x \qquad \text{Eq. B-11}$$

n	Carbon chain length [-]
W_n	Weight fraction [wt%]
α	Chain growth probability [-]
x	Adjustment parameter [-]

Hydrogenation and fractionation. Hydrogenation and fractionation of the oligomerization products can occur similarly to processing FT crude (see B.1.1). However, compared to FT crude, more H_2 is needed for the hydrogenation since the input stream is a pure olefin mixture. Furthermore, the hydrocarbons might be more challenging to hydrogenate as

they are more branched than the linear paraffinic (linear alkanes) FT product. Analogously to the FT pathway, fractionation can be realized via rectification.

B.2 Extended information on the simulation model

B.2.1 Components and property methods

In practice, the synthesis and further downstream processes considered in the analysis lead to the production of various chemical components. Some of them differ only slightly in their structure and respective properties or are produced only in vanishingly small quantities. To reduce this product variety to an appropriate level with regard to the requirements of the analysis, only the main components that sufficiently approximate a real product mixture are considered in the simulation. In terms of hydrocarbon products, therefore, only linear olefins (C_2 to C_{24}) and linear alkanes (C_1 to C_{45}), for which all necessary parameters can be taken from the Aspen Plus databases, are considered in the model. Table B-1 lists the modeled components in the respective pathway simulations.

Table B-1: List of modeled components.

Component	CAS number	Pathway
Nitrogen (N_2)	7727-37-9	Fischer-Tropsch, Methanol
Oxygen (O_2)	7782-44-7	Fischer-Tropsch, Methanol
Hydrogen (H_2)	1333-74-0	Fischer-Tropsch, Methanol
Carbon monoxide (CO)	630-08-0	Fischer-Tropsch, Methanol
Carbon dioxide (CO_2)	124-38-9	Fischer-Tropsch, Methanol
Water (H_2O)	7732-18-5	Fischer-Tropsch, Methanol
Alkanes (C_1–C_{45}) | (C_1–C_{24})	-	Fischer-Tropsch, Methanol
Olefins (C_2–C_{24})	-	Fischer-Tropsch, Methanol
Methane (CH_4)	74-82-8	Fischer-Tropsch, Methanol
Methanol (CH_3OH)	67-56-1	Methanol
Ethanol (C_2H_5OH)	64-17-5	Methanol
Dimethyl ether (C_2H_6O)	115-10-6	Methanol
Methyl formate ($C_2H_4O_2$)	107-31-3	Methanol
Acetone (C_3H_6O)	67-64-1	Methanol
Coke ($C_{11}H_{16}$)	61827-86-9	Methanol
Sodium hydroxide (NaOH)	1310-73-2	Methanol
Sodium carbonate (Na_2CO_3)	497-19-8	Methanol
Sodium bicarbonate ($NaHCO_3$)	144-55-8	Methanol
Ions (H_3O^+, NA^+, HCO_3^-, OH^-, CO_3^{2-})	-	Methanol

Different thermodynamic modeling approaches (equation of state or activity coefficient models) must be chosen to calculate the occurring mixture states and mass and energy flows depending on the interacting components and the process conditions. For the model of the Fischer-Tropsch pathway, the “Peng-Robinson with Boston-Mathias alpha function” (PR-BM) is chosen as the global property method for analyzing hydrocarbon systems [83,

144]. For streams with considerable proportions of polar components, such as predominantly water, the combined method "Non-random two-liquid – Redlich-Kwong" (NRTL-RK) is also used [221]. Light gases – such as H_2, N_2, or CH_4 – are, in this case, considered Henry components. PR-BM is also predominantly used in the methanol pathway model (oligomerization and further downstream processes). The synthesis gas generation and methanol synthesis are modeled using the property method "Soave-Redlich-Kwong" (SRK) [221]. In the dehydration of methanol, NRTL-RK is used due to the high water formation [221, 222]. The caustic wash is simulated using "Electrolyte NRTL with Redlich-Kwong" (ELECNRTL) [221].

B.2.2 Chain growth probability variation

This subsection defines the analyzed value ranges for the variation of the chain growth probability. For this purpose, the relevant straight-run fractions of the Fischer-Tropsch synthesis and the oligomerization and their interactions with the overall concepts are described.

Figure B-2 illustrates the straight-run kerosene (C_8 to C_{16}) and wax ($\geq C_{21}$) fractions resulting from varied chain growth probabilities (α) of the assumed ASF distributions for the FT and the methanol pathway considered. "Straight-run" represents the reactant conversion in the reactor without recycling and downstream processing. The analysis of straight-run fractions serves as a means to depict the product fractions resulting from the assumed distributions and allows for the derivation of meaningful value ranges for the overall system investigation. The FT synthesis, represented by the standard ASF distribution, shows a maximum straight-run kerosene fraction of about 40 wt%, achieved at a chain growth probability value of 0.84. It is evident that the maximum straight-run kerosene fractions for all assumed methanol pathway variations are significantly higher than the maximum FT kerosene yields. The maximum shifts towards lower chain growth probabilities for the assumed hydrocarbon chain formation through oligomerization. As the monomer (olefin) size increases, fewer chain growth reactions are required to reach a kerosene chain length during the oligomerization. Consequently, the maximum achievable straight-run kerosene fraction increases with an increasing monomer size (modeled by the parameter x (Eq. B-11). Thus, for a light olefin input stream (x = 2), a maximum straight-run kerosene fraction of 54 % can be achieved at a chain growth probability of 0.78. In contrast, an oligomerization feedstock composed of longer olefins (x = 4) achieves a higher maximum straight-run kerosene fraction, which amounts to about 70 % at a chain growth probability of 0.71.

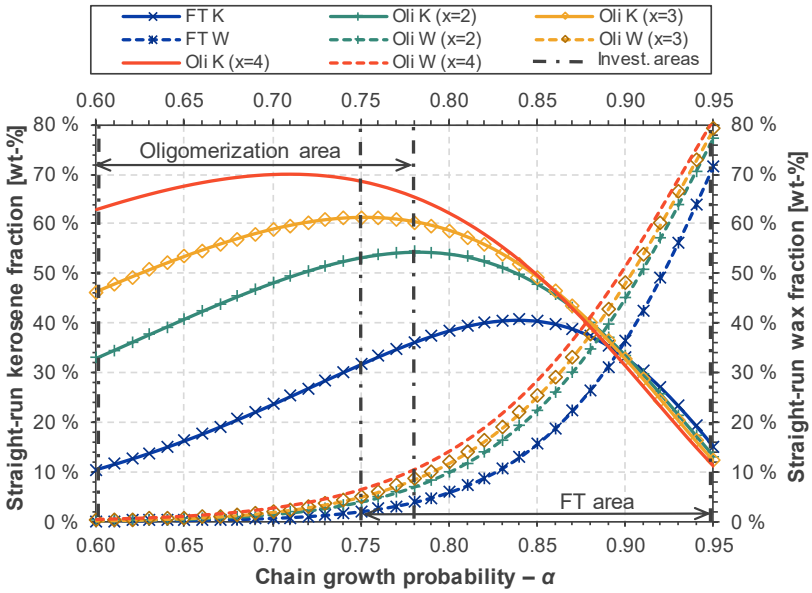

Figure B-2: Straight-run kerosene and wax fractions over chain growth probability variation (FT: Fischer-Tropsch, Invest. areas: Investigated areas in overall plant simulation, K: Kerosene, Oli.: Oligomerization, W: Wax, *x*: parameter of Eq. B-11).

Furthermore, while the share of components below the naphtha fraction (with regard to the chain length) decreases with an increasing alpha (α) value, the wax proportion significantly increases for both pathways. The plant concept of the FT pathway allows waxes to be further cracked into fuel fractions, which is why the analyzed range (FT area) is centered around the straight-run maximum. In contrast, there is no hydrocracking step in the plant concept of the methanol pathway (although this would also be technically feasible), resulting in waxes as non-fuel products, reducing the value product yield. Consequently, the analyzed range in the overall concept simulation is located to the left of the maxima of the straight-run profiles.

B.2.3 Process modeling

Compression. The selected compressor models are designed according to several criteria. Generally, a maximum compression ratio of 3 is permitted [223, 224]. If higher pressure ratios are required for compression, multistage compressors are selected. For the multistage compressor, the same pressure ratios are assumed for all stages since the total work requirement is lowest here [223]. Intermediate cooling is assumed down to 75 °C (air cooler [25 $°C_{Air}$] with minimal temperature difference gas to gas 50 K). The maximum compression temperature is considered to be below 250 °C [224]. All compressions are calculated polytropic using ASME method (see Aspen Help for further descriptions [109]). Aspen Plus default compression efficiency (72 %) is used.

Fuel gas combustion. Fuel gas combustion is modeled using stoichiometric reactor models generating combustion reactions. Oxygen is provided by air (21 $vol\%_{O2}$ / 79 $vol\%_{N2}$).

The combustion ratio is assumed with air in surplus (λ = 1.2) and a combustion temperature of 1,000 °C. The feed gas is pre-heated to 750 °C to consider heat integration potential. Peng-Robinson equation of state is used for calculating thermodynamic properties.

Fischer-Tropsch synthesis. The implementation of the FT-synthesis reactions in the flowsheet simulation takes place according to the procedure presented in [265]. A stoichiometric reactor (RStoic) is used, and the reactions Eq. B-12 ($1 \leq n < 42$) and Eq. B-13 ($2 \leq n < 24$) are implemented. The selectivity for methane, ethane, and ethene is approximated according to [159] with a value of 5.6, 1.0, and 0.1 %, respectively.

$$n\mathrm{CO} + (2n+1)\mathrm{H_2} \rightarrow \mathrm{C}_n\mathrm{H}_{2n+2} + n\mathrm{H_2O} \qquad \text{Eq. B-12}$$

$$n\mathrm{CO} + (2n)\mathrm{H_2} \rightarrow \mathrm{C}_n\mathrm{H}_{2n} + n\mathrm{H_2O} \qquad \text{Eq. B-13}$$

The amount of purge gas controls the feed gas composition. Thereby, the reactant concentration is set to 70 % (different values are reported: 50 % [83], 80 % [159]).

Olefin cleaning. The caustic wash is modeled using the Aspen Plus modeling example "ELECNRTL_Rate_Based_NaOH_Model". The "Dryer" is considered to be a molecular sieve modeled with a separator and a calculator block, which determines the required heat based on the evaporation enthalpy.

Distillation. The rectification columns were simulated for the reference cases using rigorous column models. For this purpose, "Radfrac" columns were selected, which allow the head and bottom product purities to be defined via internal design specifications, which are achieved by adjusting reflux and distillate-to-feed ratios. A preliminary design was carried out on shortcut models (DSTWU) to determine suitable stage numbers. The settings of the columns are listed in Table B-2.

Simulation changes from reference case to parameter variation. To perform the parameter variation in a simulation-based manner without violating internal design specifications under varying plant conditions, the rigorous column models of hydrocarbon fractionation were replaced by separator blocks. Due to the relatively low energy requirements of the columns, the resulting inaccuracies can be neglected.

Table B-2: Specification of column modeling (MeOH: Methanol pathway, FT: Fischer-Tropsch pathway).

Pathway	Column	Specification	Value	Unit
FT	Middle column 1	Stages	24	-
		Mass purity, head, C_{7-} and light gases	99.8	%
		Mass recovery, head, C_{7-} and light gases	99.5	%
	Middle column 2	Stages	24	-
		Mass purity, bottom, C_8-C_{20}	99.5	%
		Mass recovery, bottom, C_8-C_{20}	99.5	%
	Wax column	Stages	40	-
		Mass purity, head, $C_{21}H_{44}$	0.025	%
		Mass recovery, head, $C_{20}H_{42}$	98.0	%
	Kerosene column	Stages	50	-
		Mass purity, head, C_8-C_{16}	99.6	
		Mass recovery, head, C_{16} and lower	99.7	
	Naphtha column	Stages	24	-
		Mass purity, bottom, C_5-C_9	99.0	%
		Mass recovery, bottom, C_5-C_9	99.0	%
MeOH	Topping column	Stages	6	-
		Mass purity, bottom, CO_2	0.001	%
		Mass recovery, bottom, CH_3OH	99.9	%
	Methanol column	Stages	26	-
		Mass purity, head, CH_3OH	99.85	%
		Mass recovery, head, CH_3OH	99.95	%
	Middle column	Stages	24	-
		Mass purity, bottom, C_8 and higher	99.7	%
		Mass recovery, bottom, C_8 and higher	99.5	%
	Diesel column	Stages	50	-
		Mass purity, head, C_{16}-C_{20}	99.5	%
		Mass recovery, head, C_{16}-C_{20}	99.5	%
	Kerosene column	Stages	50	-
		Mass purity, head, C_8-C_{16}	99.5	%
		Mass recovery, head, C_8-C_{16}	99.5	%
	Naphtha column	Stages	20	-
		Mass purity, bottom, C_5-C_9	99.0	%
		Mass recovery, bottom, C_5-C_9	99.0	%

B.2.4 Heat integration approach

The heat integration carried out via pinch analysis considers a general minimum temperature difference (ΔT) of 20 K. Apart from this, a ΔT of 10 K is assumed for evaporation and condensation processes [225]. In order to approximate an ideal heat integration, heating/cooling and aggregate state changes of pure substances are simulated in separate steps. Table B-3 lists the considered utility streams used in the pinch analysis.

Table B-3: Utility streams considered in heat integration.

Task	Utility stream	Inlet T [°C]	Outlet T [°C]
Cooling	Refrigerant 1	−25	−24
	Water	15	25
	Low-pressure steam generation	124	125
	Medium-pressure steam generation	174	175
	High-pressure steam generation	249	250
Heating	Power	1,001	1,000

The demand for refrigerants from heat integration is further converted into additional cooling water and power demand for low-temperature generation. The theoretical coefficient of performance (COP) is adjusted with an approximated cooling cycle efficiency of 72 % [110].

B.3 Extended results

The following presents additional analysis results, supplementing those outlined in Chapter 4.

B.3.1 Hydrogen flows

Generally, the hydrogen flows resemble those of carbon and energy flows. Additionally, it is evident at which points molecularly bound hydrogen in the form of water is separated as a by-product.

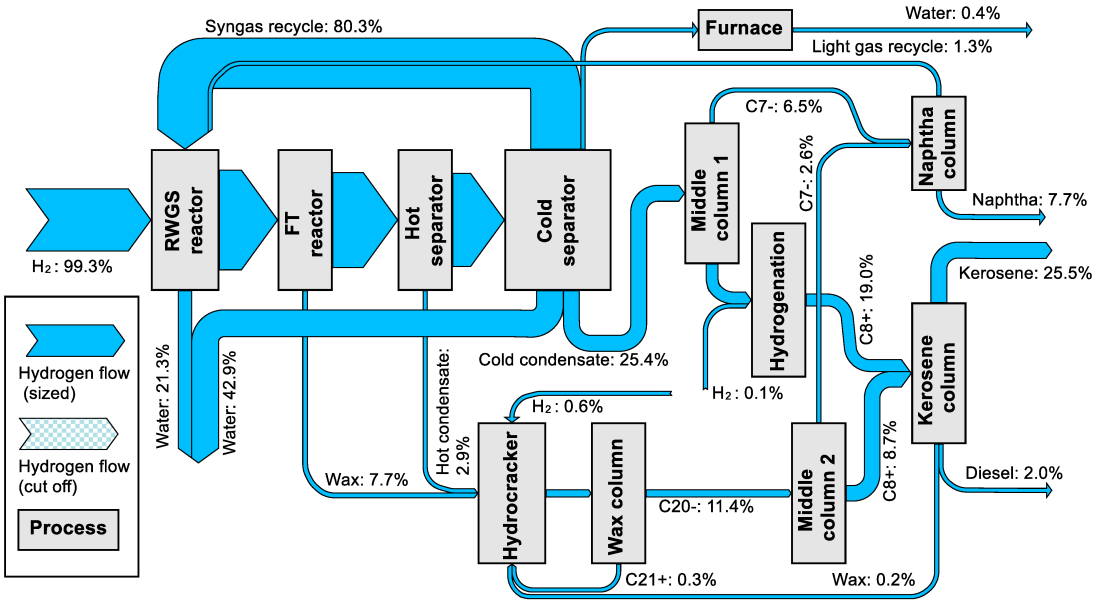

Figure B-3: Hydrogen flows of the Fischer-Tropsch pathway.

The most significant hydrogen loss in the FT pathway (Figure B-3) occurs through water separation in the cold separator. Before this, approximately half of the hydrogen amount

is separated after the RWGS. In the methanol pathway (Figure B-4), water formation occurs in methanol synthesis and dehydration in almost equal amounts. These hydrogen losses are unavoidable since water formation is stoichiometrically dictated in both process pathways. As water can be separated easily, no significant carbon losses occur. Compared to energy flow diagrams, it is apparent that the loss of hydrogen does not lead to equivalent energy losses, as most energy is transferred to the target product with the formation of hydrocarbon compounds. The difference corresponds to the reaction enthalpy. The ratios of the fractions to each other differ only slightly since the H/C ratios of the products are similar. Compared to carbon losses, hydrogen experiences a higher loss through flue gas (in the form of water), as a substantial portion of hydrogen and light, hydrogen-rich hydrocarbons are burned.

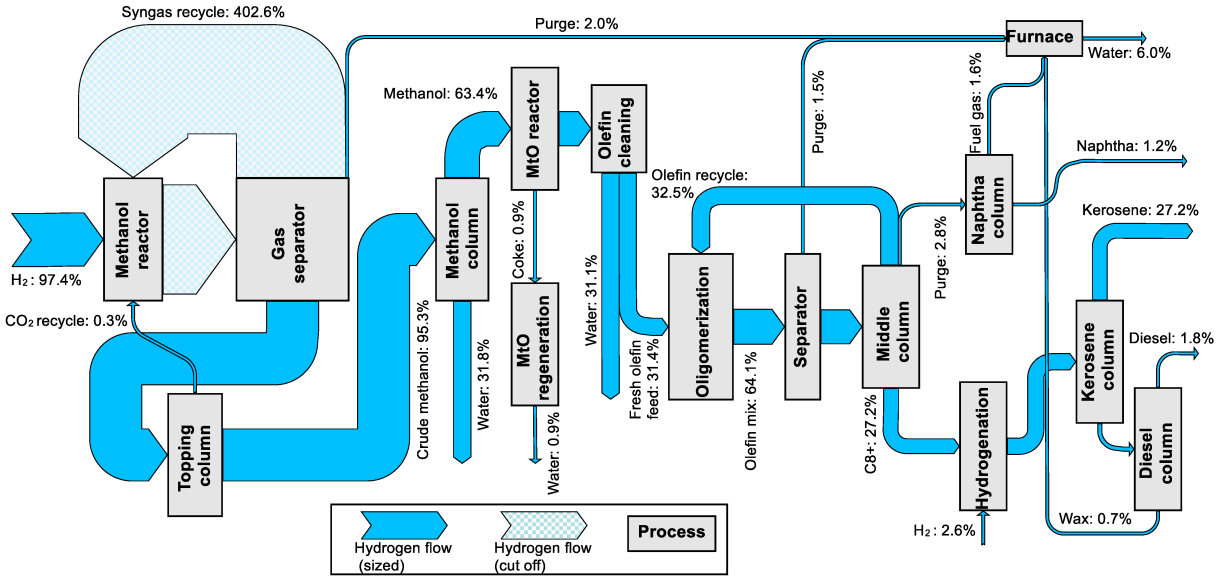

Figure B-4: Hydrogen flows of the methanol pathway.

The hydrogen efficiency regarding kerosene is 25.5 % in the FT and 27.2 % in the methanol pathway. Regarding the total fuel, the efficiencies are 35.2 % and 30.2 %, respectively.

B.3.2 Product composition

The product properties of the fuel fractions derived are decisive for their applicability as a fuel and the potentially required refining and blending steps. However, due to the quantitative consideration of the efficiencies within the scope of the work, no detailed, simulation-based analysis of the product properties of the fractions produced is possible (e.g., cold flow properties). However, essential characteristics concerning chain length distribution can be derived; these provide information about product quality and necessary adjustments in production and processing.

Figure B-5 shows the resulting chain length distribution of kerosene fractions and selected product properties. The FT kerosene shows a relatively even chain length distribution with a slight decrease in longer chain lengths. In contrast, the product distribution of

methanol-based production shows a strong shift toward light hydrocarbons and, thus, a significantly less balanced distribution. This is also reflected in the estimated product properties, especially in the low flash point. Both kerosene fractions are below the densities required in the specification but have a sufficiently high gravimetric energy content. According to the boiling curve, the distillate data are within the specification.

Even if the product fractions obtained here do not fully meet the ASTM requirements, using the fractions in the corresponding fuels is possible. Compliance with the specifications can be achieved by mixing the fuel fractions, adapting the rectification process, or making technical adjustments to the process. For the methanol pathway, in particular, the weighting of the product distribution towards shorter-chain products must be taken into account. In terms of process technology, for example, an increased return of C_{8+} components to the oligomerization process could ensure a more balanced distribution. However, the effects on the efficiencies and influencing variables considered in this work are rated low, as this does not significantly change overall carbon and energy demands.

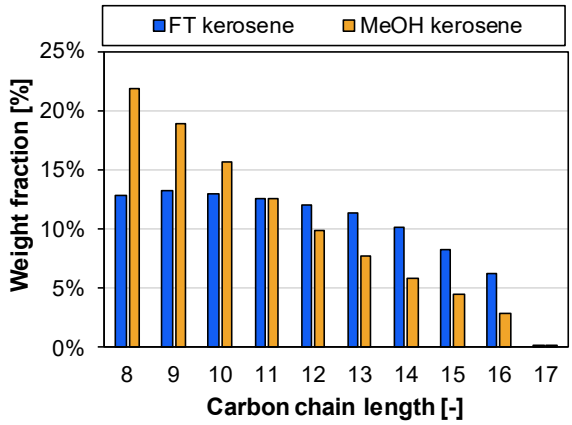

Property	Unit	ASTM D7566	FT	MeOH
Density	kg/m³	775-840	742	733
LHV	MJ/kg	42.8	44.2	44.2
Flash point	°C	>38	38	31
Dist. temp.:				
10% rec.	°C	<205	158	144
100% rec.	°C	<300	281	276

Figure B-5: Chain length distribution and specific properties of the kerosene fractions (Dist. temp. rec.: Distillation temperature at X % recovered, FT: Fischer-Tropsch pathway, MeOH: MeOH pathway).

The curves of the chain length distributions of naphtha and diesel shown in Figure B-6 differ slightly between the process pathways. Due to the wide range of applications in the chemical industry (cracking) or fuel production (gasoline), a suitable application can be expected for the naphtha fraction. Concerning the diesel fraction, it can be seen that due to the high chain length, the product fractions tend to represent heavy diesel, which can potentially be added to lighter diesel.

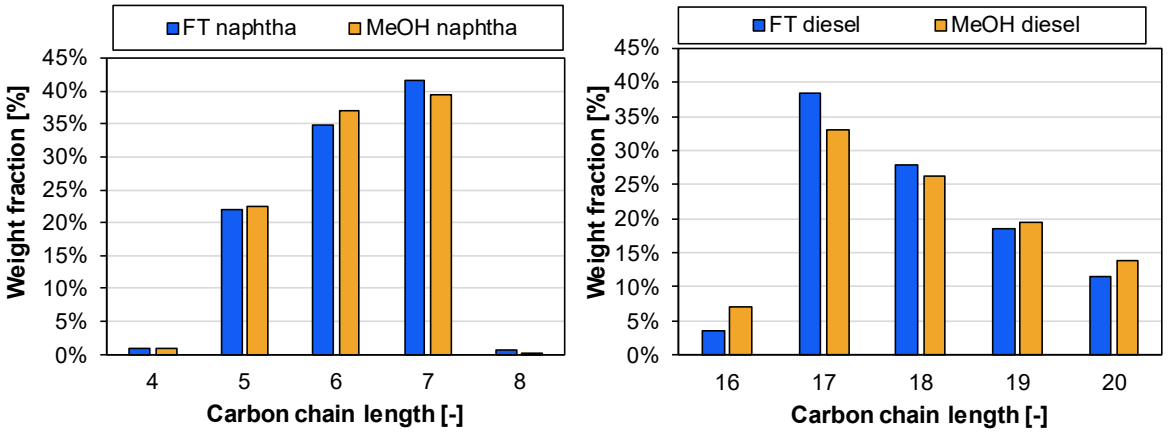

Figure B-6: Chain length distributions of the naphtha and diesel fractions (FT: Fischer-Tropsch pathway, MeOH: MeOH pathway).

Annex C – Cost analysis of kerosene production from power-based syngas via the Fischer-Tropsch and methanol pathway

This section contains the supplementary information published with the manuscript "Cost analysis of kerosene production from power-based syngas via the Fischer-Tropsch and methanol pathway" (Chapter 5). Formatting and wording are slightly adjusted to ensure consistency throughout this thesis.

C.1 Process modeling and simulation

The pathways are analyzed by coupling the Aspen plus® simulation with an additionally developed Python-Excel script, enabling automated simulation and evaluation.

Detailed information about the individual process technologies, process modeling, and the considered process data can be found in Bube et al. [175]. Adaptations of the process concepts and assumptions made in this paper result from the evaluation of [175] with recent literature and technical experts in power-based fuel production. In addition to the aspects described in Chapter 5, the most important adjustments made compared to [175] are described below.

C.1.1 Methanol pathway – Oligomerization approach

The oligomerization of an olefin mixture, particularly a blend of ethylene and higher olefins, is challenging due to the different reaction mechanisms involved. To ensure high conversions of all olefins, the use of different catalysts in multi-stage or multi-bed reactors is necessary. Nickel-based catalysts (e.g., Ni-AlSBA-15) allow for nearly complete conversion of ethene [191]. Subsequent oligomerization using acid catalysts (e.g., in mesoporous and microporous materials (MCM-41; SBA-15), zeolites or resins(Amberlyst-35)) enables the production of a high proportion of highly branched C_{10+} olefins [191, 192]. In the overall concept investigated in the methanol pathway, such advanced oligomerization of the light olefin mixture is assumed.

The model in [175] was adapted for the process concepts examined here to depict a more deterministic and feed-dependent product formation. The model is based on the assumptions and steps explained below.

The product distribution resulting from the oligomerization reactions is calculated based on the normalized molar olefin fractions of the feed stream (x_F) (i.e., non-olefin components remain unchanged during the reaction and are excluded from the following calculation) and the chain growth probability (α). Full conversion of all olefin components is

considered. The formation probability of an oligomer from n monomers ($P_{\mathrm{ASF},n}$) is obtained by assuming an Anderson-Schulz-Flory (ASF) distribution [171]. Taking into account the fact that an oligomer consists of at least two monomers, Eq. C-1 results. The carbon chain length (y) of the oligomer formed depends on the chain length of the coupled monomers (i, j) and results from the sum of the monomers chain lengths ($y = i + j$) . The probability of the monomers colliding is approximated as a multiplication of the molar fractions. The probability that an oligomer with the carbon chain length y is formed from n monomers ($P_{\mathrm{y},n}$) therefore corresponds to Eq. C-2, taking into account the feedstock composition ($x_{i,\mathrm{F}}$) and the concentration of the oligomers formed up to this point ($x_{j,n-1}$). Only oligomers up to a maximum chain length of C_{24} are considered, as it is assumed that formation restrictions occur in this range due to the shape selectivity of the catalyst. This also means that there can only be a maximum of 11 oligomerization steps; i.e., oligomers can be formed from a maximum of 12 monomers. By forming the sum of the multiplied probabilities over all oligomerization steps, the overall formation probability of a component with the chain length y ($P_{y,\mathrm{R}}$) can be calculated (Eq. C-3). The total fraction of the substance in the product ($x_{\mathrm{y,T}}$) is obtained by relating the overall formation probability of the individual olefin to the sum of the formation probabilities of all formed olefins (Eq. C-4).

$$P_{\mathrm{ASF},n} = (1-\alpha)\,\alpha^{n-2} \quad \text{for } n > 1 \qquad \text{Eq. C-1}$$

$$P_{\mathrm{y},n} = \sum_{i=2}^{24}\sum_{j=2}^{24} x_{i,\mathrm{F}} x_{j,n-1} \ (\text{für } (\mathrm{i}+\mathrm{j}) = \mathrm{y} \ \wedge (\mathrm{i}+\mathrm{j}) \leq 24 \wedge \ n > 1) \qquad \text{Eq. C-2}$$

$$P_{y,\mathrm{R}} = \sum_{n=2}^{12} P_{\mathrm{ASF},n}\, P_{\mathrm{y},n} \qquad \text{Eq. C-3}$$

$$x_{\mathrm{y,T}} = \frac{P_{y,\mathrm{R}}}{\sum_{i=2}^{24} P_{i,\mathrm{R}}} \qquad \text{Eq. C-4}$$

α	Chain growth probability [-]
$P_{\mathrm{ASF},n}$	Formation probability of an oligomer from n monomers taking into account ASF distribution [-]
$P_{\mathrm{y},n}$	Formation probability of an oligomer from n monomers with the chain length y taking into account collision probabilities
$x_{i,\mathrm{F}}$	Mole fraction of an olefin (chain length i) in the feed stream [-]
$x_{j,\mathrm{n}-1}$	Mole fraction of an olefin (chain length j) in from previous oligomerization step [-]
n	Number of monomers bound in oligomer [-]
$P_{y,\mathrm{R}}$	Overall formation probability of an oligomer (chain length y) through reaction
$x_{\mathrm{y,T}}$	Mole fraction of an olefin (chain length y) in total product [-]

The model is implemented in Aspen plus® by coupling a Calculator block with a RYield reactor. The reaction product is fractionated by using a flash and a subsequent distillation column. The flash (3 bar, 0 °C) separates light fuel gases and thus counteracts the accumulation of inert gases. The distillation column separates the oligomerization product further into a C_{8-} and C_{9+} fraction. Octene and lighter components are recycled to the oligomerization, while nonene and heavier olefins are processed in the hydrogenation and fractionation. A splitter within the olefin recycle is used to adjust the olefine fraction of the oligomerization feed to at least 80 %.

C.1.2 Energy integration approach

The plant concept is considered to convert H_2 and CO_2 into hydrocarbon fuels, with kerosene as the targeted product. Internal heat streams are integrated via pinch analysis (Aspen Energy Analyzer®). Utility streams satisfy the remaining heating and cooling demands. Reactors are usually not heated or cooled with other process streams and are excluded from direct heat integration and cooled or heated with utilities. The resulting utility requirements are balanced with the requirements of the pinch analysis to form the total utility demand. According to the system boundaries and in line with the general power-to-liquid (PtL) concept, electricity is considered as the primary energy source and, therefore, also for heat provision. Internally produced heat that exceeds the integrable requirements is considered for re-electrification via steam turbines so that only low-temperature heat (removed via cooling water) is produced in addition to the fuel products.

The heat integration carried out via pinch analysis considers a general minimum temperature difference (ΔT) of 20 K. Apart from this, a ΔT of 10 K is assumed for evaporation and condensation processes as well as product cooling, to avoid unnecessary refrigerant requirements [225]. In order to approximate an ideal heat integration, heating/cooling and aggregate state changes of pure substances are simulated in separate steps. Table C-1 lists the considered utility streams used in the pinch analysis.

Table C-1: Utility streams considered in heat integration.

Task	Utility stream	Inlet T [°C]	Outlet T [°C]
Cooling	Refrigerant	−25	−24
	Water	15	25
	Low-pressure steam generation	124	125
	Medium-pressure steam generation	174	175
	High-pressure steam generation	249	250
	Super high-pressure steam generation	324	325
Heating	Low-pressure steam	125	124
	Medium-pressure steam	175	174
	High-pressure steam	250	249
	Super high-pressure steam	325	324
	Electrical heating	1,100	1,099

Fuel gas furnace. Fuel gas combustion is assumed via stoichiometric combustion reactions. Oxygen is provided by air (21 vol%$_{O2}$/ 79 vol%$_{N2}$). The combustion ratio is assumed with air in surplus (λ = 1.2) and a combustion temperature of 1,000 °C. The feed gas is pre-heated to 750 °C to consider heat integration potential.

Low-temperature cooling. The demand for refrigerants from heat integration is further converted into additional cooling water and electricity demand, considering a conventional cooling cycle for low-temperature generation. The theoretical coefficient of performance (COP) is adjusted with an approximated cooling cycle efficiency of 72 % [110, 124].

Re-electrification. Electricity generation from waste heat using steam turbines is calculated using the Carnot efficiency. A condensation temperature of 40 °C is considered. To account for technical conversion losses, a technology factor of 85 % is applied [266].

Electrical heating. Since electricity is considered the primary energy source, it is also used for heat provision. The electricity-to-heat efficiency for steam generation is set to 100 % [267], while high-temperature heating above 325 °C has an efficiency of 95 % [268].

Vacuum generation. The energy demand for vacuum generation in distillation is derived from [186], considering a combined system of steam jet ejectors and liquid ring vacuum pumps. At an absolute pressure of 0.05 bar, the energy demand results in around 13 kWh of electrical power and 485 kWh MP-steam per ton of distillate. The energy is then released into cooling water.

The electricity demand for cooling of cooling water is assumed to be 2 % of the actual cooling demand, according to [125, 124, 269].

C.2 Cost calculation methodology

C.2.1 Fixed capital investment (*FCI*) calculation

The *FCI* (here, similar to grassroots or greenfield cost) is calculated according to Eq. C-5, representing the capital required for the plant's construction. The applied module costing technique, according to Turton et al. [110], relates all costs to the purchased cost of equipment evaluated under base conditions (C_{P}^{0}). The purchased costs for base conditions are multiplied with specific bare module cost factors individually for each equipment (l), some of which take into account additional design adjustments for pressure and material requirements (F_{BM}) and other not (F_{BM}^{0}). Contingency and fee costs (γ) and costs for, among others, site development, buildings, and utilities (auxiliary costs: β) are considered via mark-up factors multiplied by the sum of the total cost of equipment (k).

$$FCI = (1+\gamma)\sum_{l=1}^{k} C_{\mathrm{P},l}^{0}\, F_{\mathrm{BM},l} + \beta \sum_{l=1}^{k} C_{\mathrm{P},l}^{0}\, F_{\mathrm{BM},l}^{0} \qquad \text{Eq. C-5}$$

The base equipment costs are calculated for the major process equipment and can be derived from equipment-specific cost correlations (Eq. C-6) using empirical correlation parameters (K_x) [110]. For this purpose, the individual equipment is dimensioned concerning the equipment-dependent capacity parameter (A, e.g., area, volume, power) based on the simulation results and further technical specifications (e.g., gas hourly space velocity, bulk density, etc.).

$$\log_{10}(C_P^0) = K_1 + K_2 \log_{10}(A) + K_3 [\log_{10}(A)]^2 \quad \text{Eq. C-6}$$

To adjust the purchased cost for base conditions to non-base-case conditions and to take into account the direct and indirect costs of installation, C_P^0 is multiplied by the bare module cost factor (F_{BM}) (Eq. C-7).

$$F_{BM} = B_1 + B_2 F_p F_M \quad \text{Eq. C-7}$$

$$F_{BM}^0 = B_1 + B_2 \quad \text{Eq. C-8}$$

The calculation of the pressure factor (F_p) depends on the selected equipment. The selected formulas and basic assumptions are listed in Table C-2. The design pressure is chosen by multiplying a safety factor of 1.5 with the operating pressure [110]. The material factor (F_M) is selected depending on the equipment and the construction material. For a conservative cost estimate, stainless steel is assumed unless otherwise stated in this work. The specific installation cost factors (B_1 & B_2), are also available in the literature for the respective equipment. Certain components, such as compressors, have a standard bare module cost factor that is used independently of the operating conditions [110]. The bare module cost factor under standard conditions (F_{BM}^0) is used to calculate the grassroots cost since auxiliary facilities are generally unaffected by the operating conditions and material of process equipment (Eq. C-8).

Table C-2: Pressure factor (F_p) calculation.

Equipment	Pressure factor	Applied for
Vessels and column towers	1	$t < t_{min}$ and $p > -0.5$ bar
	$\frac{\frac{p \cdot D}{2S \cdot E - 1.2p} + CA}{t_{min}}$	$t > t_{min}$ and $p > -0.5$ bar
	1.25	$p < -0.5$ bar
Furnaces, heat exchangers, pumps	$\log_{10}(F_p) = C_1 + C_2 \log_{10}(p) + C_3 [\log_{10}(p)]^2$	only applied when $F_p > 1$, else 1

Formula symbols and assumptions: Equipment diameter (D [m]); absolute pressure (p [bar]); maximum allowable stress (S [bar] according to Turton [110] p. 1017); wall thickness (t [m]); corrosion allowance (CA [m]) 0.00315 m; weld efficiency (E [-])0.9; minimal allowable wall thickness (t_{min} [m]) 0.0063 m.

The literature does not provide cost functions for all equipment needed. The respective equipment costs (C_i) are derived based on literature cost values and scaled according to Eq. C-9 using an equipment-dependent scaling exponent (x), the size of the respective base equipment (s_1) and cost of the base equipment (C_1).

$$C_i = C_1 \cdot \left({}^{S_\mathrm{i}}/_{S_1}\right)^x \qquad \text{Eq. C-9}$$

C.2.2 Operational labor calculation

The number of operating employees per shift (N_OE) is calculated based on the number of process steps (N_PS) according to Eq. C-10 [110].

$$N_\mathrm{OE} = \sqrt{6.29 + 0.23 \cdot N_\mathrm{PS}} \qquad \text{Eq. C-10}$$

The annual operational labor cost (C_OL) is determined according to Eq. C-11, taking into account the gross monthly salary (S_m) and the non-wage labor costs (w). Furthermore, 5.15 shifts and 13 salaries per year are assumed.

$$C_\mathrm{OL} = 5.15 N_\mathrm{OE} \cdot 13 \cdot (1 + w) S_\mathrm{m} \qquad \text{Eq. C-11}$$

C.3 Cost calculation data

C.3.1 Equipment design data and assumptions

The main assumptions made within the equipment design are listed below for each type of equipment.

Reactors and vessels. Reactors are generally designed as vessels with an internal heat exchanger so that the vessel volume contains the reaction chamber and the heat exchanger volume. Unless otherwise stated, fixed catalyst beds with a void volume of 50 % are considered [270]. The height-to-diameter ratio of vessels is generally defined as 4 [270]. Considering these assumptions, the residence time (gas hourly space velocity, GHSV; weight hourly space velocity, WHSV; liquid hourly space velocity, LHSV) can be used for reactor dimensioning. Table C-3 lists the residence times considered for the required reactors.

Within the considered MtO technology (fluidized bed reactor), a SAPO-34 zeolite catalyst with a tap density of 826 kg/m^3 is used. The fluidized bed is assumed to have a porosity of 0.8 [271, 272]. Gas-liquid separators are designed to enable a residence time of the liquid phase of 5 min [270].

Table C-3: Residence times of reactors.

Pathway	Reactor	Residence time	Unit	Reference
Fischer-Tropsch	RWGS	36,000	h^{-1} (GHSV)	[150]
	Fischer-Tropsch	1,200	h^{-1} (GHSV)	[58, 273]
	Hydrocracker	1,5	h^{-1} (LHSV)	[58, 158, 274]
	Hydrogenation	1.2	h^{-1} (LHSV)	[160, 275]
Methanol	Methanol	7,000	h^{-1} (GHSV)	[95, 276, 277]
	MtO	1	h^{-1} (WHSV)	[168, 260, 278]
	Oligomerization	2	h^{-1} (WHSV)	[279–281]
	Hydrogenation	1.2	h^{-1} (LHSV)	[160, 275]

Heat exchanger. The heat exchangers are considered tube bundles with a tube diameter of 0.02 m [270]. The heat streams are derived by process simulation, and heat transfer coefficients are assumed according to the states/phases of the respective flows. The logarithmic mean temperature difference is calculated under the assumption of counter-flow operation.

Heaters not installed in reactors are included in the heat integration analysis (Pinch analysis). This shows the total area and the required number of heat exchangers. The area of the individual heat exchangers is assumed to be identical. The average operating pressure is defined as 25 bar. The heat integration is carried out for the reference case and is scaled within the parameter variation according to the CO_2 feed flow.

Columns. Columns are sized according to the number of stages and the stage diameter given by the flow sheet simulation. A stage height of 0.6 m, bottom height of 1.5 m, head height of 3 m, and inlet height of 1.5 m are considered [144].

Molecular sieve. The energy demand for molecular sieve regeneration is assumed to be 1.5 times the pure energy demand for heating and evaporation of water. A 3A molecular sieve, mainly used for olefin drying (CAS: 308080-99-1.; $K_{12}[(AIO_2)_{12}(SIO_2)]$-$XH_2O$), is considered. The relevant properties for the vessel design are the water adsorption maximum of 20 wt% and the bulk density (pellet) of 700 kg/m^3 [282].

C.3.2 Fixed capital investment

The parameters assumed for fixed capital investment calculation, according to the methodology mentioned above, are listed in Table C-4 and Table C-5.

Table C-4: Empirical equipment cost functions (Eq. C-6) according to Turton et al. [110].

Equipment	Parameter	Unit	Min	Max	K_1	K_2	K_3
Centrifugal compressor	Fluid power	kW	450	2,600	2.2897	1.3604	-0.1027
Drives (compressor)	Shaft power	kW	75	2,600	1.956	1.7142	-0.2282
Pump (centrifugal)	Shaft power	kW	1	300	3.3892	0.0536	0.1538
Heat exchanger (fixed tube)	Area	m^2	10	1,000	4.3247	−0.3030	0.1634
Steam boiler	Power	kW	1,200	9,400	6.9617	−1.4800	0.3161
Process vessel (horizontal)	Volume	m^3	0.1	628	3.5565	0.3776	0.0905
Process vessel (vertical)	Volume	m^3	0.3	520	3.4974	0.4485	0.1074
Column	Volume	m^3	0,3	520	3.4974	0.4485	0.1074
Stages (Sieve)	Area	m^2	0.07	12.3	2.9949	0.4465	0.3961
Turbines	Fluid power	kW	100	4,000	2.7051	1.4398	-0.1776
Furnace	Power	MW	1	100	7.3488	−1.1666	0.2028
Reformer furnace	Power	MW	3	100	3.0680	0.6597	0.0194
Reactor jacket (agitated)	Volume	m^3	0.1	35	4.1052	0.5320	-0.0005

Table C-5: Fixed capital investment assumptions and special equipment cost.

Costs	Value	Base		Reference
Contingency and fee share (γ)[%]	18	see Eq. C-5		[110]
Auxiliary cost share (β) [%]	50	see Eq. C-5		[110]
Equipment cost (Eq. C-9)	C_1	s_1	x	**Reference**
Vacuum generation	790,000 $US\$_{2016}$	11.8 t/h	0.7	[186]
High-temperature electrical heating	135,000 $US\$_{2020}$	1 MW	1.0	[268]

C.3.3 Fixed operational expenditures

The fixed operational expenditures ($OPEX_f$) are calculated according to the values listed in Table C-6. Labor costs are calculated on a European wage level. Maintenance costs are assumed in the lower range of the literature data since only fluids and no mechanical solids are processed. Relatively low costs are also assumed for distribution and selling, as the products are produced in large quantities and can be handled by the existing infrastructure.

Table C-6: Assumptions on fixed operational expenditures (*FCI*: Fixed capital investment, *KPC*: Kerosene production cost).

Costs	Value	Base	Reference
Gross monthly salary (S_m)[€/month]	5,202	-	[283]
Non-wage labor costs for EU-27 (w) [%]	32	gross monthly salary	[284]
Direct supervisory & clerical labor (C_{DS}) [%]	18	operational labor cost (C_{OL})	[110]
Maintenance and repairs ($C_{M\&R}$) [%]	3	*FCI*	[110, 124]
Operating supplies [%]	15	$C_{M\&R}$	[110]
Laboratory charges [%]	15	C_{OL}	[110]
Patents and royalties [%]	3	*KPC*	[110]
Plant overhead costs [%]	60	(C_{OL}+$C_{M\&R}$+C_{DS})	[110]
Administration costs [%]	15	(C_{OL}+$C_{M\&R}$+C_{DS})	[110]
Distribution and selling costs [%]	2	*KPC*	[110, 125]
Research and development [%]	5	*KPC*	[110, 125]

C.4 Technical results

Due to the process and modeling adjustments compared to Bube et al. [175], there are also slight deviations within the technical results. These are presented and briefly described below to assess the economic results better.

C.4.1 Carbon streams

This section shows the carbon flows of the process pathways in relation to the overall carbon input streams. The carbon share of the fuel output streams represents the carbon efficiency.

Fischer Tropsch pathway. Figure C-1 shows the relative carbon flows of the analyzed FT plant concept. The CO_2 feed stream (100 %) is the only carbon input into the process. It is supplied to the RWGS reactor along with the synthesis gas recycle (in terms of carbon, primarily CO, CO_2, and CH_4). Accumulation of inert components is prevented by a purge gas stream, which is separated from the recycle stream (cold separator). Downstream, around 50 % of the FT syncrude consists of heavy components (wax and hot condensate) which are directed to the hydrocracking unit. Approximately 70 % of this can be converted into kerosene (C_9-C_{17}), with the remaining 30 % consisting of naphtha and lighter gases (C_{8-}). The cold condensate is fractionated into kerosene (67 %) and lighter components (33 %). After subsequent hydrogenation, the kerosene fractions are combined and result in a carbon efficiency of 70.3 %. The remaining naphtha stream contains 27.7 % of the carbon used. The remaining 2.0 % are recognized as losses.

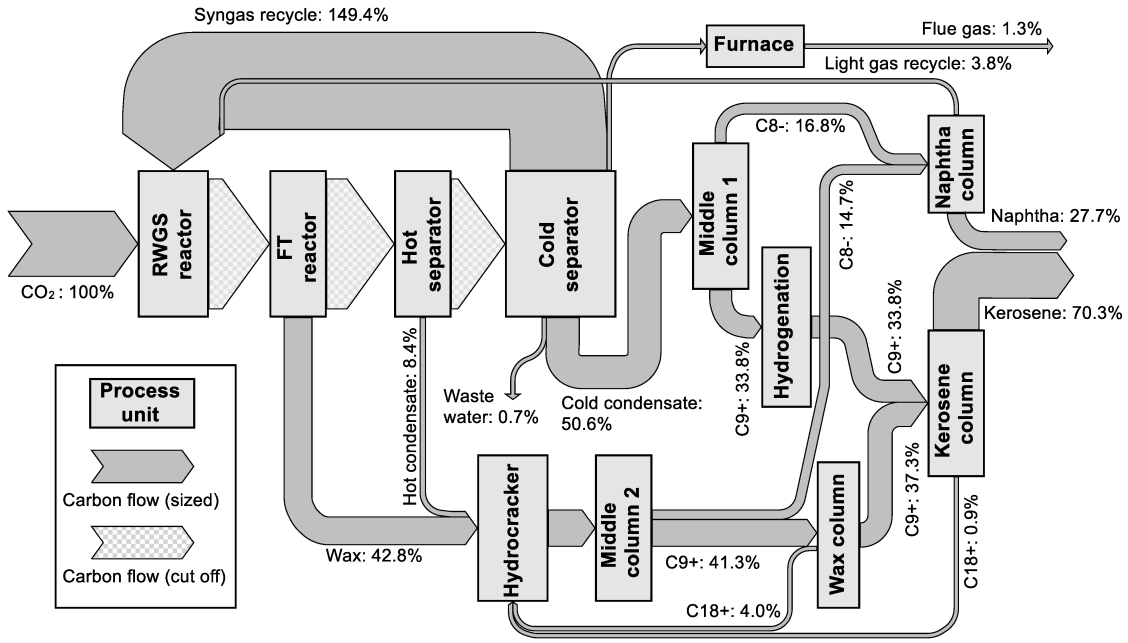

Figure C-1: Carbon flow diagram of the Fischer-Tropsch pathway (Diagram represents the reference case; FT: Fischer-Tropsch).

Methanol pathway. Figure C-2 shows the relative carbon flows of the methanol pathway. Again, the CO_2 stream serves as the only carbon input. Upstream, methanol production yields a carbon efficiency of almost 98 %, with purge gases being the only significant losses. The major carbon losses occur downstream, as upstream methanol production only shows carbon losses of around 2 %. Within the MtO reactor, 3 % of the carbon is discharged from the process as coke. Purge gas losses in the oligomerization loop add up to overall carbon losses of 16.7 %. The kerosene fraction contains 75.7 % of the carbon used, naphtha (2.3 %) and diesel (5.3 %) add up to a total fuel carbon efficiency of 83.3 %.

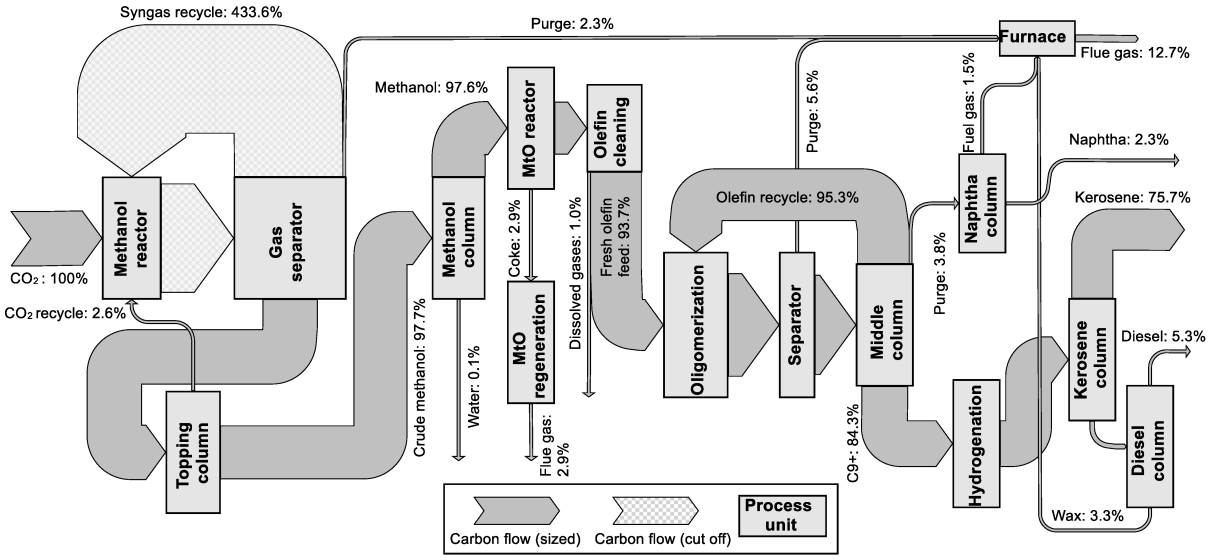

Figure C-2: Carbon flow diagram of the methanol pathway (Diagram represents the reference case; MeOH: Methanol; MtO: Methanol-to-olefins).

C.4.2 Energy streams

The energy flows shown in the following are normalized to the total energy input of each pathway, including electricity, heat, and chemical energy (higher heating value) flows.

Fischer-Tropsch pathway. The energy flows of the FT pathway are shown in Figure C-3. The main energy is provided by H_2, accounting for around 88 % of the total energy requirement. The main energy consumption in the process arises from electrical heating within the RWGS (950 °C). This energy is needed both for the endothermic RWGS reaction and for the endothermic reforming of light hydrocarbons in the syngas recycle. While some of this energy is subsequently released during the highly exothermic FT synthesis, heat integration is significantly constrained due to the much lower reaction temperature (220 °C). By implementing heat integration and re-electrification using steam turbines, the external electricity demand can be reduced to ca. 12 %.

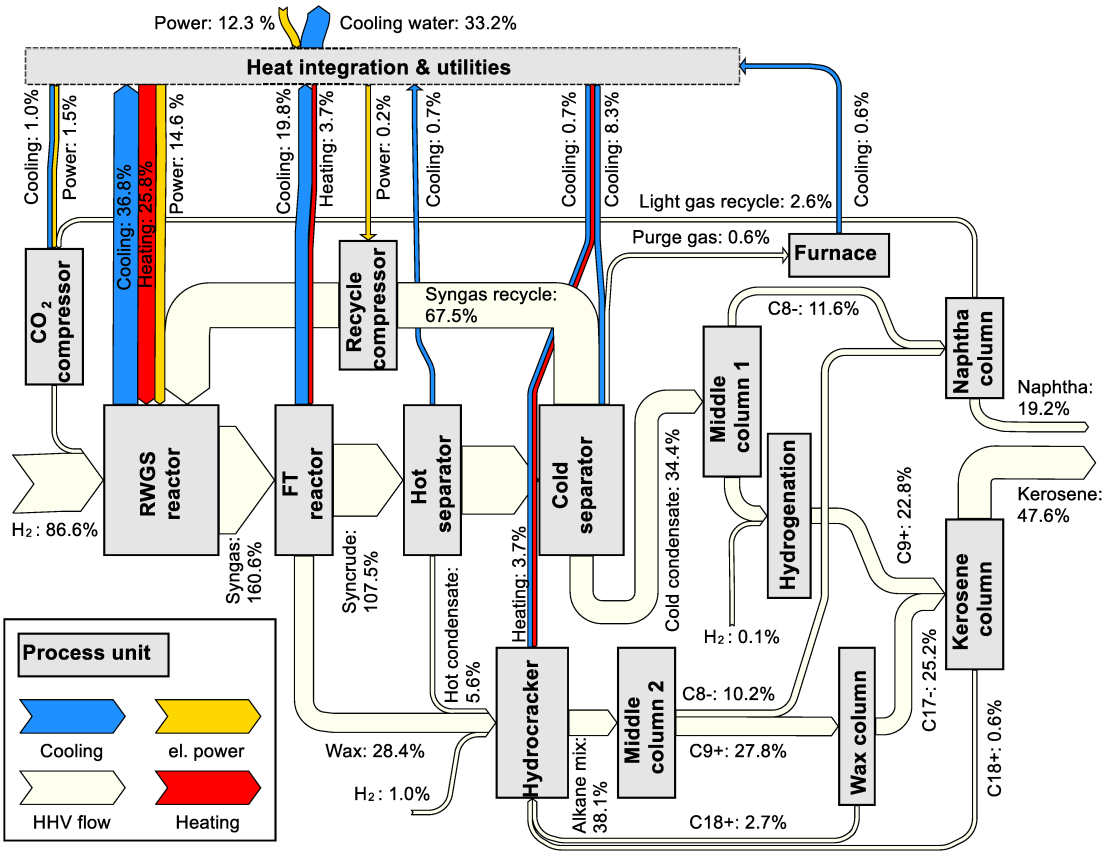

Figure C-3: Energy flow diagram of the Fischer-Tropsch pathway (Diagram represents the reference case; FT: Fischer-Tropsch).

Methanol pathway. The relative energy flows of the MeOH pathway are shown in Figure C-4. The H_2 input accounts for 99.7 % of the total energy input. Due to the higher pressure level and lower conversion of the methanol synthesis compared to the FT synthesis, as well as the increased pressure of the oligomerization reactor, the energy demand for compression is relatively high. However, the electricity demand is almost completely covered by internal re-electrification of waste heat, leading to an amount of external electricity of only 0.3 %.

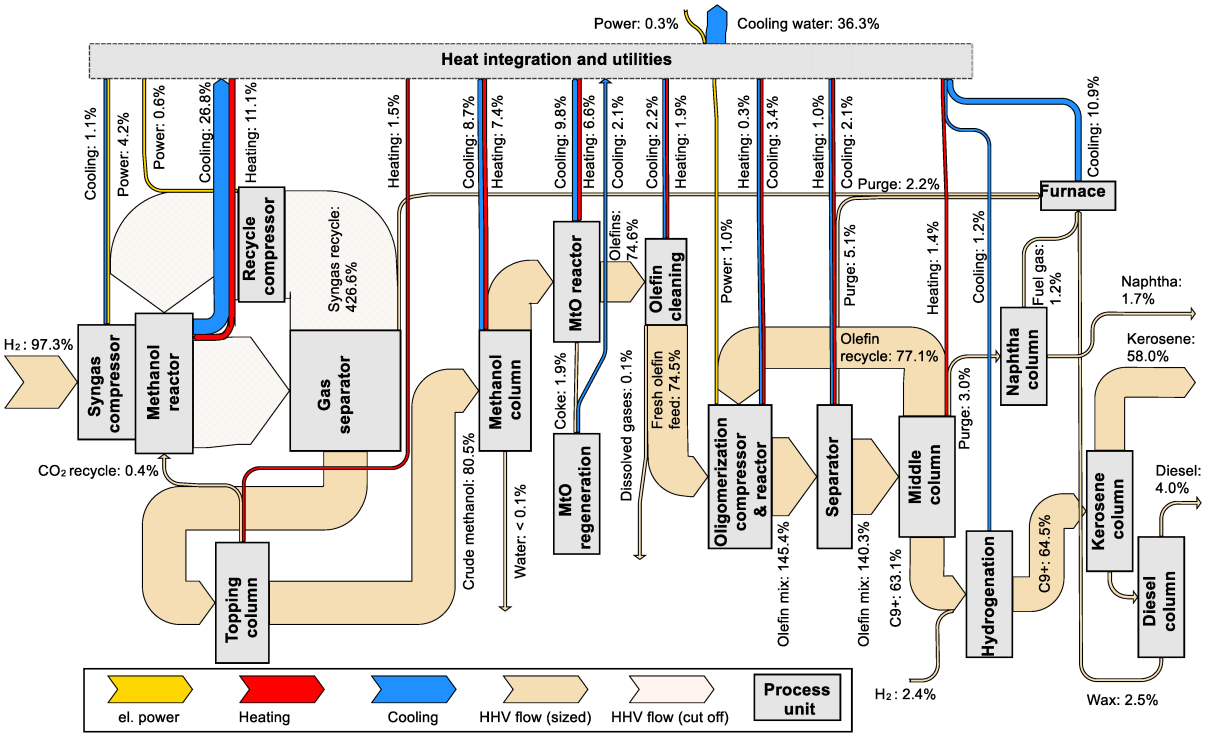

Figure C-4: Energy flow diagram of the methanol pathway (Diagram represents the reference case; MeOH: Methanol).

C.4.3 Carbon efficiency

Carbon efficiency is defined as the ratio of carbon atoms in fuel products (naphtha, kerosene, diesel) to carbon atoms provided by feedstock (CO_2). Figure C-5 shows the carbon efficiencies of both pathways under varying technical parameters. In the FT pathway, the chain growth probability within the FT reactor and the degree of hydrocracking, i.e., single (pri.), double (sec.), and triple (ter.) cracking possibility per reactor pass, are varied as higher-level process parameters (see Section 5.3.1). In the MeOH pathway, the olefin-selectivity (S_O) of the methanol dehydration and the chain growth probability within the oligomerization are varied.

Within the FT pathway, the carbon efficiency of the total fuel fraction, similarly to [175], exhibits an almost constant value across variations in chain growth probability without being influenced by the assumed hydrocracking behavior. This is because only the proportions of the product fractions change, but the total amount of fuel produced remains the same. However, differences are observed in the carbon efficiency of the kerosene fraction. Due to the complete recycling of the diesel fraction, the amount of kerosene continuously increases with increasing chain growth probability until the maximum achievable chain growth probability is reached. Since waxes and diesel from the hydrocracking product are also recycled, particularly mild hydrocracking (primary HC) is advantageous, as it produces fewer light components (naphtha). The additional hydrocracking of the diesel fraction reduces the total fuel carbon efficiency compared to [175] by around 1 %. Although this increases the amount of kerosene, it is reduced to a similar extent by the

changed assumptions of the kerosene fraction (C_8-C_{16} in [175](Chapter 4); C_9-C_{17} here (Chapter 5)).

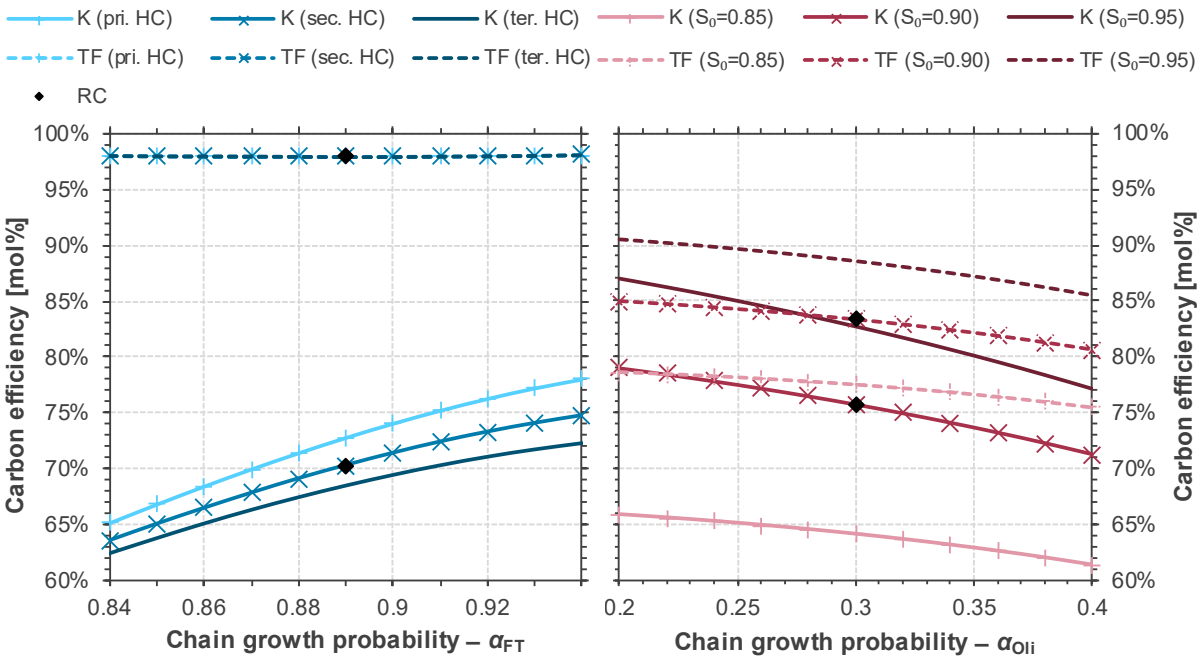

Figure C-5: Carbon efficiency of the Fischer-Tropsch and methanol pathway (K: Kerosene fraction, TF: Total fuel fraction, S_0: Olefin selectivity pri.: primary, sec.: secondary, ter.: tertiary, HC: Hydrocracking, RC: Reference case).

For the methanol pathway, similar trends are observed as simulated in [175], though at significantly lower chain growth probabilities due to the extended oligomerization model. A maximum is also observed here at very low chain growth probabilities, as the formation of heavier fractions (diesel) can be reduced. However, this results in additional effort due to the increased recycling of light fractions, which is not reflected in the carbon efficiency. The MtO olefin selectivity is the most important parameter within the methanol pathway. Industrial MtO plants can reach around 90 % selectivity. A further increase could reduce direct carbon losses within the MtO reactor (lower coke and CO_2 formation) and, even more importantly, reduce purge gas demands within the oligomerization loop. Lower selectivities significantly reduce the kerosene and total fuel carbon efficiency. However, total fuel efficiency is less affected since naphtha can partly be recovered from the purge gas.

The higher selectivity towards kerosene of oligomerization compared to FT synthesis primarily results from two factors. First, the monomers used in oligomerization (ethylene, propylene) are larger building blocks than carbon monoxide (FT synthesis), requiring fewer chain growth reactions to achieve the chain lengths of the kerosene fraction. The ASF distribution shows broader product distributions, with increasing chain growth probabilities, reducing the selectivity for specific chain lengths. Therefore, low chain growth probabilities combined with larger monomers result in higher kerosene selectivity. The second factor is that light product fractions in oligomerization can be directly re-

cycled, i.e., the chain length generated during the first reactor pass can further be increased. In FT synthesis, recycling is only possible after prior reforming, i.e., the synthesized chains are fully cracked before chain growth can start again. However, to achieve this higher selectivity in real processes, the catalysts and reaction conditions must enable sufficient activity for all olefins and sufficient chain growth probability. The oligomerization of olefins for hydrocarbon production in the kerosene range has already been demonstrated, but industrial validation of kerosene-optimized production is still pending [155, 171, 191, 285].

C.4.4 Energy efficiency

Figure C-6 shows the energy efficiencies of both pathways under varying technical parameters. In the FT pathway, the energy efficiency regarding the total fuel fraction exhibits a slightly curved profile, reaching a maximum of around 67 % at 90 % chain growth probability. At higher alpha values, the efficiency decreases due to the increasing amount of recycled light components from hydrocracking, which raises the heat demand of the RWGS, i.e., the reforming occurring here. In addition, the energy requirement for rectification in the hydrocracking unit is increased as more heavy components are formed and have to be fractionated after hydrocracking. For kerosene-related efficiency, this increasing energy demand is offset by the growing amount of kerosene, resulting in a rise in energy efficiency across the entire parameter variation.

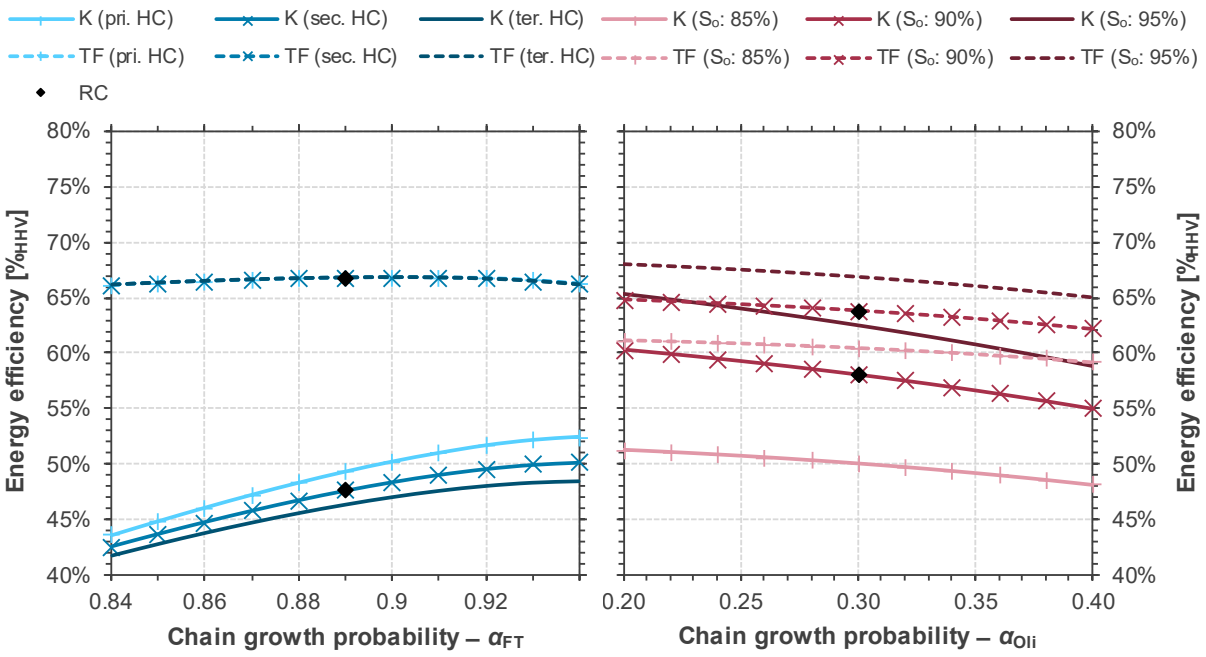

Figure C-6: Energy efficiency of the Fischer-Tropsch and methanol pathway (K: Kerosene allocation, TF: Total fuel allocation, S_0: Olefin selectivity pri.: primary, sec.: secondary, ter.: tertiary, HC: Hydrocracking, RC: Reference case).

In the methanol pathway, decreasing chain growth probabilities increase the compression demands for the oligomerization recycle. However, this is overcompensated by a

growing amount of fuel product resulting from reduced non-fuel hydrocarbon formation (C_{20+}). Low-chain growth probabilities prevent the formation of longer-chain fractions and allow for the targeted separation of kerosene. Significant quantities of the oligomerization recycle must be removed, particularly at low olefin selectivity in the MtO reactor, decreasing kerosene yield. The total product quantity decreases less significantly, as naphtha can still be partially separated from the purge gas.

C.4.5 Product composition

The fuel properties of the produced kerosene fractions play a critical role in determining their suitability for use as fuels, as well as the refining or blending processes that may be required. These properties, primarily cold flow properties, density, and also the distillation curve, are highly dependent on the exact composition of the fuel.

In addition to chain length, these characteristics are influenced by factors such as the degree of branching of paraffin and the proportion of cyclic components. In the modeling conducted here, chain length was primarily used as the key factor to quantify the resulting product fractions. While this common approach does not allow for the precise determination of specific fuel properties, as they are influenced by the factors mentioned above, the chain length distribution obtained from the simulation results provides an approximate basis for discussing fuel characteristics.

Figure C-7 shows the resulting chain length distribution of the kerosene fractions and selected product properties derived from the simulation. The distribution of the kerosene fraction resulting from the FT pathway is relatively even. The methanol-based kerosene exhibits a higher proportion of lighter components, particularly C_9 and C_{10}. This could potentially be adjusted, if necessary, by modifying the recycle flow in the oligomerization process. The properties of the fractions derived from the simulation largely fall within the required ASTM specifications. Only the simulated density is below the standard, although this further depends on the types of components formed (e.g., cyclic components can increase the density [30, 58]).

Regarding boiling points, a reduction in boiling temperature and flash point can be expected, depending on the degree of branching in the actual mixture. Overall, the properties are close to the ASTM requirements, suggesting that compliance with ASTM standards could realistically be achieved, possibly with adjustments to process parameters. However, the effects on the efficiencies and costs derived in this work are rated low, as this does not significantly change overall carbon and energy demands.

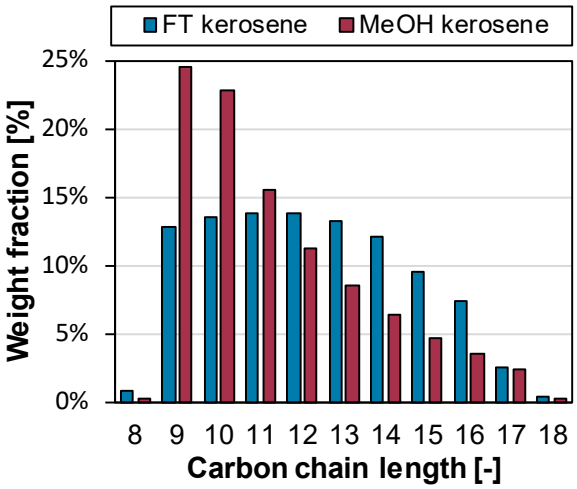

Property	Unit	ASTM D7566	FT	MeOH
Density	kg/m³	755-840	749.7	744.6
LHV	MJ/kg	>42.8	44.1	44.1
Flash point	°C	>38	54	48
Dist. temp.:				
10% rec.	°C	<205	176	168
100% rec.	°C	<300	296	292

Figure C-7: Chain length distribution and specific properties of the kerosene fractions (Dist. temp. rec.: Distillation temperature at X % recovered, LHV: Lower heating value, FT: Fischer-Tropsch pathway, MeOH: Methanol pathway).

C.5 Economic results

Figure C-8 presents the breakdown of the fixed capital investments determined for both production pathways in the reference case. Due to the calculation methodology (see Section C.2 and C.3), heat exchangers outside reactors are reported separately and not assigned to specific process units. The utilities include steam turbines, fuel gas furnaces, and vacuum generation.

The electrically heated reverse water-gas shift unit in the FT pathway represents the most capital-intensive section. Heat integration, the FT synthesis unit, and plant utilities contribute similar cost shares, while hydrotreatment, compressors, and distillation account for smaller shares.

In the methanol pathway, higher capital costs arise from the direct methanol synthesis, which, in addition to the inherently higher pressures compared to FT synthesis, exhibits much lower per-pass conversions, necessitating a substantially larger design. This also impacts the required compressor capacities and their associated costs. The oligomerization unit also requires a large-scale design due to the high product recycling rate, which also necessitates distillation for the targeted separation of fuel fractions. The methanol-to-olefins (MtO) unit is also relatively capital-intensive, as the selected reactor concept involves two fluidized bed reactors.

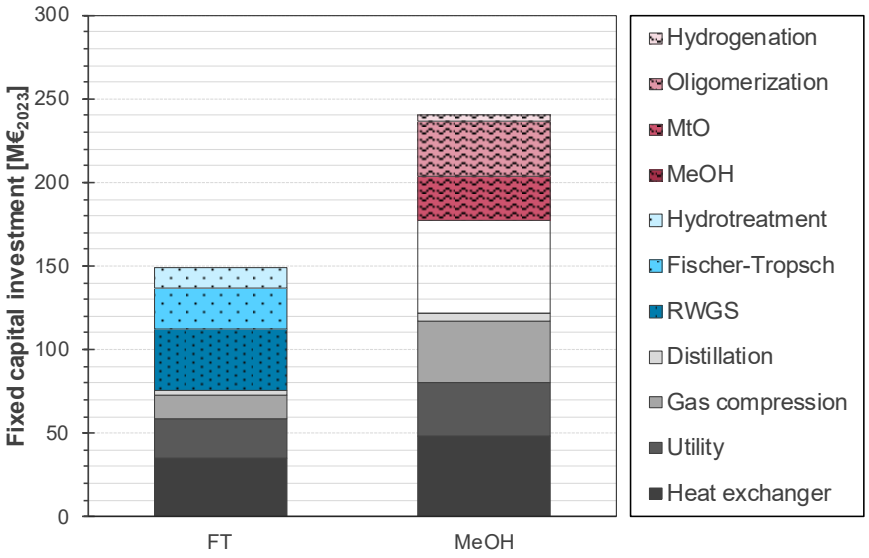

Figure C-8: Fixed capital investment of the Fischer-Tropsch and methanol pathway (Reference case; MtO: Methanol-to-olefins, MeOH: Methanol, RWGS: Reverse water-gas shift unit).

References

1. IPCC (2023) Summary for Policymakers. In: Climate Change 2023: Synthesis Report. Contribution of Working Groups I, II and III to the Sixth Assessment Report of the Intergovernmental Panel on Climate Change [Core Writing Team, Lee H and Romero J (eds.)]. IPCC, Geneva, Switzerland, pp. 1-34, doi: 10.59327/IPCC/AR6-9789291691647.001. Intergovernmental Panel on Climate Change (IPCC)
2. Abbass K, Qasim MZ, Song H, Murshed M, Mahmood H, Younis I (2022) A review of the global climate change impacts, adaptation, and sustainable mitigation measures. Environ Sci Pollut Res Int 29:42539–42559. doi:10.1007/s11356-022-19718-6
3. Kemp L, Xu C, Depledge J, Ebi KL, Gibbins G, Kohler TA, Rockström J, Scheffer M, Schellnhuber HJ, Steffen W, Lenton TM (2022) Climate Endgame: Exploring catastrophic climate change scenarios. Proc Natl Acad Sci U S A 119:e2108146119. doi:10.1073/pnas.2108146119
4. Lee DS, Fahey DW, Skowron A, Allen MR, Burkhardt U, Chen Q, Doherty SJ, Freeman S, Forster PM, Fuglestvedt J, Gettelman A, León RR de, Lim LL, Lund MT, Millar RJ, Owen B, Penner JE, Pitari G, Prather MJ, Sausen R, Wilcox LJ (2021) The contribution of global aviation to anthropogenic climate forcing for 2000 to 2018. Atmos Environ (1994) 244:117834. doi:10.1016/j.atmosenv.2020.117834.
5. Bergero C, Gosnell G, Gielen D, Kang S, Bazilian M, Davis SJ (2023) Pathways to net-zero emissions from aviation. Nat Sustain 6:404–414. doi:10.1038/s41893-022-01046-9
6. Quante G, Voigt C, Kaltschmitt M (2025) Climate Impacts of Aviation and the Potential of Aviation Powerfuels Toward Their Mitigation. In: Bullerdiek N, Neuling U, Kaltschmitt M (eds) Powerfuels. Springer Nature Switzerland, Cham, pp 879–904
7. Klöwer M, Allen MR, Lee DS, Proud SR, Gallagher L, Skowron A (2021) Quantifying aviation's contribution to global warming. Environ Res Lett 16:104027. doi:10.1088/1748-9326/ac286e
8. Grewe V, Gangoli Rao A, Grönstedt T, Xisto C, Linke F, Melkert J, Middel J, Ohlenforst B, Blakey S, Christie S, Matthes S, Dahlmann K (2021) Evaluating the climate impact of aviation emission scenarios towards the Paris agreement including COVID-19 effects. Nat Commun 12:3841. doi:10.1038/s41467-021-24091-y
9. International Air Transport Association (2021) Resolution on the industry's commitment to reach net zero carbon emissions by 2050: Press Release No: 66
10. International Civil Aviation Organization (2022) Resolution A41-21.: Consolidated statement of continuing ICAO policies and practices related to environmental protection - Climate change., Montréal
11. Bullerdiek N (2024) Kerosinoptionen auf Basis regenerativer Energien im internationalen Luftverkehr. Dissertation, Technische Universität Hamburg; Verlag Dr. Kovač
12. Dray L, Schäfer AW, Grobler C, Falter C, Allroggen F, Stettler MEJ, Barrett SRH (2022) Cost and emissions pathways towards net-zero climate impacts in aviation. Nat Clim Chang 12:956–962. doi:10.1038/s41558-022-01485-4

13. Jing L, El-Houjeiri HM, Monfort J-C, Littlefield J, Al-Qahtani A, Dixit Y, Speth RL, Brandt AR, Masnadi MS, MacLean HL, Peltier W, Gordon D, Bergerson JA (2022) Understanding variability in petroleum jet fuel life cycle greenhouse gas emissions to inform aviation decarbonization. Nat Commun 13:7853. doi:10.1038/s41467-022-35392-1
14. International Air Transport Association (2024) Industry Statistics: Fact sheet, Montréal
15. Pechstein J (2025) Klimaschutz im internationalen Luftverkehr. Dissertation, Technische Universität Hamburg; Verlag Dr. Kovač; Technische Universität Hamburg
16. International Air Transport Association (2022) Net zero 2050: sustainable aviation fuels. Fact sheet., Montréal
17. International Air Transport Association (2023) SAF Volumes Growing but Still Missing Opportunities: Press Release No: 69. https://www.iata.org/en/pressroom/2023-releases/2023-12-06-02/. Accessed 11 Dec 2024
18. International Air Transport Association (2024) Disappointingly Slow Growth in SAF Production: Press Release No: 60. https://www.iata.org/en/pressroom/2024-releases/2024-12-10-03/. Accessed 11 Dec 2024
19. Wen J, Zhao D, Zhang C (2020) An overview of electricity powered vehicles: Lithium-ion battery energy storage density and energy conversion efficiency. Renewable Energy 162:1629–1648. doi:10.1016/j.renene.2020.09.055
20. Choi JW, Aurbach D (2016) Promise and reality of post-lithium-ion batteries with high energy densities. Nat Rev Mater 1. doi:10.1038/natrevmats.2016.13
21. Adu-Gyamfi BA, Good C (2022) Electric aviation: A review of concepts and enabling technologies. Transportation Engineering 9:100134. doi:10.1016/j.treng.2022.100134
22. Atanasov G, van Wensveen J, Peter F, Zill T (2019) Electric Commuter Transport Concept Enabled by Combustion Engine Range Extender. Deutscher Luft-und Raumfahrtkongress vol 68, Darmstadt, Germany
23. Graver B, Zhang K, Rutherford D (2019) CO2 emissions from commercial aviation, 2018
24. Bullerdiek N, Voß S, Neuling U, Kaltschmitt M (2022) Direct alcohol vs. alcohol-to-jet SPK utilisation in commercial aviation – an energetic-operational analysis. Int. J. Sustainable Aviation
25. Penner, J., Lister, D., Griggs, D., Dokken, D., McFarland, M. (ed) (1999) Aviation and the global atmosphere: Aircraft Technology and Its Relation to Emissions, 1. publ. Cambridge University Press, Cambridge
26. Bullerdiek N, Quante G, Bube S, Neuling U, Kaltschmitt M (2022) Non Drop-In Kraftstoffe im Luftverkehr – Ein gesamtsystemischer Vergleich von Nutzungs- und Einsatzmöglichkeiten., Hamburg, Berlin
27. International Civil Aviation Organization Conversion processes: Approved Conversion Processes. https://www.icao.int/environmental-protection/GFAAF/Pages/Conversion-processes.aspx. Accessed 11 Dec 2024
28. ASTM (2021) Specification for Aviation Turbine Fuel Containing Synthesized Hydrocarbons(D7566)
29. Pires, A., Han, Y., Kramlich, J., Garcia-Perez, M (2018) Chemical Composition and Fuel Properties of Alternative Jet Fuels. BioResources:2632–2657. doi:10.15376/biores.13.2.2632–2657
30. Cookson DJ, Lloyd CP, Smith BE (1987) Investigation of the chemical basis of kerosene (jet fuel) specification properties. Energy Fuels 1:438–447. doi:10.1021/ef00005a011

31. Quante G, Voigt C, Kaltschmitt M (2024) Targeted use of paraffinic kerosene: Potentials and implications. Atmospheric Environment: X 23:100279. doi:10.1016/j.aeaoa.2024.100279
32. Morrison K., Miller J. , Rodrigues PF., Mulholland E, Zhou Y., Baldino C., Benoit J. (2024) Cleaning up Germany's vehicle stock: Strategies to decarbonize the passenger car fleet
33. Slowik P., Isenstadt A., Pierce L., Searle S. (2022) ASSESSMENT OF LIGHT-DUTY ELECTRIC VEHICLE COSTS AND CONSUMER BENEFITS IN THE UNITED STATES IN THE 2022–2035 TIME FRAME
34. Pasini G, Lutzemberger G, Ferrari L (2023) Renewable Electricity for Decarbonisation of Road Transport: Batteries or E-Fuels? Batteries 9:135. doi:10.3390/batteries9020135
35. Agora Verkehrswende (2023) E-Fuels zwischen Wunsch und Wirklichkeit. Was strombasierte synthetische Kraftstoffe für die Energiewende im Verkehr leisten können und was nicht.
36. (2023) DIRECTIVE (EU) 2023/2413 OF THE EUROPEAN PARLIAMENT AND OF THE COUNCIL: RED III
37. Hoogwijk M, Faaij A, van den Broek R, Berndes G, Gielen D, Turkenburg W (2003) Exploration of the ranges of the global potential of biomass for energy. Biomass and Bioenergy 25:119–133. doi:10.1016/S0961-9534(02)00191-5
38. Quante G, Bullerdiek N, Bube S, Neuling U, Kaltschmitt M (2023) Renewable fuel options for aviation – A System-Wide comparison of Drop-In and non Drop-In fuel options. Fuel 333:126269. doi:10.1016/j.fuel.2022.126269
39. Kost C, Müller P, Schweiger JS, Fluri V, Thomsen J (2024) Levelized Cost of Electricity Renewable Energy Technologies
40. Hassan Q, Viktor P, J. Al-Musawi T, Mahmood Ali B, Algburi S, Alzoubi HM, Khudhair Al-Jiboory A, Zuhair Sameen A, Salman HM, Jaszczur M (2024) The renewable energy role in the global energy Transformations. Renewable Energy Focus 48:100545. doi:10.1016/j.ref.2024.100545
41. IEA - International Energy Agency (2024) Renewables 2024. https://www.iea.org/reports/renewables-2024. Accessed Licence: CC BY 4.0
42. Moriarty P, Honnery D (2012) What is the global potential for renewable energy? Renewable and Sustainable Energy Reviews 16:244–252. doi:10.1016/j.rser.2011.07.151
43. Resch G, Held A, Faber T, Panzer C, Toro F, Haas R (2008) Potentials and prospects for renewable energies at global scale. Energy Policy 36:4048–4056. doi:10.1016/j.enpol.2008.06.029
44. Khan MA, Al-Attas T, Roy S, Rahman MM, Ghaffour N, Thangadurai V, Larter S, Hu J, Ajayan PM, Kibria MG (2021) Seawater electrolysis for hydrogen production: a solution looking for a problem? Energy Environ Sci 14:4831–4839. doi:10.1039/D1EE00870F
45. Santana L, Santos Gd, Santos A, Marinho C, Bispo A, Villardi H, Pessoa F (2024) Evaluating the economic influence of water sources on green hydrogen production: A cost analysis approach. International Journal of Hydrogen Energy 89:353–363. doi:10.1016/j.ijhydene.2024.09.274
46. Neuling U, Kaltschmitt M (2018) Techno-economic and environmental analysis of aviation biofuels. Fuel Processing Technology 171:54–69. doi:10.1016/j.fuproc.2017.09.022

47. Mission Possible Partnership (2022) Making Net-Zero Aviation Possible. https://missionpossiblepartnership.org/action-sectors/aviation/. Accessed 28.09.22
48. Voß S, Bube S, Kaltschmitt M (2024) Hybrid Biomass- and Electricity-Based Kerosene Production—A Techno-Economic Analysis. Energy Fuels 38:5263–5278. doi:10.1021/acs.energyfuels.3c04876
49. Rojas-Michaga MF, Michailos S, Cardozo E, Akram M, Hughes KJ, Ingham D, Pourkashanian M (2023) Sustainable aviation fuel (SAF) production through power-to-liquid (PtL): A combined techno-economic and life cycle assessment. Energy Conversion and Management 292:117427. doi:10.1016/j.enconman.2023.117427
50. Agora Verkehrswende and PtX Hub (2024) Defossilising aviation with e-SAF: An introduction to technologies, policies, and markets for sustainable aviation fuels
51. Dieckmann C, Kaltschmitt M, Kretzschmar J, Liebetrau J, Oldenburg S, Ritzkowski M, Scherzinger M, Scholwin F, Schultz J, Weinrich S (2024) Biogaserzeugung. In: Kaltschmitt M, Scherzinger M, Gescher J (eds) Energie aus Biomasse. Springer Fachmedien Wiesbaden, Wiesbaden, pp 229–401
52. Uddin MM, Wright MM (2023) Anaerobic digestion fundamentals, challenges, and technological advances. Physical Sciences Reviews 8:2819–2837. doi:10.1515/psr-2021-0068
53. Benedikt F, Fleck S, Fuchs J, Hofbauer H, Kaltschmitt M, Keil F, Klemm M (2024) Verfahren der Gaserzeugung in der Gasatmosphäre. In: Kaltschmitt M, Hofbauer H, Lenz V (eds) Energie aus Biomasse. Springer Fachmedien Wiesbaden, Wiesbaden, pp 669–802
54. Molino A, Chianese S, Musmarra D (2016) Biomass gasification technology: The state of the art overview. Journal of Energy Chemistry 25:10–25. doi:10.1016/j.jechem.2015.11.005
55. Puig-Arnavat M, Bruno JC, Coronas A (2010) Review and analysis of biomass gasification models. Renewable and Sustainable Energy Reviews 14:2841–2851. doi:10.1016/j.rser.2010.07.030
56. Bube S, Hofbauer H, Kaltschmitt M, Klemm M, Neuling U, Voß S, Zitscher T (2024) Synthese- und Weiterverarbeitungsverfahren. In: Kaltschmitt M, Hofbauer H, Lenz V (eds) Energie aus Biomasse. Springer Fachmedien Wiesbaden, Wiesbaden, pp 1011–1099
57. Hiller H, Reimert R, Marschner F, Renner H-J, Boll W, Supp E, Brejc M, Liebner W, Schaub G, Hochgesand G, Higman C, Kalteier P, Müller W-D, Kriebel M, Schlichting H, Tanz H, Stönner H-M, Klein H, Hilsebein W, Gronemann V, Zwiefelhofer U, Albrecht J, Cowper CJ, Driesen HE Gas Production. In: Ullmann's Encyclopedia of Industrial Chemistry
58. Klerk A de (2011) Fischer-Tropsch refining. Wiley-VCH, Weinheim
59. Nedolivko VV, Zasypalov GO, Vutolkina AV, Gushchin PA, Vinokurov VA, Kulikov LA, Egazar'yants SV, Karakhanov EA, Maksimov AL, Glotov AP (2020) Carbon Dioxide Reforming of Methane. Russ J Appl Chem 93:765–787. doi:10.1134/S1070427220060014
60. Abdulrasheed A, Jalil AA, Gambo Y, Ibrahim M, Hambali HU, Shahul Hamid MY (2019) A review on catalyst development for dry reforming of methane to syngas: Recent advances. Renewable and Sustainable Energy Reviews 108:175–193. doi:10.1016/j.rser.2019.03.054
61. Owgi AHK, Jalil AA, Hussain I, Hassan NS, Hambali HU, Siang TJ, Vo DVN (2021) Catalytic systems for enhanced carbon dioxide reforming of methane: a review. Environ Chem Lett 19:2157–2183. doi:10.1007/s10311-020-01164-w

62. Jang W-J, Jeong D-W, Shim J-O, Kim H-M, Roh H-S, Son IH, Lee SJ (2016) Combined steam and carbon dioxide reforming of methane and side reactions: Thermodynamic equilibrium analysis and experimental application. Applied Energy 173:80–91. doi:10.1016/j.apenergy.2016.04.006
63. Zhao X, Joseph B, Kuhn J, Ozcan, S (2020) Biogas Reforming to Syngas: A Review. iScience 23:101082. doi:10.1016/j.isci.2020.101082
64. Görner K, Hübner K, Behr P, Heischkamp E, Rehfeldt S, Bergins C, Oeljeklaus G, Jönsson S, Kniesburges P, Epple B, Förster M, Wallus S, Schwendig F, Multhaupt S, Majoros ÖJ, Bockhorn H, Pfeifer H, Hoenig V, Hoppe H, Fleiger K, Middelhauve R, Doncheva-Albrecht D, Schwarz G, Ruf S, Engel C, Kortenbach K, Gerling JP, Knopf S, Müller C, May F, Kühn M, Streibel M (2015) CCS-Prozesskette. In: Fischedick M, Görner K, Thomeczek M (eds) CO2: Abtrennung, Speicherung, Nutzung. Springer Berlin Heidelberg, Berlin, Heidelberg, pp 255–482
65. Buttler A, Spliethoff H (2018) Current status of water electrolysis for energy storage, grid balancing and sector coupling via power-to-gas and power-to-liquids: A review. Renewable and Sustainable Energy Reviews 82:2440–2454. doi:10.1016/j.rser.2017.09.003
66. Lange H, Klose A, Lippmann W, Urbas L (2023) Technical evaluation of the flexibility of water electrolysis systems to increase energy flexibility: A review. International Journal of Hydrogen Energy 48:15771–15783. doi:10.1016/j.ijhydene.2023.01.044
67. Shiva Kumar S, Lim H (2022) An overview of water electrolysis technologies for green hydrogen production. Energy Reports 8:13793–13813. doi:10.1016/j.egyr.2022.10.127
68. Chatenet M, Pollet BG, Dekel DR, Dionigi F, Deseure J, Millet P, Braatz RD, Bazant MZ, Eikerling M, Staffell I, Balcombe P, Shao-Horn Y, Schäfer H (2022) Water electrolysis: from textbook knowledge to the latest scientific strategies and industrial developments. Chem Soc Rev 51:4583–4762. doi:10.1039/d0cs01079k
69. Rodin V, Lindorfer J, Böhm H, Vieira L (2020) Assessing the potential of carbon dioxide valorisation in Europe with focus on biogenic CO2. Journal of CO2 Utilization 41:101219. doi:10.1016/j.jcou.2020.101219
70. Lindsey R DE (2024) Climate Change: Atmospheric Carbon Dioxide. https://www.climate.gov/news-features/understanding-climate/climate-change-atmospheric-carbon-dioxide. Accessed 07 Jan 2025
71. Fischedick M, Görner K, Thomeczek M (eds) (2015) CO2: Abtrennung, Speicherung, Nutzung. Springer Berlin Heidelberg, Berlin, Heidelberg
72. Fasihi M, Efimova O, Breyer C (2019) Techno-economic assessment of CO2 direct air capture plants. Journal of Cleaner Production 224:957–980. doi:10.1016/j.jclepro.2019.03.086
73. Sievert K, Schmidt TS, Steffen B (2024) Considering technology characteristics to project future costs of direct air capture. Joule 8:979–999. doi:10.1016/j.joule.2024.02.005
74. Young J, McQueen N, Charalambous C, Foteinis S, Hawrot O, Ojeda M, Pilorgé H, Andresen J, Psarras, P. Renforth, P., Garcia S, van der Spek M (2023) The cost of direct air capture and storage can be reduced via strategic deployment but is unlikely to fall below stated cost targets. One Earth 6:899–917. doi:10.1016/j.oneear.2023.06.004
75. Rezaei E, Dzuryk S (2019) Techno-economic comparison of reverse water gas shift reaction to steam and dry methane reforming reactions for syngas production. Chemical Engineering Research and Design 144:354–369. doi:10.1016/j.cherd.2019.02.005

76. Wolf A, Jess A, Kern C (2016) Syngas Production via Reverse Water-Gas Shift Reaction over a Ni-Al 2 O 3 Catalyst: Catalyst Stability, Reaction Kinetics, and Modeling. Chem Eng Technol 39:1040–1048. doi:10.1002/ceat.201500548
77. Voß S, Bube S, Bullerdiek N, Kaltschmitt M (2025) Reverse Water–Gas Shift for Synthesis Gas Provision—A Core Technology for Powerfuel Production. In: Bullerdiek N, Neuling U, Kaltschmitt M (eds) Powerfuels. Springer Nature Switzerland, Cham, pp 515–537
78. Bertau M, Offermanns H, Plass L, Schmidt F, Wernicke H-J (2014) Methanol: The Basic Chemical and Energy Feedstock of the Future. Springer Berlin Heidelberg, Berlin, Heidelberg
79. Keil FJ (1999) Methanol-to-hydrocarbons: process technology. Microporous and Mesoporous Materials 29:49–66. doi:10.1016/S1387-1811(98)00320-5
80. Avidan AA (1988) Gasoline and Distillate Fuels From Methanol. In: Methane Conversion, Proceedings of a Symposium on the Production of Fuels and Chemicals from Natural Gas, vol 36. Elsevier, pp 307–323
81. Kaltschmitt M, Neuling U (eds) (2018) Biokerosene. Springer Berlin Heidelberg, Berlin, Heidelberg
82. Chiaramonti D, Prussi M, Buffi M, Tacconi D (2014) Sustainable bio kerosene: Process routes and industrial demonstration activities in aviation biofuels. Applied Energy 136:767–774. doi:10.1016/j.apenergy.2014.08.065
83. König DH (2016) Techno-ökonomische Prozessbewertung der Herstellung synthetischen Flugturbinentreibstoffes aus CO2 und H2: Dissertation, Universität Stuttgart
84. Meurer A, Kern J (2021) Fischer–Tropsch Synthesis as the Key for Decentralized Sustainable Kerosene Production. Energies 14:1836. doi:10.3390/en14071836
85. Pfeifer P, Biffar L, Timm F, Böltken T (2020) Influence of Power-to-Fuel Plant Flexibility Towards Power and Plant Utilization and Intermediate Hydrogen Buffer Size. Chemie Ingenieur Technik 92:1976–1982. doi:10.1002/cite.202000084
86. Dieterich V, Buttler A, Hanel A, Spliethoff H, Fendt S (2020) Power-to-liquid via synthesis of methanol, DME or Fischer–Tropsch-fuels: a review. Energy Environ Sci 13:3207–3252. doi:10.1039/D0EE01187H
87. Maitlis PM, Klerk A de (2013) Greener Fischer-Tropsch Processes for Fuels and Feedstocks. Wiley
88. Pérez-Fortes M, Schöneberger JC, Boulamanti A, Tzimas E (2016) Methanol synthesis using captured CO2 as raw material: Techno-economic and environmental assessment. Applied Energy 161:718–732. doi:10.1016/j.apenergy.2015.07.067
89. Goeppert A, Czaun M, Jones J-P, Surya Prakash GK, Olah GA (2014) Recycling of carbon dioxide to methanol and derived products - closing the loop. Chem Soc Rev 43:7995–8048. doi:10.1039/c4cs00122b
90. Anicic B, Trop P, Goricanec D (2014) Comparison between two methods of methanol production from carbon dioxide. Energy 77:279–289. doi:10.1016/j.energy.2014.09.069
91. IRENA and the Methanol Institute (2021) Innovation Outlook: Renewable Methanol, International Renewable Energy Agency, Abu Dhabi.
92. Mbatha S, Everson RC, Musyoka NM, Langmi HW, Lanzini A, Brilman W (2021) Power-to-methanol process: a review of electrolysis, methanol catalysts, kinetics, reactor designs and modelling, process integration, optimisation, and techno-economics. Sustainable Energy Fuels 5:3490–3569. doi:10.1039/D1SE00635E
93. Otto A Chemische, verfahrenstechnische und ökonomische Bewertung von Kohlendioxid als Rohstoff in der chemischen Industrie. Dissertation, Techn. Hochsch Aachen

94. Umweltbundesamt Atmosphärische Treibhausgas-Konzentrationen. https://www.umweltbundesamt.de/daten/klima/atmosphaerische-treibhausgas-konzentrationen#kohlendioxid-. Accessed 14 Nov 2022
95. Ott J, Gronemann V, Pontzen F, Fiedler E, Grossmann G, Kersebohm DB, Weiss G, Witte C (2012) Methanol. In: Ott J (ed) Ullmann's Encyclopedia of Industrial Chemistry: Methanol. Wiley-VCH Verlag GmbH & Co. KGaA, Weinheim, Germany
96. IEA - International Energy Agency (2018) The future of petrochemicals. OECD
97. Entesari N, Goeppert A, Prakash GKS (2020) Renewable Methanol Synthesis through Single Step Bi-reforming of Biogas. Ind Eng Chem Res 59:10542–10551. doi:10.1021/acs.iecr.0c00755
98. Acquarola C, Bhatelia T, Pareek V, Ao M, Shah MT (2022) Optimized Process for Methanol Production via Bi-reforming Syngas. Ind Eng Chem Res 61:5557–5567. doi:10.1021/acs.iecr.1c04904
99. Acquarola C, Ao M, Bhatelia T, Prakash B, Faka S, Pareek V, Shah MT (2021) Simulations and Optimization of a Reduced CO 2 Emission Process for Methanol Production Using Syngas from Bi-reforming. Energy Fuels 35:8844–8856. doi:10.1021/acs.energyfuels.1c00227
100. Chein R-Y, Chen W-H, Chyuan Ong H, Loke Show P, Singh Y (2021) Analysis of methanol synthesis using CO2 hydrogenation and syngas produced from biogas-based reforming processes. Chemical Engineering Journal 426:130835. doi:10.1016/j.cej.2021.130835
101. Hernandez B, Martin M (2018) Optimization for biogas to chemicals via tri-reforming. Analysis of Fischer-Tropsch fuels from biogas. Energy Conversion and Management 174:998–1013. doi:10.1016/j.enconman.2018.08.074
102. Chein R-Y, Hsu W-H (2018) Analysis of Syngas Production from Biogas via the Tri-Reforming Process. Energies 11:1075. doi:10.3390/en11051075
103. Farsi M, Lari MF (2020) Methanol production based on methane tri-reforming: Process modeling and optimization. Process Safety and Environmental Protection 138:269–278. doi:10.1016/j.psep.2020.03.014
104. Zhang Y, Cruz J, Zhang S, Lou HH, Benson TJ (2013) Process simulation and optimization of methanol production coupled to tri-reforming process. International Journal of Hydrogen Energy 38:13617–13630. doi:10.1016/j.ijhydene.2013.08.009
105. Lim D, Lee B, Lee H, Byun M, Lim H (2022) Projected cost analysis of hybrid methanol production from tri-reforming of methane integrated with various water electrolysis systems: Technical and economic assessment. Renewable and Sustainable Energy Reviews 155:111876. doi:10.1016/j.rser.2021.111876
106. Choe C, Byun M, Lee H, Lim H (2022) Techno-economic and environmental assessments for sustainable bio-methanol production as landfill gas valorization. Waste Manag 150:90–97. doi:10.1016/j.wasman.2022.06.040
107. Moioli E, Schildhauer T (2022) Eco-Techno-Economic Analysis of Methanol Production from Biogas and Power-to-X. Ind Eng Chem Res 61:7335–7348. doi:10.1021/acs.iecr.1c04682
108. Sens L, Piguel Y, Neuling U, Timmerberg S, Wilbrand K, Kaltschmitt M (2022) Cost minimized hydrogen from solar and wind – Production and supply in the European catchment area. Energy Conversion and Management 265:115742. doi:10.1016/j.enconman.2022.115742
109. aspentech Aspen Plus. Aspen Technology Inc, Bedford
110. Turton R (op. 2018) Analysis, synthesis, and design of chemical processes, fifth edition. Prentice Hall International Series in the Physical and Chemical Engineering Sciences. Prentice Hall, Boston [etc.]

111. Association for the Advancement of Cost Engineering (2020) COST ESTIMATE CLASSIFICATION SYSTEM-AS APPLIED IN ENGINEERING, PROCUREMENT, AND CONSTRUCTION FOR THE PROCESS INDUSTRIES: AACE® International Recommended Practice No. 18R-97. TCM Framework: 7.3 – Cost Estimating and Budgeting
112. Wismann ST, Engbæk JS, Vendelbo SB, Bendixen FB, Eriksen WL, Aasberg-Petersen K, Frandsen C, Chorkendorff I, Mortensen PM (2019) Electrified methane reforming: A compact approach to greener industrial hydrogen production. Science 364:756–759. doi:10.1126/science.aaw8775
113. Danish Energy Agency Technology Data for Industrial Process Heat: Datasheet for industrial process heat
114. Topsoe eREACT™ Fuels: New technology essential for electrofuels production. https://www.topsoe.com/our-resources/knowledge/our-products/equipment/e-react-fuels. Accessed 19 Dec 2023
115. BASF (2023) BASF, SABIC und Linde beginnen mit dem Bau der weltweit ersten Demonstrationsanlage für großtechnische elektrisch beheizte Steamcracker-Öfen. https://www.basf.com/global/de/media/news-releases/2022/09/p-22-326.html. Accessed 19/12.2023
116. Ciambelli P (2021) 2 Catalytic autothermal reforming for hydrogen production: from large-scale plant to distributed energy system. In: van de Voorde M (ed) Hydrogen Production and Energy Transition. De Gruyter, pp 171–192
117. Kaltschmitt M, Hartmann H, Hofbauer H (eds) (2016) Energie aus Biomasse: Grundlagen, Techniken und Verfahren, 3., aktualisierte und erweiterte Auflage. Springer Vieweg, Berlin
118. Fachagentur Nachwachsende Rohstoffe e. V. (2023) Nachwachsende Rohstoffe: Basisdaten Bioenergie Deutschland 2022
119. Vita A, Italiano C, Previtali D, Fabiano C, Palella A, Freni F, Bozzano G, Pino L, Manenti F (2018) Methanol synthesis from biogas: A thermodynamic analysis. Renewable Energy 118:673–684. doi:10.1016/j.renene.2017.11.029
120. Butera G, Fendt S, Jensen SH, Ahrenfeldt J, Clausen LR (2020) Flexible methanol production units coupling solid oxide cells and thermochemical biomass conversion via different gasification technologies. Energy 208:118432. doi:10.1016/j.energy.2020.118432
121. Hansen JB, Hjlund Nielsen PE Methanol Synthesis. In: Ertl, Knözinger, Schüth, Weitkamp (eds) 2008 – Handbook of Heterogeneous Catalysis
122. M. Dreher, M. Memmler, S. Rother, S. Schneider (2011) Bioenergie - Datengrundlagen für die Statistik der erneuerbaren Energien und Emissionsbilanzierung: Ergebnisbericht zum Workshop vom Juli 2011
123. Fasihi M, Breyer C (2020) Baseload electricity and hydrogen supply based on hybrid PV-wind power plants. Journal of Cleaner Production 243:118466. doi:10.1016/j.jclepro.2019.118466
124. Towler GP, Sinnott RK (2013) Chemical engineering design: Principles, practice, and economics of plant and process design, 2nd ed. Butterworth-Heinemann, Boston MA
125. Peters MS, Timmerhaus KD, West RE (2006) Plant design and economics for chemical engineers, 5. ed., internat. ed., [Nachdr.]. McGraw-Hill chemical engineering series. McGraw-Hill, Boston
126. Martin Wietschel (2019) Klimabilanz, Kosten und Potenziale verschiedener Kraftstoffarten und Antriebssysteme für Pkw und Lkw: Endbericht. doi:10.24406/publica-fhg-299856
127. Umweltbundesamt (2020) Optionen für Biogas-Bestandsanlagen bis 2030 aus ökonomischer und energiewirtschaftlicher Sicht: Abschlussbericht

128. Eurostat (2023) Electricity prices for non-household consumers - bi-annual data (from 2007 onwards): Online data code: nrg_pc_205. https://ec.europa.eu/eurostat/databrowser/view/nrg_pc_205/default/table?lang=en
129. Boulamanti A, Moya JA (2017) Production costs of the chemical industry in the EU and other countries: Ammonia, methanol and light olefins. Renewable and Sustainable Energy Reviews 68:1205–1212. doi:10.1016/j.rser.2016.02.021
130. EEA E (2023) Preisentwicklung von CO2-Emissionsrechten im europäischen Emissionshandel (EU-ETS) von 2005 bis 2022. https://de.statista.com/statistik/daten/studie/1304069/umfrage/preisentwicklung-von-co2-emissionsrechten-in-eu/. Accessed 03 Nov 2023
131. Svanberg M, Ellis J, Lundgren J, Landälv I (2018) Renewable methanol as a fuel for the shipping industry. Renewable and Sustainable Energy Reviews 94:1217–1228. doi:10.1016/j.rser.2018.06.058
132. Kajaste R, Hurme M, Oinas P (2018) Methanol-Managing greenhouse gas emissions in the production chain by optimizing the resource base. AIMS Energy 6:1074–1102. doi:10.3934/energy.2018.6.1074
133. Kärcher B (2018) Formation and radiative forcing of contrail cirrus. Nat Commun 9:1824. doi:10.1038/s41467-018-04068-0.
134. Surgenor C. LanzaJet opens the world's first-of-a-kind ethanol to jet fuel production facility. https://www.greenairnews.com/?p=5251. Accessed 10 Jan 2024
135. Schmidt P, Weindorf W, Roth A, Batteiger V, Riegel F (2016) Power-to-Liquids: Potentials and Perspectives for the Future Supply of Renewable Aviation Fuel
136. Panzone C, Philippe R, Chappaz A, Fongarland P, Bengaouer A (2020) Power-to-Liquid catalytic CO2 valorization into fuels and chemicals: focus on the Fischer-Tropsch route. Journal of CO2 Utilization 38:314–347. doi:10.1016/j.jcou.2020.02.009
137. Bellussi G, Mizia F, Calemma V, Pollesel P, Millini R (2012) Oligomerization of olefins from Light Cracking Naphtha over zeolite-based catalyst for the production of high quality diesel fuel. Microporous and Mesoporous Materials 164:127–134. doi:10.1016/j.micromeso.2012.07.020
138. Atsonios K, Li J, Inglezakis VJ (2023) Process analysis and comparative assessment of advanced thermochemical pathways for e-kerosene production. Energy 278:127868. doi:10.1016/j.energy.2023.127868
139. Al-Malah KIM (2017) Aspen plus: Chemical engineering applications. Wiley, Hoboken, New Jersey
140. Haydary J (2019) Chemical process design and simulation: Aspen Plus and Aspen HYSYS applications. Wiley, Hoboken, N.J.
141. Schefflan R (2011) Teach Yourself the Basics of Aspen Plus™. Wiley
142. Siemens Energy (2020) Silyzer 300: The next paradigm of PEM electrolysis. https://assets.siemens-energy.com/siemens/assets/api/uuid:a193b68f-7ab4-4536-abe2-c23e01d0b526/datasheet-silyzer300.pdf. Accessed 18 Jan 2024
143. Pearson K Hydrogen Production by Partial Catalytic Dehydrogenation of Kerosene. Dissertation, Institut für Energiespeicherung, Universität Stuttgart
144. Schemme S (2020) Techno-ökonomische Bewertung von Verfahren zur Herstellung von Kraftstoffen aus H2 und CO2: Dissertation. Energie & Umwelt / Energy & Environment, Jülich
145. Wei J, Ge Q, Yao R, Wen Z, Fang C, Guo L, Xu H, Sun J (2017) Directly converting CO2 into a gasoline fuel. Nat Commun 8:15174. doi:10.1038/ncomms15174
146. Wang Y, Kazumi S, Gao W, Gao X, Li H, Guo X, Yoneyama Y, Yang G, Tsubaki N (2020) Direct conversion of CO2 to aromatics with high yield via a modified Fischer-Tropsch

synthesis pathway. Applied Catalysis B: Environmental 269:118792. doi:10.1016/j.apcatb.2020.118792
147. Yang Q, Kondratenko VA, Petrov SA, Doronkin DE, Saraçi E, Lund H, Arinchtein A, Kraehnert R, Skrypnik AS, Matvienko AA, Kondratenko EV (2022) Identifying Performance Descriptors in CO2 Hydrogenation over Iron-Based Catalysts Promoted with Alkali Metals. Angew Chem Int Ed Engl 61:e202116517. doi:10.1002/anie.202116517
148. Corrao E, Salomone F, Giglio E, Castellino M, Ronchetti SM, Armandi M, Pirone R, Bensaid S (2023) CO2 conversion into hydrocarbons via modified Fischer-Tropsch synthesis by using bulk iron catalysts combined with zeolites. Chemical Engineering Research and Design 197:449–465. doi:10.1016/j.cherd.2023.07.052
149. Shi B, Davis BH (2005) Fischer–Tropsch synthesis: The paraffin to olefin ratio as a function of carbon number. Catalysis Today 106:129–131. doi:10.1016/j.cattod.2005.07.159
150. Kaiser P, Unde RB, Kern C, Jess A (2013) Production of Liquid Hydrocarbons with CO2 as Carbon Source based on Reverse Water-Gas Shift and Fischer-Tropsch Synthesis. Chemie Ingenieur Technik 85:489–499. doi:10.1002/cite.201200179
151. Nestler F, Krüger M, Full J, Hadrich MJ, White RJ, Schaadt A (2018) Methanol Synthesis - Industrial Challenges within a Changing Raw Material Landscape. Chemie Ingenieur Technik 90:1409–1418. doi:10.1002/cite.201800026
152. Maus W (ed) (2019) Zukünftige Kraftstoffe. Springer Berlin Heidelberg, Berlin, Heidelberg
153. Sydora OL, Jones TC, Small BL, Nett AJ, Fischer AA, Carney MJ (2012) Selective Ethylene Tri-/Tetramerization Catalysts. ACS Catal 2:2452–2455. doi:10.1021/cs300488t
154. Britovsek GJP, Malinowski R, McGuinness DS, Nobbs JD, Tomov AK, Wadsley AW, Young CT (2015) Ethylene Oligomerization beyond Schulz–Flory Distributions. ACS Catal 5:6922–6925. doi:10.1021/acscatal.5b02203
155. Nicholas CP (2017) Applications of light olefin oligomerization to the production of fuels and chemicals. Applied Catalysis A: General 543:82–97. doi:10.1016/j.apcata.2017.06.011
156. Unde RB Kinetics and Reaction Engineering Aspects of Syngas Production by the Heterogeneously Catalysed Reverse Water Gas Shift Reaction. Dissertation, Lehrstuhl für Chemische Verfahrenstechnik, Universität Bayreuth
157. Rafati M, Wang L, Dayton DC, Schimmel K, Kabadi V, Shahbazi A (2017) Techno-economic analysis of production of Fischer-Tropsch liquids via biomass gasification: The effects of Fischer-Tropsch catalysts and natural gas co-feeding. Energy Conversion and Management 133:153–166. doi:10.1016/j.enconman.2016.11.051
158. Bouchy C, Hastoy G, Guillon E, Martens JA (2009) Fischer-Tropsch Waxes Upgrading via Hydrocracking and Selective Hydroisomerization. Oil & Gas Science and Technology - Rev IFP 64:91–112. doi:10.2516/ogst/2008047
159. Klerk A de (2008) Fischer–Tropsch refining: technology selection to match molecules. Green Chem 10:1249. doi:10.1039/b813233j
160. Lamprecht D (2007) Hydrogenation of Fischer–Tropsch Synthetic Crude. Energy Fuels 21:2509–2513. doi:10.1021/ef060612q
161. Haag S, Castillo-Welter F, Schuhmann T, Williams BA, Oelmann T, Günther A, Gorny M (2018) How to Convert CO2 to Green Methanol: Challenges for Petrochemicals and Fuels: Integration of Value Chains and Energy Transition, Berlin

162. Gogate MR (2019) Methanol-to-olefins process technology: current status and future prospects. Petroleum Science and Technology 37:559–565. doi:10.1080/10916466.2018.1555589
163. Samanta C, Das RK (2021) C3-Based Petrochemicals: Recent Advances in Processes and Catalysts. In: Pant KK, Gupta SK, Ahmad E (eds) Catalysis for Clean Energy and Environmental Sustainability. Springer International Publishing, Cham, pp 149–204
164. Ortiz-Espinoza AP, Noureldin MM, El-Halwagi MM, Jiménez-Gutiérrez A (2017) Design, simulation and techno-economic analysis of two processes for the conversion of shale gas to ethylene. Computers & Chemical Engineering 107:237–246. doi:10.1016/j.compchemeng.2017.05.023
165. Independent Commodity Integrence Service UOP/Hydro work MTO magic: MTO MATERIAL BALANCE. https://www.icis.com/explore/resources/news/1996/06/01/9793/uop-hydro-work-mto-magic/. Accessed 18 Oct 2021
166. Yang M, Fan D, Wei Y, Tian P, Liu Z (2019) Recent Progress in Methanol-to-Olefins (MTO) Catalysts. Adv Mater 31:e1902181. doi:10.1002/adma.201902181
167. Ye M, Tian P, Liu Z (2021) DMTO: A Sustainable Methanol-to-Olefins Technology. Engineering 7:17–21. doi:10.1016/j.eng.2020.12.001
168. Kianfar E (2019) Comparison and assessment of zeolite catalysts performance dimethyl ether and light olefins production through methanol: a review. Reviews in Inorganic Chemistry 39:157–177. doi:10.1515/revic-2019-0001
169. Vora BV, Marker TL, Barger PT, Nilsen HR, Kvisle S, Fuglerud T (1997) Economic route for natural gas conversion to ethylene and propylene. In: Natural Gas Conversion IV, vol 107. Elsevier, pp 87–98
170. Dimian AC, Bildea CS (2018) Energy efficient methanol-to-olefins process. Chemical Engineering Research and Design 131:41–54. doi:10.1016/j.cherd.2017.11.009
171. Eagan NM, Kumbhalkar MD, Buchanan JS, Dumesic JA, Huber GW (2019) Chemistries and processes for the conversion of ethanol into middle-distillate fuels. Nat Rev Chem 3:223–249. doi:10.1038/s41570-019-0084-4
172. Tao L, Markham JN, Haq Z, Biddy MJ (2017) Techno-economic analysis for upgrading the biomass-derived ethanol-to-jet blendstocks. Green Chem 19:1082–1101. doi:10.1039/C6GC02800D
173. Gong A, Verstraete D (2017) Fuel cell propulsion in small fixed-wing unmanned aerial vehicles: Current status and research needs. International Journal of Hydrogen Energy 42:21311–21333. doi:10.1016/j.ijhydene.2017.06.148
174. Focus Roland Berger (2020) Hydrogen: A future fuel for aviation?
175. Bube S, Bullerdiek N, Voß S, Kaltschmitt M (2024) Kerosene production from power-based syngas – A technical comparison of the Fischer-Tropsch and methanol pathway. Fuel 366:131269. doi:10.1016/j.fuel.2024.131269
176. Schemme S, Breuer JL, Köller M, Meschede S, Walman F, Samsun RC, Peters R, Stolten D (2020) H2-based synthetic fuels: A techno-economic comparison of alcohol, ether and hydrocarbon production. International Journal of Hydrogen Energy 45:5395–5414. doi:10.1016/j.ijhydene.2019.05.028
177. Drünert S, Neuling U, Zitscher T, Kaltschmitt M (2020) Power-to-Liquid fuels for aviation – Processes, resources and supply potential under German conditions. Applied Energy 277:115578. doi:10.1016/j.apenergy.2020.115578
178. Seymour K, Held M, Stolz B, Georges G, Boulouchos K (2024) Future costs of power-to-liquid sustainable aviation fuels produced from hybrid solar PV-wind plants in Europe. Sustainable Energy Fuels 8:811–825. doi:10.1039/D3SE00978E

179. Colelli L, Segneri V, Bassano C, Vilardi G (2023) E-fuels, technical and economic analysis of the production of synthetic kerosene precursor as sustainable aviation fuel. Energy Conversion and Management 288:117165. doi:10.1016/j.enconman.2023.117165
180. Raab M, Dietrich R-U (2023) Techno-economic assessment of different aviation fuel supply pathways including LH2 and LCH4 and the influence of the carbon source. Energy Conversion and Management 293:117483. doi:10.1016/j.enconman.2023.117483
181. Meurer A, Jochem P, Kern J (2024) Decentralised production of e-fuels for aviation: implications and trade-offs of a targeted small-scale production of sustainable aviation fuel based on Fischer–Tropsch synthesis. Sustainable Energy Fuels 8:752–765. doi:10.1039/D3SE01156A
182. Peacock J, Cooper R, Waller N, Richardson G (2024) Decarbonising aviation at scale through synthesis of sustainable e-fuel: A techno-economic assessment. International Journal of Hydrogen Energy 50:869–890. doi:10.1016/j.ijhydene.2023.09.094
183. Hirunsit P, Senocrate A, Gómez-Camacho CE, Kiefer F (2024) From CO 2 to Sustainable Aviation Fuel: Navigating the Technology Landscape. ACS Sustainable Chem Eng. doi:10.1021/acssuschemeng.4c03939
184. Porter RT, Fairweather M, Pourkashanian M, Woolley RM (2015) The range and level of impurities in CO2 streams from different carbon capture sources. International Journal of Greenhouse Gas Control 36:161–174. doi:10.1016/j.ijggc.2015.02.016
185. Kadlecek D (2023) Methanol to Jet (MTJ): ASTM D02.0J AC724 Task Force. www.caafi.org/resources/pdf/Methanol-to-Jet_CAAFI_Kadlecek_07_25_2023.pdf. Accessed 17 Jul 2024
186. Reddy C, Rangaiah GP (2016) Retrofit of Vacuum Systems in Process Industries. In: Rangaiah GP (ed) Chemical Process Retrofitting and Revamping. Wiley, pp 317–346
187. Adelung S, Dietrich R-U (2022) Impact of the reverse water-gas shift operating conditions on the Power-to-Liquid fuel production cost. Fuel 317:123440. doi:10.1016/j.fuel.2022.123440
188. Wesenberg MH (2006) Gas heated steam reformer modelling. NTNU, Trondheim
189. Grabke HJ (2003) Metal dusting. Materials & Corrosion 54:736–746. doi:10.1002/maco.200303729
190. Hamelinck C, Faaij A, Denuil H, Boerrigter H. (2004) Production of FT transportation fuels from biomass; technical options, process analysis and optimisation, and development potential. Energy 29:1743–1771. doi:10.1016/j.energy.2004.01.002
191. Babu BH, Lee M, Hwang DW, Kim Y, Chae H-J (2017) An integrated process for production of jet-fuel range olefins from ethylene using Ni-AlSBA-15 and Amberlyst-35 catalysts. Applied Catalysis A: General 530:48–55. doi:10.1016/j.apcata.2016.11.020
192. Lacarriere A, Robin J, Swierczyński D, Finiels A, Fajula F, Luck F, Hulea V (2012) Distillate-range products from non-oil-based sources by catalytic cascade reactions. ChemSusChem 5:1787–1792. doi:10.1002/cssc.201200092
193. Liu H, Xie Z, Zhao G The Progress of SINOPEC Methanol-To-Olefins (S-MTO) Technology: Shanghai Research Institute of Petrochemical Technology SINOPEC, China. In: October 9 - 11, 2013, Dresden, Germany
194. Bundesministerium der Finanzen (1995) AfA-Tabelle für den Wirtschaftszweig "Chemische Industrie": § 193ff AO , § 7 Abs 1 EStG
195. Oeko-Institut, Agora Energiewende & Agora Industry (2024) PTX Business Opportunity Analyser

196. Smith E, Morris J, Kheshgi H, Teletzke G, Herzog H, Paltsev S (2021) The cost of CO2 transport and storage in global integrated assessment modeling. International Journal of Greenhouse Gas Control 109:103367. doi:10.1016/j.ijggc.2021.103367
197. EZB Jährliche Entwicklung des Wechselkurses des Euro gegenüber dem US-Dollar von 1999 bis 2022. https://de.statista.com/statistik/daten/studie/200194/umfrage/wechselkurs-des-euro-gegenueber-dem-us-dollar-seit-2001/. Accessed 12 Jan 2023
198. Ruokonen J, Nieminen H, Dahiru AR, Laari A, Koiranen T, Laaksonen P, Vuokila A, Huuhtanen M (2021) Modelling and Cost Estimation for Conversion of Green Methanol to Renewable Liquid Transport Fuels via Olefin Oligomerisation. Processes 9:1046. doi:10.3390/pr9061046
199. Schröder J, Naumann K (2022) Monitoring erneuerbarer Energien im Verkehr: DBFZ Report 44. DBFZ Deutsches Biomasseforschungszentrum gemeinnützige GmbH
200. Bube S (2024) Produktionsverfahren für Sustainable Aviation Fuels - Wo wir aktuell stehen. https://www.airliners.de/status-quo-klimaschutz-2-produktionsverfahren-sustainable-aviation-fuels-aktuell-stehen/76542
201. IEA - International Energy Agency ETP Clean Energy Technology Guide. https://www.iea.org/data-and-statistics/data-tools/etp-clean-energy-technology-guide. Accessed 02 Mar 2025
202. Commercial Aviation Alternative Fuels Initiative Tools From CAAFI: Fuel Readiness Level (FRL). https://www.caafi.org/tools. Accessed 23 Jan 2025
203. Schaadt A (2024) Perspectives on Methanol to Jet Fuel – SAFari Project: aireg Webinar on Sustainable Aviation
204. (2023) REGULATION (EU) 2023/2405 OF THE EUROPEAN PARLIAMENT AND OF THE COUNCIL: ReFuelEU Aviation
205. Li Y, Zhang R, Liu G, Chen C, He Y, Liu X (2013) Comparison of methane production potential, biodegradability, and kinetics of different organic substrates. Bioresour Technol 149:565–569. doi:10.1016/j.biortech.2013.09.063
206. Voß S, Bube S, Kaltschmitt M (2023) Aviation fuel production pathways from lignocellulosic biomass via alcohol intermediates – A technical analysis. Fuel Communications 17:100093. doi:10.1016/j.jfueco.2023.100093
207. (2018) DIRECTIVE (EU) 2018/2001 OF THE EUROPEAN PARLIAMENT AND OF THE COUNCIL: RED II
208. Sens L, Neuling U, Kaltschmitt M (2022) Capital expenditure and levelized cost of electricity of photovoltaic plants and wind turbines – Development by 2050. Renewable Energy 185:525–537. doi:10.1016/j.renene.2021.12.042
209. Kost C, Shammugam S, Fluri V, Peper D, Memar AD, Schlegl T (2021) STROMGESTEHUNGSKOSTEN ERNEUERBARE ENERGIEN
210. Ouda M, Hank C, Nestler F, Hadrich M, Full J, Schaadt A, Hebling C (2019) Power-to-Methanol: Techno-Economical and Ecological Insights. In: Maus W (ed) Zukünftige Kraftstoffe. Springer Berlin Heidelberg, Berlin, Heidelberg, pp 380–409
211. Cummins Inc. HyLYZER® WATER ELECTROLYZERS: Electrolyzer brochure. https://www.cummins.com/new-power/applications/about-hydrogen. Accessed 01 May 2022
212. Paglini R, Gandiglio M, Lanzini A (2022) Technologies for Deep Biogas Purification and Use in Zero-Emission Fuel Cells Systems. Energies 15:3551. doi:10.3390/en15103551
213. Reppich M, Datzmann S, Li X, Rosenbauer S, Schlecht C, Tschepur S (2009) Vergleich verschiedener Aufbereitungsverfahren von Biogas zur Einspeisung in das Erdgasnetz. Chemie Ingenieur Technik 81:211–223. doi:10.1002/cite.200800125

214. Jensen C, Duyar MS (2021) Thermodynamic Analysis of Dry Reforming of Methane for Valorization of Landfill Gas and Natural Gas. Energy Technol 9:2100106. doi:10.1002/ente.202100106
215. Soleimani S, Lehner M (2022) Tri-Reforming of Methane: Thermodynamics, Operating Conditions, Reactor Technology and Efficiency Evaluation—A Review. Energies 15:7159. doi:10.3390/en15197159
216. Alipour Z, Babu Borugadda V, Wang H, Dalai AK (2023) Syngas production through dry reforming: A review on catalysts and their materials, preparation methods and reactor type. Chemical Engineering Journal 452:139416. doi:10.1016/j.cej.2022.139416
217. De Heer J (1957) The principle of Le Châtelier and Braun. University of Colorado. JOURNAL OF CHEMICAL EDUCATION:375–380
218. Cunha AF, Morales-Torres S, Pastrana-Martínez LM, Maldonado-Hódar FJ, Caetano NS (2022) Syngas production by bi-reforming of methane on a bimetallic Ni-ZnO doped zeolite 13X. Fuel 311:122592. doi:10.1016/j.fuel.2021.122592
219. García-Vargas JM, Valverde JL, Lucas-Consuegra A de, Gómez-Monedero B, Dorado F, Sánchez P (2013) Methane tri-reforming over a Ni/β-SiC-based catalyst: Optimizing the feedstock composition. International Journal of Hydrogen Energy 38:4524–4532. doi:10.1016/j.ijhydene.2013.02.001
220. Reuß M, Grube T, Robinius M, Stolten D (2019) A hydrogen supply chain with spatial resolution: Comparative analysis of infrastructure technologies in Germany. Applied Energy 247:438–453. doi:10.1016/j.apenergy.2019.04.064
221. Aspen Physical Property System: Physical Property Methods and Models 11.1
222. Carlson EC (1996) Don't Gamble With Physical Properties For Simulations: Succeeding at simulation. CHEMICAL ENGINEERING PROGRESS
223. Böge W (2007) Verdichter. In: Böge A (ed) Vieweg Handbuch Maschinenbau. Vieweg+Teubner, Wiesbaden, pp 904–912
224. Grote K-H, Bender B, Göhlich D (2018) Dubbel: Taschenbuch für den Maschinenbau. Springer Berlin Heidelberg, Berlin, Heidelberg
225. VDI e. V. (2013) VDI-Wärmeatlas. Springer Berlin Heidelberg, Berlin, Heidelberg
226. K. Hoyer, Hulteberg C. , Svensson M. , Jernberg J., Norregard Ø. (2016) Biogas upgrading - Technical review
227. Parks G, Boyd R, Cornish J, Remick R (2014) Hydrogen Station Compression, Storage, and Dispensing Technical Status and Costs: Systems Integration
228. ENERGY.GOV (2015) 3.2 Hydrogen Delivery: DELIVERY SECTION. https://www.energy.gov/sites/prod/files/2015/08/f25/fcto_myrdd_delivery.pdf. Accessed 07 Nov 2023
229. Reuß M, Grube T, Robinius M, Preuster P, Wasserscheid P, Stolten D (2017) Seasonal storage and alternative carriers: A flexible hydrogen supply chain model. Applied Energy 200:290–302. doi:10.1016/j.apenergy.2017.05.050
230. Nexant (2008) H2A Hydrogen Delivery Infrastructure Analysis Models and Conventional Pathway Options Analysis Results
231. INTERNATIONAL ENERGY AGENCY (2019) The Future of Hydrogen, Paris
232. Vartiainen E, Masson G, Breyer C, Moser D, Román Medina E (2020) Impact of weighted average cost of capital, capital expenditure, and other parameters on future utility-scale PV levelised cost of electricity. Progress in Photovoltaics 28:439–453. doi:10.1002/pip.3189
233. Prognos, Öko-Institut, Wuppertal Institut (2021) Klimaneutrales Deutschland.: Datenanhang. Studie im Auftrag von Agora Energiewende, Agora Verkehrswende und Stiftung Klimaneutralität

234. W. Cole, A. W. Frazier (2020) Cost Projections for Utility-Scale Battery Storage: 2020 Update: NREL/TP-6A20-75385. Contract No. DE-AC36-08GO28308
235. S. Kreidelmeyer, H. Dambeck, A. Kirchner, M. Wünsch (2020) Kosten und Transformationspfade für strombasierte Energieträger: Endbericht zum Projekt „Transformationspfade und regulatorischer Rahmen für synthetische Brennstoffe". Studie im Auftrag des Bundesministeriums für Wirtschaft
236. Michalski J, Bünger U, Crotogino F, Donadei S, Schneider G-S, Pregger T, Cao K-K, Heide D (2017) Hydrogen generation by electrolysis and storage in salt caverns: Potentials, economics and systems aspects with regard to the German energy transition. International Journal of Hydrogen Energy 42:13427–13443. doi:10.1016/j.ijhydene.2017.02.102
237. Saba SM, Müller M, Robinius M, Stolten D (2018) The investment costs of electrolysis – A comparison of cost studies from the past 30 years. International Journal of Hydrogen Energy 43:1209–1223. doi:10.1016/j.ijhydene.2017.11.115
238. L. Bertuccioli, A. Chan, D. Hart, F. Lehner, B. Madden, E. Standen (2014) Development of Water Electrolysis in the European Union
239. F. Merten, A. Scholz, C. Krüger, S. Heck, Y. Girard, M. Mecke, M. George (2020) Bewertung der Vor- und Nachteile von Wasserstoffimporten im Vergleich zur heimischen Erzeugung – Update
240. Fasihi M, Bogdanov D, Breyer C (2016) Techno-Economic Assessment of Power-to-Liquids (PtL) Fuels Production and Global Trading Based on Hybrid PV-Wind Power Plants. Energy Procedia 99:243–268. doi:10.1016/j.egypro.2016.10.115
241. Interreg Norht-West Europe H2SHIPS (2020) System-Based Solutions for H2-Fuelled Water Transport in North-West Europe: Comparative report on alternative fuels for ship propulsion
242. Schmidt O, Gambhir A, Staffell I, Hawkes A, Nelson J, Few S (2017) Future cost and performance of water electrolysis: An expert elicitation study. International Journal of Hydrogen Energy 42:30470–30492. doi:10.1016/j.ijhydene.2017.10.045
243. Ali Khan MH, Daiyan R, Han Z, Hablutzel M, Haque N, Amal R, MacGill I (2021) Designing optimal integrated electricity supply configurations for renewable hydrogen generation in Australia. iScience 24:102539. doi:10.1016/j.isci.2021.102539
244. Caldera U, Bogdanov D, Breyer C (2016) Local cost of seawater RO desalination based on solar PV and wind energy: A global estimate. Desalination 385:207–216. doi:10.1016/j.desal.2016.02.004
245. Ram M, Bogdanov D, Aghahosseini A, Gulagi A, Oyewo AS, Child M, Caldera U, Sadovskaia K, Farfan J, Barbosa L, Fasihi M, Khalili S, Breyer C (2019) Global energy system based on 100% renewable energy–power, heat, transport and desalination sectors. Berlin
246. Bründlinger R, Christ D, Fechner H, Kaltschmitt M, Müller J, Peharz G, Schulz D, Sens L (2020) Photovoltaische Stromerzeugung. In: Kaltschmitt M, Streicher W, Wiese A (eds) Erneuerbare Energien. Springer Berlin Heidelberg, Berlin, Heidelberg, pp 339–460
247. International Renewable Energy Agency (2019) Future of solar photovoltaic: Deployment, investment, technology, grid integration and socio-economic aspects. International Renewable Energy Agency, [Abu Dhabi]
248. M. Fette, H. C. Gils, J. Schaffert, E. Tali, N. Brücken (2020) Multi-Sektor-Kopplung: Modellbasierte Analyse der Integration erneuerbarer Stromerzeugung durch die Kopplung der Stromversorgung mit dem Wärme-, Gas- und Verkehrssektor. Endbericht
249. Danish Energy Agency (2016) Technology Data: Generation of Electricity and District heating

250. Kaltschmitt M, Özdirik B, Reimers B, Schlüter M, Schulz D, Sens L (2020) Stromerzeugung aus Windenergie. In: Kaltschmitt M, Streicher W, Wiese A (eds) Erneuerbare Energien. Springer Berlin Heidelberg, Berlin, Heidelberg, pp 461–582
251. International Renewable Energy Agency (2019) Future of wind: Deployment, investment, technology, grid integration and socio-economic aspects. International Renewable Energy Agency, [Abu Dhabi]
252. National Renewable Energy Laboratory Electricity Annual Technology Baseline: (ATB Spreadsheet). https://atb-archive.nrel.gov/electricity/2020/data.php. Accessed 05 Sep 2023
253. Krieg D (2012) Konzept und Kosten eines Pipelinesystems zur Versorgung des deutschen Straßenverkehrs mit Wasserstoff. Zugl.: Aachen, Techn. Hochsch., Diss., 2012. Schriften des Forschungszentrums Jülich Reihe Energie & Umwelt, vol 144. Forschungszentrum Jülich, Jülich
254. U. Kramer (2018) Defossilisierung des Transportsektors: Optionen und Voraussetzungen in Deutschland
255. Rivard E, Trudeau M, Zaghib K (2019) Hydrogen Storage for Mobility: A Review. Materials (Basel) 12. doi:10.3390/ma12121973
256. Marchese M, Giglio E, Santarelli M, Lanzini A (2020) Energy performance of Power-to-Liquid applications integrating biogas upgrading, reverse water gas shift, solid oxide electrolysis and Fischer-Tropsch technologies. Energy Conversion and Management: X 6:100041. doi:10.1016/j.ecmx.2020.100041
257. Steynberg A, Dry M (2004) Fischer-Tropsch technology. Studies in Surface Science and Catalysis, vol 152. Elsevier, Amsterdam, London
258. Iglesia E, Reyes SC, Madon RJ, Soled SL (1993) Selectivity Control and Catalyst Design in the Fischer-Tropsch Synthesis: Sites, Pellets, and Reactors. In: vol 39. Elsevier, pp 221–302
259. Pellegrini LA, Gamba S, Calemma V, Bonomi S (2008) Modelling of hydrocracking with vapour–liquid equilibrium. Chemical Engineering Science 63:4285–4291. doi:10.1016/j.ces.2008.06.002
260. Sun Q, Xie Z, Yu J (2018) The state-of-the-art synthetic strategies for SAPO-34 zeolite catalysts in methanol-to-olefin conversion. National Science Review 5:542–558. doi:10.1093/nsr/nwx103
261. Xue Y, Li S, Li J, Cui X, Wang P, Zheng H, Niu Y, Ma Q, Ding L (2021) Enhancing propene selectivity in methanol and/or butene conversion by regulating channel systems over ZSM-5/ZSM-48 composite zeolites. Microporous and Mesoporous Materials 312:110803. doi:10.1016/j.micromeso.2020.110803
262. Geleynse S, Brandt K, Garcia-Perez M, Wolcott M, Zhang X (2018) The Alcohol-to-Jet Conversion Pathway for Drop-In Biofuels: Techno-Economic Evaluation. ChemSusChem 11:3728–3741. doi:10.1002/cssc.201801690
263. Pechstein J, Neuling U, Gebauer J, Kaltschmitt M (2018) Alcohol-to-Jet (AtJ). In: Kaltschmitt M, Neuling U (eds) Biokerosene. Springer Berlin Heidelberg, Berlin, Heidelberg, pp 543–574
264. Keim W (2013) Oligomerization of ethylene to α-olefins: discovery and development of the shell higher olefin process (SHOP). Angew Chem Int Ed Engl 52:12492–12496. doi:10.1002/anie.201305308
265. Pondini M EM (2013) Process synthesis and design of low temperature Fischer-Tropsch crude production from biomass derived syngas: Master's Thesis within the Sustainable Energy Systems programme. Master's Thesis, CHALMERS UNIVERSITY OF TECHNOLOGY

266. Wiesche S aus der, Joos F (eds) (2018) Handbuch Dampfturbinen: Grundlagen, Konstruktion, Betrieb. Springer Vieweg, Wiesbaden, Heidelberg
267. Bless F, Arpagaus C, Bertsch SS, Schiffmann J (2017) Theoretical analysis of steam generation methods - Energy, CO 2 emission, and cost analysis. Energy 129:114–121. doi:10.1016/j.energy.2017.04.088
268. Thiel GP, Stark AK (2021) To decarbonize industry, we must decarbonize heat. Joule 5:531–550. doi:10.1016/j.joule.2020.12.007
269. Smith R (2016) Chemical process: Design and integration, Second edition. Wiley, Chichester, West Sussex, United Kingdom
270. Biegler LT, Grossmann IE, Westerberg AW (1998) Solutions Manual: Systematic methods for chemical process desing, 5st ed. Prentice Hall, Upper Saddle River (NJ)
271. Hemming W, Wagner W (2017) Verfahrenstechnik: 7.2 Berechnung der Wirbelschichtzustandsgrößen, 12., korrigierte Auflage. Kamprath-Reihe. Vogel Business Media, Würzburg
272. ACS Material MATERIALS CATALOG - SAPO-34: Technical parameters. https://www.acsmaterial.com/sapo-34.html. Accessed 04 Mar 2025
273. Jahangiri H, Bennett J, Mahjoubi P, Wilson K, Gu S (2014) A review of advanced catalyst development for Fischer–Tropsch synthesis of hydrocarbons from biomass derived syngas. Catal. Sci. Technol. 4:2210–2229. doi:10.1039/C4CY00327F
274. Couper JR, Penny WR, Fair JR 17 - CHEMICAL REACTORS. In: Chemical Process Equipment, pp 581–640
275. Morawski I, Mosio-Mosiewski J (2006) Effects of parameters in Ni–Mo catalysed hydrocracking of vacuum residue on composition and quality of obtained products. Fuel Processing Technology 87:659–669. doi:10.1016/j.fuproc.2006.01.006
276. Choi E, Song K, An S, Lee K, Youn M, Park K, Jeong S, Kim H (2018) Cu/ZnO/AlOOH catalyst for methanol synthesis through CO2 hydrogenation. Korean J Chem Eng 35:73–81. doi:10.1007/s11814-017-0230-y
277. Pontzen F, Liebner W, Gronemann V, Rothaemel M, Ahlers B (2011) CO2-based methanol and DME – Efficient technologies for industrial scale production. Catalysis Today 171:242–250. doi:10.1016/j.cattod.2011.04.049
278. Lu K, Huang J, Ren L, Li C, Guan Y, Hu B, Xu H, Jiang J, Ma Y, Wu P (2020) High Ethylene Selectivity in Methanol-to-Olefin (MTO) Reaction over MOR-Zeolite Nanosheets. Angew Chem Int Ed Engl 59:6258–6262. doi:10.1002/anie.202000269
279. Yarlagadda P, Lund C, Ruckenstein E (1990) Oligomerization of ethene and propene over composite zeolite catalysts. Applied Catalysis 62:125–139. doi:10.1016/S0166-9834(00)82242-3
280. Balshakou S (2024) Production of fuel fractions from renewable ethene-propene mixture over Ni/HZSM-5. Master Thesis, LUT, Lappeenranta-Lahti University of Technology
281. Monama W, Mohiuddin E, Thangaraj B, Mdleleni MM, Key D (2020) Oligomerization of lower olefins to fuel range hydrocarbons over texturally enhanced ZSM-5 catalyst. Catalysis Today 342:167–177. doi:10.1016/j.cattod.2019.02.061
282. JALON Zeolite 3A Molekularsieb: Technische Daten. https://www.jalonzeolite.com/de/product-item/zeolite-3a/. Accessed 06 Mar 2025
283. Verband der Chemischen Industrie e. V. (2023) Chemiewirtschaft in Zahlen: 2023, Frankfurt
284. Statistisches Bundesamt (2021) Lohnnebenkosten auf 100 Euro Bruttoverdienst in der Privatwirtschaft in den Mitgliedstaaten der Europäischen Union in den Jahren 2018 bis 2020. https://de.statista.com/statistik/daten/studie/182879/umfrage/lohnnebenkosten-in-der-eu/. Accessed 15 Jul 2024

285. Saavedra Lopez J, Dagle RA, Dagle VL, Smith C, Albrecht KO (2019) Oligomerization of ethanol-derived propene and isobutene mixtures to transportation fuels: catalyst and process considerations. Catal Sci Technol 9:1117–1131. doi:10.1039/C8CY02297F